

**Alkali Metal Mediated Bimetallic Main Group and
Transition Organometallic Chemistry**

By

Ross Campbell

A thesis submitted to the Department of Pure and Applied Chemistry, University of
Strathclyde, in part fulfilment of the requirements for the degree of Doctor of
Philosophy

March 2012

This thesis is the result of the author's original research. It has been composed by the author and has not been previously submitted for examination which has led to the award of a degree.

The copyright of this thesis belongs to the author under the terms of the United Kingdom Copyright Acts as qualified by the University of Strathclyde Regulation 3.50. Due acknowledgement must always be made of the use of any material contained in, or derived from, this thesis.

To my mum and dad, here's to all the good times shared and all the adventures yet to
come!

1 Acknowledgements

First and foremost I must thank Prof. Mulvey for giving me this opportunity to study for a PhD with him, and the EPSRC for funding the project. Rab has helped immeasurably with all things chemistry; conceiving projects and guiding them, the preparation and delivery of oral presentations, and the proof reading of papers and reports, including this thesis for which the reader should also be eternally thankful. I hope in the years ahead that I will feature in a few of his stories alongside the many greats of time gone by.

Special note must also go to my second supervisor, Dr. Charlie O'Hara. Without the help of his technical wizardry I think my frustrations with MS Word, End Note etc. may have become too much to bare. It is thanks to him that my computer and I are now enjoying a fruitful relationship and that I have not become the first person to submit a hand written 9 month report to this department in the 21st century!

The important contribution made to the whole Mulvey group by our dedicated crystallographers cannot be overstated. The remarkable fact is that, despite all the hours toiling away running our crystals, often during unsociable hours, Stuart, Pablo and Jan are also the most dependable members of the fun gang come Friday night!

My final thanks go to the rest of our group that I have not mentioned by name. My gratitude cannot adequately be portrayed in one page of text (or even the "extended highlights" at the back of this thesis). For making our lab an enjoyable place to work, for our various excursions bowling, go-karting and the likes, and for the countless acts of generosity that have been too quickly forgotten to mention, I am eternally grateful.

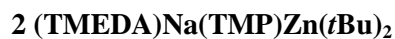
Ross Campbell

2 Abbreviations

CIPE	Complex Induced Proximity Effect
THF	Tetrahydrofuran
TMEDA	<i>N,N,N',N'</i> -tetramethylethylenediamine
Boc	COO(<i>t</i> Bu)
<i>Do</i> M	Directed <i>ortho</i> Metallation
TMP(H)	2,2,6,6-tetramethylpiperidine
HMPA	Hexamethylphosphoric triamide
HMDS(H)	1,1,1,3,3,3-hexamethyldisilazane
DA(H)	diisopropylamine
DPEDA(H ₂)	<i>N,N'</i> -diisopropylethylenediamine
DBEDA(H ₂)	<i>N,N'</i> -di- <i>tert</i> -butylethylenediamine
DFT	Density Functional Theory
OAc	OOCMe
Dipp	Diisopropylphenyl – 2,6-(<i>i</i> Pr)C ₆ H ₃
DOSY	Diffusion Ordered Spectroscopy
Cp*	pentamethylcyclopentadienyl
CCDB	Cambridge Crystallographic Database
EXSY	Exchange Spectroscopy
PMDETA	<i>N,N,N',N'',N''</i> -pentamethyldiethylenetriamine
TMCDA	<i>N,N,N',N'</i> -(1 <i>R</i> ,2 <i>R</i>)-tetramethylcyclohexane-1,2-diamine
Me ₆ -TREN	Tris[2-(dimethylamino)ethyl]amine
PET	Positron Emission Tomography
DIBA(H)	Diisobutylamine
NPPDA	NeoPentylPhenylDiAmide - Ph[1,2-N(CH ₂ ^{<i>t</i>} Bu)] ₂
DAIB	3- <i>exo</i> -(dimethylamino)isoborneol
DMP(H)	(<i>cis</i>)-2,6-dimethylpiperidine
NOESY	Nuclear Overhauser Effect Spectroscopy
Cy	cyclohexyl
Tol	tolyl
Py	Pyridine

DMF	<i>N,N</i> -dimethylformamide
EPR	Electro Paramagnetic Resonance
MM	Multipole Model
MDME	1-methoxy-2-dimethylaminoethane
THFFA	<i>N,N</i> -dimethyltetrahydrofurfurylamine
DME	1,2-dimethoxyethane
TMDAE	TetraMethylDiAminoEther - bis[2-(<i>N,N</i> -dimethylamino)ethyl] ether
MAC	Metal Anionic Crown

3 Numbered compounds

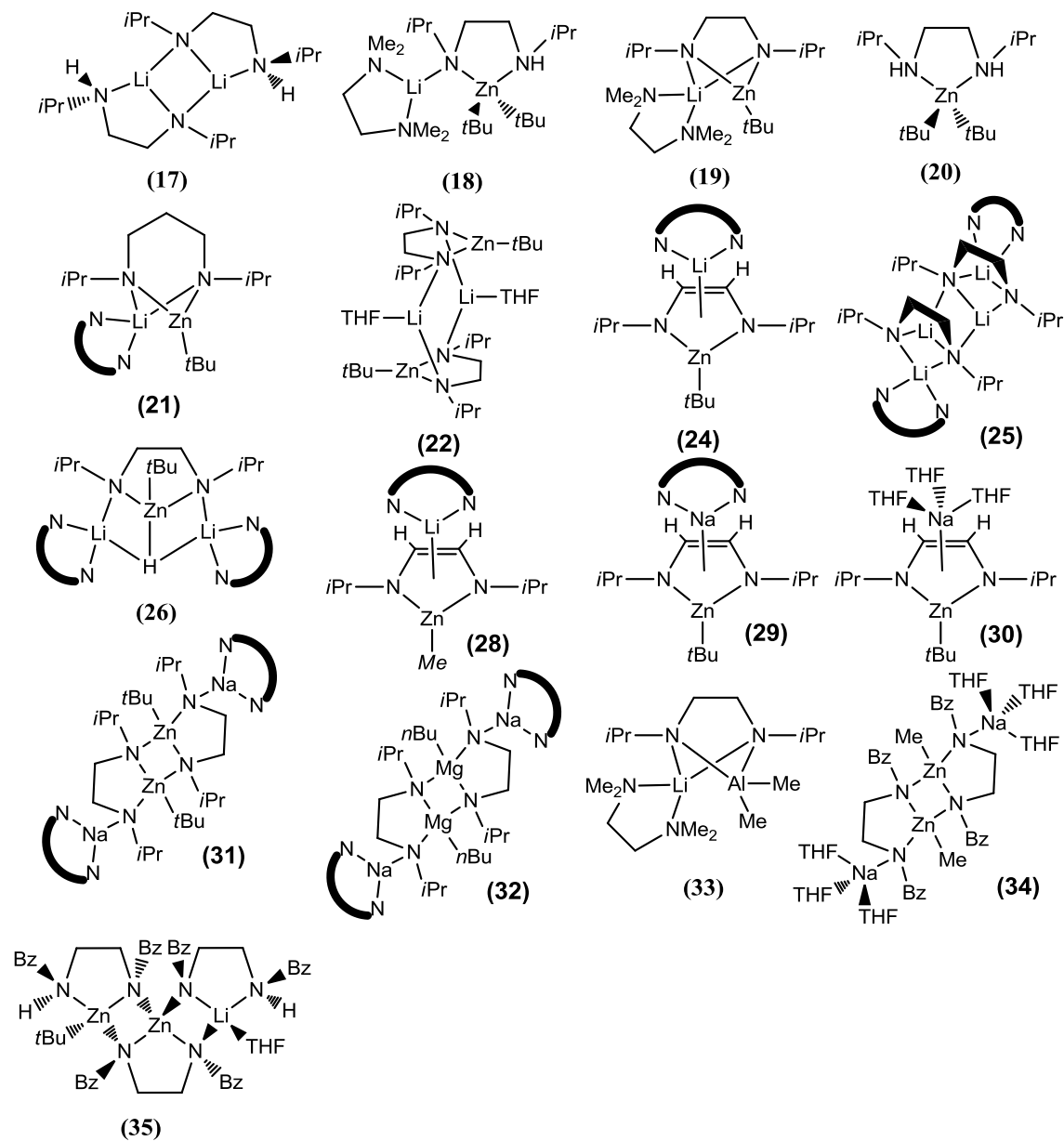


- 16 $\text{Me}_2\text{NCH}_2\text{CH}_2\text{N}(\text{Me})_2\text{C}_6\text{H}_4\text{Zn}(t\text{Bu})_2$
- 17 $\{\text{Li}[(i\text{Pr})\text{NCH}_2\text{CH}_2\text{N}(\text{H})(i\text{Pr})]\}_2$
- 18 $(\text{TMEDA})\text{Li}[(i\text{Pr})\text{NCH}_2\text{CH}_2\text{N}(\text{H})(i\text{Pr})]\text{Zn}(t\text{Bu})_2$
- 19 $(\text{TMEDA})\text{Li}[(i\text{Pr})\text{NCH}_2\text{CH}_2\text{N}(i\text{Pr})]\text{Zn}(t\text{Bu})$
- 20 $[(i\text{Pr})\text{N}(\text{H})\text{CH}_2\text{CH}_2\text{N}(\text{H})(i\text{Pr})]\text{Zn}(t\text{Bu})_2$
- 21 $(\text{TMEDA})\text{Li}[(i\text{Pr})\text{NCH}_2\text{CH}_2\text{CH}_2\text{N}(i\text{Pr})]\text{Zn}(t\text{Bu})$
- 22 $\{(\text{THF})\text{Li}[(i\text{Pr})\text{NCH}_2\text{CH}_2\text{N}(i\text{Pr})]\text{Zn}(t\text{Bu})\}_2$
- 23 $\text{K}_2[(t\text{Bu})\text{N}(\text{H})\text{C}(\text{O})\text{NCH}_2\text{CH}_2\text{NC}(\text{O})\text{NH}(t\text{Bu})]_2\text{Zn}$
- 24 $(\text{TMEDA})\text{Li}[(i\text{Pr})\text{NCH}=\text{CHN}(i\text{Pr})]\text{Zn}(t\text{Bu})$
- 25 $[(\text{TMEDA})\text{Li}(i\text{Pr})\text{NCH}_2\text{CH}_2\text{N}(i\text{Pr})\text{Li}]_2$
- 26 $[(\text{TMEDA})\text{Li}]_2[(i\text{Pr})\text{NCH}_2\text{CH}_2\text{N}(i\text{Pr})]\text{Zn}(t\text{Bu})\text{H}$
- 27 $[(\text{TMEDA})\text{Li}]_2[(i\text{Pr})\text{NCH}=\text{CHN}(i\text{Pr})]\text{Zn}(t\text{Bu})\text{H}$
- 28 $(\text{TMEDA})\text{Li}[(i\text{Pr})\text{NCH}=\text{CHN}(i\text{Pr})]\text{Zn}(\text{Me})$
- 29 $(\text{TMEDA})\text{Na}[(i\text{Pr})\text{NCH}=\text{CHN}(i\text{Pr})]\text{Zn}(t\text{Bu})$
- 30 $(\text{THF})_3\text{Na}[(i\text{Pr})\text{NCH}=\text{CHN}(i\text{Pr})]\text{Zn}(t\text{Bu})$
- 31 $\{(\text{TMEDA})\text{Na}[(i\text{Pr})\text{NCH}_2\text{CH}_2\text{N}(i\text{Pr})]\text{Zn}(t\text{Bu})\}_2$
- 32 $\{(\text{TMEDA})\text{Na}[(i\text{Pr})\text{NCH}_2\text{CH}_2\text{N}(i\text{Pr})]\text{Mg}(n\text{Bu})\}_2$
- 33 $(\text{TMEDA})\text{Li}[\text{N}(i\text{Pr})\text{CH}_2\text{CH}_2\text{N}(i\text{Pr})]\text{Al}(\text{Me})_2$
- 34 $\{(\text{THF})_3\text{Na}[(\text{Bz})\text{NCH}_2\text{CH}_2\text{N}(\text{Bz})]\text{Zn}(\text{Me})\}_2$
- 35 $(\text{THF})\text{Li}[(\text{Bz})\text{N}(\text{H})\text{CH}_2\text{CH}_2\text{N}(\text{Bz})]_2\text{Zn}_2[(\text{Bz})\text{NCH}_2\text{CH}_2\text{N}(\text{Bz})](t\text{Bu})$
- 36 $\{(\text{THF})\text{Li}(\text{DIBA})\}_2$
- 37 $\{(\text{TMEDA})[\text{Li}(\text{DIBA})]_2\}_\infty$
- 38 $[(\text{TMEDA})_2\text{Li}]\{(i\text{Bu})_2\text{N}[(\text{Zn}(t\text{Bu})_2)_2]\}$
- 39 $(\text{THF})_3\text{Li}[(\text{Dipp})\text{NH}]\text{Zn}(\text{Me})[(\text{Dipp})\text{NH}]\text{Zn}(\text{Me})_2$
- 40 $(\text{TMEDA})\text{Na}(\text{DIBA})_2\text{Zn}(t\text{Bu})$
- 41 $(\text{C}_{10}\text{H}_7)[\text{N}(i\text{Bu})_2]\text{C}=\text{N}[\text{Zn}(t\text{Bu})_2]\text{Li}(\text{TMEDA})$

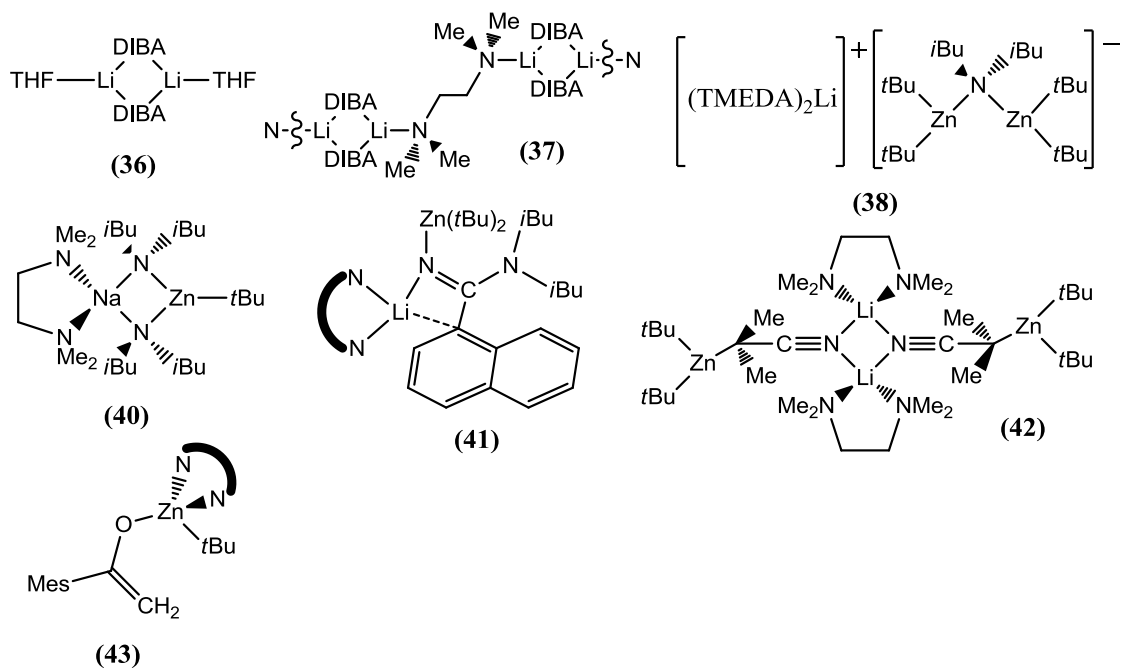
- 42 $\{(\text{TMEDA})\text{Li}[\text{NCC}(\text{Me}_2)\text{Zn}(t\text{Bu})_2]\}_2$
- 43 $(\text{TMEDA})\text{Zn}(t\text{Bu})\text{OC}(=\text{CH}_2)\text{Mes}$
- 44 $[(\text{Et}_2\text{O})_4\text{Na}]_4\text{Cr}_2\text{Me}_8$
- 45 $[(\text{TMEDA})\text{Na}]_3\text{Cr}_2\text{Me}_7$
- 46 $[(\text{TMEDA})\text{Na}]_3\text{Cr}_2\text{Me}_7$
- 47 $[(\text{TMEDA})\text{Na}]\text{Mo}_2\text{Me}_8$
- 48 $[\text{LiTMP} + (i\text{Bu})_2\text{Al}(\text{TMP})]$
- 49 $(\text{THF})\text{Li}(\text{TMP})\text{Al}(i\text{Bu})_3$
- 50 $(\text{MDME})\text{Li}(\text{TMP})\text{Al}(i\text{Bu})_3$
- 51 $(\text{THFFA})\text{Li}(\text{TMP})\text{Al}(i\text{Bu})_3$
- 52 $(\text{DME})\text{Li}(\text{TMP})\text{Al}(i\text{Bu})_3$
- 53 $(\text{MDME}^*)\text{Li}(\text{TMP})\text{Al}(i\text{Bu})_2$
- 54 $(\text{THFFA}^*)\text{Li}(\text{TMP})\text{Al}(i\text{Bu})_2$
- 55 $\{(\text{THFFA})[\text{Li}(\text{TMP})]_2\text{LiCl}\}_2$
- 56 $(\text{DME})[(\text{DME}^*)\text{Li}(\text{TMP})\text{Al}(i\text{Bu})_2]_2$
- 57 $(\text{TMDAE}^*)\text{Li}(\text{TMP})\text{Al}(i\text{Bu})_2$

4 Compounds prepared within this thesis

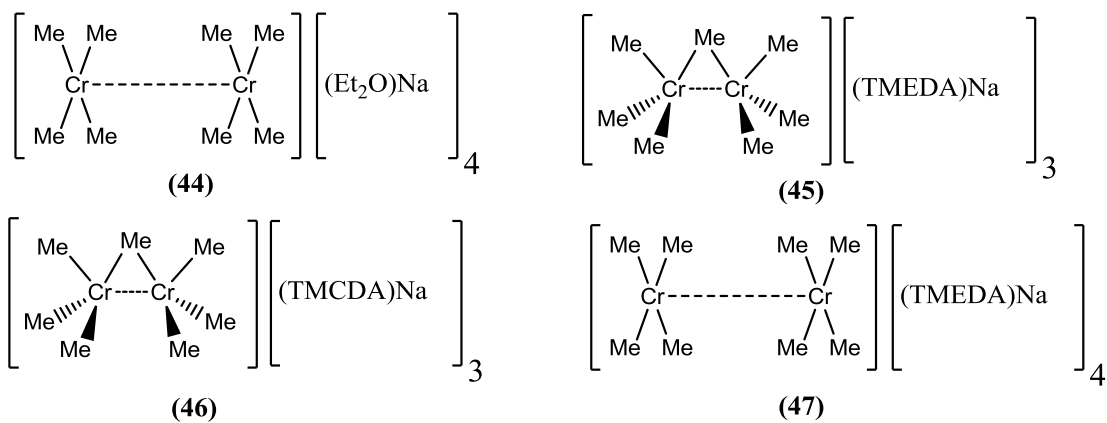
9. Alkali-Metal-Mediated multiple main group C-H activation



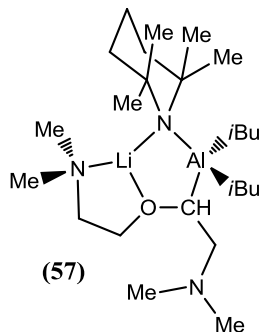
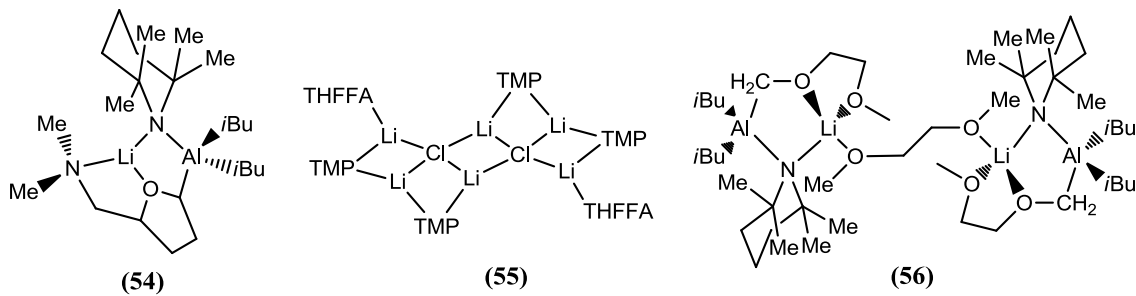
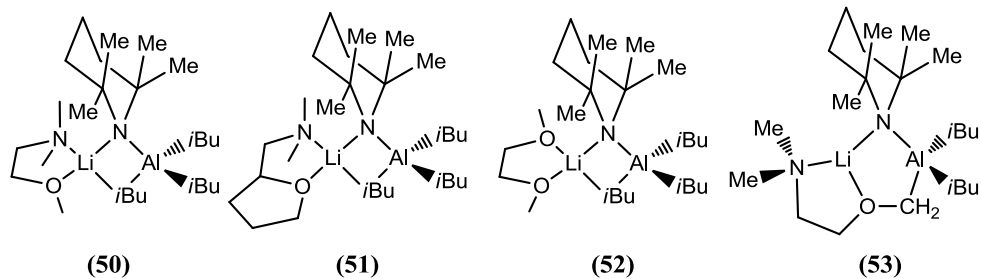
10. New alkyl amido zincates: a disproportionation reaction and novel stoichiometries



11. Alkali metal control of the metal-metal bonding properties of the group VI metals



12. sp^3 C-H metallation mediated by synergic bimetallic alluminate bases



5 Abstract

The work reported may appear as an eclectic mix of zinc, magnesium, aluminium and transition metal chemistry. However, at the heart of all the investigations is the prominent role of lithium or sodium within a bi-metallic species in either 1) facilitating unusual reactivity or 2) resulting in novel structural chemistry.

The surprising transformation of saturated diamine (*i*Pr)NHCH₂CH₂NH(*i*Pr) to the unsaturated diazaethene [(*i*Pr)NCH=CHN(*i*Pr)]²⁻ via the synergic mixture BuM, (*t*Bu)₂Zn and TMEDA (where M = Li, Na) has been investigated by NMR spectroscopy and DFT calculations. Isolated compounds (TMEDA)Li[(*i*Pr)NCH₂CH₂NH(*i*Pr)]Zn(*t*Bu)₂ **18**, (TMEDA)Li[(*i*Pr)NCH₂CH₂CH₂N(*i*Pr)]Zn(*t*Bu) **21**, {(THF)Li[(*i*Pr)NCH₂CH₂N(*i*Pr)]Zn(*t*Bu)}₂ **22**, and {(TMEDA)Na[(*i*Pr)NCH₂CH₂N(*i*Pr)]Zn(*t*Bu)}₂ **31**, are discussed in relation to their role in forming (TMEDA)M[(*i*Pr)NCH=CHN(*i*Pr)]Zn(*t*Bu) (M = Li, **24**; Na, **29**). Also, the dilithiozincate molecular hydride [(TMEDA)Li]₂[(*i*Pr)NCH₂CH₂N(*i*Pr)]Zn(*t*Bu)H **26** is reported. Its ⁷Li NMR spectrum reveals a rare scalar ¹J_{Li-H} coupling constant of 13.3 Hz.

The diisobutylamide ligand (DIBA) has been investigated in both a homo-metallic (Li) and bi-metallic (Li/Zn, Na/Zn) context. A zinc-rich zincate [(TMEDA)₂Li]⁺{(DIBA)[Zn(*t*Bu)₂]₂}⁻ **38** and bis-amide (TMEDA)Na(DIBA)₂Zn(*t*Bu)₂ **40** have been made.

Reported also is the synthesis of the sodium complex [(Et₂O)Na]₄Cr₂Me₈ **44**. Its drastically elongated Cr–Cr separation [3.24 Å], relative to the lithium species [1.98 Å], has revealed the important alkali metal role in dictating the nature of metal–metal interactions. The reactivity of **44** has been investigated towards Lewis bases, resulting in the novel heptamethyl chromium complex [(TMEDA)Na]₃Cr₂Me₇ **45**. This new family

of group VI sodium methyl compounds has also been extended to molybdenum via $[(\text{TMEDA})\text{Na}]_4\text{Mo}_2\text{Me}_8$ **47**.

Finally, bimetallic aluminates $(\text{THF})\text{Li}(\text{TMP})\text{Al}(\text{iBu})_3$ **49** and “ $\text{Li}(\text{TMP})_2\text{Al}(\text{iBu})_2$ ” **48** have both previously demonstrated a propensity towards heteroatom activated sp^3 deprotonation. To extend this potentially useful synthetic methodology the reactivity of both reagents has been systematically investigated towards a series of bi and tridentate substrates incorporating both nitrogen and oxygen atoms. A family of adducts of **49** have been prepared.

6 Publications

- Main Group Multiple C–H/N–H Bond Activation of a Diamine and Isolation of a Molecular Dilithium Zincate Hydride: Experimental and DFT Evidence for Alkali Metal – Zinc Synergistic Effects – **J. Am. Chem. Soc.** 2011, **133**, 13706-13717.
- Sodium Congener of the Classical Lithium Methylchromate Dimer: Synthetic, X-Ray Crystallographic, and Magnetic Studies of $\text{Me}_8\text{Cr}_2[\text{Na}(\text{OEt}_2)]_4$ – **Inorg. Chem.** 2011, **50**, 4656-4659.
- Synergic Transformation of an Ethylenediamine to a Lithium 1,3-Diaza-2-zincacyclopentene via an Alkylolithium/Bis(alkyl)zinc Mixture – **Chem. Eur. J.** 2010, **16**, 9964-9968.
- cis-2,6-Dimethylpiperidide: a structural mimic for TMP (2,2,6,6-tetramethylpiperidide) or DA (diisopropylamide)? – **Dalton. Trans.** 2010, **39**, 511-519.

7 Conference Presentations

- Alkali Metal Control in Transition Metal Chemistry: Synthesis and Structure of New Chromates and Molybdates – Oral presentation, Universities of Scotland Inorganic Conference, Glasgow University, 2011.
- Synergic Transformation of an Ethylenediamine to a Lithium 1,3-diaza-2-zincacyclopentene – Poster presentation, Pacificchem conference, Hawaii, 2010.
- Alkali Metal Control in Transition Metal Chemistry: Synthesis and Structure of New Chromates and Molybdates – Oral presentation, WestCHEM colloquia, University of Strathclyde, 2010.
- Synergic Transformation of an Ethylenediamine to a Lithium 1,3-diaza-2-zincacyclopentene – Poster presentation, Universities of Scotland Inorganic Conference, Durham University, 2010.
- Alkali Metal Control in Transition Metal Chemistry: Synthesis and Structure of New Chromates and Molybdates – Oral presentation, Postgraduate talks, University of Strathclyde, 2010.

Contents

1	Acknowledgements	iv
2	Abbreviations	v
3	Numbered compounds	vi
4	Compounds prepared within this thesis	ix
5	Abstract	xii
6	Publications	xiv
7	Conference Presentations	xiv
8	Introduction	1
8.1	Organolithium reagents	1
8.1.1	Synthesis of simple organolithiums through reductive lithiation	1
8.1.2	Deprotonative metallation	3
8.1.3	Lithium–halogen exchange	10
8.2	Mixed Metal Organometallics	12
8.2.1	Mechanistic Insight	14
8.2.2	Synergy in action: reactivity exclusive to bimetallics	25
9	Alkali-metal-mediated multiple main group C-H activation	35
9.1	Co-complexation with a diamide and subsequent synergic zincation	35
9.2	Unexpected CH activation and experimental evidence for a hydride intermediate	48
9.3	DFT calculations	66
9.4	Scope and limitations	79
9.5	Conclusions and future work	92
10	New alkyl amido zincates: a disproportionation reaction and novel stoichiometries 96	
10.1	Introducing diisobutylamide and a new zinc rich zincate	96
10.2	The disproportionation reaction	106
10.3	New amidinato zincate compounds	111
10.4	α -Nitriles, a potential new area for zincates	118
10.5	An expansion of zincate enolate chemistry	123
10.6	Conclusions and future work	127
11	Alkali metal control of the metal–metal bonding properties of the group VI metals 131	
11.1	Structural studies of sodium methylchromates	134

11.2	Examining the electronic structures of the new chromium complexes	141
11.3	Synthesis of a sodium methylmolybdate	147
11.4	Conclusions and future work	149
12	sp^3 C–H metallation mediated by synergic bimetallic aluminate bases.....	152
12.1	Reactions with the mono TMP aluminate base	153
12.2	Reactions with the bis TMP aluminate base.....	161
12.3	Conclusions and future work	175
13	Experimental	178
13.1	General procedures	178
13.1.1	Schlenk Techniques	178
13.1.2	Use of a Glove Box.....	179
13.1.3	Solvents and Liquid Reagents.....	179
13.1.4	Reagents Used.....	180
13.1.5	Standardisation of Reagents.....	180
13.1.6	Preparation of Salicylaldehyde Phenylhydrazone.....	180
13.1.7	Standardisation of Alkyl lithium Compounds	181
13.2	Preparation of Starting Materials.....	181
13.2.1	Preparation of BuNa.....	181
13.2.2	Preparation of tBu_2Zn	182
13.3	Instrumentation	182
13.4	Synthesis for chapter 8.....	183
13.4.1	Synthesis of $\{Li[N(iPr)CH_2CH_2N(H)(iPr)]\}_2$ 17.....	183
13.4.2	Synthesis of (TMEDA)Li[(<i>iPr</i>)NCH ₂ CH ₂ N(H)(<i>iPr</i>)Zn(<i>tBu</i>) ₂] 18.....	183
13.4.3	Synthesis of [(<i>iPr</i>)N(H)CH ₂ CH ₂ N(H)(<i>iPr</i>)Zn(<i>tBu</i>) ₂] 19.....	183
13.4.4	Synthesis of (TMEDA)Li[(<i>iPr</i>)NCH ₂ CH ₂ CH ₂ N(<i>iPr</i>)Zn(<i>tBu</i>)] 21	184
13.4.5	Synthesis of $\{(THF)Li[(iPr)NCH_2CH_2N(iPr)]Zn(tBu)\}_2$ 22	184
13.4.6	Synthesis of (TMEDA)Li[(<i>iPr</i>)NCH=CHN(<i>iPr</i>)Zn(<i>tBu</i>)] 24	185
13.4.7	Synthesis of [(TMEDA)Li(<i>iPr</i>)NCH ₂ CH ₂ N(<i>iPr</i>)Li] ₂ 25.....	185
13.4.8	Synthesis of [(TMEDA)Li] ₂ [(<i>iPr</i>)NCH ₂ CH ₂ N(<i>iPr</i>)Zn(<i>tBu</i>)H] 26.....	185
13.4.9	Synthesis of [LiOCH(<i>tBu</i>) ₂] ₄	186
13.4.10	Synthesis of (TMEDA)Li[(<i>iPr</i>)NCH=CHN(<i>iPr</i>)Zn(Me)] 28	186
13.4.11	Synthesis of (TMEDA)Na[(<i>iPr</i>)NCH=CHN(<i>iPr</i>)Zn(<i>tBu</i>)] 29	187
13.4.12	Synthesis of (THF) ₃ Na[(<i>iPr</i>)NCH=CHN(<i>iPr</i>)Zn(<i>tBu</i>)] 30.....	187
13.4.13	Synthesis of $\{(TMEDA)Na[(iPr)NCH_2CH_2N(iPr)]Zn(tBu)\}_2$ 31.....	188

13.4.14	Synthesis of $\{(TMEDA)Na[(iPr)NCH_2CH_2N(iPr)]Mg(nBu)_2\}_2$ 32.....	188
13.4.15	Synthesis of $(TMEDA)Li[(iPr)NCH_2CH_2N(iPr)]Al(Me)_2$ 33.....	189
13.5	Synthesis for chapter 9.....	189
13.5.1	Synthesis of $(TMEDA)Li[DIBA]_2$ 37	189
13.5.2	Synthesis of $[(TMEDA)_2Li]\{(DIBA)[Zn(tBu)_2]_2\}$ 38	190
13.5.3	Alternative synthesis of $[(TMEDA)_2Li]\{(DIBA)[Zn(tBu)_2]_2\}$ 38.....	190
13.5.4	Synthesis of $[(TMEDA)_2Li][Zn(tBu)_3]$	191
13.5.5	Synthesis of $(TMEDA)Na[DIBA]_2Zn(tBu)$ 40.....	191
13.5.6	Synthesis of $(C_{10}H_7)C[N(iBu)_2]N[Zn(tBu)_2]Li(TMEDA)$ 41.....	191
13.5.7	Synthesis of $\{(TMEDA)Li[NCC(Me)_2Zn(tBu)_2]\}_2$ 42	192
13.5.8	Synthesis of $(TMEDA)Zn(tBu)OC(=CH_2)Mes$ 43	192
13.6	Synthesis for chapter 10.....	192
13.6.1	Synthesis of $[Na(OEt_2)]_4Cr_2Me_8$ 44.....	193
13.6.2	Synthesis of $[(TMEDA)Na]_3Cr_2Me_7$ 45.....	193
13.6.3	Synthesis of $[(TMCDA)Na]_3Cr_2Me_7$ 46	193
13.6.4	Synthesis of $[(TMEDA)Na]_4Mo_2Me_8$ 47	194
13.7	Synthesis for chapter 11.....	194
13.7.1	Synthesis of $(MDME)Li(TMP)Al(iBu)_3$ 50.....	194
13.7.2	Synthesis of $(THFFA)Li(TMP)Al(iBu)_3$ 51.....	195
13.7.3	Synthesis of $(DME)Li(TMP)Al(iBu)_3$ 52	195
13.7.4	Synthesis of $(MDME^*)Li(TMP)Al(iBu)_2$ 53.....	196
13.7.5	Synthesis of $(THFFA^*)Li(TMP)Al(iBu)_2$ 54.....	196
13.7.6	Synthesis of $(DME)[(DME^*)Li(TMP)Al(iBu)_2]_2$ 56.....	197
13.7.7	Synthesis of $(TMDAE^*)Li(TMP)Al(iBu)_2$ 57	198
14	References	199
15	X-ray Crystallographic data	211
16	Extended Acknowledgements.....	239

8 Introduction

8.1 Organolithium reagents

Since their initial preparation by the German chemists Schlenk and Holtz, who first described the synthesis of methyllithium, ethyllithium and phenyllithium in 1917,^[1] alkyl lithium reagents have been indispensable reagents in organic and organometallic synthesis and as polymerization initiators both in academic research and on an industrial scale. Collum captured a sense of their staggering influence on synthetic chemistry with the following quote.

“The chemistry of lithium is pervasive in organic chemistry...for example, well over 95% of natural product syntheses rely upon lithium-based reagents in one form or another.”

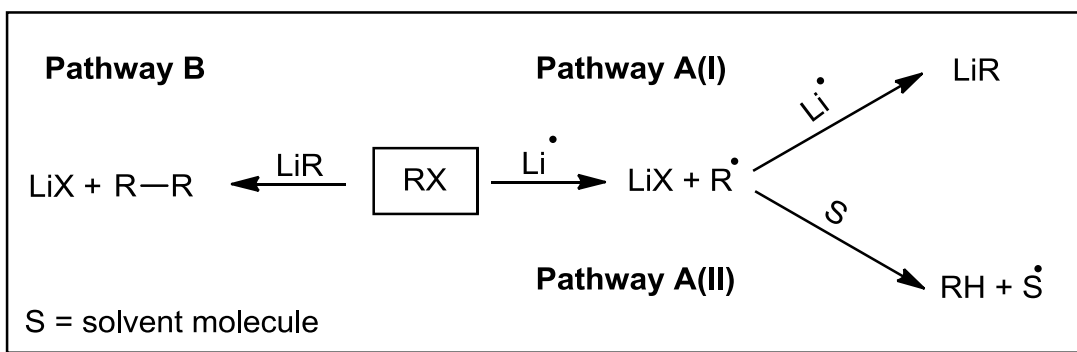
D. B. Collum^[2]

The industrial requirement for lithium organometallics shows no sign of abating either, with new plants recently opening in China and India to satisfy demand. As a result improving our understanding of the properties, reactivity and uses of such lithium species is not simply of interest to the research community, but critical if we are to continue to meet the ever increasing expectations imposed on us by an ever aspiring public.

8.1.1 Synthesis of simple organolithiums through reductive lithiation

The oldest and most direct general synthetic technique for the generation of an organolithium compound is through the reductive lithiation of an alkyl halide with lithium metal.^[1] The reaction of RX with lithium metal first proceeds through the generation of an organic radical species with concomitant formation of salt LiX.^[3] The newly formed organic radical can then couple with another equivalent of lithium metal to

provide the desired organolithium species [Scheme 8.1, Pathway A(I)]. However, the tuning of reaction conditions such as temperature and solvent choice may be required to prevent the decomposition of the radical species prior to the formation of the lithiated compound [Scheme 8.1, Pathway A(II)], or indeed the decomposition of the organolithium once formed. Perhaps the more problematic side reaction however is the so called Wurtz coupling; the reaction of the organolithium species with unreacted organohalide to give the organo-coupling product and salt LiX [Scheme 8.1, Pathway B]. This degradation route can be limited by ensuring that the halide species is efficiently consumed through the desired formation of the organolithium species [Scheme 8.1, Pathway A(I)], thus eliminating as much as possible the length of time LiR remains in contact with RX. Formation of LiR is rate limited by the ease of formation of the initial organo-radical species and as such reductive lithiation is most applicable to the formation of organolithiums with the most stable conjugate radicals, primarily alkyl or benzyl compounds.^[3b] Utilization of soluble molecular radical lithium reducing agents such as lithium naphthalenide or 4,4'-bis(tert-butyl)biphenyl lithium in place of lithium metal is an effective technique favouring formation of the desired lithiated species.^[4] Indeed, it has been shown that even the addition of a catalytic quantity of the appropriate arene in the presence of lithium metal can help mediate the process.^[5]



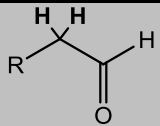
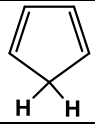
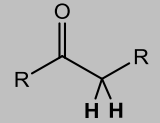
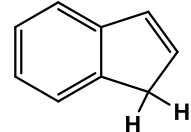
Scheme 8.1: Synthesis of an organolithium through the reductive lithiation of an organohalide [Pathway A(I)] and potentially problematic side reactions.

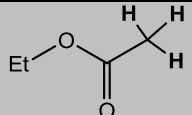
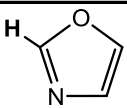
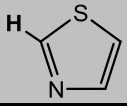
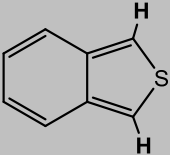
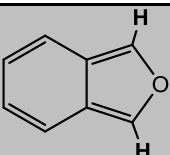
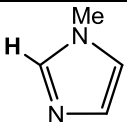
8.1.2 Deprotonative metallation

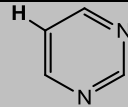
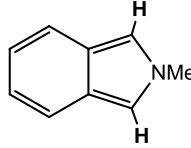
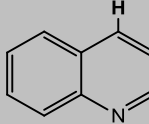
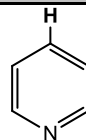
Reductive lithiation is a highly effective method for the synthesis of simple organolithiums such as the near ubiquitous, commercially available reagents *n*BuLi, *s*BuLi and *t*BuLi. These reagents can then be utilized in the synthesis of aryl, vinyl or functionalized organolithium species, the synthesis of which by direct reductive lithiation is problematic, through a sacrificial proton lithium exchange reaction. In principle, a proton should be removed from a substrate by the conjugate base of any substance with a greater pK_a than its own. In practice the structure of the organolithium species also plays an important role in determining the feasibility of any such reaction, particularly the aggregation state. The situation is further complicated by the difficulties extrapolating reliable pK_a data for weak carbon acids as well as the dependence of such data on the solvent it was determined in.^[6] Despite these limitations however, pK_a data are still instructive when designing new deprotonation reactions and a representative set of examples is presented in table 7.1. It should also be noted that such reactions represent equilibria with the notable exception of when one of the organic acids can be released as a gas such as butane. This evolution drives the numerous deprotonation reactions carried out by butyllithium reagents.

The pK_a of any substance is intuitively inversely proportional to the stability of its conjugate base. Several different factors can combine to contribute to this stability.^[7] Any effect that helps to dissipate the anionic charge throughout the substrate reduces the reactivity of the conjugate base, and hence decreases the pK_a of the acid. Electron withdrawing groups can stabilize an adjacent carbanion in this way through an inductive effect (compare entries 3 and 12 or 5 with 9). The delocalization of charge through resonance also has a similar effect (compare entries 12, 14, and 23 or 5, 7, and 29). The achievement of aromaticity is a particularly effective example of this form of stabilization (compare entries 2 and 6 with 25). Finally, s orbitals are fundamentally of lower energy than p orbitals, thus the greater the s character of a carbanion, the lower its overall energy. Hence acetylenes are stronger acids than alkenes which are themselves stronger acids than alkanes (compare entries 8, 27, and 29).

Table 8.1: pK_a data for various organic substrates. Acidic protons in bold.

Entry	Compound	Approximate pK _a (relative to water)
1		16 ^[8]
2		16 ^[8]
3	(C₆F₅)₃CH	16 ^[8]
4	R₃COH	17 ^[8]
5		19-20 ^[8]
6		20 ^[8]
7	RCH₂CN	25 ^[8]
8	HC≡CH	25 ^[8]

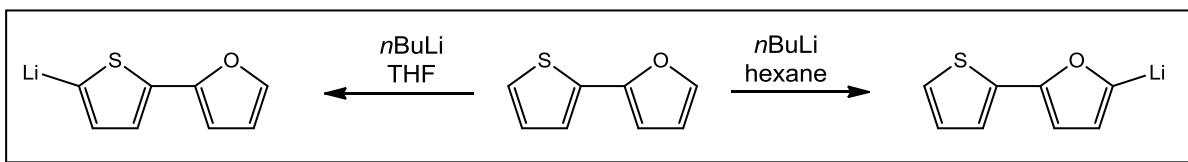
9		25.6 ^[8]
10		27.1 ^[9]
11		29.5 ^[9]
12	Ar₃CH	31.5 ^[8]
13		31.8 ^[9]
14	Ar₂CH₂	33.5 ^[8]
15		33 ^[9]
16	C₄H₄S	33.5 ^[9]
17	C₄H₄O	35 ^[9]
18		35.1 ^[9]

19		36.9 ^[9]
20		37.7 ^[9]
21		39.2 ^[9]
22	C₄H₄NMe	39.6 ^[9]
23	ArCH₃	40 ^[8]
24		40.3 ^[9]
25	CH₂=CHCH₃	43 ^[8]
26	PhH	43 ^[8]
27	H₂C=CH₂	44 ^[8]
28	CH₄	48 ^[8]
29	C₂H₆	50 ^[8]
30	Me₃CH	53 ^[8]

When discussing the acidity of heterocycles it is appropriate to consider five and six membered rings separately. With five membered heterocycles, it can be seen that the electron withdrawing heteroatom increases the acidity of adjacent protons relative to benzene through an inductive effect (compare entries 16, 17, and 18 with 26). Also, due to its greater electronegativity, oxygen has a greater inductive effect than nitrogen (compare entries 15 and 20 as well as 17 and 22). Comparison between oxygen and sulphur is more complex, presumably due to a combination of two conflicting effects. Oxygen is more electronegative than sulphur and as such is expected to have a greater inductive effect. However, sulphur has a larger atomic radius than oxygen and as such destabilizing repulsive interactions between its lone pairs of electrons and any newly formed carbanion are minimized. This dichotomy may explain the apparently contradictory results of more acidic oxygen cycles when comparing entry 10 with 11, yet a greater acidifying effect of sulphur when comparing entries 13 and 16 with 15 and 17. It may also be noted that an increase in number of heteroatoms in a ring generally leads to a decrease in pK_a (compare entries 10, 11, and 18 with 16, 17, and 22) and also that a greater resonance stabilization generally results in lower pK_a 's in benzo-coupled heterocycles (compare entries 13, 15, and 20 with 16, 17, and 20). In comparison with five member heterocycles, the hydrogens of 6 membered rings generally have higher pK_a 's (compare entries 18 with 19 and 22 with 24). The position of the most acidic proton also changes away from the nitrogen atom. This fundamental change is the result of repulsive interactions between the lone pair on the nitrogen of the six membered heterocycle and the negative charge associated with the new conjugate base. This is in contrast to a five membered heterocycle, where the heteroatom must sacrifice its lone pair to complete an aromatic sextet of electrons within the ring. Otherwise six membered heterocycles behave in the same manner as their five membered counterparts; that is, an increase in acidity with increasing numbers of heteroatoms (compare entry 18 with 24) and with increasing conjugation (compare entry 21 with 24).

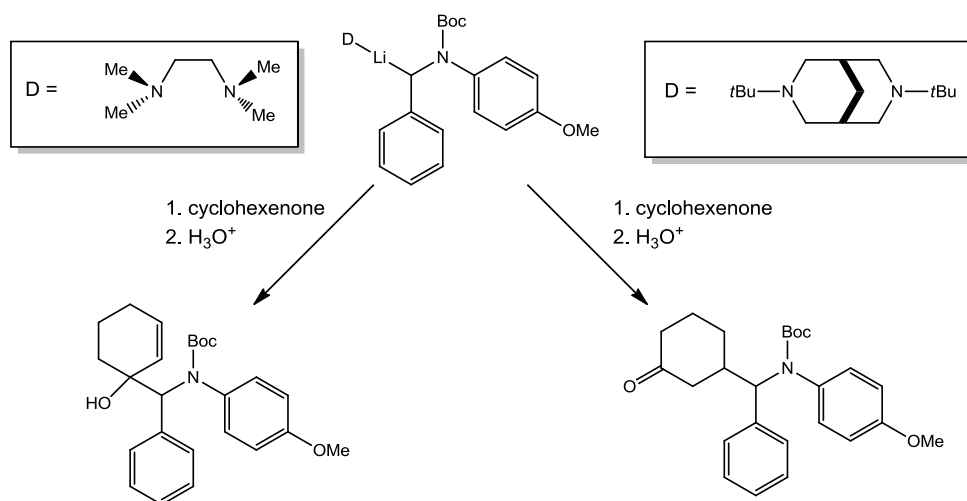
However, the relative acidities of the hydrogens within a substrate is not the sole factor in determining the selectivity of a lithiation reaction. Precomplexation of the metallating agent by the substrate can result in the reactive species being held captive by an

appropriate “directing group”, coerced into reacting with an adjacent proton source and denied the opportunity to exchange with potentially lower pK_a substituents. However, diligent choice of reaction media and co-solvent has the potential to liberate the base from the controlling grasp of a directing group and instead relinquish control to the researcher. Taken together these concepts have been termed a “Complex Induced Proximity Effect” (CIPE).^[10] An excellent illustrative example of how manipulating a CIPE can permit a greater level of control over a reaction is in the lithiation of the bis-aryl (C_4H_3S)(C_4H_3O) with $nBuLi$.^[11] When the reaction is carried out in hexane solution the furan moiety captures the lithiating agent and dictates that metallation occurs at its α -site. Alternatively, if the reaction is carried out in THF solution, the strongly electron donating solvent apparently frees the base from the directing influence of the furan solvation and the base switches its deprotonation advances towards the more acidic α proton on the thiophene ring (Scheme 8.2).



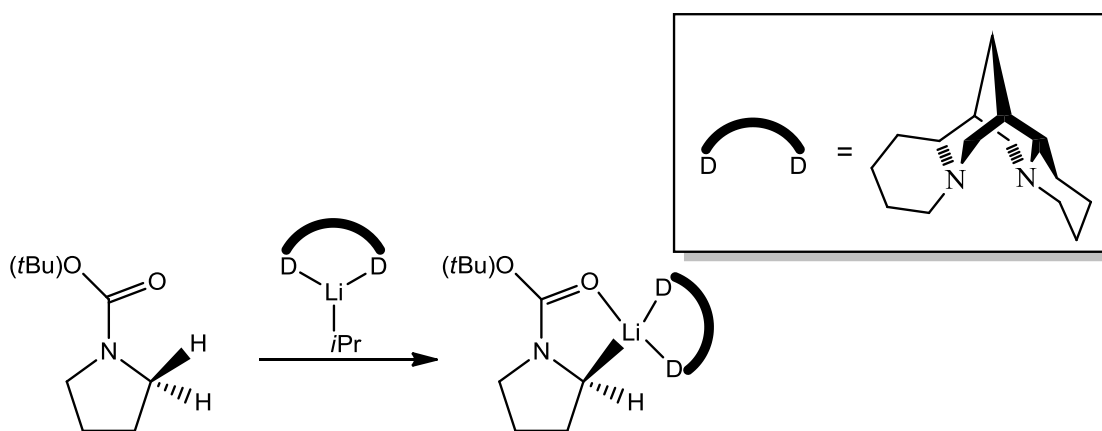
Scheme 8.2: Lithiation of (C_4H_3S)(C_4H_3O). An example of regioselectivity dependent on solvent choice.

CIPE's have also been inferred to direct the quenching of organolithium species with electrophiles. For example the product formed on quenching $PhCH(Li)N(Boc)(p-CH_3OC_6H_4)$ with cyclohexenone can be altered depending on the choice of co-solvent.^[12] If TMEDA (N,N,N',N' -tetramethylethylenediamine) is chosen then coordination of the lithium to the ketone functionality results in the 1,2-addition product. However, if the sterically restrictive diamine dibutyl bispidine is enrolled, the lithium species can be shielded from the coordination effect of the ketone and instead a 1,4 adduct is the result (Scheme 8.3).



Scheme 8.3: Contrasting quenching products of the lithium species $\text{PhCH}(\text{Li})\text{N}(\text{Boc})(p\text{-CH}_3\text{OC}_6\text{H}_4)$ depending on the donor ligand used, suggestive of a CIPE post metallation.

Utilizing CIPE's, metallating agents can be empowered into abstracting protons with ordinarily stubbornly oppressive $\text{p}K_{\text{a}}$ values. The α protons of a pyrrolidine ring are typically resistant to attack by lithium reagents on a synthetically relevant timescale. If a suitable anchoring site is provided though, such as a Boc protecting group [Boc = $\text{COO}(t\text{Bu})$], then pre-coordination can significantly improve the reaction rate. This has been exploited to great effect in the preparation of enantioenriched organolithium compounds using the chiral (-) sparteine adduct $(\text{C}_{15}\text{H}_{26}\text{N}_2)\text{Li}(i\text{Pr})$ (Scheme 8.4).^[13]



Scheme 8.4: Enantioselective lithiation of the relatively non-acidic α -hydrogen of N-Boc pyrrolidine utilizing the chiral diamine (-) sparteine.

These concepts have perhaps been most extensively studied in the deprotonative metallation reactions of substituted arenes. An extensive library of functional groups has been investigated to determine their ability to direct metallation to an ortho site, now commonly referred to as Directed *ortho* Metallation (DoM).^[10, 14] A representative list is provided in Figure 8.1.^[10] Again, the directing group's efficiency is based on a combination of its ability to complex with the incoming base and on the strength of its inductive effect on the substrate.

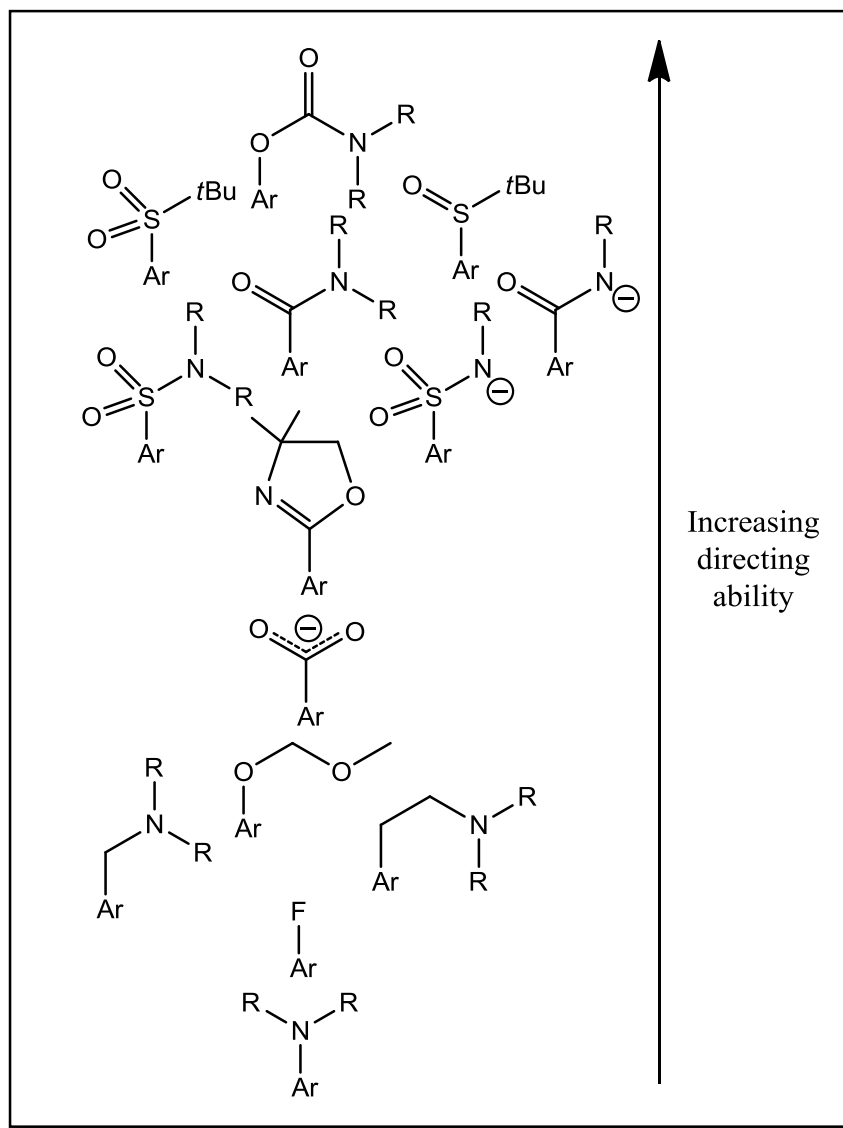
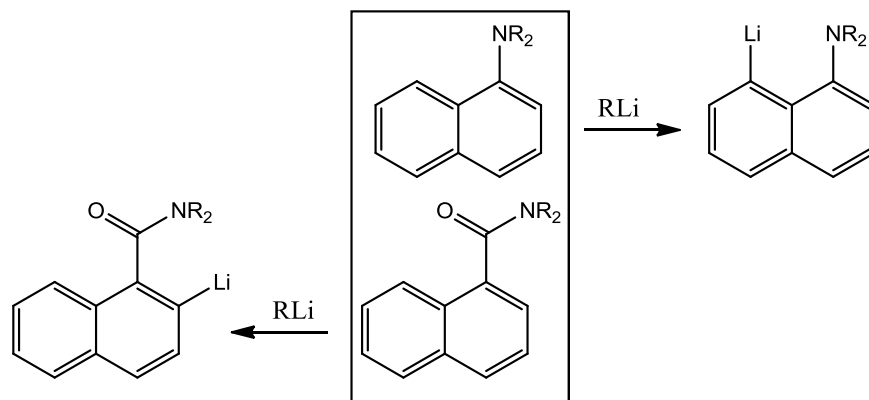


Figure 8.1: Relative directing ability of selected commonly utilized DoM functional groups.

A long established method for decoupling the inductive and coordination effects of a directing group is to monitor the metallation patterns of 1-substituted naphthalene

derivatives. Amine directing groups lead to *peri* metallation indicating induction has little to do with the action of such substituents. By comparison, amido groups were found to generate almost exclusively *ortho* metallated species suggesting a strong inductive effect (Scheme 8.5).^[15]



Scheme 8.5: Comparison of the inductive effect of different directing groups through the monitoring of *ortho/peri* metallation patterns of various 1-substituted naphthalenes.

Such decoupling of coordination and inductive effects can lead to an increased level of control of the selectivity of a reaction through an appropriate choice of metallating agent. The lithiation of 4-methoxy-N,N-dimethylaniline by BuLi leads to metallation *ortho* to the amino group. However, if the BuLi is first complexed with the diamine TMEDA, the resulting base [(TMEDA)Li(*n*Bu)]₂ has a less electropositive, less Lewis acidic metal centre which is thus less susceptible to coordination. This leads to preferential metallation adjacent to the more inductively electron withdrawing methoxy group (Figure 8.2). Similar results were obtained on metallation of 1-(4-methoxyphenyl)-N,N-dimethylmethanamine (Figure 8.2).

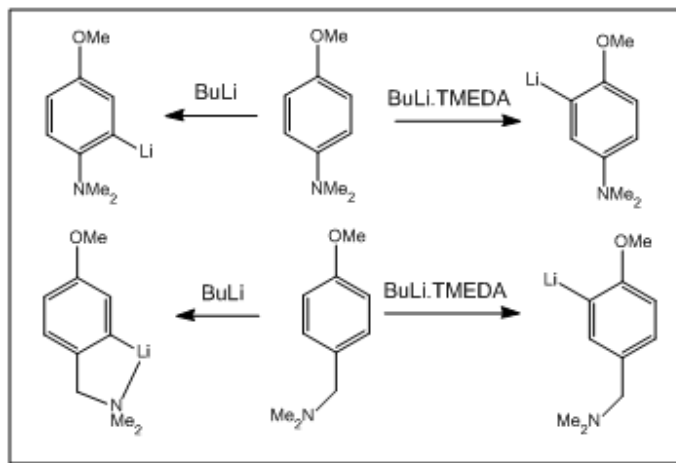


Figure 8.2: Example of varying the selectivity of a directed ortho metallation by addition of the diamine TMEDA.

8.1.3 Lithium–halogen exchange

Direct metal–hydrogen exchange is the protocol of choice when conditions can be found to produce a clean, efficient transformation. However, more complex systems may contain several potential metallating sites that no reaction conditions can suitably differentiate. Also, it is often desirable to metallate in a position contrary to the common deprotonation sites. In such cases it is often preferable to carry out metal–halogen exchange. The conversion of a carbon–bromine or carbon–iodine bond to carbon–lithium is orders of magnitude faster than the equivalent exchange of a hydrogen.^[3] As such, it is a facile process to develop metal–halogen exchange reactions that occur chemo-selectively, even in the presence of relatively strong carbon acids.^[8, 14] The carbon–chlorine bond is much less suitable for metal–halogen exchange, although there are precedents,^[16] while the carbon–fluorine bond is essentially inert to such transformations.^[3] This step-change in reactivity of the carbon–halide bond (I > Br > Cl >> F) also allows for sequential metallation and quenching protocols through halide discrimination. Furthermore, because the reactive lithiating agent can be consumed rapidly, even at low temperature, metal–halogen exchange reactions can be achieved in

the presence of reactive substituents that could not tolerate the conditions required to achieve the equivalent direct proton abstraction.

It has been postulated that metal–halogen exchange reactions take place via a hypervalent iodide species.^[3a, 17] While it is impossible to prove any reaction mechanism, it has been conclusively demonstrated, through kinetic and spectroscopic measurements, that the reaction conditions under which metal–halogen exchange reactions are typically performed also lead to the formation of hypervalent species.^[17a, 18] Indeed, the reaction of pentafluorophenyl lithium with pentafluorophenyl iodide at -78°C followed by the addition of the diamine TMEDA allowed for the isolation and crystallographic characterization of the hypervalent species $[(\text{TMEDA})_2\text{Li}][(\text{C}_6\text{F}_5)_2\text{I}]$.^[19] Hypervalent iodide species have attracted much attention in organic synthesis, not least because they are capable of facilitating coupling reactions without the need for costly transition metal catalysts.^[20] It may therefore be inferred that Wurtz type coupling, discussed previously (Scheme 8.1), can be explained through a hypervalent iodide intermediate.

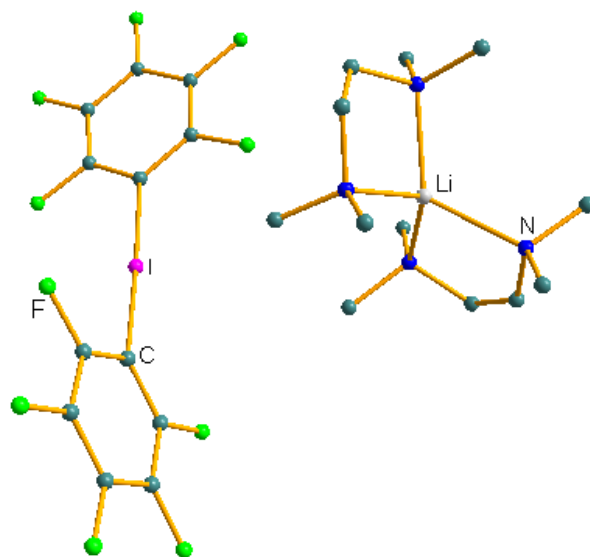
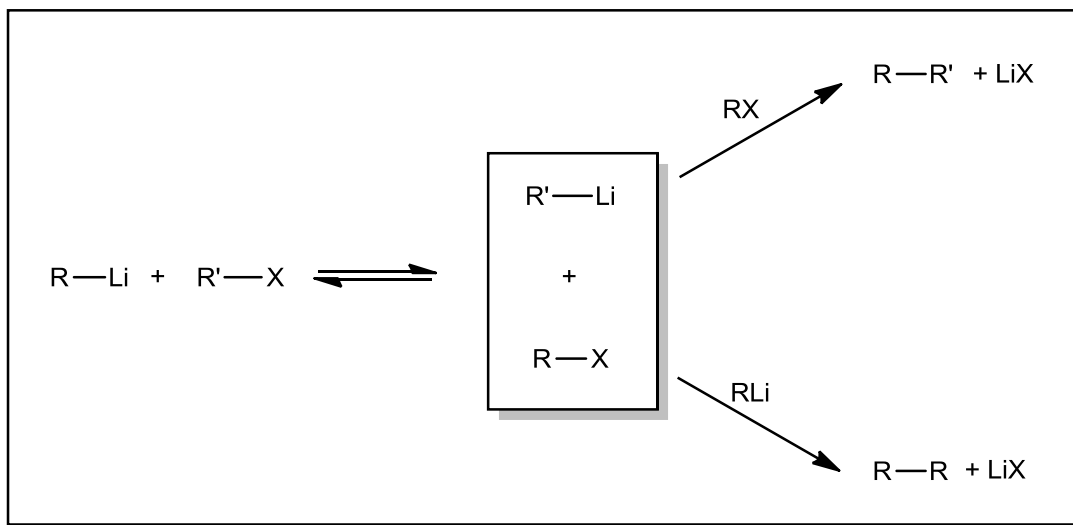


Figure 8.3: Molecular structure of the hypervalent $[(\text{TMEDA})_2\text{Li}][(\text{C}_6\text{F}_5)_2\text{I}]$.

Wurtz coupling reactions can be highly problematic in metal–halogen exchange reactions because it provides a pathway for the alkyl halide by-product to destroy the desired organolithium species. This difficulty can be overcome by applying a second, sacrificial

equivalent of base that can consume the alkyl halide to produce LiX (Scheme 8.6). This process also drives the equilibrium to completion.^[3]



Scheme 8.6: Equilibrium of a general lithium-halogen exchange reaction and demonstration of how a second equivalent of base can protect the desired organolithium species.

8.2 Mixed Metal Organometallics

Although alkali metal reagents are widely used throughout synthetic chemistry their highly reactive nature does lead to some drawbacks. Most notably, sensitive functionals, such as amides, esters, ketones or nitriles, can be liable to participate in undesirable side reactions with the base. As a result of this high reactivity it is often necessary and common practice to carry out reactions at low temperature. This is particularly important when scaling up a reaction for industrial processes as cryogenic cooling can be prohibitively expensive. For these reasons there is considerable interest in developing metallating agents with an attenuated reactivity relative to group I organometallics.

One method for the design of reagents with a more controlled reactivity is to switch to a metal that exhibits less ionic organometallic bonding. Applying Pauling's mathematical description of a chemical bond,^[21] Schlosser has estimated the relative ionic character of

organometallic bonding for various metals (Table 8.2).^[3a] This highly crude yet informative approach reveals that variation of the metal employed should provide access to an entire graduation of reactivity profiles.

Table 8.2: Approximate guide to the ionic nature of different carbon–metal bonds.

Bond	Relative ionic nature
C – Cs	90 %
C – K	80 %
C – Na	60 %
C – Li	40 %
C – Mg	20 %
C – Zn	10 %
C – Hg	5 %
C – H	0 %

While homometallic complexes of less polarised organometallics, most notably organomagnesium reagents, are undoubtedly highly important in synthetic chemistry, producing organometallic intermediates with a far greater stability than that observed for their alkali metal counter parts, and in the presence of sensitive functional groups at elevated temperatures, they also have severe limitations. Perhaps most critically, they are only capable of metallating relatively strong carbon acids (having low pK_a values) with powerful directing groups. The controlled metallation of poorly or non-activated carbon acids in the presence of sensitive functionals and/or at elevated temperatures remains a challenging task for the synthetic chemist. An approach to limiting the disruptive reactivity of the alkali metal reagents while at the same time maintaining a high level of Brønsted basicity is to produce a mixed metal species. The partnering of an alkali metal with a less polar metal, such as magnesium, zinc or aluminium, has not only led to the achievement of this lofty goal in many instances, but the unique chemistry of these

“synergic” bimetallic mixtures have often brought about transformations inaccessible to their homometallic constituents.

8.2.1 Mechanistic Insight

While mixed metal systems of a diverse mixture of ligands and metals have been prepared and applied in the field of deprotonative metallation,^[22] the heteroleptic lithium or sodium alkyl amido zincates are perhaps the best understood. Kondo and Uchiyama originally prepared the lithium zincate base “Li(TMP)Zn(*t*Bu)₂” (TMP = 2,2,6,6-tetramethylpiperidine) *in situ* from the reaction of ZnCl₂ with two molar equivalents of *t*BuLi in bulk THF solution followed by the addition of a pre-prepared THF solution of LiTMP.^[23] Mulvey succeeded in the isolation and crystallographic identification of the lithium zincate (THF)Li(TMP)Zn(*t*Bu)₂ **1** (Figure 8.4) through the co-complexation of LiTMP with *t*Bu₂Zn (purified through sublimation therefore avoiding LiCl incorporation) in hexane solution with one molar equivalent of the Lewis basic THF.^[24] The sodium analogue (TMEDA)Na(TMP)Zn(*t*Bu)₂ **2** (Figure 8.5) was similarly prepared from the mixture of NaTMP, *t*Bu₂Zn and the diamine TMEDA.^[25] Both reagents adopt a similar structural motif. The alkali metal and zinc centres are bridged by the TMP anion while a *t*Bu ligand on the zinc completes a central five membered AM–N–Zn–C–C ring through a weak electrostatic interaction between a β carbon atom and the alkali metal. The trigonal planar zinc is completed by a terminal *t*Bu ligand while the coordination of the lithium and sodium cations are satisfied by the neutral donor ligands THF and TMEDA respectively. Both TMP anions are in the thermodynamically preferred chair conformation, although the chair “overhangs” the zinc in the lithium derivative but the alkali metal in the sodium species.

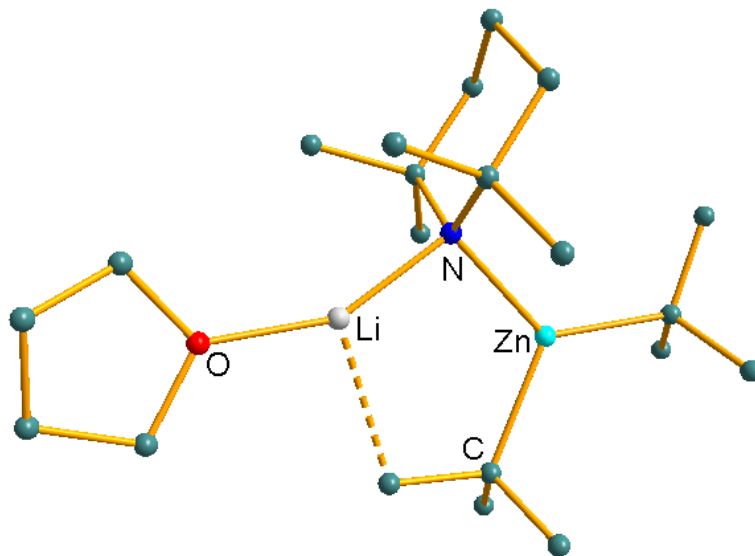


Figure 8.4: Molecular structure of the alkyl amido lithium zincate (THF)Li(TMP)Zn(*t*Bu)₂ **1**.

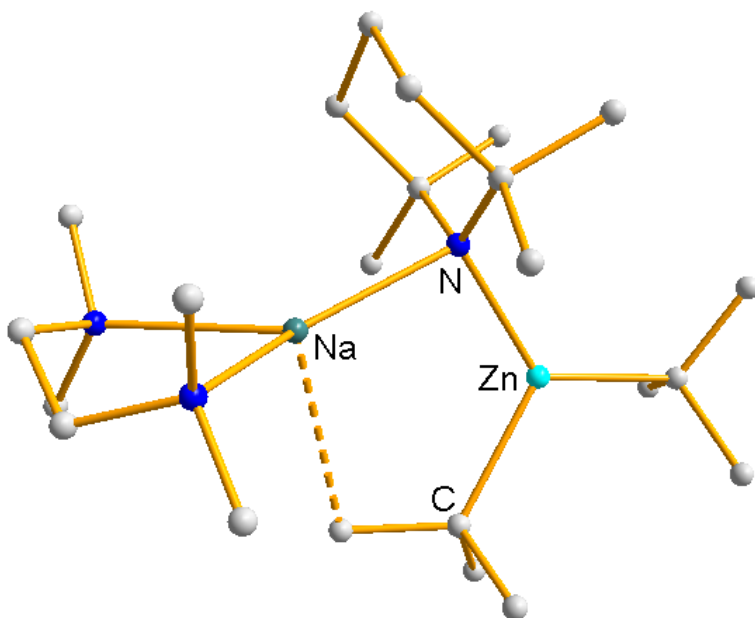


Figure 8.5: Molecular structure of the prolific alkyl amido sodium zincate (TMEDA)Na(TMP)Zn(*t*Bu)₂ **2**.

A detailed mechanistic understanding of the mode of action of these two reagents has now been developed through an accumulation of both experimental and theoretical evidence. The structural elucidation of many metallated intermediates produced by the reaction of the lithium zincate **1** and various substrates including anisole,^[26] trimethylphenoxy silane^[27] and *N,N*-diisopropylbenzamide,^[28] as well as various zincated

structures of many substrates such as *N,N*-dimethylaniline^[29], anisole^[30], *N,N*-diisopropylbenzamide^[24, 28] and toluene^[31] when the sodium zincate is employed has now been achieved. In all cases where it has been possible to confirm the nature of the metallated species, the appropriate C–H bond has been replaced with a strong Zn–C σ -bond. This marks these reactions as direct zincations. The zincated species largely adopt the same general motif. In common with the starting bases, the metallated intermediates have a backbone consisting of an AM–TMP–Zn–*t*Bu chain (AM = Alkali Metal). The metallated substrate then bridges to the zinc, through a strong σ -bond, and to the alkali metal, either through the donor site of a functional group or, in the absence of a strong Lewis basic arm, via a π -interaction with an aromatic ring. Even in the presence of strongly donating functional groups the alkali metal often maintains a direct interaction with the aromatic ring. THF or TMEDA donor ligands complete the coordination sphere of the alkali metal. This loose set of structural characteristics shall from here on be referred to as the bi-axial motif. The metallation of anisole by the lithium zincate^[32] and the mono deprotonation of benzene^[25] and *ortho* zincation of *N,N*-diethylbenzamide^[33] by the sodium zincate exemplify these common characteristics of the vast majority of the structurally characterised zincated intermediates while demonstrating that the π -interaction with the aromatic ring becomes less prominent in the company of more powerful donating groups.

The structural determination of many substrates with these mixed metal bases have repeatedly established that such reagents exhibit overall alkyl basicity. Uchiyama *et al* performed a theoretical study modelling the reactivity of the hypothetical (TMEDA)Li(NMe₂)ZnMe₂ **3** with benzene and proposed the mechanism shown in Scheme 8.7.^[34] It was argued that, although there was a thermodynamic preference to lose the alkyl group, it was the amido group that was lost first in a kinetically driven process. The relative strength of the Zn–C bond over the Zn–N bond provided a theoretical activation energy difference of 20.5 Kcal mol⁻¹ (45.6 Kcal mol⁻¹ versus 25.1 Kcal mol⁻¹).

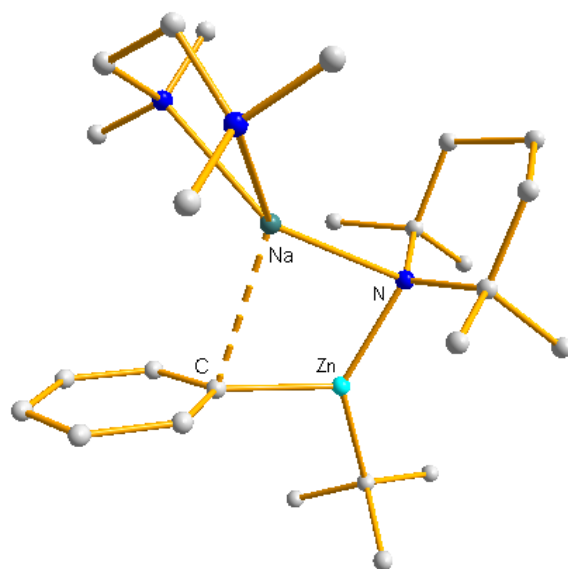


Figure 8.6: Molecular structure of the product of benzene zincation by sodium zincate 2 showing C–Zn σ and C–Na π interactions.

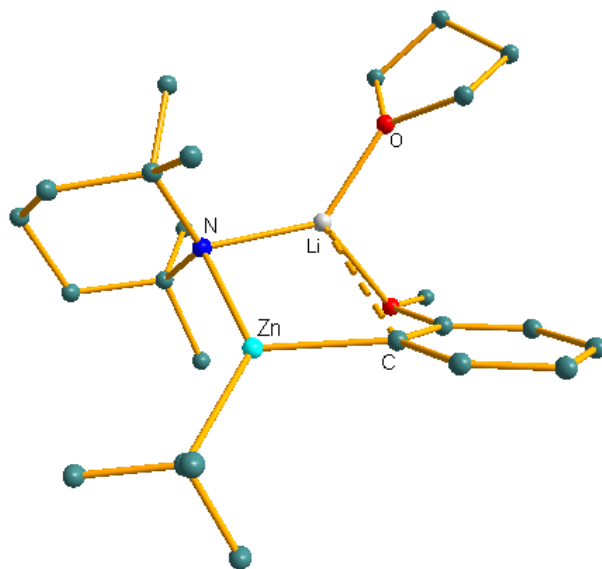


Figure 8.7: Molecular structure of anisole zincated by lithium zincate 1 showing the π -aryl and methoxy coordination to the alkali metal. Hydrogen atoms have been omitted for clarity.

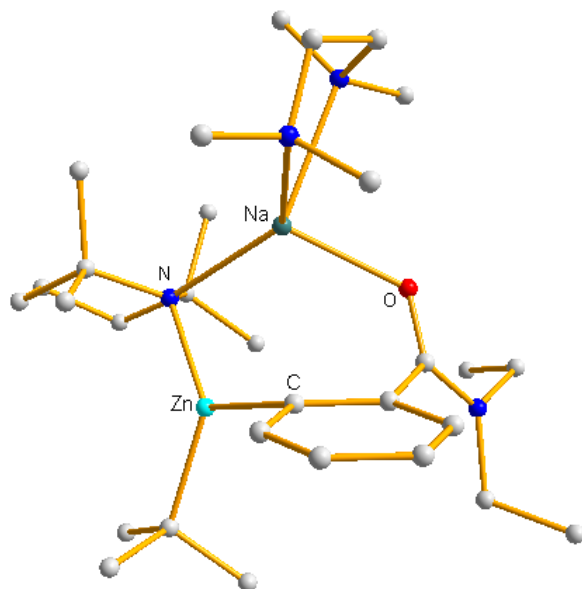
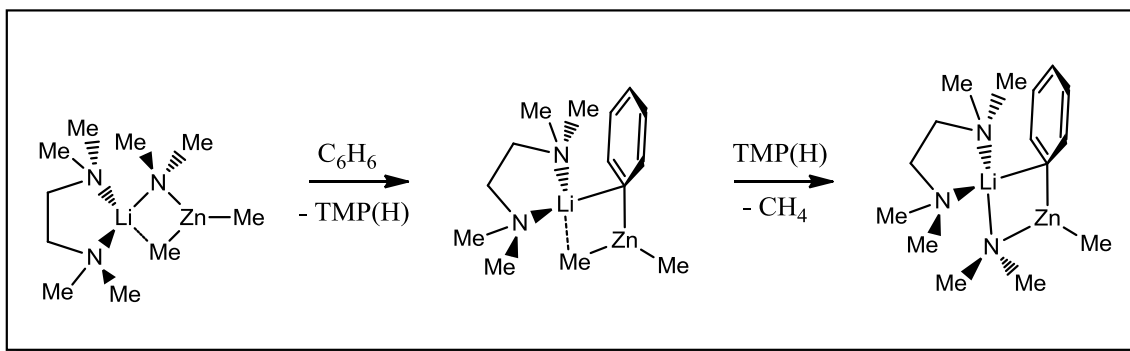


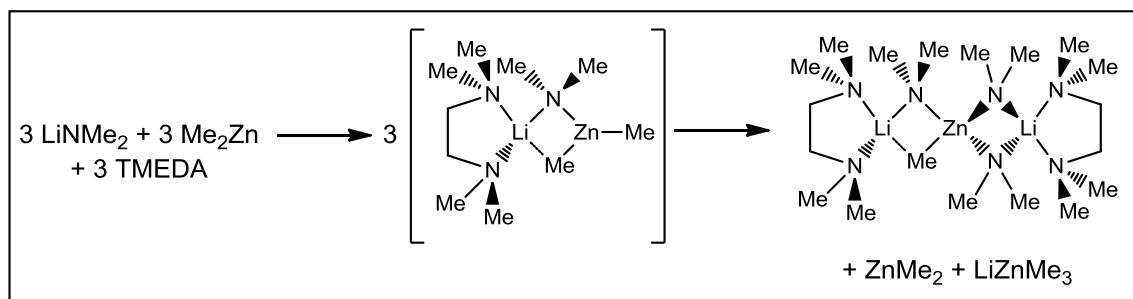
Figure 8.8: Molecular structure of *N, N* - diethylbenzamide *ortho* deprotonated by the sodium zincate base **2** where the sodium bonds predominantly to the directing group.



Scheme 8.7: Depiction of the two step deprotonation of benzene by the hypothetical dimethylamido methyl zincate **3** as predicted computationally by Uchiyama.

These predictions were made without the aid of any substantial direct experimental evidence. Furthermore, the recent attempted synthesis of the dimethylamido zincate **3** has highlighted the caution that should be applied when modelling organometallics which have yet to be structurally determined.^[35] In fact, the target zincate apparently rapidly disproportionates to furnish the unsymmetrical tetraorganozincate (TMEDA)Li(NMe₂)₂Zn(NMe₂)(Me)Li(TMEDA) (Scheme 8.8).^[35] This is supported by

NMR spectroscopic data, with the identification of Me_2Zn and LiZnMe_3 in the mother liquors. Furthermore, as opposed to acting as an amido base, the disproportionation product was found to be completely inert towards anisole, *N,N*-diisopropylbenzamide and benzonitrile.^[35]

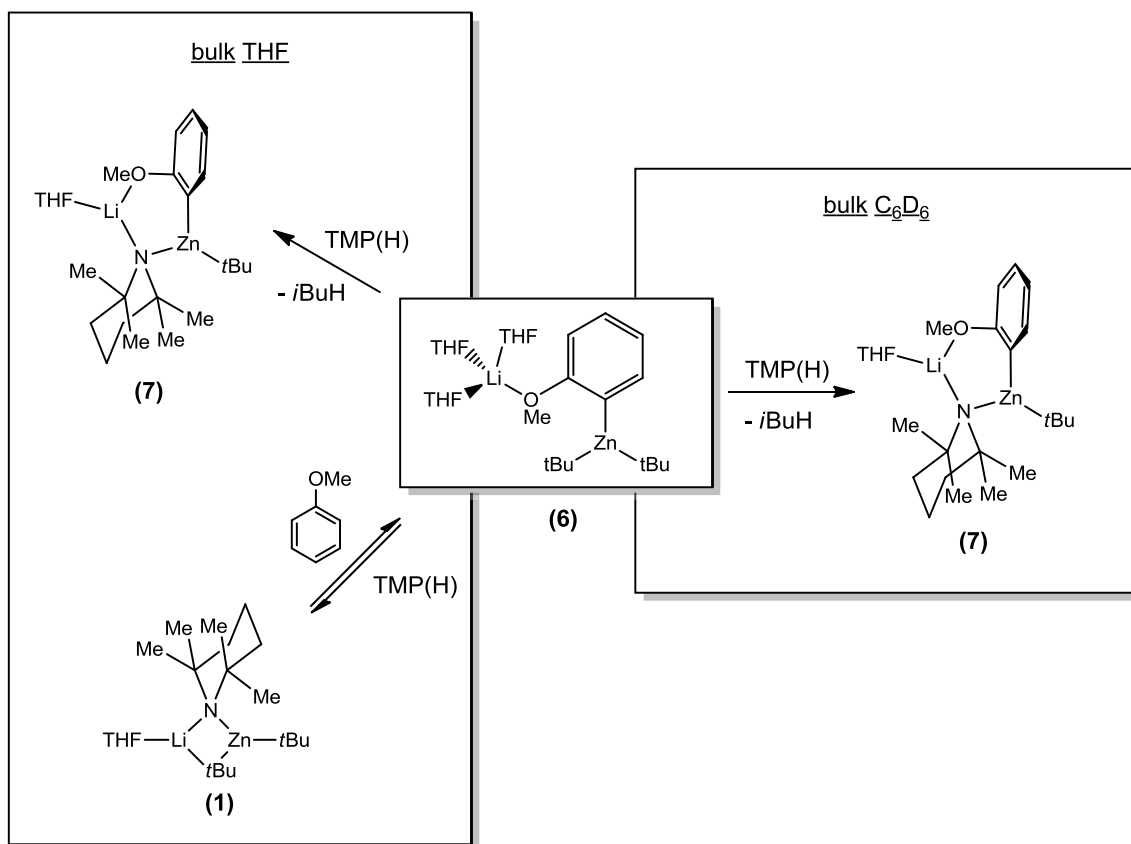


Scheme 8.8: Attempted synthesis of the postulated dimethylamido zincate **3** revealed that the sterically generous dimethyl amide instead facilitates the formation of the tetra coordinated zincate $(\text{TMEDA})\text{Li}(\text{NMe}_2)_2\text{Zn}(\text{NMe}_2)(\text{Me})\text{Li}(\text{TMEDA})$.

Despite this however the theoretical preference to act as a kinetic amido base should not be ignored. To the contrary, some compelling experimental evidence now seems to confirm the two-step reaction pathway proposed with stronger bases by Uchiyama. The reactions of $(\text{THF})\text{Li}(\text{TMP})\text{ZnMe}_2$ **4** and $(\text{THF})\text{Li}(\text{TMP})\text{Zn}(t\text{Bu})_2$ **1** with anisole were studied by Hevia *et al.*^[36] If these reagents were to act as amido bases then the intermediates $(\text{THF})_2\text{Li}(2\text{-C}_6\text{H}_4\text{OMe})\text{ZnMe}_2$ **5** and $(\text{THF})_3\text{Li}(2\text{-C}_6\text{H}_4\text{OMe})\text{Zn}(t\text{Bu})_2$ **6** would be expected to form. The postulated intermediates **5** and **6** were indirectly synthesised by the *ortho* lithiation of anisole followed by the co-complexation of the produced $(\text{THF})_2\text{Li}_4(2\text{-C}_6\text{H}_4\text{OMe})_4$ with Me_2Zn or $(t\text{Bu})_2\text{Zn}$ respectively. The reaction of **6** with $\text{TMP}(\text{H})$ proceeded as Uchiyama predicted to produce $(\text{THF})\text{Li}(\text{TMP})\text{Zn}(2\text{-C}_6\text{H}_4\text{OMe})^t\text{Bu}$ **7** (Figure 8.7) and butane when carried out in C_6D_6 solution as followed by NMR spectroscopic studies (Scheme 8.9).

The same reaction carried out in THF-D_8 solution surprisingly was in competition with the metallation of $\text{TMP}(\text{H})$, to regenerate the zincate base with concomitant elimination of free anisole (Scheme 8.9).^[36] This result, as well as demonstrating the importance of

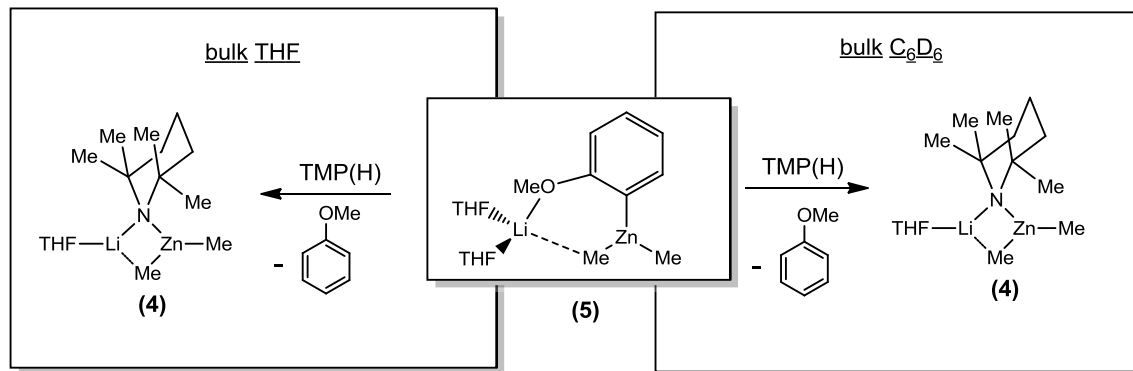
solvent effects on zincate reactivity, produced an ideal opportunity to emphasize the likelihood that the reaction of **1** with anisole does indeed pass through the intermediate **6**. The apparent increase in prevalence of the retro reaction when carried out in polar THF-D₈, relative to C₆D₆, could be expected to result in a reduced yield if the deprotonation is attempted in this Lewis basic media. Indeed, the reaction of alkyl amido zincate **1** with anisole in THF-D₈ for two hours at room temperature provided the *ortho* metallated product, the triplectic **7**, with a conversion of 62%. By comparison, the same reaction in the non-donating solvent hexane results in near complete conversion.



Scheme 8.9: Depiction of the contrasting fates of **6**, the postulated intermediate in the metallation of anisole by the lithium zincate base **1**, in both THF and C₆D₆ solution in the presence of TMP(H).

The reaction of the methyl derivative **5** with TMP(H) in both C₆D₆ and THF-D₈ solution exhibited complete discrimination for aryl over alkyl basicity to produce the methyl amido zincate **4** and free anisole (Scheme 8.10).^[36] This result emphasizes the importance

of the alkyl group to the reactivity of the base even if it is the amido ligand that initiates deprotonation. If the alkyl group is not more basic than the metallated substrate then the incoming TMP(H) will only serve to reproduce the starting materials in a retro reaction rather than the desired product.



Scheme 8.10: Methyl derivative 5 is incapable of retaining the metallated anisole in the presence of TMP(H) in either ethereal or arene media.

The first direct interception of intermediates of alkyl amido zincate deprotonations clearly displaying amido basicity were isolated from the reaction of the sodium zincate **2** with a series of nitrile compounds.^[37] The base was able to cleanly deprotonate both *meta*-tolunitrile and 1-cyanonaphthalene in the *ortho* position, with no discernable side reactions resulting from attack of the nitrile functionality. The intermediates detected adopt a different structural motif from the standard cycle of alkali metal π interactions and zinc sigma bonding described previously. Taking first the product of deprotonation of 1-cyanonaphthalene, (TMEDA)₂NaN≡CC₁₀H₆[Zn(*t*Bu)₂] **8** (Figure 8.9), the strongly Lewis basic cyano group succeeds in isolating the sodium ion from the carbanionic sites of the *t*Bu and naphthyl ligands. Similarly, in the zincation of *meta*-tolunitrile, in the product, [(TMEDA)₂Na{N≡CC₆H₃(Me)[Zn(*t*Bu)₂]}₂][(TMEDA)₂Na{N≡CC₆H₃(Me)}₂] **9** (Figure 8.10), the nitrile substituent succeeds in ensuring that the alkali metal is again remote from the potentially reactive anions. In this case two zincated nitrile moieties succeed in coordinating to a (TMEDA)₂Na ion in a trans fashion resulting in an overall anion. This is balanced by a (TMEDA)₂Na cation solvated by two neutral *meta*-tolunitrile ligands. It is not unusual for sodium tert-butyl zincates in the absence of a TMP or other

amido ligand to deviate from the strictly contact ion pair bi-axial motif. Both complexes $(\text{TMEDA})\text{Na}[\text{N}(\text{Me})_2\text{C}_6\text{H}_4]_2\text{Zn}(t\text{Bu})$ ^[38] and $(\text{TMEDA})_2\text{Na}(\text{CH}_2\text{C}_6\text{H}_5)\text{Zn}(t\text{Bu})_2$,^[31] synthesised through indirect transmetallation protocols, exhibit little evidence of any interaction between the *t*Bu ligands and sodium ions. It can be postulated, given the wealth of examples now elucidated,^[22a, 22c] that there is an inherent stability associated with the contact ion pair bi-axial motif and that the attainment of such a stable arrangement is, at least in part, responsible for the reactivity associated with deprotonations using such alkyl amido zincates. Extending this argument, it is conceivable that the putative TMP complexes $(\text{TMEDA})\text{Na}(\text{TMP})(\text{N}\equiv\text{CC}_{10}\text{H}_6)\text{Zn}(t\text{Bu})$ and $(\text{TMEDA})\text{Na}(\text{TMP})[\text{N}\equiv\text{CC}_6\text{H}_3(\text{Me})]\text{Zn}(t\text{Bu})$ do not form on reaction of **8** or **9** with TMP(H) respectively, because, even on incorporation of the potential bridging ligand TMP, the bi-axial motif remains inaccessible due to the stranglehold the strongly Lewis basic nitrile groups have on the alkali metal. In this way, both the success of the zincate reagents **1** and **2** in deprotonative metallation, and the overall amido basicity exhibited on deprotonation of 1-cyanonaphthalene and *meta*-tolunitrile can be explained. It also gives rise to the encouraging rationale for the drop off in efficiency observed when the metallation of anisole is attempted in bulk THF as opposed to the non-polar C₆D₆ (Scheme 8.9);^[36] that the strongly donating solvent can at least partially disrupt the construction of a stable bi-axial motif arrangement.

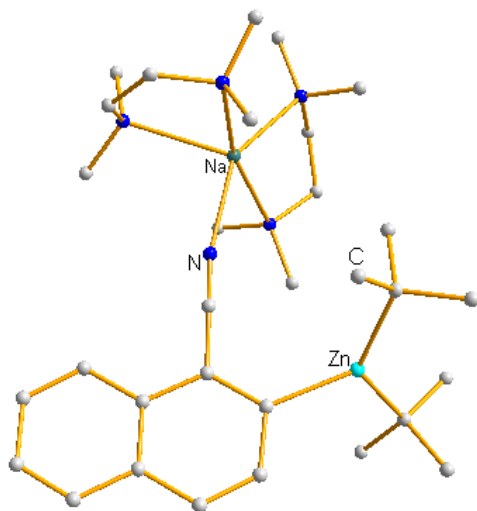


Figure 8.9: Molecular structure of the TMP free zincate $(\text{TMEDA})_2\text{NaN}\equiv\text{CC}_{10}\text{H}_6[\text{Zn}(t\text{Bu})_2]$ **8**, product of the reaction between the sodium zincate **2** and 1-cyanonaphthalene.

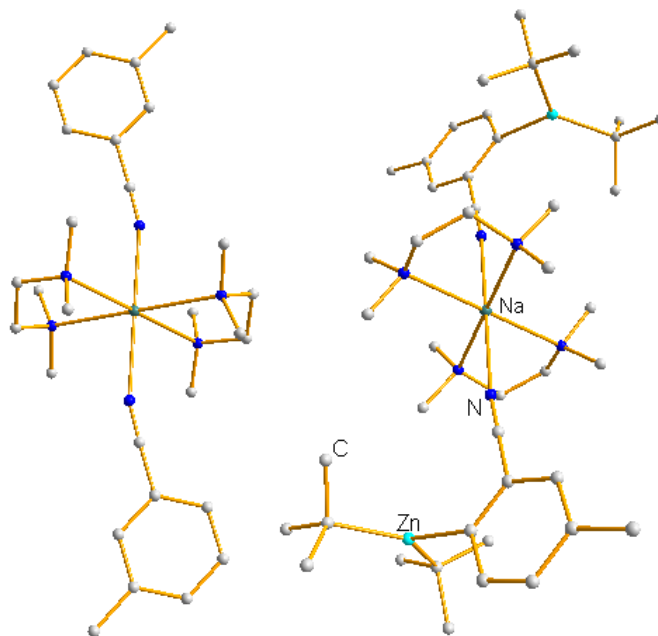
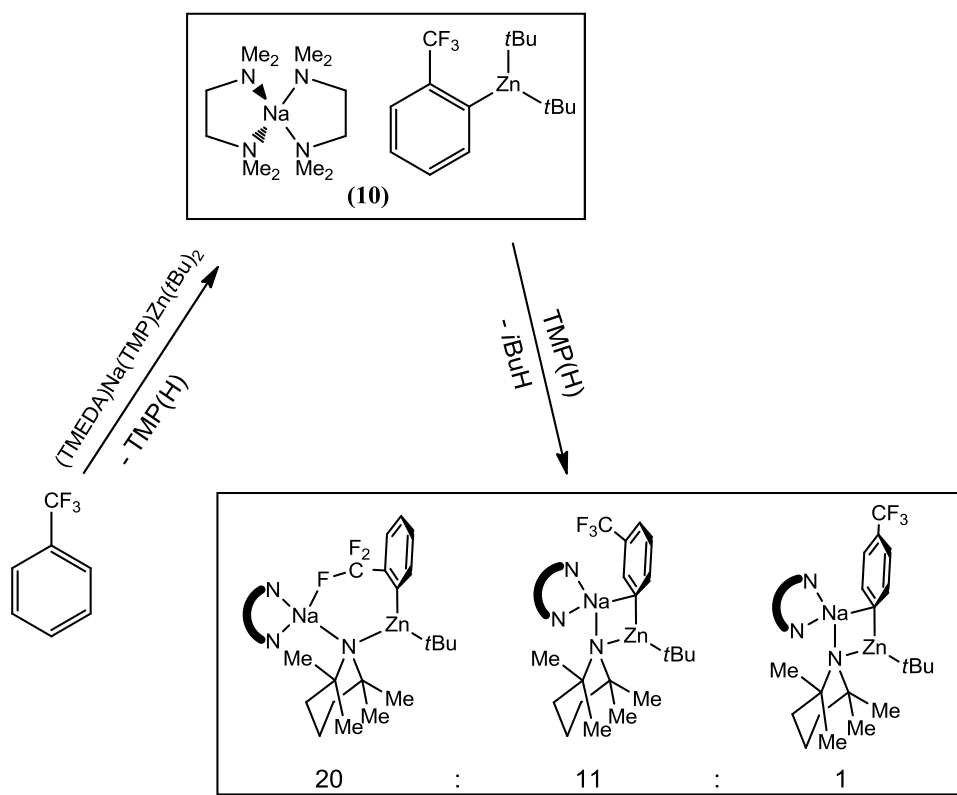


Figure 8.10: Molecular structure of the solvent separated zincate $[(\text{TMEDA})_2\text{Na}\{\text{N}\equiv\text{CC}_6\text{H}_3(\text{Me})\}_2]^+[(\text{TMEDA})_2\text{Na}\{\text{N}\equiv\text{CC}_6\text{H}_3(\text{Me})[\text{Zn}(\text{tBu})_2]\}_2]^-$ **9**. Cation LHS, anion RHS.

The metallation of trifluorotoluene by the sodium zincate **2** has further improved our understanding of the mechanics of such reactions through the isolation of several different intermediates along the reaction pathway.^[39] When the base is combined with trifluorotoluene at 0°C in hexane then the kinetic product $[(\text{TMEDA})_2\text{Na}][(\text{C}_6\text{H}_4\text{CF}_3)\text{Zn}(\text{tBu})_2]$ **10** can be isolated (Scheme 8.11). The base can therefore be confirmed to have exhibited amido basicity. Like the sodium tert-butyl zincates discussed previously, the tert-butyl ligands fail to bridge the two metal centres in **10**, resulting in a solvent separated structure. If the kinetic **10** is isolated and then treated with TMP(H) at room temperature, or the sodium zincate **2** is allowed to react with trifluorotoluene under ambient conditions, then a mixture of the *ortho*, *meta* and *para* isomers of $(\text{TMEDA})\text{Na}(\text{TMP})(\text{C}_6\text{H}_4\text{CF}_3)\text{Zn}(\text{tBu})$ is produced in a 20:11:1 ratio (Scheme 8.11). Crystalline samples of the *ortho* and *meta* isomers could be prepared and X-Ray diffraction analysis revealed that the reincorporation of the amido ligand has permitted the formation of bi-axial motifs in both instances. In the case of the *ortho* metallation the sodium ion is supported by a strong interaction with one of the fluorine atoms while in

the case of the meta deprotonation the alkali metal interacts with the trifluorotoluene solely through a π interaction with the carbanion. This result is important for two reasons. 1) It further supports the now well established argument that alkyl amido zincates act via a two-step mechanism, initially as an amido base but ultimately demonstrating overall alkyl basicity. 2) That it may only be with reincorporation of the amido ligand that access to the less acidic *meta* and *para* protons is permitted. Examining the structure of (TMEDA)Na(TMP)(*m*-C₆H₄CF₃)Zn(*t*Bu), it is highly tempting to attribute this selectivity to the stabilisation that the alkali metal enjoys through its π interaction with the aromatic ring, the interaction that it repeatedly neglects in the absence of its amido tether to the zinc. In short, the unique reactivities often displayed by alkyl amido zincates (to be discussed in section 8.2.2 Synergy in action: reactivity) can be attributed to the formation of stable bi-axial motif structures when deprotonating in positions where significant stabilisation is unavailable to the homo-metallic analogues.



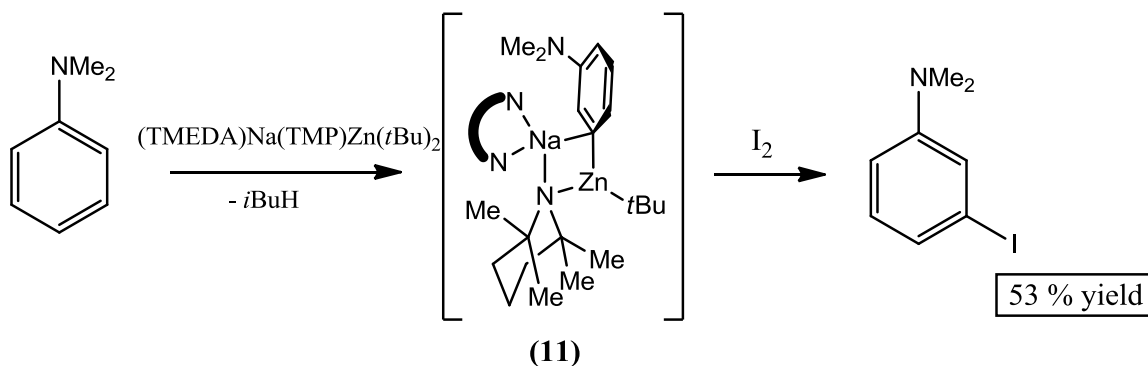
Scheme 8.11: Metallation of trifluorotoluene by the sodium zincate 2. The reaction has been shown to pass through an *ortho* metallated amido free zincate before the re-introduction of TMP(H) results in partial isomerisation of the product.

8.2.2 Synergy in action: reactivity exclusive to bimetallics

Mixed metal bases have proven to be adept at efficiently metallating a wide range of substrates, tolerating a range of sensitive functional groups and without the need for cryogenics.^[22] Most exciting of all though is that these bimetallic systems have repeatedly demonstrated an ability to perform transformations that are unavailable to their monometallic counterparts. In this sense it can be said that the different metal centres must successfully cooperate to achieve such unprecedented chemistry. Examples of where this synergic relationship has been exploited to deliver potential new frontiers for the creative synthetic chemist will now be discussed in greater detail.

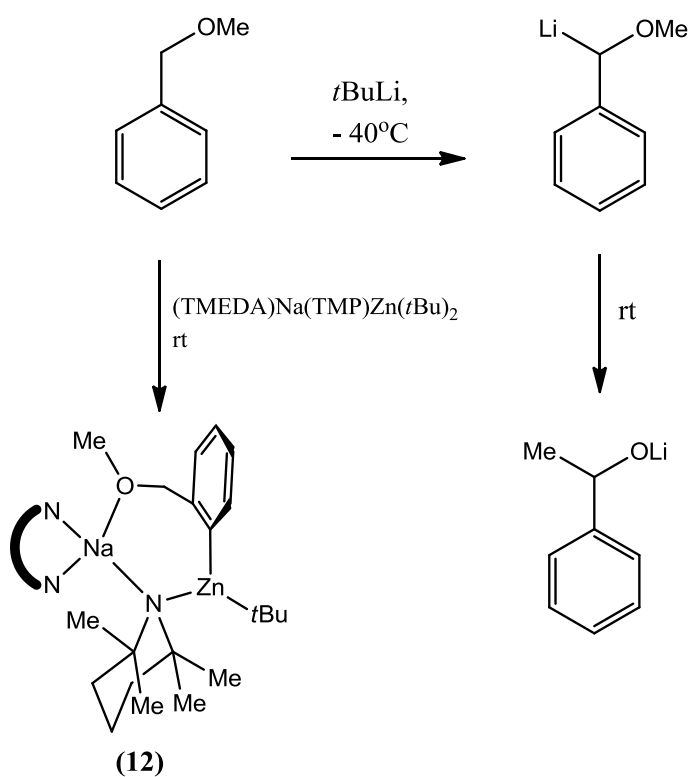
As has been discussed previously, directed *ortho* metallation has become one of the cornerstones of organic chemistry, allowing for the reliable synthesis of a wide variety of functionalised aromatics.^[14] The reaction of the sodium alkyl amido zincate **2** with *N,N*-dimethylaniline or *N,N*-dimethyl-3-methylaniline has given rise to the beginning of an alternative concept in synthetic chemistry, namely directed *meta* metallation.^[29] Refluxing either substrate with the zincate base **2** in hexane for two hours allowed for the isolation of crystalline (TMEDA)Na(TMP){Me₂N-3-[Zn(*t*Bu)]-C₆H_{4}} **11** and (TMEDA)Na(TMP){Me₂N-3-Me-5-[Zn(*t*Bu)]-C₆H_{4}} in a 39% and 43% yield respectively (Scheme 8.12). DFT calculations comparing the *meta* deprotonated dimethylaniline **11** with the postulated products upon metallation *ortho* and *para* to the dimethylamino directing group, as well as lateral metallation of the directing group itself, have confirmed that *meta* deprotonation is indeed the thermodynamic outcome when using this bimetallic protocol. The conventional *ortho* metallated product was found to be 4.53 kcal/mol higher in energy, presumably due to the steric interaction between the dimethylamino unit disrupting the construction of a stable bi-axial motif while simultaneously failing to provide enough stabilisation itself, owing to the weak Lewis basicity of the directing group. *Meta* deprotonation was also more favoured than *para* substitution by a miniscule 0.74 kcal/mol, in this case likely due to the inductive effect of the now remote amino functionality. This may explain why quenching with iodine produces a moderate level of the *para* substituted species, though the *meta* product}}

remains prevalent (*ortho:meta:para* 6:73:21).^[38] This ground-breaking regioselective metallation is thus distinct from access to similarly remote deprotonations, utilising for example the Lochmann–Schlosser “LIKOR” superbases, that are delivered as part of an indiscriminate mess of kinetic products. However, owing to the modest incorporation of *para* substituted product, which upon electrophilic quenching is liable to provide an organic compound difficult to separate from the desired *meta* derivative, this first example of directed *meta* metallation is likely to have limited use to synthetic organic chemists. Now that the concept has been conceived and successfully demonstrated the challenge for the future is to develop directing groups more able to discern *meta* and *para* substitution. Given the discrimination between these substitutions is most probably controlled through simple acidity principles then such a directing group is liable to require a greater inductive effect relative to the dimethylamino functionality while also ensuring that it is incapable of providing meaningful stabilisation of the metallated intermediate through Lewis acid/base interactions that would result in *ortho* substitution. This latter consideration is probably most easily achieved through steric protection of the directing group. A bulkier substituent may also be capable of forcing deprotonation yet further round the ring to provide access to the first example of directed *para* metallation. And finally, the influence of the mixed metal base should not be ignored. Increasing the steric bulk of the ligand sets employed to produce such reagents may well also be capable of directing metallation further from any respective directing group.



Scheme 8.12: Reaction of sodium zincate base 2 with dimethylaniline gives rise to the first confirmed example of a genuine directed *meta* metallation. Using I_2 as an electrophile gives the *meta* substituted species in a 53% yield.

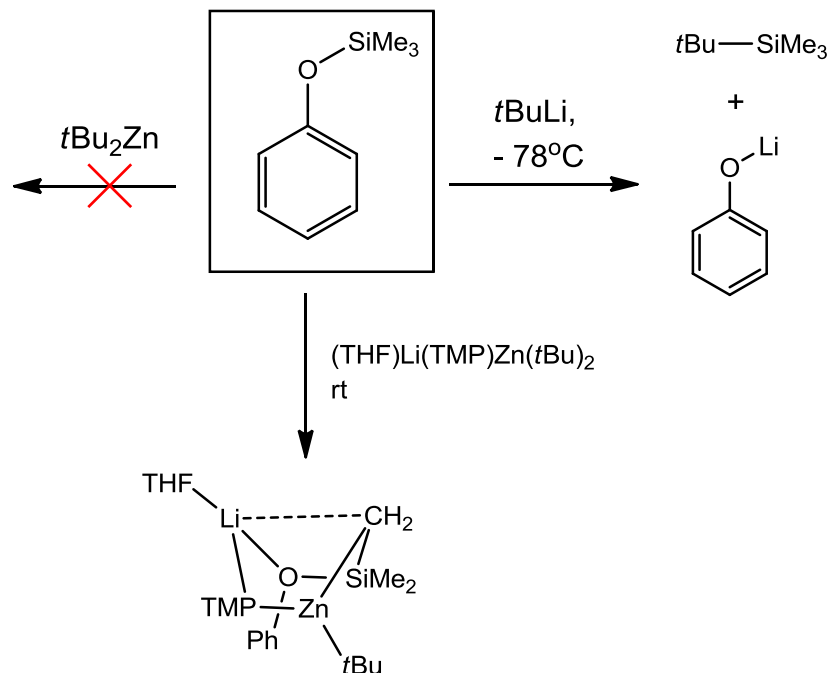
A further example of a mixed metal reagent induced unprecedented regioselectivity is the reaction between sodium zincate **2** and benzyl methyl ether. When the reaction is carried out in hexane at 20°C then the zincated intermediate (TMEDA)Na(TMP)(MeOCH₂C₆H₄)Zn(*t*Bu) **12** can be crystallised in a 49% yield (Scheme 8.13).^[40] If the reaction is instead directly followed by electrophilic quenching with iodine then the *ortho* substituted species can be isolated as the only detectable product in a 59% yield, or an 88% isolated yield when two equivalents of the base are employed. The CH₂OMe functionality is thus acting as an efficient *ortho* directing group when subjected to the synergic base. However, reaction of benzyl methyl ether with *n*BuLi at -40°C in THF results in complete discrimination for the benzylic site, as determined by subsequent deuteration of the lithiated intermediate.^[41] Furthermore, the lithiated intermediate proves to be far less stable than the *ortho* zincated **12** as at room temperature a Wittig rearrangement takes place to yield the alcohol PhCH(Me)OH on quenching with water.



Scheme 8.13: Contrasting regioselectivities and stabilities of the metallation products upon reacting benzyl methyl ether with *t*BuLi or the mixed metal base **2.**

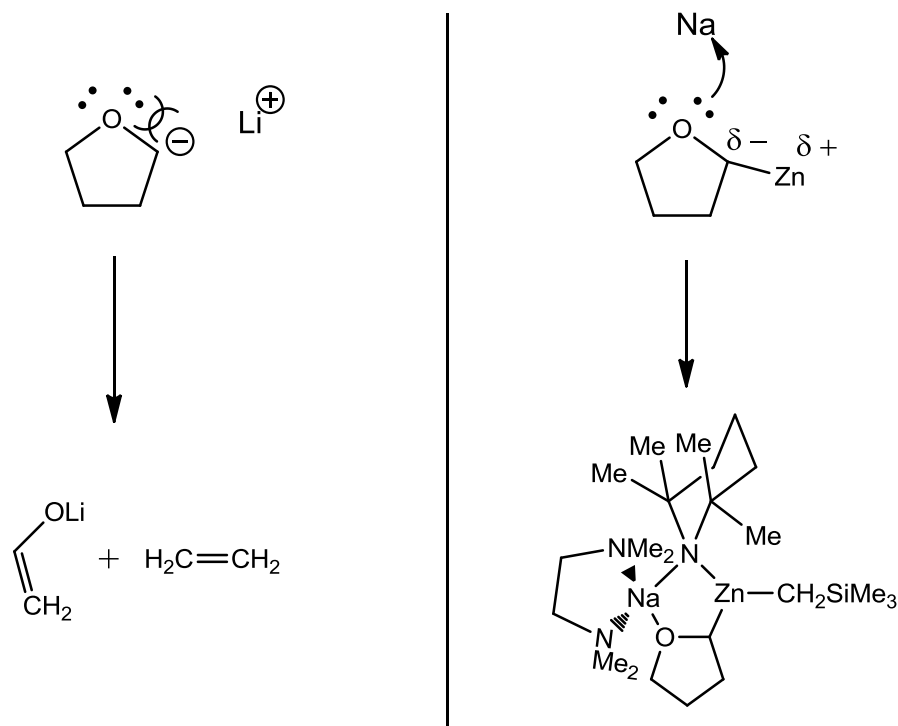
Synergic bases can not only induce unprecedented regio-selectivity, they can also promote deprotonation of substrates that prove resistant to such transformations under the influence of conventional mono-metallic reagents. The reaction of phenoxytrimethylsilane with *t*BuLi in THF at -78°C furnishes (*t*Bu)SiMe₃ and LiOPh, the product of nucleophilic substitution, with no detectable metallated species.^[42] Homonuclear (*t*Bu)₂Zn was found to be completely inert towards the same silane.^[42] However, when the bi-metallic lithium zincate reagent **1** was employed no Si–O cleavage was observed. Instead the selective lateral zincation of the trimethylsilyl group was the result (Scheme 8.14).^[42] The product (THF)Li(TMP)[CH₂Si(Me)₂OPh]Zn(*t*Bu)₂ adopts an unusual boat conformation allowing for a weak stabilising interaction between the lithium and the newly formed carbanion. Thus the synergic cooperativity between lithium and zinc has either successfully reduced the stability of the appropriate metal phenoxy species such as to switch the thermodynamic preference for the reaction compared with reaction with *t*BuLi or, perhaps more likely, succeeds in stabilising the transition state along the deprotonative reaction pathway, relative to direct lithiation, allowing for the selective synthesis and isolation of a kinetic product. The α metallation of silanes has found great utility in synthesis^[43] but, owing to the prevalence to undergo nucleophilic substitution, such synthetic strategies had previously been limited for aryloxy derivatives.^[44]

The metallation of ethereal solvents such as THF has long constituted an often problematic ill desired side reaction.^[45] Conventional lithiation of THF is quickly followed by decomposition, most often resulting in the formation of the lithium enolate LiOCH=CH₂ and ethene, owing to the repulsion between the newly formed carbanion and the lone pairs on the oxygen.^[46] However, when the sodium zincate base (TMEDA)Na(TMP)Zn(CH₂SiMe₃)₂ **13** is dissolved in neat THF and stirred for two weeks at room temperature, then the THF metallation product (TMEDA)Na(TMP)(2-OC₄H₇)Zn(CH₂SiMe₃) can be crystallised in a 53% yield from a hexane/THF mixture at -30°C.^[47] Remarkably, the integrity of the cyclic ether, minus the cleaved hydrogen atom, remains intact and can be successfully quenched with benzoyl chloride to furnish the desired organic product 2-[C(O)Ph]-C₄H₇O, thus this synergic metallation has provided



Scheme 8.14: Synergic metallation of phenoxytrimethylsilane with the lithium zincate base **1 compared with nucleophilic substitution when it is subjected to $t\text{BuLi}$.**

access to a useful new synthon in organic synthesis produced from a ubiquitous ethereal solvent. The success of this reaction is only possible because of the cooperativity between the two metal centres of the zincate base **13**. The THF ring is helped to retain its structural integrity because the metallation is carried out directly by the non-polar metal zinc. The newly formed “carbanion” thus enjoys a largely covalent interaction with the metal centre and so the build-up of charge that leads to ring cleavage is greatly reduced. However, organozinc reagents are kinetically retarded bases and are incapable of deprotonating THF out with a synergic mixture such as **13**. It can also be argued that repulsion between the carbanion and the oxygen lone pair is further reduced owing to the latter’s interaction with the alkali metal. These combined stabilising effects have been termed “synergic sedation” (Scheme 8.15). This metallation strategy was also effectively extended to the six-membered homologue tetrahydropyran.

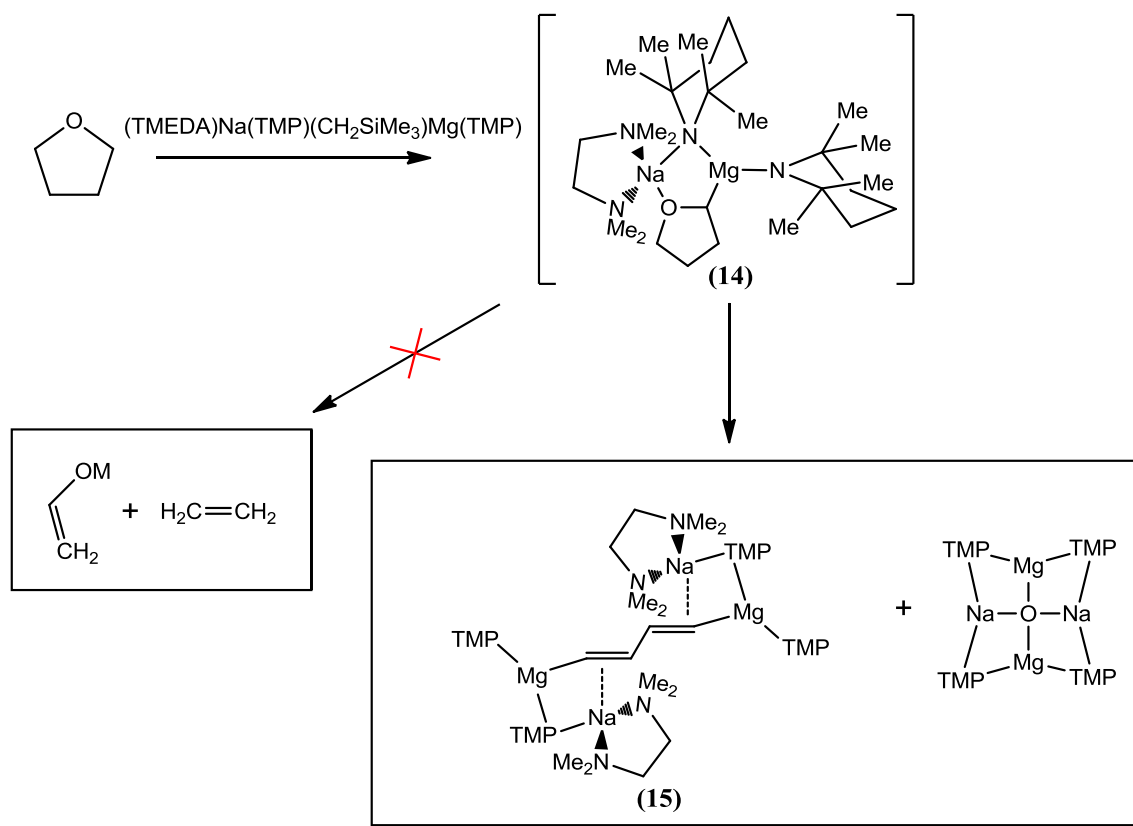


Scheme 8.15: Conventional lithiation of THF followed by decomposition vs. synergic zincation followed by trapping (“sedation”) within a sterically protecting mixed metal complex.

A further advancement of the synthesis of stable deprotonated THF molecules came from the reaction of the lithium aluminate synergic mixture of LiTMP and (TMP)Al(*i*Bu)₂ with two equivalents of THF in bulk hexane. The reaction produced the bimetallic (THF)Li(TMP)(2-C₄H₇O)Al(*i*Bu)₂ containing an aluminated THF anion.^[48] This does not merely constitute an alternative route to the creation of what had previously been an unprecedented synthon but, importantly, the aluminate base is capable of converting a stoichiometric quantity of the ether rather than reacting with a bulk solvent in the previous case. This methodology may therefore be compatible with the further functionalization of more sophisticated cyclic ethers that would prove too expensive to be utilised as a solvent.

In stark contrast to the gentle caressing of THF by both the zinc and aluminium reagents is the outright mutilation of the same cyclic ether at the hands of the sodium magnesiate base (TMEDA)Na(TMP)(CH₂SiMe₃)Mg(CH₂SiMe₃). As previously stated, metallation of THF usually results in a reverse [3 + 2] cycloaddition to yield the appropriate metal enolate and ethene. One rare example of an alternative fragmentation pathway has been realised from the reaction of (HMPA)Li(*t*Bu) (HMPA = hexamethylphosphoric triamide) with THF to give, after aqueous workup, the five-membered chain CH₂=CHCH₂CH₂OH. The sodium magnesiate **14**, more reactive than the zincate **13** or the synergic mixture of LiTMP and (TMP)Al(*t*Bu)₂, presides over a cascade of reactions cumulating in the preparation of the di-metallated butadiene fragment (TMEDA)Na(TMP)₂Mg(CH=CHCH=CH)Mg(TMP)₂Na(TMEDA) **15** (Scheme 8.16). Repeating the reaction with deuterated THF resulted in a butadiene fragment containing deuterium, confirming the cyclic ether as its source. To produce **15** from THF requires the severing of six of the thirteen bonds from which it is constructed. So the mixed metal system is not only altering the initial selectivity of the reaction, effectually suppressing the formation of an enolate species, but the entrapment of the THF fragment within a bi-metallic synergic shell unlocks a multi-step reaction pathway post metallation to produce an exotic di-ion from an inexpensive, abundant cyclic ether (Scheme 8.16). The reproducible isolation of the oxo-inverse crown species Na₂Mg₂(TMP)₄(O) from the same reaction mixture strongly implies that this is the final resting place for the oxygen from the THF molecule. The analogous reaction products can also be obtained with manganese in place of magnesium if the manganate base (TMEDA)Na(TMP)(CH₂SiMe₃)Mn(TMP) is used in place of **14**.

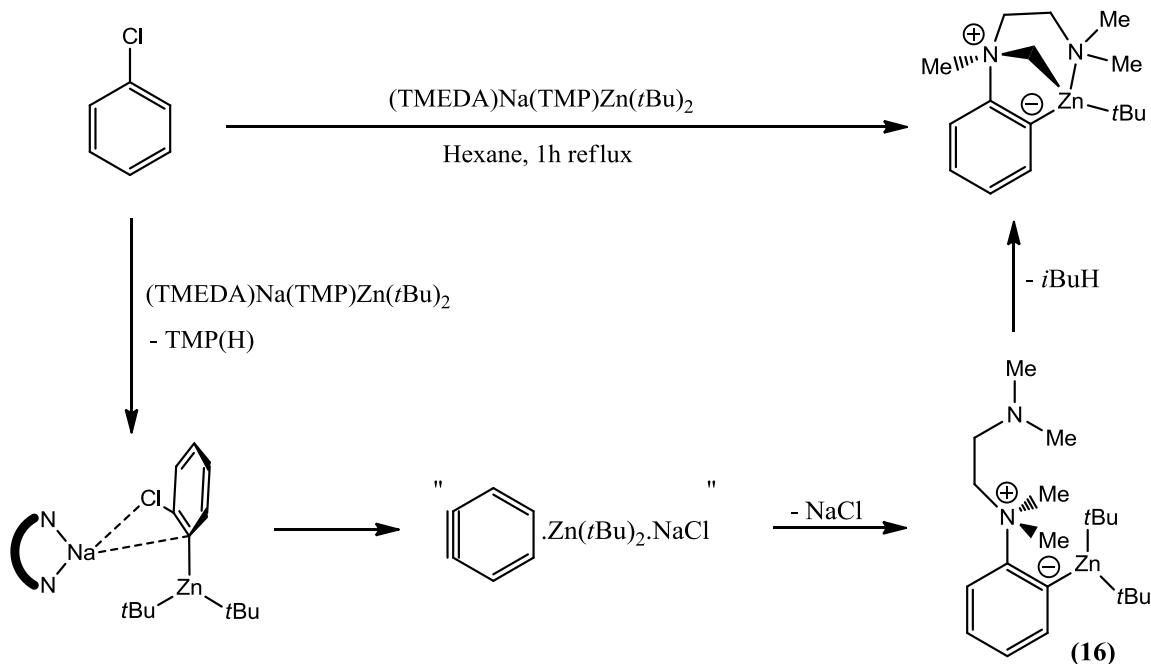
Another example of a sequence of reactions instigated by a mixed metal system to produce a highly irregular, unexpected result came upon the attempted zincation of chlorobenzene by the sodium zincate base **2**. The expected product of reaction (TMEDA)Na(TMP)(C₆H₄I)Zn(*t*Bu) is presumed to form but is then quickly followed by elimination of NaCl to provide a benzyne intermediate (Scheme 8.17). This is contrary to the reactivity displayed by “Li(TMP)Zn(*t*Bu)₂” in a study by Uchiyama towards the same substrate that displayed no salt elimination or benzyne formation. The distinction



Scheme 8.16: Synergic cleavage of THF within a mixed metal environment to produce a di-metallated butadiene and an oxo-inverse crown.

could be as a result of the changing of the alkali metal, moving from hexane to bulk THF as a reaction media or non-innocent behaviour of the too often discounted LiCl salt silently present within Uchiyama's reagent. However, Uchiyama does report high yielding benzyne formation when utilising the related "Li(TMP)Zn(Me)₂" reagent. The formal addition of (TMEDA)Zn(*t*Bu)₂ across the benzyne produces the unusual zwitterionic Me₂NCH₂CH₂N(Me)₂C₆H₄Zn(*t*Bu)₂ **16** where the positive charge of the TMEDA derived ammonium ion is balanced by the newly formed carbanion on the aromatic ring. Upon refluxing **16** for one hour a further transformation takes place to yield the peculiar tricyclic Me₂NCH₂CH₂N(Me)(CH₂)C₆H₄Zn(*t*Bu). This is the product of the extraordinary deprotonation of a hydrogen on an α carbon to a nitrogen by an unactivated alkylzinc. Extraordinary because alkylzinc reagents are such weakly deprotonating bases that under certain conditions they have even been known to tolerate

water. However, the combination of a forcing complex induced proximity effect and the lack of a lone pair of electrons on the nitrogen facilitates this most unlikely of metallations.



Scheme 8.17: Formation of the zwitterionic $\text{Me}_2\text{NCH}_2\text{CH}_2\text{N}(\text{Me})(\text{CH}_2)\text{C}_6\text{H}_4\text{Zn}(\text{tBu})$ from chlorobenzene and sodium zincate 2.

As the enterprise of this group has thus illustrated, the inclusion of an alkali metal within an organometallic system to give a hetero bimetallic complex permits the formation of otherwise inaccessible structural motifs. In return, such architectures can lead to a diverse array of unexpected reactivities, whether that is gaining access to a previously unprecedented regioselectivity such as the *meta* deprotonation of dimethylaniline, or facilitating an entire cascade of reactions to give products which are somewhat alien to the starting materials employed such is the transformation induced, for example the synthesis of butadiene from THF or the formation of the zwitterionic $\text{Me}_2\text{NCH}_2\text{CH}_2\text{N}(\text{Me})(\text{CH}_2)\text{C}_6\text{H}_4\text{Zn}(\text{tBu})$ from chlorobenzene. The aim of this project is thus to seek out new examples of alkali metal induced structural motifs and hence new examples of alkali metal instigation of unusual reactivity. To ensure the discovery of novel examples of this chemistry, a set of *hitherto* unexplored ligand sets has been

identified and the project shall also cross the seldom crossed frontier into transition metal chemistry, where the role of the alkali metal has often been marginalised in the past.

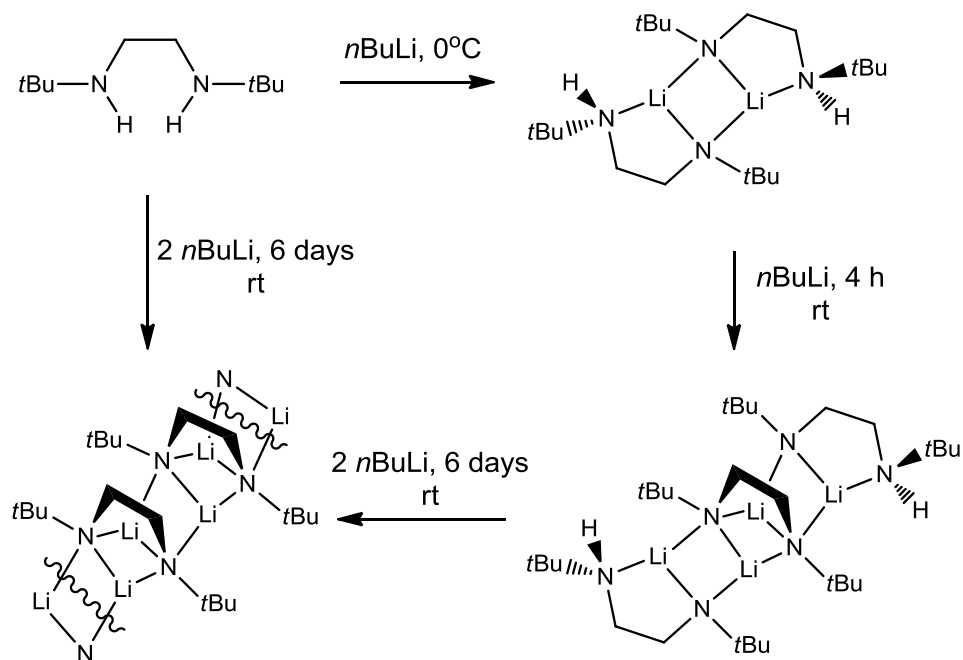
9 Alkali-metal-mediated multiple main group C-H activation

As can be gleaned from the introduction to this thesis (8.2 Mixed Metal Organometallics), the sterically demanding secondary amine 2,2,6,6-tetramethylpiperidine [TMP(H)] has been at the forefront of investigations into synergic mixed metal reactivity. Other amines such as 1,1,1,3,3,3-hexamethyldisilazane [HMDS(H)]^[49] and diisopropylamine [DA(H)]^[50] have also played important, if less prominent roles, in furthering this area of chemistry. However, until this body of work was undertaken, no bisamido ligand had yet been investigated specifically within the remit of synergic bimetallics. Thus this chapter details the extension of such chemistry to the diamine *N,N'*-diisopropylethylenediamine [(*i*Pr)N(H)CH₂CH₂N(H)(*i*Pr), DPEDA(H₂)] to explore how a bimetallic mixture might respond to the inclusion of a second acidic proton and how the inclusion of a dianionic ligand might affect any further reactivity of the mixed metal reagent.

9.1 Co-complexation with a diamide and subsequent synergic zincation

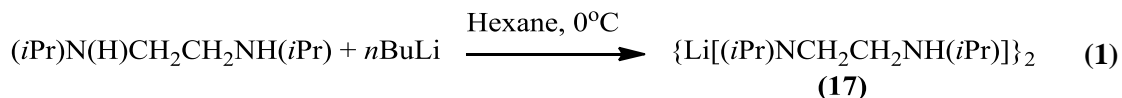
The lithiation of the closely related *N,N'*-di-*tert*-butylethylenediamine [(*t*Bu)N(H)CH₂CH₂N(H)(*t*Bu), DBEDA(H₂)] has been extensively studied by Gardiner and Raston (Scheme 9.1).^[51] Reaction of *n*BuLi or MeLi with the diamine in a 1:1 molar ratio at 0°C in hexane yields exclusively the dimeric monolithiated species {Li[N(*t*Bu)CH₂CH₂N(H)(*t*Bu)]₂. Following the deprotonation by NMR spectroscopy established the essentially quantitative transformation confirming that no other species were observed in solution such as the plausible solvated complex [(*t*Bu)N(H)CH₂CH₂N(H)(*t*Bu)]Li[N(*t*Bu)CH₂CH₂N(H)(*t*Bu)]. DFT calculations were performed suggesting that such solvation is discouraged by severe steric clashing of the *tert*-butyl ligands.^[51] When the diamine DBEDA(H₂) is subjected to one and a half molar

equivalents of $n\text{BuLi}$, or the monolithiated complex $\text{Li}[\text{N}(\text{tBu})\text{CH}_2\text{CH}_2\text{N}(\text{H})(\text{tBu})]$ is allowed to react with half an equivalent of $n\text{BuLi}$, at 0°C followed by warming to room temperature and stirring for four hours allowed the preparation and isolation of the mixed mono/di-lithiate $\{\text{Li}[\text{N}(\text{tBu})\text{CH}_2\text{CH}_2\text{N}(\text{H})(\text{tBu})]\text{Li}\}_2[\text{N}(\text{tBu})\text{CH}_2\text{CH}_2\text{N}(\text{tBu})]$. This mixed species, which crystallises as an extended ladder, clearly exhibits a reasonable degree of stability as complete synthesis of the dimetallated (twofold deprotonated) compound $\text{Li}_2[\text{N}(\text{tBu})\text{CH}_2\text{CH}_2\text{N}(\text{tBu})]$ requires the combination of the diamine $\text{DBEDA}(\text{H}_2)$ and $n\text{BuLi}$ followed by extended reaction times of up to six days at room temperature. The dilithiate can be obtained in one of two different polymorphs. If the reaction mixture is allowed to stand for six days followed by concentration and storage at -30°C then a microcrystalline white solid is obtained which is believed to be the polymeric infinite ladder $\{\text{Li}_2[\text{N}(\text{tBu})\text{CH}_2\text{CH}_2\text{N}(\text{tBu})]\}_\infty$. If instead after a one day stir at room temperature the hexane solution is frozen in liquid nitrogen and allowed to slowly warm to -30°C then a crystalline product of the molecular, distorted cubane species $\{\text{Li}_2[\text{N}(\text{tBu})\text{CH}_2\text{CH}_2\text{N}(\text{tBu})]\}_2$ can be isolated, albeit in a small (apparently immeasurable) yield.



Scheme 9.1: Illustration of the various stages of Gardiner and Raston's lithiation of the diamine $(\text{tBu})\text{N}(\text{H})\text{CH}_2\text{CH}_2\text{N}(\text{H})(\text{tBu})$ [$\text{DBEDA}(\text{H}_2)$].

Turning now to our own investigations, the monolithiate $\{\text{Li}[(i\text{Pr})\text{NCH}_2\text{CH}_2\text{N}(\text{H})(i\text{Pr})]\}_2$ - $\{\text{Li}[\text{DPEDA}(\text{H})]\}_2$ - **17** was produced upon introducing one molar equivalent of $n\text{BuLi}$ to the diamine $\text{DPEDA}(\text{H}_2)$ in hexane solution at 0°C [equation (1)]. Storage at -30°C allowed for the isolation of a crystalline sample of **17** in a 79% yield.



NMR spectroscopic analysis of **17** confirms the abstraction of one proton from the diamine and no solvated species such as $[(i\text{Pr})\text{N}(\text{H})\text{CH}_2\text{CH}_2\text{N}(\text{H})(i\text{Pr})]\text{Li}[\text{N}(i\text{Pr})\text{CH}_2\text{CH}_2\text{N}(\text{H})(i\text{Pr})]$ could be detected suggesting that complexes of $\text{DPEDA}(\text{H}_2)$ behave in a similar manner to the homologous $\text{DBEDA}(\text{H}_2)$ studied by Gardner and Raston.^[51] Therefore, to avoid the duplication of work, no X-Ray diffraction analysis was deemed necessary and **17** is presumed to adopt the same structural motif as the related *tert*-butyl analogue $\{\text{Li}[\text{N}(t\text{Bu})\text{CH}_2\text{CH}_2\text{N}(\text{H})(t\text{Bu})]\}_2$. Also, akin to the observations of Gardiner and Raston, the ^1H NMR spectrum of **17** (Figure 9.1) exhibits two broad resonances for the methylene hydrogens at 2.65 ppm and 3.25 ppm as well as two similarly broad signals for the alkyl substituents at 0.90 ppm and 1.35 ppm intimating the presence of a dynamic equilibrium. Also, the C-H resonances of the isopropyl groups overlap with the methylene signals of the diamine backbone. Unlike in the case of $\{\text{Li}[\text{N}(t\text{Bu})\text{CH}_2\text{CH}_2\text{N}(\text{H})(t\text{Bu})]\}_2$, the N-H resonance is clearly split into two separate signals at 0.40 ppm and 0.55 ppm in approximately a 2:1 ratio. Gardiner and Raston demonstrated that at -40°C the equilibrium for $\{\text{Li}[\text{N}(t\text{Bu})\text{CH}_2\text{CH}_2\text{N}(\text{H})(t\text{Bu})]\}_2$ can be frozen to produce an NMR spectrum with four inequivalent methylene resonances consistent with what would be expected on examining the crystal structure. The fluxional behaviour was ascribed to an association/disassociation of the solvating amino arm.^[51] Again it was deemed unnecessary to duplicate this work for our own system given their similarity.

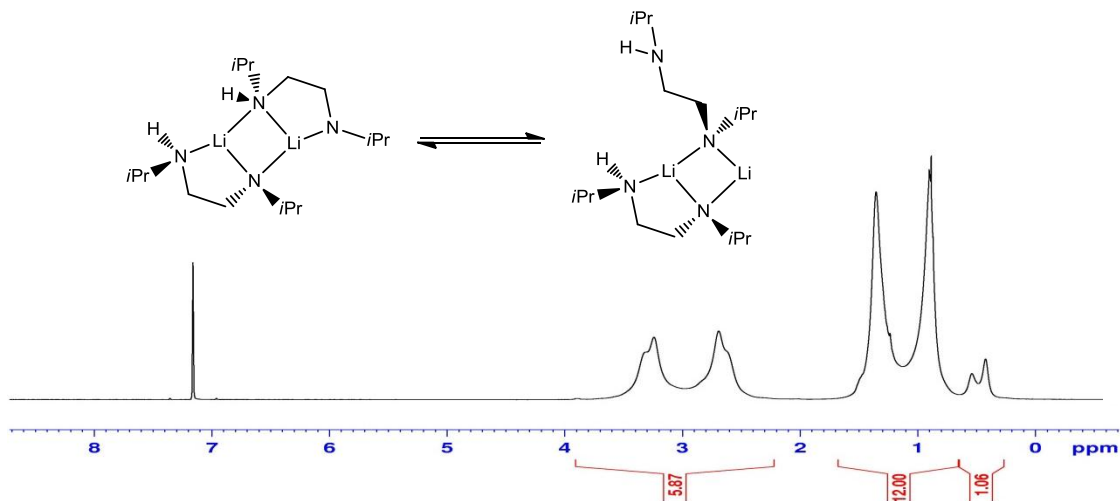


Figure 9.1: ^1H NMR spectrum of the monolithiated $\{\text{Li}[(i\text{Pr})\text{NCH}_2\text{CH}_2\text{N}(\text{H})(i\text{Pr})]\}_2$ in C_6D_6 and a postulated equilibria to explain the broad signals and inequivalent N-H signals.

The co-complexation of the monolithiated diamine **17**, either synthesised *in situ* or utilising a pre-prepared crystalline sample, with $(t\text{Bu})_2\text{Zn}$ and a molar equivalent of the tertiary diamine TMEDA in hexane at 0°C followed by immediate storage at -30°C permitted the formation and isolation of transparent colourless crystals suitable for X-Ray diffraction analysis. Following such an analysis, the product was revealed to be the adduct $(\text{TMEDA})\text{Li}[(i\text{Pr})\text{NCH}_2\text{CH}_2\text{N}(\text{H})(i\text{Pr})]\text{Zn}(t\text{Bu})_2$ **18** [equation (2), Figure 9.2].



Akin with the TMP lithium zincate **1** (Figure 8.4, page 15), **18** adopts a contacted ion pair motif with the amido N2 bridging the lithium and zinc centres. The zinc is in a distorted tetrahedral geometry (bond angles averaging 107.23°) owing in part to the narrow bite angle of the DPEDA(H) ligand [N1-Zn1-N2 $83.10(5)^\circ$]. Again comparing **18** with the TMP lithium zincate **1**, the switch from a trigonal planar to a tetrahedral zinc coordination, due to solvation by the amino N1 arm, results in the displacement of the *tert*-butyl ligands from the Li-N2-Zn plane [Li1-N2-Zn1-C5 torsion angle $7.72(13)^\circ$ compared with Li-N-Zn-C $0.00(14)^\circ$ in **1**]. This precludes the establishment of an electrostatic interaction between the *tert*-butyl ligand and the lithium centre that would

result in the familiar five-membered Li-N-Zn-C-C ring. Consequently the Li1-C8 separation [3.036(4) Å] is significantly elongated in comparison to the equivalent distance in **1** [Li-C 2.409(5)] and a more open structure is the result with a Li1-N2-Zn1 angle of 112.29(12) compared with Li-N-Zn angle of 100.24(14) in **1**. No apparent bonding interaction exists between Li1 and N1 given the extremely long separation [Li1-N1 4.123(3) Å]. Li1 is thus three coordinate, in a distorted trigonal planar geometry again due to the narrow bite angle of the TMEDA ligand (bond angles totalling 355.32). Further distortion of the coordination around Li1 [N2-Li1-N3 127.12(5) compared with N2-Li1-N4 141.06(16)] can be explained by steric clashing between the N2 isopropyl group and the N4 arm of the TMEDA ligand. The anionic nature of N2 is evident from the shorter N2-Zn1 [2.127(1) Å] and N2-Li1 [1.993(3) Å] bond lengths compared with N1-Zn1, N3-Li1 and N4-Li1 bond distances of 2.326(1) Å, 2.143(3) Å and 2.173(3) Å respectively. The five atoms Zn1-N1-C12-C13-N2 occupy a puckered five-membered ring with a N1-C12-C13-N2 torsion angle of 65.74(18). The isopropyl groups of the DPEDA(H) ligand lying *anti* to each other.

From a mechanistic perspective, one of the areas of alkali metal alkyl amido zincate chemistry to generate much debate is whether they exhibit alkyl or amido basicity and the two-step mechanism initially proposed by Uchiyama (see chapter 8.2.1). It has been proposed that zincate reagents such as (TMEDA)Na(TMP)Zn(*t*Bu)₂ **2** act first kinetically as amido bases, followed by a resurrection of the TMP anion through a thermodynamic preference to exhibit overall alkyl basicity on the basis of DFT (Density Functional Theory) calculations.^[34] This view has since become widely accepted, aided by a growing mass of experimental evidence (chapter 8.2.1). While it has indeed been demonstrated that (THF)₃Li(C₆H₄OMe)Zn(*t*Bu)₂ **6**, the postulated intermediate of the reaction between lithium zincate (THF)Li(TMP)Zn(*t*Bu)₂ **1** and anisole, can be synthesised indirectly and when subjected to TMP(H) displays alkyl basicity to form (THF)Li(TMP)(C₆H₄OMe)Zn(*t*Bu) **7** with concomitant release of isobutane, there is little experimental or theoretical data on the precise mode of reaction that results in the regeneration of the amido ligand. The lithium zincate **18** can be viewed as a model

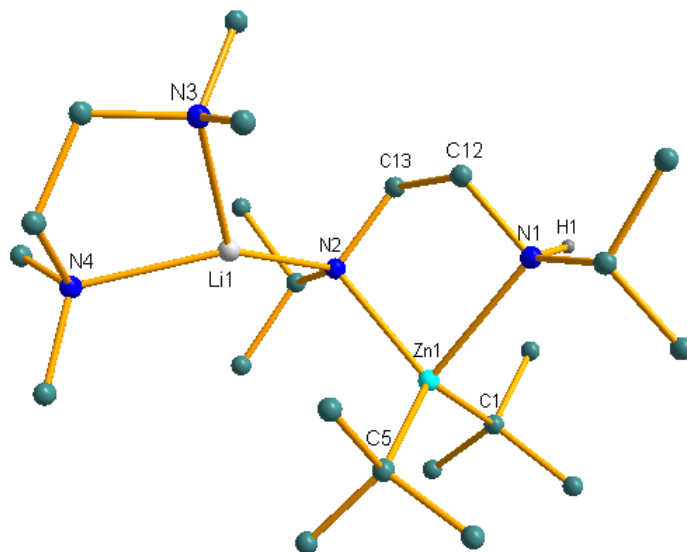
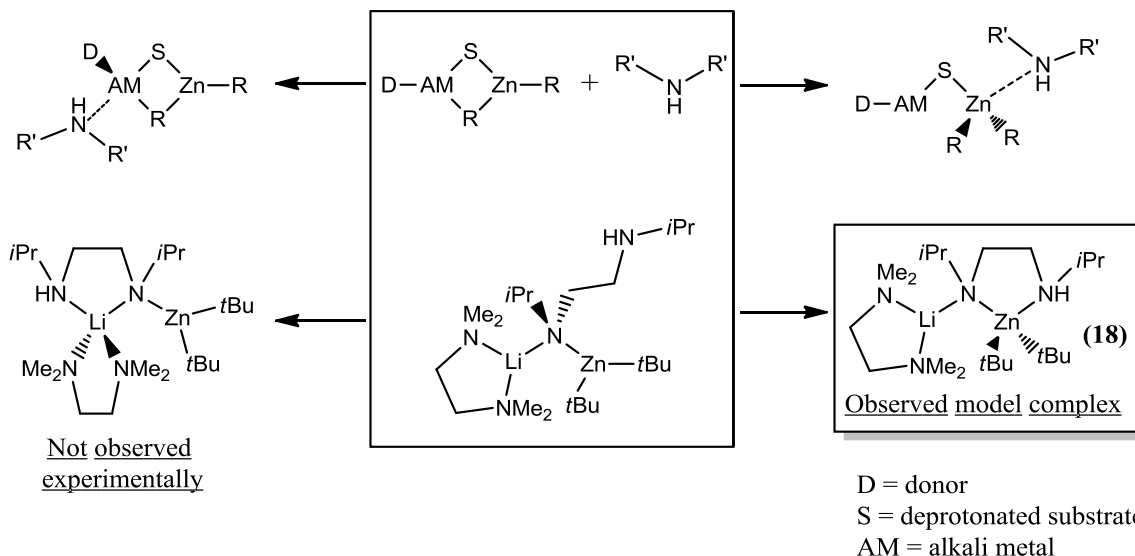


Figure 9.2: Molecular structure of **18** with hydrogen atoms (except N-*H*) omitted for clarity. Selected bond lengths [Å] and angles [°]: Zn1-C1 2.073(2), Zn1-C5 2.068(2), Zn1-N1 2.326(1), Zn1-N2 2.127(1), Li1-N2 1.993(3), Li1-N3 2.143(3), Li1-N4 2.173(3), N1-C12 1.470(2), N2-C13 1.461(2), C12-C13 1.517(2); C5-Zn1-C1 125.65(7), C5-Zn1-N2 111.49(6), C5-Zn1-N1 108.98(5), C5-Zn1-N2 111.49(56), C1-Zn1-N1 102.67(6), N2-Zn1-N1 83.10(5), N2-Li1-N3 127.12(15), N2-Li1-N4 141.06(16), N3-Li1-N4 87.1(1).

compound for an intermediate along such a two-step reaction pathway, with the amino pendant arm of the DPEDA(H) ligand representing the returning amino ligand immediately prior to the final execution of alkyl basicity which leads to the reincorporation of an amido ligand (Scheme 9.2). However, unlike the calculations performed by Uchiyama on the theoretical reaction of (TMEDA)Na(NMe₂)Zn(Me)₂ **3** with benzene (Scheme 8.7),^[34] which suggests the liberated Me₂NH re-enters the complex via pre-coordination to the alkali metal, the amino arm in **18** chooses instead to coordinate to the more Lewis acidic zinc. It is of course true that **18** does not accurately reproduce the true steric interactions that may affect the reactivity of TMP zincates such as **2**, and the anchimeric nature of the amino functionality may have a bearing on its solvation properties, but then the simplistic model compound **3** is not an accurate model for the sterics involved in TMP zincates either. Experimental evidence for pre-coordination of substrates at the alkali metal rather than zinc exists, for example as in the case of the isolation and X-ray characterisation of the pre-complex

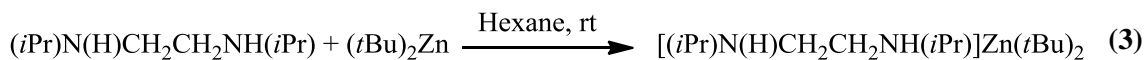
$[\text{C}_6\text{H}_5\text{C}(\text{O})\text{N}(\text{iPr})_2]\text{Li}(\text{TMP})\text{Zn}(\text{tBu})_2$ on route to the eventual ortho deprotonation of the benzamide with overall loss of isobutane.^[24] However, the second step of the reaction involves the incoming proton source (the now liberated amino ligand) approaching a fundamentally different zincate species as, evidently, the amide has been replaced by a deprotonated substrate. The different steric situation of this intermediary zincate may result in a switching from alkali metal to zinc sited pre-coordination. The amino solvation of zinc in **18** does not justify a belief that metallation by zincate bases must proceed via pre-coordination at zinc. However, it does suggest that, at least in certain cases where the zincate reagent employed or the steric nature of the substrate metallated result in less crowded complexes, that pre-coordination at zinc represents a feasible reaction pathway. Computational evidence for coordination at zinc can be gleaned from a DFT study into the theoretical metallation of anisole by the lithium zincate $(\text{Me}_2\text{O})\text{Li}(\text{NMe}_2)\text{Zn}(\text{Me})_2$.^[52] The calculations suggest initial pre-coordination of anisole at the alkali metal which ultimately leads to deprotonation by the amido ligand. The species produced post metallation retains the formed Me_2NH coordinated to the Lewis acidic zinc centre, thus displaying the same fundamental characteristics as observed experimentally in **18**. This offers the enticing notion, supported by the formulation of **18**, that a transient zincate intermediate may, at least in some instances, be formed upon a zincate reagent acting as an amido base in which the newly formed amine is retained complexed to the zinc, ready to act as a speedy proton shuttle between the deprotonated substrate and the more sluggish alkyl ligand without ever being liberated from the zincate. This could also provide an explanation for why deprotonation reactions by zincate reagents can prove to be more efficient in hexane than the donor solvent THF, as the Lewis basic THF may encourage the expulsion of the amine from the zincate before alkyl basicity can be realised. This is in agreement with NMR spectroscopic studies performed by Uchiyama on the reaction of $(\text{THF})\text{Li}(\text{TMP})\text{Zn}(\text{tBu})_2$ with anisole in bulk THF which exhibited amido basicity with little evidence for loss of isobutane. DFT calculations by Mongin have also suggested that the cadmation of anisole by the putative base $\text{LiCd}(\text{TMP})_3$ proceeds via precomplexation of the incoming anisole at the larger Cd centre over the alkali metal prior to metallation and that this might be key to the reactivity of this reagent.^[53] However, it is perhaps not surprising that the sterically deficient model

complex $(\text{Me}_2\text{O})\text{Li}(\text{NMe}_2)_2\text{Cd}(\text{NMe}_2)$ might crave additional solvation of the sizable cadmium ion.



Scheme 9.2: Depiction of how complex **18** can be viewed as a model for the second stage of the two-step mechanism proposed by Uchiyama (see Scheme 8.7).

Complex **18** is thermally unstable and rapidly decomposes at room temperature with loss of isobutane to furnish the diamido complex $(\text{TMEDA})\text{Li}[(i\text{Pr})\text{NCH}_2\text{CH}_2\text{N}(i\text{Pr})]\text{Zn}(t\text{Bu})$ **19**. As such, satisfactory NMR data is unavailable. For comparison, the reaction of $(t\text{Bu})_2\text{Zn}$ with $\text{DPEDA}(\text{H}_2)$ was investigated. The 1:1 combination of $(t\text{Bu})_2\text{Zn}$ and $\text{DPEDA}(\text{H}_2)$ in hexane, after 18 hours at room temperature, yielded the simple non-deprotonated chelate $[(i\text{Pr})\text{N}(\text{H})\text{CH}_2\text{CH}_2\text{N}(\text{H})(i\text{Pr})]\text{Zn}(t\text{Bu})_2$ **20** as colourless crystals suitable for X-ray diffraction analysis upon storage at -30°C [equation (3)].



The zinc adopts a distorted tetrahedral geometry due to the natural bite angle of the $\text{DPEDA}(\text{H}_2)$ ligand with a N1-Zn1-N1 angle of $79.53(17)$. Zinc is held centrally by the diamine ligand with near identical Zn-N bond lengths [Zn1-N1 2.245(5) Å, Zn1-N2 2.254(5) Å]. These bond distances are consistent with the Zn-N bond lengths observed in $[\text{PhCH}(\text{Me})\text{N}(\text{H})\text{CH}_2\text{CH}_2\text{N}(\text{H})\text{CH}(\text{Me})\text{Ph}]\text{Zn}(\text{Me})_2$ of 2.231(3) Å^[54]; however, they are

slightly shorter than the N(H)-Zn bond distance observed in the mixed metal complex **18** [Zn1-N1 2.326(1) Å] due to the greater affinity of the zinc for the amido nitrogen in this species. The Zn-C bond distances in **20** [Zn1-C1 2.063(5) Å, Zn1-C5 2.042(7) Å] differ little from those observed in the zincate **18** [Zn1-C1 2.073(2) Å, Zn1-C5 2.068(2) Å] and only marginally longer than the Zn-Me bond lengths in [PhCH(Me)N(H)CH₂CH₂N(H)CH(Me)Ph]Zn(Me)₂ [Zn-Me 2.006(5) Å]. The five atoms Zn1-N1-C13-C12-N2 connect to generate a puckered five-membered ring with a N1-C13-C12-N2 torsion angle of 58.16(65). This is consistent with that in the symmetrical complex [PhCH(Me)N(H)CH₂CH₂N(H)CH(Me)Ph]Zn(Me)₂ [N-C-C-N 59.89(42)]^[54] while the mixed metal complex **18** is distorted slightly further from planarity [N1-C12-C13-N2 65.74(18)]. In all three complexes the alkyl groups of the diamino ligands adopt an *anti* configuration.

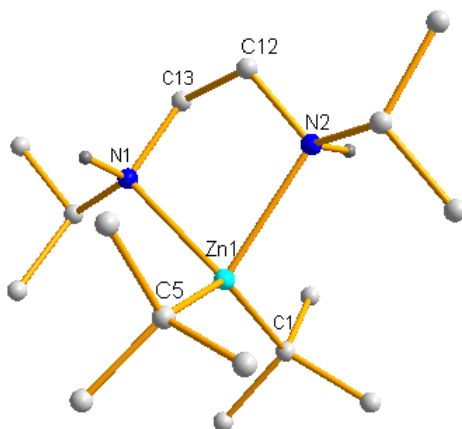


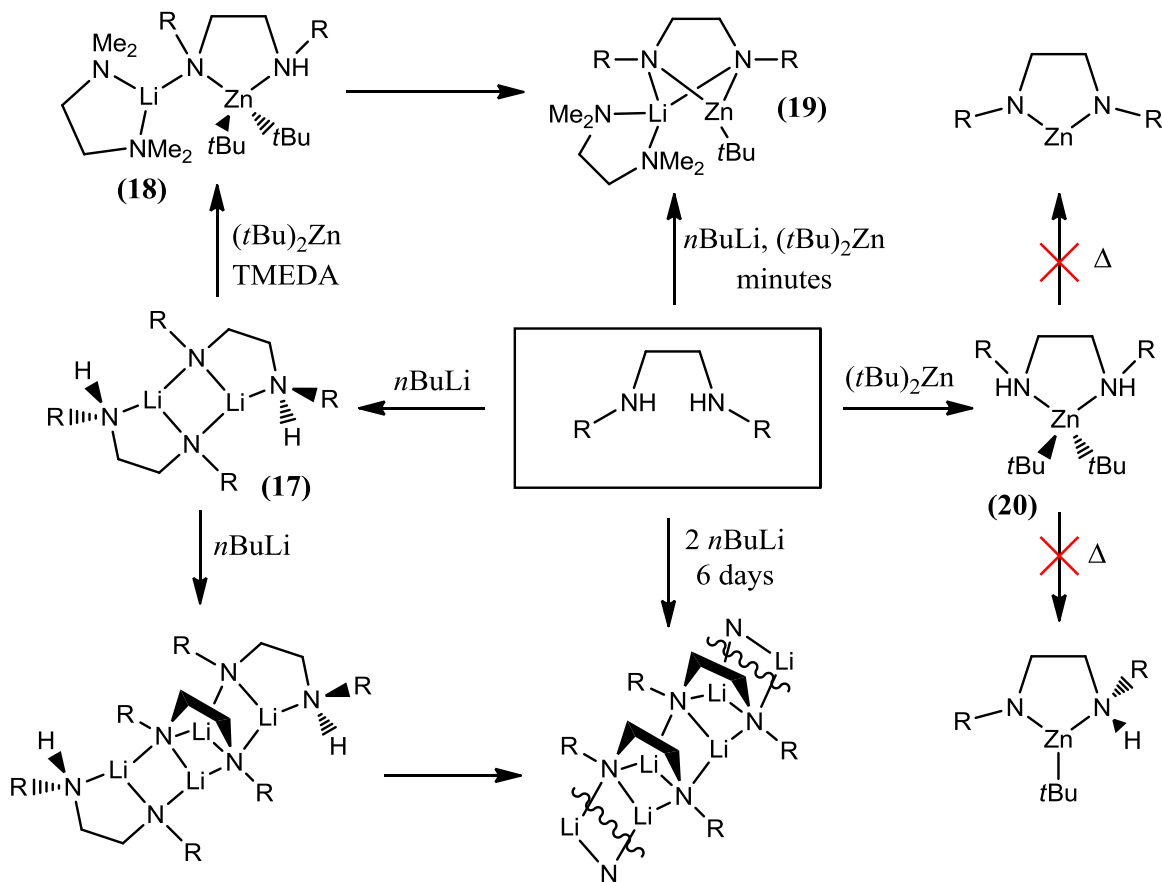
Figure 9.3: Molecular structure of the simple adduct [(*i*Pr)N(H)CH₂CH₂N(H)(*i*Pr)]Zn(*t*Bu)₂ **20** with hydrogen atoms (except N-H) omitted for clarity. Selected bond lengths [Å] and angles [°]: Zn1-C1 2.063(5), Zn1-C5 2.042(7), Zn1-N1 2.245(5), Zn1-N2 2.254(5), N1-C13 1.459(7), N2-C12 1.459(7), C12-C13 1.512(8), C5-Zn1-C1 133.9(2), C5-Zn1-N1 105.7(2), C1-Zn1-N1 109.7(2), C5-Zn1-N2 110.5(2), C1-Zn1-N2 104.3(2), N1-Zn1-N2 79.6(2).

Repeating the synthesis of **20** and analysing the solution obtained by NMR spectroscopy revealed no detectable level of deprotonation, even after refluxing of the solution for ten minutes. This control reaction has thus demonstrated that the direct zincation of the DPEDA(H) ligand, or even of the DPEDA(H₂) ligand, is not possible with zinc on its

own but requires the participation of an alkali metal. The rapid loss of isobutane from **18** is thus a rare example of an intramolecular alkali metal mediated zincation. Remarkably, this represents a synergic acceleration even compared with complete di-deprotonation when two equivalents of *n*BuLi are employed, contrasting with reaction times as long as six days to fully deprotonate the related DBEDA(H₂).^[51] A possible explanation for this extraordinary observation of an alkylzinc reagent, with the aid of the diamine TMEDA, demonstrating greater kinetic basicity than *n*BuLi can be formulated when considering the transformation from the lithium complex {Li[(*i*Pr)NCH₂CH₂N(H)(*i*Pr)]}₂ **17** to the mixed lithium-zinc complex (TMEDA)Li[(*i*Pr)NCH₂CH₂N(H)(*i*Pr)]Zn(*t*Bu)₂ **18**. A combination of the Lewis acidity and steric bulk of the (*t*Bu)₂Zn facilitates the monomerisation of the mono-lithiated dimer **17** which, in turn, precludes the formation of a mixed species such as the hypothetical Li₂[DPEDA][DPEDA(H)]Zn₂(*t*Bu)₃, analogous to that of the lithiated compound {Li[N(*t*Bu)CH₂CH₂N(H)(*t*Bu)]Li}₂[N(*t*Bu)CH₂CH₂N(*t*Bu)].^[51] This monomerisation thus necessitates the smooth, direct transformation from mono to di-deprotonation (Scheme 9.3).

While the formation of the di-deprotonated complex has been confirmed by NMR spectroscopy, no definitive structural data could be obtained from X-ray crystallographic techniques. However, the successful isolation and crystallographic characterisation of several closely related species has been achieved. Turning to the homologous (*i*Pr)N(H)CH₂CH₂CH₂N(H)(*i*Pr) (diisopropylpropylenediamine), the combination of Li[(*i*Pr)NCH₂CH₂CH₂NH(*i*Pr)] with (*t*Bu)₂Zn(TMEDA) allowed for the preparation and crystallographic characterization of the di-metallated diamide (TMEDA)Li[(*i*Pr)NCH₂CH₂CH₂N(*i*Pr)]Zn(*t*Bu) **21**, establishing that this synergic zincation can be extended to different diamine ligands. Unfortunately the crystal data are of insufficient quality to allow discussion of the geometric parameters of the structure but the connectivity is definite (Figure 9.4). The lithium diamidozincate **21** contains an NCCCZn six membered ring in a boat type conformation. The diamido ligand thus chelates the Zn centre while its two *i*Pr arms are oriented out of the plane of the ring in an *anti* configuration. The (TMEDA)Li cation is coordinated to the hull of the boat,

anchored exclusively to the two secondary amido groups to produce a puckered LiNZnN four membered ring. A *tert*-butyl anion completes the distorted trigonal planar coordination of the zinc atom.



Scheme 9.3: Synergic direct intramolecular zincation contrasted with coordination to $(t\text{Bu})_2\text{Zn}$ and a slow di-lithiation process.

On utilising THF as a donor ligand in the absence of TMEDA, in a repeat of the synthesis of **19**, the dimeric THF-solvated product $\{(\text{THF})\text{Li}[(i\text{Pr})\text{NCH}_2\text{CH}_2\text{N}(i\text{Pr})\text{Zn}(t\text{Bu})]\}_2$ **22** was isolated and subsequently crystallographically characterised.



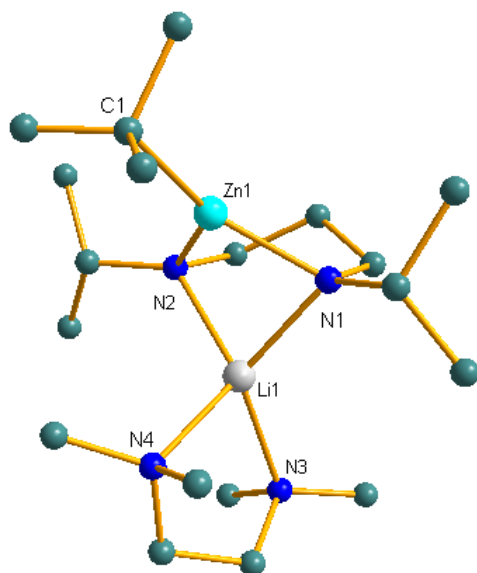


Figure 9.4: Molecular structure of the diamidozincate (TMEDA)Li[(*i*Pr)NCH₂CH₂CH₂N(*i*Pr)]Zn(*t*Bu) **21**. Hydrogen atoms and disordered *t*Bu/TMEDA components have been omitted for clarity.

Lithium zincate **22** has a centrosymmetric dimeric structure consisting of two [(*i*Pr)NCH₂CH₂N(*i*Pr)]Zn(*t*Bu) complex anions, juxtaposed, and bridged by two (THF)Li cations to produce an eight-membered (LiNZnN)₂ ring (Figure 9.5). The cyclic conformation of **22** allows for the near symmetrical coordination of each amido group to one lithium [N1-Li1 2.001(4), N2-Li1' 2.041(4)] and one zinc centre [N1-Zn1 2.019(2), N2-Zn1 1.986(2)]. Both sets of metal centres occupy distorted trigonal planar geometries with bond angles totalling 359.6° and 359.9° for lithium and zinc respectively. The *i*Pr groups on the amido ligands lie *syn* with respect to the ZnNCCN ring which, while still puckered, deviates less from planarity than both the ZnNCCN rings in **18** and **20** with a N1-C4-C5-N2 torsion angle of 50.0°.

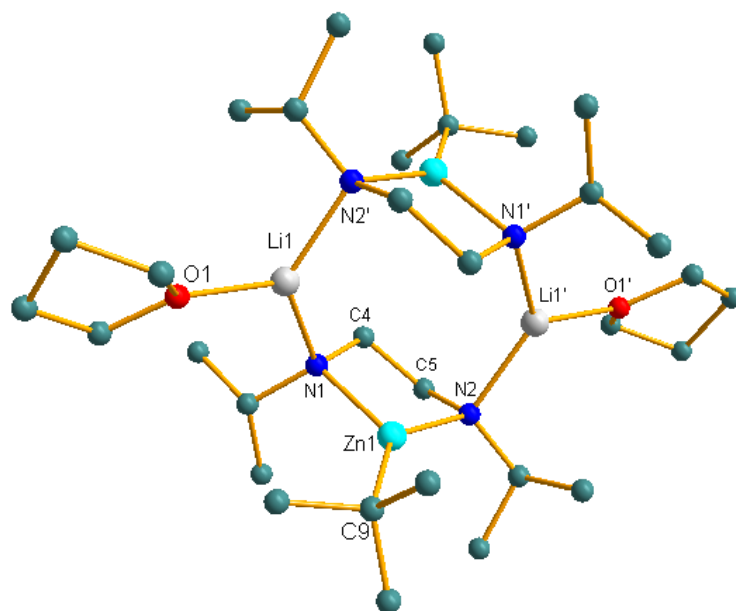


Figure 9.5: Molecular structure of THF-solvated lithium zincate [(THF)Li[(*i*Pr)NCH₂CH₂N(*i*Pr)]Zn(*t*Bu)]₂ **22**. Hydrogen atoms and minor disordered *t*Bu/THF components have been omitted for clarity. Symmetry operations to generate equivalent atoms: 1-*x*, -*y*, 1-*z*. Selected bond lengths [Å] and angles [°]: Zn1–N1 2.019(2), Zn1–N2 1.986(2), Zn–C9 2.019(9), Li1–N1 2.001(4), Li1–N2' 2.041(4), Li1–O1 2.004(4), N1–C4 1.471(3), N2–C5 1.470(3), C4–C5 1.530(3), N1–Zn1–N2 91.20(7), N1–Zn1–C9 127.5(2), N2–Zn1–C9 141.2(2), N1–C4–C5–N2 50.0, N1–Li1–N2' 127.0(2), N1–Li1–O1 117.7(2), N3–Li1–O1 114.9(2).

Both the propylene bridged **21** and the ethylene bridged THF solvate **22** are rare examples of structurally characterised diamido alkali metal zincates with a saturated linker. Perhaps the closest structurally analogous compound, and, to our knowledge, the only structurally characterised complex to strictly fit the description of an alkali metal diamido zincate with a saturated bridge, was synthesised by Borovik.^[55] The transmetallation of (*t*Bu)N(H)C(O)N(K)CH₂CH₂N(K)C(O)NH(*t*Bu) with half a molar equivalent of Zn(OAc)₂ in *N,N*-dimethylacetamide provided access to the bimetallic [(Me)₂NC(O)CH₃]₂K₂[(*t*Bu)N(H)C(O)NCH₂CH₂NC(O)NH(*t*Bu)]₂Zn **23** with the concomitant precipitation of potassium acetate. It was hoped that **23** could be used as a model complex to investigate hydrogen bonding, which is of fundamental importance to

the action of metallo-biomolecules. The zinc centre in **23** is sequestered by the two chelating diamido ligands while short NH-Zn bond lengths (average 2.75 Å) were used to imply the presence of hydrogen bonding to the metal. Each potassium cation bridges two asymmetric units through coordination of the carbonyls of the urea side arms, giving rise to an infinite polymeric structure. A similar transmetallation protocol was successfully employed by the same group to synthesise a series of trisamido species including the potassium zincates $\text{K}\{\text{N}[\text{CH}_2\text{C}(\text{O})\text{NCH}(\text{Me})\text{Ph}]_3\}\text{Zn}^{[56]}$ and the hydroxo complex $\text{K}_2\{\text{N}[\text{CH}_2\text{C}(\text{O})\text{N}(t\text{Bu})]_3\}\text{ZnOH}^{[57]}$. To the best of our knowledge there is no previous precedent for the synthesis of saturated diamido or trisamido zincate species by direct deprotonation by a zinc reagent. However, precedent does exist for the synthesis of unsaturated analogues, such as the functionalization of a pyrrole based porphyrin ring through deprotonation by Et_2Zn followed by addition of $\text{KCl}^{[58]}$.

9.2 Unexpected CH activation and experimental evidence for a hydride intermediate

While exploring the properties of the mixed lithium-zinc diamide complex $(\text{TMEDA})\text{Li}[(i\text{Pr})\text{NCH}_2\text{CH}_2\text{N}(i\text{Pr})]\text{Zn}(t\text{Bu})$ **19** it was discovered that, upon refluxing in hexane, the solution colour changed from pale yellow to a vibrant orange. It was found that this was due to the surprising formal elimination of hydrogen gas from **19**, resulting in the formation of the unsaturated diazadiene complex $(\text{TMEDA})\text{Li}[(i\text{Pr})\text{NCH}=\text{CHN}(i\text{Pr})]\text{Zn}(t\text{Bu})$ **24** (Figure 9.6). Refluxing an *in situ* generated hexane solution of **19** for two hours followed by storage of the resulting orange solution at -70°C allowed for the isolation of a yellow crystalline sample of the unsaturated **24**, in a 40% yield suitable for X-ray diffraction analysis. The crystallographic data obtained are of insufficient quality to permit a detailed discussion of the geometric parameters of **24**, though the connectivity is unequivocal. Qualitatively it can be observed that the NCCN chelating section of the diazadiene ligand $(i\text{Pr})\text{NCH}=\text{CHN}(i\text{Pr})$ is considerably closer to planarity compared to the diamido structures of **20** and **22** which is consistent with dehydrogenation of the backbone of the

ligand. The Zn centre is in a distorted trigonal planar geometry, lying below the plane of the diazadiene ligand, while the Li is chelated by the neutral diamine TMEDA ligand and its coordination sphere is completed by an η^4 interaction with the upper face of the diazadiene ligand.

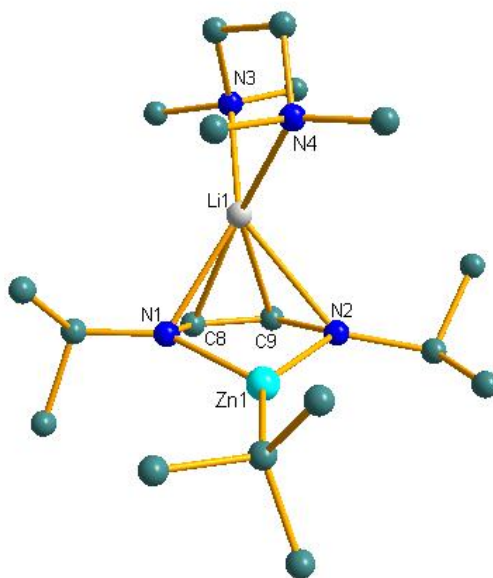


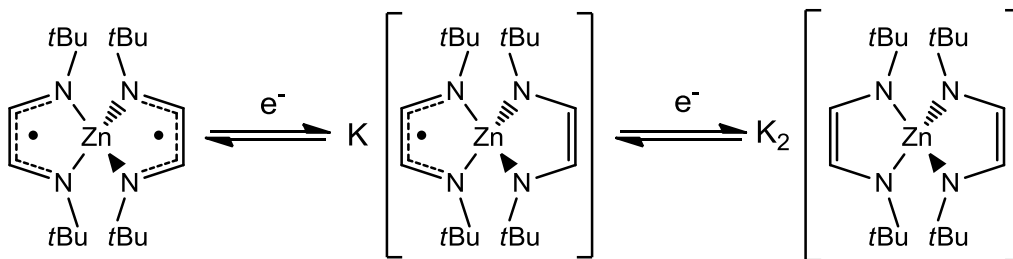
Figure 9.6: Molecular structure of the diazadiene zincate complex (TMEDA)Li[(*i*Pr)NCH=CHN(*i*Pr)]Zn(*t*Bu) **24**. Hydrogen atoms and disorder within the *t*Bu ligand are omitted for clarity.

Ligands of type RNCH=CHNR have proven popular in synthetic chemistry owing to the ease with which their steric properties can be tuned and their versatile electronic nature; properties which result in a ligand set particularly adept at stabilising low valent complexes such as In(I),^[59] Ga(I)^[60] and Cr(I).^[61] Accordingly, within alkali metal zincate chemistry, diazadiene ligands have played an important role in the synthesis of compounds containing Zn–Zn bonds. Complexes containing a formal Zn(I) cation have been systematically generated by the chemical reduction of a mixture of ZnCl₂ and a diimine ligand of form RN=CR'–CR'=NR by an alkali metal. Examples include the sodium zincates $\{(\text{Et}_2\text{O})\text{Na}[(\text{Dipp})\text{NCH}=\text{CHN}(\text{Dipp})]\text{Zn}\}_2$ ^[62] and $\{(\text{THF})_2\text{Na}[(\text{Dipp})\text{NC}(\text{Me})=\text{C}(\text{Me})\text{N}(\text{Dipp})]\text{Zn}\}_2$,^[63] as well as the potassium analogue

$\{(\text{THF})_2\text{K}[(\text{Dipp})\text{NC}(\text{Me})=\text{C}(\text{Me})\text{N}(\text{Dipp})]\text{Zn}\}_2$ [Dipp = 2,6-(*i*Pr) C_6H_3].^[64] When the sterics of the diazadiene ligand are not conducive to the formation of a Zn–Zn bond then divalent complexes akin to **24** are often the result. When ZnCl_2 is utilised then complexes with a 2:1 diazadiene:zinc stoichiometry is the result, such as $[(\text{THF})\text{Na}]_2[(\text{Mes})\text{NC}(\text{Me})=\text{C}(\text{Me})\text{N}(\text{Mes})]_2\text{Zn}$,^[62] $[(\text{Et}_2\text{O})\text{Na}]_2[(\text{Dipp})\text{NC}(\text{Me})=\text{C}(\text{Me})\text{N}(\text{Dipp})]_2\text{Zn}$ ^[64] and $\text{K}_2\{[2,6\text{-(Et)}\text{C}_6\text{H}_3]\text{NC}(\text{Me})=\text{C}(\text{Me})\text{N}[2,6\text{-(Et)}\text{C}_6\text{H}_3]\}_2\text{Zn}$.^[64] If the zinc source is changed for an alkyl reagent then alkyl amido complexes such as $\{(\text{Et}_2\text{O})\text{K}[(t\text{Bu})\text{NCH}=\text{CHN}(t\text{Bu})]\text{Zn}(\text{Bz})\}_\infty$ ^[65] and $\{(\text{THF})\text{K}[(t\text{Bu})\text{NCH}=\text{CHN}(t\text{Bu})]\text{Zn}(\text{Me})\}_\infty$,^[66] are the result; in both cases the coordination sphere of the potassium being supplemented by intermolecular interactions to adjoining diazadiene ligands to produce polymeric chains. In all of the examples above, as in **24**, the diazadiene adopts a *cis*-conformation chelating the zinc centre. However, within zincate chemistry there is one example, $[(\text{Et}_2\text{O})\text{K}]_2[(\text{Dipp})\text{NCH}=\text{CHN}(\text{Dipp})]_3\text{Zn}_2$,^[62] of a diazadiene ligand in a *trans*-conformation adopting a bridging role between two zinc cations. The electronic versatility of diazadiene ligands was exploited by van Koten to synthesise the homologous series of zinc complexes $\text{K}_x[(t\text{Bu})\text{NCHCHN}(t\text{Bu})]_2\text{Zn}$ ($X = 0, 1, 2$ Scheme 9.4) through successive one electron reductions with stoichiometric quantities of elemental potassium.^[67] This series highlights the diazadienes ability to reside in the formal 0, -1, and -2 oxidation states. No successful synthesis of a lithium zincate diazadiene complex had previously been achieved although other metal combinations such as $\text{K}:\text{Mg}$,^[68] $\text{Li}:\text{Ga}$ ^[69] and $\text{K}:\text{Ga}$ ^[70] have been reported. Again these complexes were synthesised starting from diimino precursors. Importantly, our synthesis of **24** is, to the best of our knowledge, the only synthesis of a diazadiene “ate” complex starting from a saturated diamine.

The closest analogy to the synthesis of **24** was reported by Veith who formed 1,3-diaza-2-silacyclopentene by the double lithiation of $(t\text{Bu})\text{NHCH}_2\text{CH}_2\text{NH}(t\text{Bu})$ with $n\text{BuLi}$ followed by an electrophilic quench with $\text{Cl}_2\text{Si}(\text{Me})\text{N}(\text{H})t\text{Bu}$ (Scheme 9.5).^[71] It was

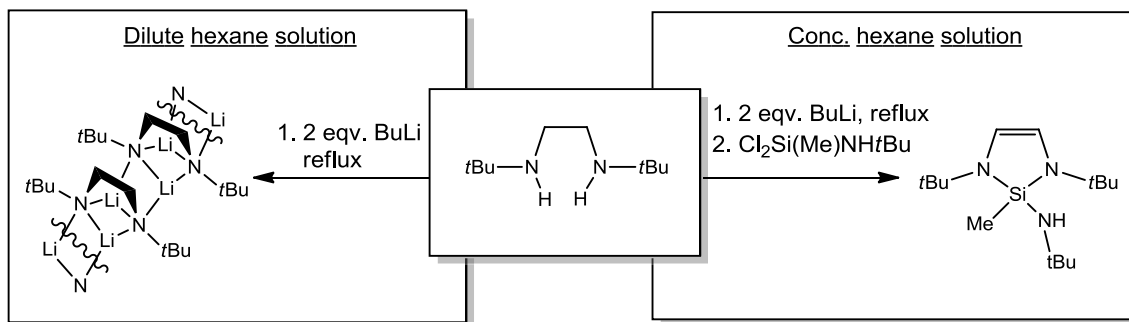
acknowledged at the time that the process leading to this dehydrogenation was unclear



Scheme 9.4: Homologous series of potassium zincates demonstrating the electronic versatility of the diazadiene ligand.

but it was noted that the reaction was highly concentration dependent. For dehydrogenation to occur the lithiation step needed to be carried out in a highly concentrated $n\text{BuLi}$ hexane solution (ca. 2M). The lithiated intermediates were never characterised in Veith's study. We have confirmed by NMR spectroscopy that $(i\text{Pr})\text{NHCH}_2\text{CH}_2\text{NH}(i\text{Pr})$, like its homologue $(t\text{Bu})\text{NHCH}_2\text{CH}_2\text{NH}(t\text{Bu})$, can be activated when refluxed in a concentrated $n\text{BuLi}$ solution. Importantly, when the reaction was carried out at concentrations akin to that used in the synthesis of **24** then no unsaturated products were observed. This concentration dependence infers a different mechanism of hydrogen activation in the homometallic transformation from that which results in the synthesis of **24**, possibly involving either larger aggregates or an intermolecular process. The dilithiated species, produced on refluxing two molar equivalents of $n\text{BuLi}$ in a dilute hexane solution of the diamine $(i\text{Pr})\text{NHCH}_2\text{CH}_2\text{NH}(i\text{Pr})$ could be crystallised as a TMEDA solvate (Figure 9.7). This product, $[(\text{TMEDA})\text{Li}(i\text{Pr})\text{NCH}_2\text{CH}_2\text{N}(i\text{Pr})\text{Li}]_2$ **25** has a distorted ladder structure in the solid state with the diamido ligands adopting a trans-bent conformation allowing them to bridge between opposite corners of alternate rungs. The rungs of the ladder differ little in length with Li–N bond distances in the range of 1.977(3) Å– 2.025(2) Å. In contrast, the edges exhibit distinct variation in length with Li–N bond distances of 2.227(2) Å and 1.971(2) Å between the outer rungs and 2.057(2) Å between the inner rungs. Maintaining the C_2 axis of symmetry, the long and short edges of the ladder alternate as the ladder is ascended. The distortion in the edge lengths generates a screw twist along the ladder. Both outer lithium centres adopt distorted

tetrahedral geometries while the internal lithium atoms are three coordinate. Gardiner postulated that donor free $\text{Li}(t\text{Bu})\text{NCH}_2\text{CH}_2\text{N}(t\text{Bu})\text{Li}$ polymerised as an infinite ladder (Scheme 9.5).^[51] This trapping of a ladder segment instigated by the Lewis base TMEDA supports Gardiner's assertions.



Scheme 9.5: Contrasting fates of the diamine $(t\text{Bu})\text{N}(\text{H})\text{CH}_2\text{CH}_2\text{NH}(t\text{Bu})$ on reflux with two molar equivalents of BuLi depending on the concentration of the reaction.

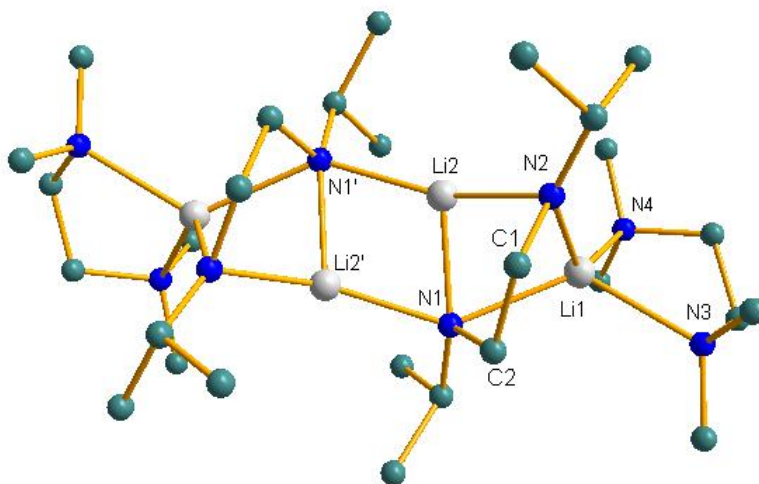


Figure 9.7: Molecular structure of the di-lithium diamido $[(\text{TMEDA})\text{Li}(i\text{Pr})\text{NCH}_2\text{CH}_2\text{N}(i\text{Pr})\text{Li}]_2$ 25. Hydrogen atoms and minor disordered TMEDA components have been omitted for clarity. Symmetry operations to generate equivalent atoms: $-x, y, 0.5-z$. Selected bond lengths [\AA] and angles [$^\circ$]: Li1-N1 2.227(2), Li1-N2 1.977(3), Li1-N3 2.209(3), Li1-N4 2.199(3), Li2-N1 2.025(2), Li2-N2 1.971(2), Li2-N1' 2.057(2), N1-C2 1.460(2), N2-C1 1.458(2), C1-C2 1.521(2), N1-Li1-N2 81.23(9), N1-Li1-N3 125.9(1), N1-Li1-N4 129.1(1), N2-Li1-N3 117.3(1), N2-Li1-N4 125.26(1), N3-Li1-N4 83.34(1), N1'-Li2-N1 109.6(1), N1'-Li2-N2 151.4(1), N1-Li2-N2 86.7(1).

In an attempt to understand the process by which the saturated diamido complex **19** converts to the diazadiene **24**, ^7Li NMR spectroscopy was employed, allowing for the facile monitoring of this highly unusual transformation. A ^7Li NMR spectrum of isolated crystals of the cocomplexation product $(\text{TMEDA})\text{Li}[(i\text{Pr})\text{NCH}_2\text{CH}_2\text{NH}(i\text{Pr})]\text{Zn}(t\text{Bu})_2$ **18**, with a fully saturated $\text{NCH}_2\text{CH}_2\text{N}$ backbone and one N–H bond, in C_6D_6 solution reveals two major resonances at -0.37 ppm and 0.63 ppm, suggesting a mixture of products. When this solution is gently warmed and reanalysed, the resonance at -0.37 ppm is absent, intimating that the product associated with this low-frequency resonance has been fully consumed, and only the resonance at 0.63 ppm remains (Figure 6.8). This is consistent with the disappearing resonance at -0.37 ppm representing the bisalkyl zincate **18** which, in an intramolecular deprotonation with concomitant release of isobutane, forms the diamido complex **19**, in which the two N–H bonds have been deprotonated. Further support for this interpretation can be found when considering how close the signal assigned to complex **19** (0.63 ppm) comes to that of the structurally analogous propylene derivative **21** (0.75 ppm, that is, a difference of only 0.12 ppm). When the reaction was repeated *in situ* at 0°C and an aliquot removed and analysed by ^7Li NMR spectroscopy, two pertinent resonances at -2.39 ppm, and 1.71 ppm, as well as the resonance belonging to the previously identified intermediate **19**, can be observed (Figure 6.8). ^7Li DOSY (diffusion ordered spectroscopy) NMR experiments reveal that the intermediate responsible for the resonance at 1.71 ppm has a molecular weight similar to that of **19**, presumably ruling out an aggregation process for the formation of this, as yet, unidentified species. Comparison with the ^7Li NMR spectra of the diazaethene **24** in C_6D_6 reveals that the signal at -2.39 ppm is the result of a trace amount of this final product. Due to the highly reactive, transient existence of the bis-alkylzincate **18**, its presence is not detected in this *in situ* NMR study. Another aliquot of the solution was removed after a 2-day stir at room temperature, but the recorded ^7Li NMR spectrum indicated no significant further compositional change had taken place. Aliquots were then removed after intervals of 5 min, 1 h, and 2 h reflux time, and the recorded spectra revealed a gradual transformation from the saturated intermediate **19** to the unsaturated final product **24** (Scheme 9.6). After 2 h reflux, decomposition of the reaction mixture is evidenced by

the deposition of a black solid. Any further intermediates along the reaction pathway must be too short lived to be visible on the NMR time scale.

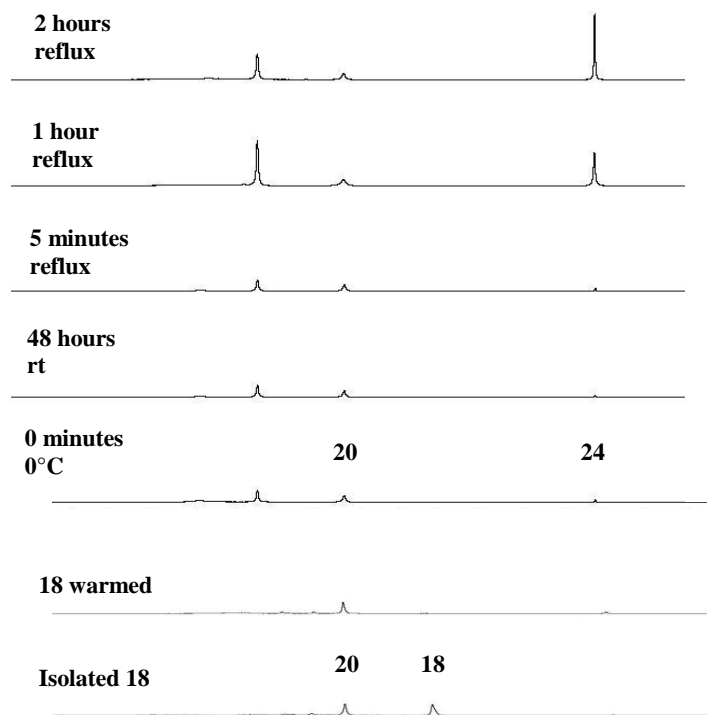
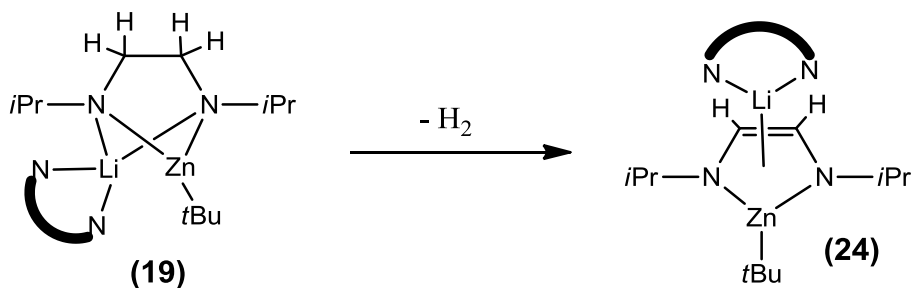


Figure 9.8: Monitoring of the conversion of 18 to 24 by ^7Li NMR spectroscopy. All spectra are scaled to a consistent peak height for the resonance associated with zincate 19.



Scheme 9.6: Conversion of 19 to 24 on reflux with the formal elimination of H_2 .

A highly effective protocol for dehydrogenation adjacent to nitrogen has been developed by Brookhart utilising the cobalt catalyst $(\text{Cp}^*)\text{Co}(\text{CH}_2=\text{CHSiMe}_3)_2$ (Cp^* = pentamethylcyclopentadienyl). Reaction of a variety of cyclic tertiary amino substrates bearing a dimethylvinylsilane side arm were investigated.^[72] Dissociation of one

vinyltrimethylsilane ligand to give the 16 electron complex $(\text{Cp}^*)\text{Co}(\text{CH}_2=\text{CHSiMe}_3)$ followed by association of the substrate through its vinylic silyl group is believed to open the catalytic cycle (Figure 9.9). This is then believed to be followed by CH activation adjacent to the nitrogen producing an 18 electron Co(III) hydride complex. Next, addition across the vinylic silyl group is expected to produce a Co(III) complex containing a five-membered Co-C-N-Si-CH(CH₃) ring. β -hydride elimination completes the unsaturation adjacent to the nitrogen followed by reductive elimination to provide the final product. The protocol was also successfully extended to the noncyclic diamine (*cyclo*-CH₂CH₂OCH₂CH₂N)CH₂CH₂N[Si(Me)₂CH=CH₂][Si(Me)₂CH₂CH₃] with no interference from the morpholine side arm. Goldman has also demonstrated that the iridium catalyst employing a PCP pincer ligand {2,6-[(*t*Bu)₂PCH₂]₂C₆H₃}IrH₂ can be utilised to form enamines from tertiary amines.^[73] In this case an intermolecular mechanism is envisaged with two molar equivalents of *tert*-butylethylene added to the reaction to provide a final resting place for the cleaved hydrogen atoms. Interestingly, similar results cannot be produced for secondary amines, the same catalyst instead selectively furnishing the imine.^[74] While superficially the transformations achieved by Brookhart and Goldman resemble the synthesis of the diazadiene **24** from the diamide **19**, the synthesis of the latter must be mechanistically distinct. Firstly, in our own synthesis there are no redox active metals capable of facilitating oxidative addition or reductive elimination reactions. This can have major cost implications for the utility of these competing reaction protocols with Alfa Aesar currently selling ZnCl₂ for £1.00 per gram (for 99.99% pure material), compared with £10.00 per gram CoCl₂ (for 99.9% pure material) and £92.20 per gram IrCl₃ (for 99.99% pure material).^[75] If such a main group synthesis could be developed which was as widely applicable as these transition metal catalysts it could constitute a significant advancement. However, the scope of our protocol remains unproven (see later 9.4 Scope and limitations). Secondly, unlike the reactions of Brookhart and Goldman, there is no obvious hydrogen acceptor in our synthesis of the diazaethene **24**.

Instead, we hypothesise that the dehydrogenation of the diamide **19** could be the result of a β -hydride elimination process followed by deprotonation via the hydride to produce the

unsaturated **24** with concomitant release of hydrogen gas (Figure 9.10). A similar reaction mechanism has been postulated for the transformation of the dibenzylamido species $\text{NaN}(\text{CH}_2\text{Ph})_2$ into the aza-allyl species $\text{Na}(\text{PhCHNCHPh})$.^[76] The insoluble (in non-donating media) donor free sodium amide $[\text{NaN}(\text{CH}_2\text{Ph})_2]_\infty$, and the TMEDA

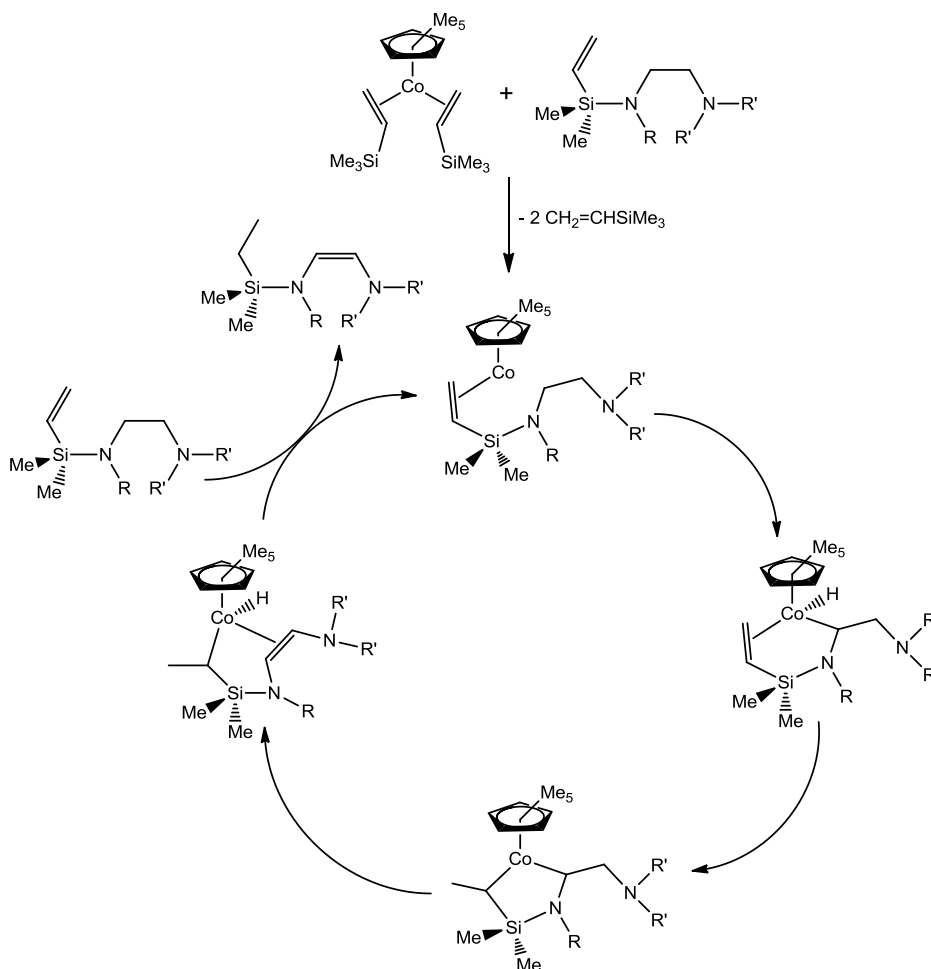


Figure 9.9: Proposed catalytic cycle for the unsaturation adjacent to nitrogen utilising the cobalt catalyst $(\text{Cp}^*)\text{Co}(\text{CH}_2=\text{CHSiMe}_3)_2$.

solvated dimer species $[(\text{TMEDA})\text{NaN}(\text{CH}_2\text{Ph})_2]_2$ are both stable under an inert atmosphere at room temperature. However, the PMDETA solvate $(\text{PMDETA})\text{NaN}(\text{CH}_2\text{Ph})_2$, or the TMEDA solvate in the additional presence of THF were both found to rapidly convert to the aza-allyl complexes $(\text{PMDETA})\text{Na}(\text{PhCHNCHPh})$ and $(\text{THF})(\text{TMEDA})\text{Na}(\text{PhCHNCHPh})$ respectively.

These observations are consistent with an initial β -hydride elimination, the transition state of which requires monomerisation to take place to set up a four membered transition state. The apparent dependency of aza-allyl formation on the aggregation state of the amido complex is in agreement with the strict steric conditions required for β -hydride elimination to proceed, passing through a stereospecific cyclic transition state.^[77] Deprotonation of the expected imino product $\text{PhCH}=\text{NCH}_2\text{Ph}$, a known compound, by the *in situ* generated NaH can then yield the aza-allyl species. The plausible nature of this final deprotonation step was confirmed by reacting commercially available NaH with an authentic sample of the imine in the presence of PMDETA, which resulted in the formation of the aza-allyl species $(\text{PMDETA})\text{Na}(\text{PhCHNCHPh})$. Importantly however, despite in theory being a more direct synthesis, the formation of the aza-allyl species from the imine and NaH resulted in a much reduced yield compared with the *in situ* synthesis starting from the sodium amide. This is most probably a reflection of the poor solubility of NaH, and implies that the *in situ* reaction mixture is playing an important role in solubilising, and hence activating, the produced NaH.

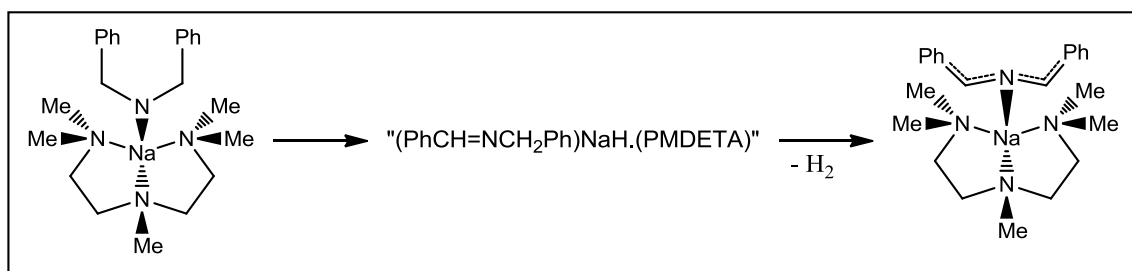
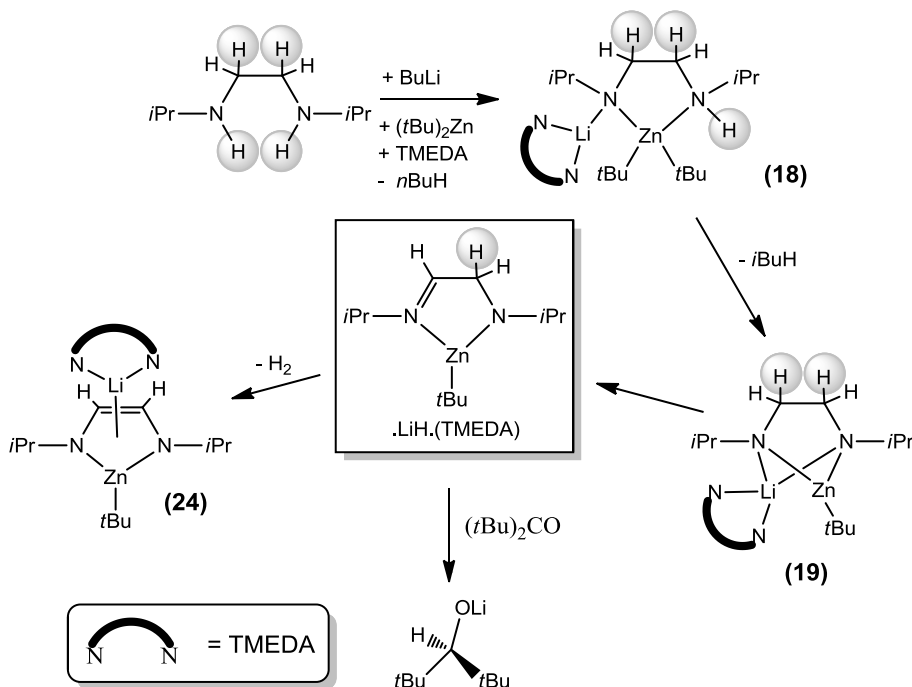


Figure 9.10: Spontaneous conversion of a sodium amide to an aza-allyl formulation postulated to proceed via β -hydride elimination.

In order to probe whether the transformation of the diamide **19** to the diazaethene **24** involves a similar mechanism involving a hydrido intermediate the reaction was repeated in the presence of the electrophilic ketone $(t\text{Bu})_2\text{CO}$ (Scheme 9.7). It was proposed that a hydride intermediate might be evidenced by the formation of the alkoxide ligand $(t\text{Bu})_2\text{C}(\text{H})\text{O}^-$. The bulky ketone $(t\text{Bu})_2\text{CO}$ was chosen to discourage the possibility of competitive alkylation reactions. The *in situ* generation of the diamide **19**, through the co-complexation of $\text{Li}[(i\text{Pr})\text{NCH}_2\text{CH}_2\text{NH}(i\text{Pr})]$ with $t\text{Bu}_2\text{Zn}(\text{TMEDA})$, followed by the

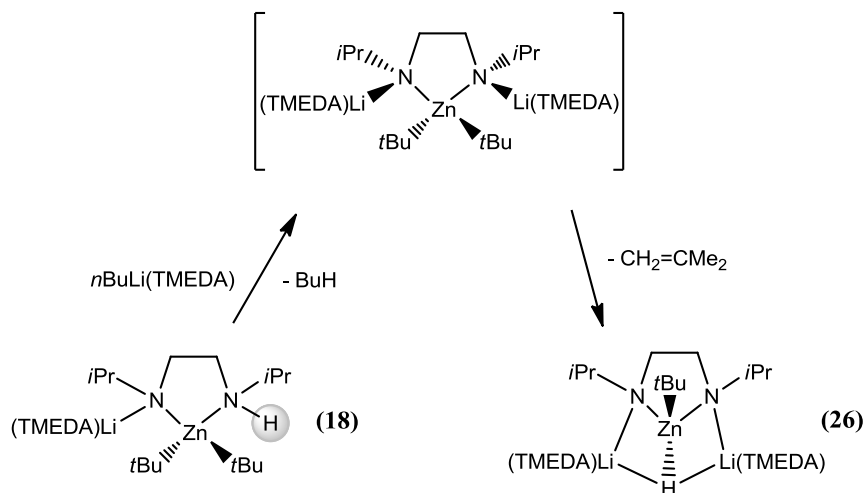
addition of the ketone resulted in a complex mixture of products after twenty-four hours as determined by multinuclear NMR spectroscopy. Comparison of the ^1H , ^{13}C and ^7Li NMR spectra of an aliquot from the reaction in C_6D_6 with a genuine sample of the lithium alkoxide $\text{LiOC}(\text{H})(t\text{Bu})_2$ clearly indicated the reduction of the ketone had taken place. To ensure that the reduction of the ketone was not as a result of its reaction with unreacted BuLi a control reaction was undertaken which revealed that BuLi successfully alkylates $(t\text{Bu})_2\text{CO}$ with no detectable formation of the reduced product. The *tert*-butyl ligands on the zinc were similarly eliminated as a potential source of the hydride by repeating the reaction with Me_2Zn in place of $t\text{Bu}_2\text{Zn}$. Analysis of the resulting liquors again confirmed the presence of the lithium alkoxide $\text{LiOC}(\text{H})(t\text{Bu})_2$.



Scheme 9.7: Proposed reaction mechanism for the formation of 24 highlighting the overall loss of 4 protons from the initial diamine and the trapping of a hydride species by a ketone.

Exploring the chemistry of the initial pre-complex **18** provided further evidence that this mixed metal system can support a hydride species. While maintaining the temperature of a pre-prepared solution of the lithium zincate **18** at 0°C , to prevent zincation of the remaining amino functionality, a molar equivalent of $n\text{BuLi}(\text{TMEDA})$ was introduced in an attempt to synthesise the “higher order” lithium zincate (defined as having more

lithium than zinc atoms, most often a 2:1 stoichiometry)^[78] [(TMEDA)Li]₂[(iPr)NCH₂CH₂N(iPr)]Zn(*t*Bu)₂ (Scheme 9.8). A white precipitate was formed that upon heating dissolved to give a vibrant red solution. Storage of this solution at -30°C provided colourless crystals suitable for X-ray diffraction in a 35% yield. These studies revealed the reaction product to be the higher order lithium zincate molecular hydride species [(TMEDA)Li]₂[(iPr)NCH₂CH₂N(iPr)]Zn(*t*Bu)H **26** (Figure 9.11).



Scheme 9.8: Proposed synthesis of the dilithio zincate hydride via a “higher order” alkyl amido zincate.

Although metal hydride complexes are notoriously insoluble, a reputation perpetuated by common hydride reagents such as LiH and CaH₂, the hydride carrier **26** is soluble in the non polar solvent hexane. This high solubility is achieved despite maintaining the polar alkali metal hydride bond. The structure of zinc hydride **26** bears a partial resemblance to that of the THF solvated dimer **22**, with a [(iPr)NCH₂CH₂N(iPr)]Zn(*t*Bu) complex anion having a lithium cation bound to each nitrogen atom. The Li–N amido bond distances in **26** (average 1.984 Å) are close to those in dimer **22** (average 2.021 Å). Likewise the Zn–N bond distances in hydride **26** [2.074(2) Å and 2.043(2) Å] are only marginally longer than those in alkylamido **22** (average, 2.002 Å) owing to the increased number of anions bound to the zinc. The *tert*-butyl group has been pushed out of the plane of the amido ligand to allow the zinc centre to enter a distorted tetrahedral geometry by binding to the hydride ligand. As in the lithium zincate **22**, the N–C [1.481(3) Å and 1.448(3) Å] and C–C [1.523(4) Å] bond lengths in **26** are consistent with an unactivated ethylene bridge.

Thus the diamide ligand does not appear to be the source of the hydride ligand. The trapped μ_3 -hydride was successfully located and freely refined in the X-ray diffraction study. It caps a Li_2Zn triangle asymmetrically with unequal Li–H bond distances [1.96(2) Å and 2.07(2) Å] and a longer Zn–H bond [2.14(2) Å]. The CCDB^[79] at the time of writing contains only 45 compounds exhibiting a Zn-hydride bond. Excluding an anomalously long contact within a zinc borohydride compound (2.409 Å),^[80] Zn-hydride bond lengths range from 1.409 Å^[81] to 2.167 Å^[82] with an average distance of 1.771 Å. The Zn-hydride contact in **26** is thus long range; to the best of our knowledge, the longest Zn-hydride contact in a non borohydride complex to date (the value of 2.167 Å mentioned above also comes from a borohydride complex). There are currently 147 compounds in the CCDB^[79] (Cambridge Crystallographic Database) containing Li-hydride contacts with their lengths spanning the wide range 1.607 Å^[83] to 2.802 Å.^[84] The average distance (2.044 Å) is comparable with those found in **26**. To the best of our knowledge there are no previously reported zinc μ_3 -hydride complexes. However, there have been various dilithio μ_3 -hydride compounds reported with other metals such as the main group metals Ga,^[85] Al,^[83, 86] the transition metals Zr,^[87] W,^[88] Ta^[88b] Fe^[89]; and the lanthanide Sm.^[90]

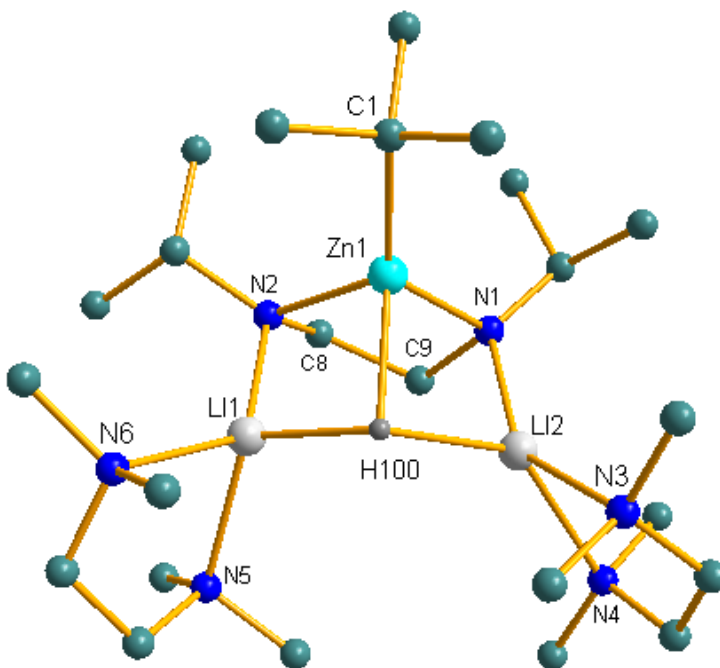


Figure 9.11: Molecular structure of the zincate hydride complex $[(\text{TMEDA})\text{Li}]_2[(i\text{Pr})\text{NCH}_2\text{CH}_2\text{N}(i\text{Pr})]\text{Zn}(t\text{Bu})\text{H}$ **26** with hydrogen atoms (except for the

hydride ion) omitted for clarity. Selected bond lengths [Å] and angles [°]: Li–H100 1.96(2), Li2–H100 2.07(2), Zn1–H100 2.14(2), Li1–N2 1.979(4), Li2–N1 1.989(4), Zn1–N1 2.043(2), Zn1–N2 2.074(2), Zn1–C1 2.045(3), N1–C9 1.481(3), N2–C8 1.448(3), C8–C9 1.523(4), N1–Zn1–H100 92.8(6), N1–Zn1–N2 89.66(8), N1–Zn1–C1 133.1(1), N2–Zn1–C1, 125.19(9), N2–Zn1–H100 92.8(5), H100–Zn1–C1 113.0(6), N2–Li1–N5 121.8(2), N2–Li1–N6 129.6(2), N2–Li1–H100 101.5(6); N5–Li1–N6 85.7(2), N5–Li1–H100 115.9(6), N6–Li1–H100 101.6(6).

Variable-concentration multinuclear (^1H , ^{13}C and ^7Li) NMR spectroscopic studies of **26**, as well as exchange spectroscopic (EXSY) NMR experiments, confirm the presence of a dynamic equilibrium in C_6D_6 solution. As well as resonances consistent with the solid state structure of **26**, resonances attributable to **19** are also observed. This suggests that lithium hydride is associating with and dissociating from **19** (Figure 9.12). Mixed metal zincate complex **19** can thus be thought of as a molecular scaffold for the molecularisation of the usually insoluble polymeric lithium hydride. This association could be important for the synthesis of the diazadiene complex **24** by providing a mechanism to prevent the precipitation of polymeric lithium hydride. Additional control experiments combining lithium hydride powder with the diamido zincate **19** failed to produce the hydride species **26** or to dissolve the ionic lithium hydride suggesting that, while zincate **19** can prevent the aggregation and hence the precipitation of LiH, it is incapable of breaking up the ionic lattice of the solid material (note lithium hydride has a lattice energy of 217.9 Kcal/mol).^[91] An examination of the ^7Li NMR spectrum reveals a doublet with a $^1J_{\text{Li}-\text{H}}$ coupling constant of 13.3 Hz, confirming the retention of the Li–H bond in solution. Observations of such $^1J_{\text{Li}-\text{H}}$ scalar coupling constants are rare. Only a few examples have been detected since the first measurement by Bergman of the iridium metallocene $(\text{Cp}^*)\text{IrH}_2\text{SiMe}_3\text{Li}(\text{PMDETA})$ ($\text{Cp}^* = \text{C}_5\text{Me}_5$, PMDETA = *N,N,N',N'',N'''*-pentamethyldiethylenetriamine) in 1985.^[92] Those detected have coupling constants in the range 6.4 to 14.7 Hz, placing our example at the upper end of those in the literature. Taking advantage of this direct Li–H coupling, a two dimensional ^7Li – ^1H HSQC experiment was performed to determine the chemical shift of the hydride resonance. Surprisingly, two independent ^1H resonances, at 3.27 ppm and 3.19 ppm, were detected coupling with the doublet in the ^7Li NMR spectrum (Figure 9.13). These resonances had previously been masked by others assigned to the diamide ligand. This result can be tentatively assigned to the ^7Li resonance pertaining to the zincate hydride **26** sharing the same chemical shift as “dissociated” (TMEDA)LiH, in agreement with the presence of a

dynamic equilibrium in solution. Alternatively, the two hydride signals in the ^7Li - ^1H HSQC could be the result of an intramolecular flux within complex **26**, for example interchange between the hydride and *tert*-butyl ligands.

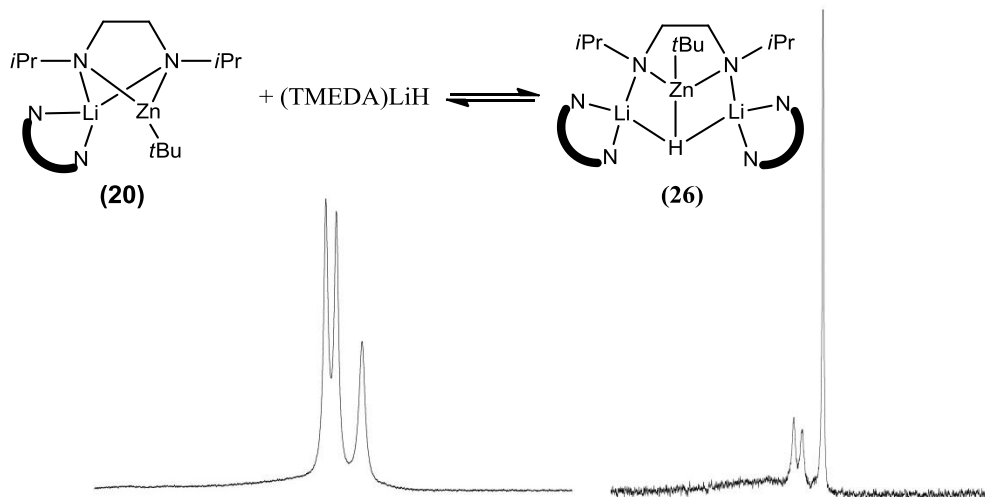


Figure 9.12: High (left) and low (right) concentration ^7Li NMR spectra of the zincate hydride species **26** in C_6D_6 solution with a depiction of the postulated equilibrium.

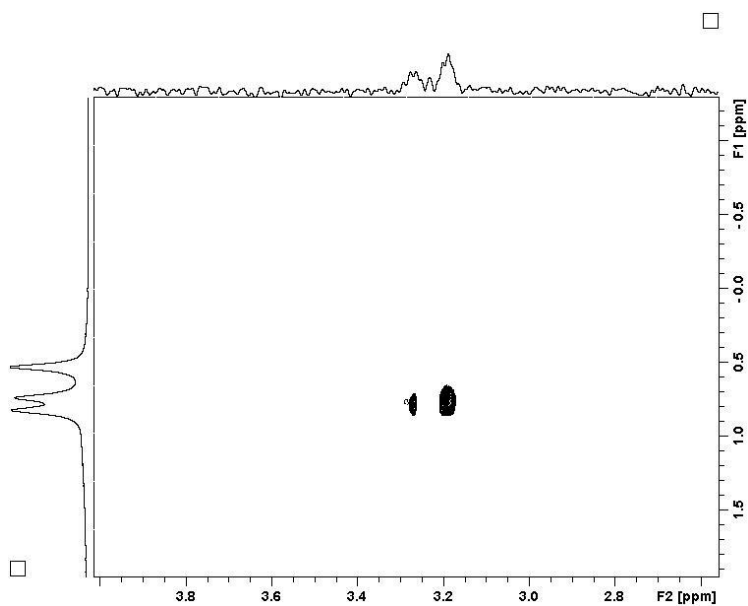
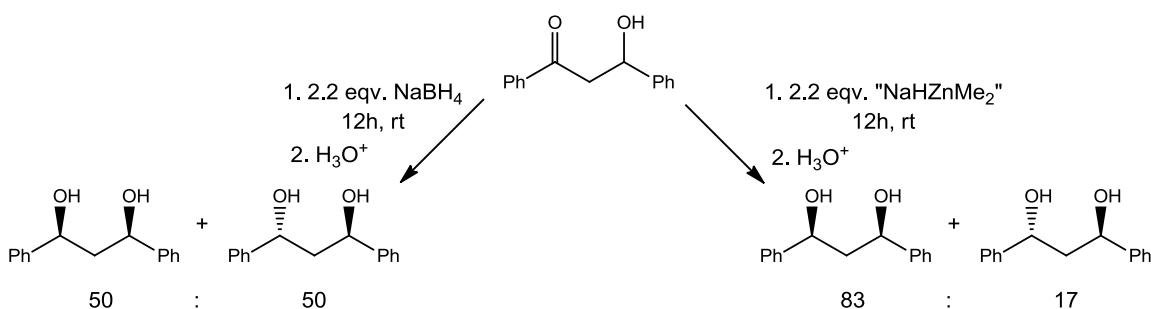


Figure 9.13: ^1H - ^7Li HSQC spectrum of the lithium hydrido species **26** revealing two distinct hydrido signals.

Mixed metal zincate hydrides have repeatedly demonstrated their utility in organic synthesis as reagents for chemoselective, diastereoselective and catalytic reductions.^[93]

Of particular note is the synergic mixture of NaH and Me₂Zn developed by Uchiyama.^[93c] This mixture has been shown to selectively reduce a series of aldehydes, ketones, esters, epoxides and amides in high yielding reactions with effectively no competing alkylation reactions. For example the “NaHZnMe₂” selectively converted the epoxide styrene oxide to the secondary alcohol PhCH(OH)Me in a 92% yield. This result was largely reproduced (94%; 97:3 secondary:primary alcohol) even when Me₂Zn was used catalytically (20 mol%). By comparison, the conventional borohydride reagent NaBH₄ proved unreactive. Betraying the conventional wisdom that more reactive equals less selective, when investigating the reduction of β-hydroxy ketones the zincate “NaHZnMe₂” achieved the diastereoselective reduction of 3-hydroxy-1,3-diphenyl-1-propanone with a pronounced preference for the *anti* product (83:17) while NaBH₄ displayed no selectivity at all (50:50) (Scheme 9.9). Finally the lithium congener “LiHZnMe₂” was shown to selectively partially reduce carboxylic acids to give aldehydes when conventional hydride reagents are known to give exclusively the “fully reduced” alcohols. It is postulated that reduction of the carboxylic acid is advantageously halted at the aldehyde stage by the formation of a highly stable mixed metal zincate species. Despite this undoubted synthetic promise, structurally defined alkali metal zincate hydrides are extremely rare. To date the only examples in the CCDB^[79] are the zinc-zinc bonded ArZn(μ-H)(μ-Na)ZnAr (Ar = C₆H₃-2,6-[C₆H₃-(*i*Pr)₂]₂),^[94] the hetero-cubanes [(*t*BuO)ZnH]_n[(*t*BuO)Li(THF)]_(4-n) (n = 1-4)^[95] and the higher order zincates Na₂[(Et)₂ZnH]₂ and Na₃[(*i*Pr)₃Zn(μ-H)Zn(*i*Pr)₃].^[96] The synthesis and isolation of very soluble, stable and well defined alkali metal zincate hydride species is thus highly desirable.



Scheme 9.9: Selective reduction of a β-hydroxy ketone by the zincate hydride “NaHZnMe₂” contrasted by the aselective reduction by NaBH₄.

As a test reaction to determine how the lithium hydrido-zincate **26** might behave as a reducing agent, the sterically demanding ketone $(t\text{Bu})_2\text{CO}$ was introduced to a pre-prepared hexane solution of the hydride **26** before being stored at -30°C overnight producing colourless crystals. X-ray diffraction and NMR spectroscopic studies revealed the product to be the homometallic alkoxide $[\text{LiOCH}(t\text{Bu})_2]_4$, a tetramer with a distorted cubane structure. The pseudo-tetrahedral geometry around the oxo carbons indicates a successful reduction of the ketone. Also the average C–O bond length of 1.41 \AA is consistent with the formation of an alkoxide. The CCDB^[79] currently holds ten examples of structurally characterised lithium alkoxide cubanes with C–O bond lengths ranging from $1.338 \text{ \AA} - 1.422 \text{ \AA}$.^[97] Of the ten examples, which includes $[\text{LiOCH}(t\text{Bu})_2]_4$,^[97d] seven exhibit solvation of the lithium cations.^[97a-c, 97e, 97f, 97h, 97j] The new alkoxide, $[\text{LiOCH}(t\text{Bu})_2]_4$ is thus one of only three examples of lithium alkoxide cubanes where the steric bulk of the ligands preclude any additional stabilisation of the lithium centres (Figure 9.14).^[97d, 97g, 97i] It is important to note that no mixed metal species has been formed on reaction with the zincate hydride **26**. Instead, this complex reducing agent appears to have behaved as simple LiH. This is perhaps unsurprising given the especially long Zn–H contact in **26** [$2.14(2) \text{ \AA}$] and the apparent dissociation of the complex in C_6D_6 solution to yield the mono-metallic hydride (Figure 9.12). The dilithio zincate hydride **26** is thus of potential utility as a reagent when the product of lithium hydride addition is desired in a non-donor solvent.

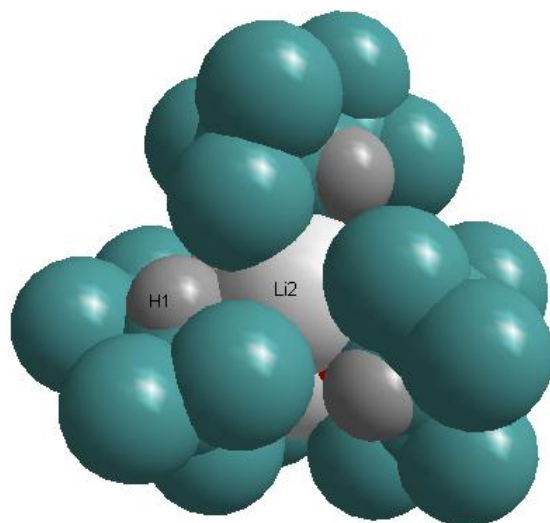


Figure 9.14: Space filling model of the tetrameric cubane $[\text{LiOCH}(t\text{Bu})_2]_4$ demonstrating the considerable steric protection the bulky alkoxide ligands afford the lithium cations.

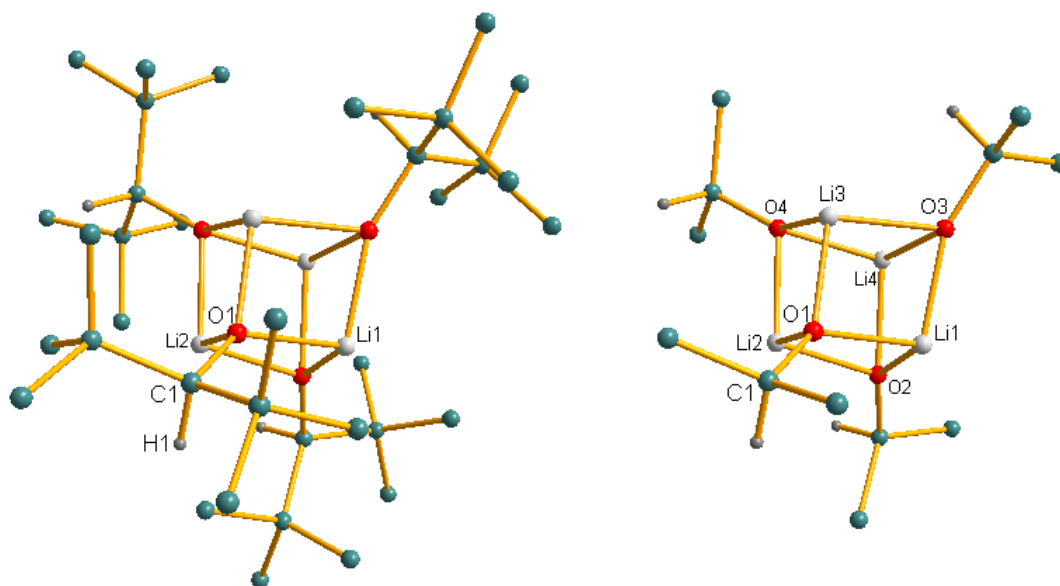


Figure 9.15: Molecular structure of $[\text{LiOCH}(t\text{Bu})_2]_4$ with hydrogen atoms (except OC-H) omitted for clarity (left) and additionally the simplification of *t*Bu groups (right). Selected bond lengths [Å] and angles [°]: Li(1)-O(3) 1.891(3), Li(1)-O(2) 1.929(3), Li(1)-O(1) 1.929(3), Li(2)-O(2) 1.941(3), Li(2)-O(4) 1.947(3), Li(2)-O(1) 1.948(3), Li(3)-O(1) 1.888(3), Li(3)-O(4) 1.901(3), Li(3)-O(3) 1.941(3), Li(4)-O(4) 1.884(3), Li(4)-O(2) 1.943(3), Li(4)-O(3) 1.946(3), O(1)-C(1) 1.410(2), O(2)-C(10) 1.4225(19), O(3)-C(19) 1.4150(18), O(4)-C(28) 1.412(2), O(3)-Li(1)-O(2) 100.51(16),

O(3)-Li(1)-O(1) 98.44(15), O(2)-Li(1)-O(1) 99.71(15), O(2)-Li(2)-O(4) 99.08(15), O(2)-Li(2)-O(1) 98.67(15), O(4)-Li(2)-O(1) 98.49(13), O(1)-Li(3)-O(4) 102.27(14), O(1)-Li(3)-O(3) 98.15(15), O(4)-Li(3)-O(3) 98.22(15), O(4)-Li(4)-O(2) 101.23(15), O(4)-Li(4)-O(3) 98.65(16), O(2)-Li(4)-O(3) 98.12(15), Li(3)-O(1)-Li(1) 80.83(14), Li(3)-O(1)-Li(2) 79.24(13), Li(1)-O(1)-Li(2) 79.79(14), Li(1)-O(2)-Li(2) 79.97(14), Li(1)-O(2)-Li(4) 79.41(14), Li(2)-O(2)-Li(4) 78.53(13), Li(1)-O(3)-Li(3) 80.44(14), Li(1)-O(3)-Li(4) 80.27(14), Li(3)-O(3)-Li(4) 79.25(14), Li(4)-O(4)-Li(3) 81.82(15), Li(4)-O(4)-Li(2) 79.79(14), Li(3)-O(4)-Li(2) 78.92(13).

9.3 DFT calculations

In order to investigate any potential hydride intermediates involved in the synthesis of the diazadiene **24** from the diamido **19**, and to gain insight into how this unexpected transformation may be facilitated by a synergic effect between the two metals, we turned to DFT. All reaction intermediates and transition states were optimised at the M06L^[98] level of theory, the basis set used was 6-311++G(d,p).^[99] Geometry optimizations were carried out with standard procedures based on analytical energy gradients. Frequency calculations were performed to characterize the optimized structures as minima or transition states, where the transition states were found to each have a single imaginary frequency. In addition, the vibrational frequencies were used to obtain temperature corrected energies, enthalpies, entropies, and free energies. All calculations were performed within the Gaussian 09 package.^[100] We first required a suitable model for the starting diamido species **19**. Based on the crystal structure for the propylene homologue **21**, a monomeric structure was computed and found to represent a minimum on the potential energy surface (Figure 9.16). While a direct comparison of the bonding parameters of this model complex **19a** with those obtained experimentally for complex **21** is not possible owing to disorder within the crystal it can be said that the two structures are qualitatively similar. Like complex **21**, model compound **19a** has a tetrahedral lithium centre and trigonal planar zinc lying above and below the plane of the (*i*Pr)NCH₂CH₂N(*i*Pr) ligand respectively. The near symmetrical binding of the lithium and zinc ions by the diamide ligand results in bond lengths which are entirely sensible [Li–N (2.02 Å, 2.05 Å), Zn–N (2.04 Å, 1.99 Å)] and the diamide ligand its self is puckered, with a N-C-C-N torsion angle of 31.4°, as is expected for a fully saturated backbone.

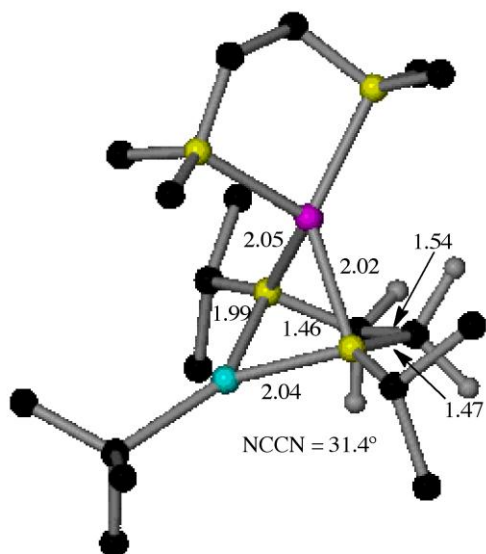


Figure 9.16: Optimized geometry of **19a** with key distances shown in Å. All H atoms, except those involved in the reaction, are omitted for clarity. NCCN refers to the dihedral angle (in degrees) of the diamido ligand.

Two separate mechanisms were envisaged to be plausible for the hydride abstraction from the ethylene backbone; either transfer of one of the lower hydrogens to produce a zinc hydride species [pathway (a)] or alternatively transfer of one of the upper hydrogens to the lithium [pathway (b)]. Plausible intermediates for both processes were found to correspond to minima on the potential energy surface and transition states were successfully computed for both mechanisms. Transference of the hydride to zinc via **19TS(a)** resulted in structure **19Int(a)** (Figure 9.17). Within the transition state the Zn–H contact is computed to be 1.75 Å, in good agreement with the average Zn–H contact contained within the CCDB^[79] of 1.771 Å but considerably shorter than that found in hydrido complex **26** [2.14(2) Å]. This, coupled with the significant C–H bond distance of 1.61 Å reveals that the removal of the hydrogen from the backbone of the ligand is already well progressed at this stage. As an obvious consequence of this hydrogen abstraction the formation of an imino functionality is evidenced by a shortening of the C–N bond distance to 1.33 Å from 1.47 Å calculated for the starting model **19(a)**. As a consequence of gaining a hydrido ligand the zinc centre has broken contact with the imino (previously amido) nitrogen of the (*i*Pr)N=CHCH₂N(*i*Pr) ligand, in order to remain three coordinate, with Zn–N contacts of 2.01 Å and 3.39 Å comparing with 1.99 Å and 2.04 Å found within model complex **19(a)**. Meanwhile the lithium centre within **19TS(a)**

remains tightly bound to both nitrogens of the (*i*Pr)N=CHCH₂N(*i*Pr) ligand and solvated by the diamine TMEDA. Structurally little changes on moving from **19TS(a)** to **19Int(a)**. The Zn–H bond distance has settled at 1.62 Å, which is short but well within the lower limit of 1.409 Å^[81] for Zn–H contacts within the CCDB.^[79] The hydride ligand now resides directly above the C–C bond of the backbone, now 2.93 Å from the carbon from which it was plucked. The fully formed imino N=C double bond is 1.28 Å.

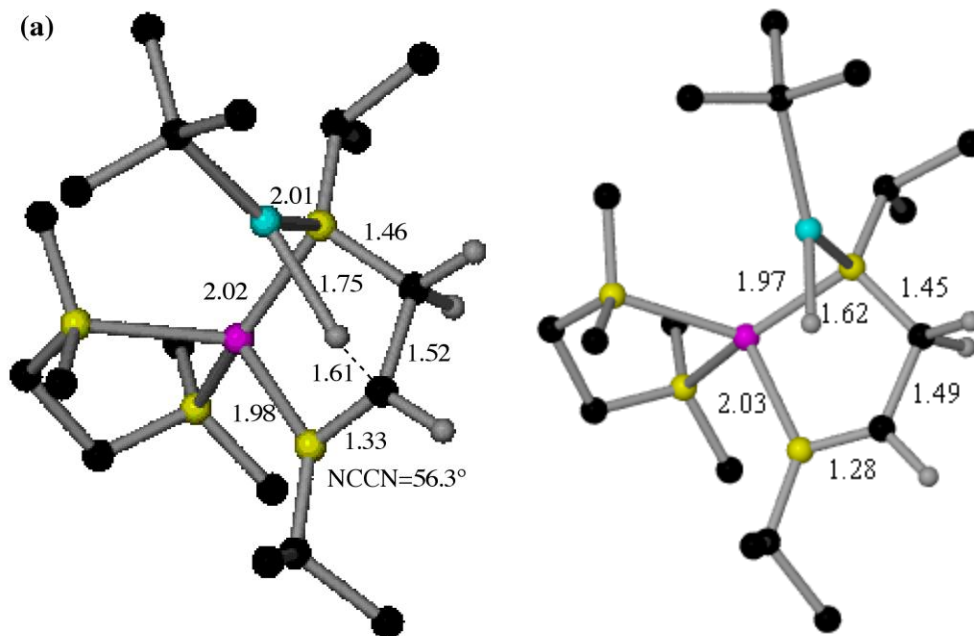


Figure 9.17: Optimised geometry for transition state 19TS(a) (left) and intermediate 19Int(a) (right) along the reaction pathway (a). All distances shown are in Å. All hydrogen atoms, except those involved in the reaction, omitted for clarity.

Considering now abstraction of a hydrogen from the ethylene bridge by the lithium, **19TS(b)** leads to the intermediate **19Int(b)** (Figure 9.18). The Li–H bond distance within the transition state of 1.75 Å is already short when compared to the average Li–H contact within the CCDB^[79] of 2.044 Å. This is indicative of a β -hydride elimination which is essentially complete; a fact further supported by an appropriately elongated C–H “contact” (2.40 Å) and an essentially fully formed imino N=C double bond (1.28 Å). Analogous to the formation of the zinc hydride transition state **19TS(a)**, the formation of the new Li–H bond comes at the expense of a Li–N contact with bond lengths of 2.05 Å and 2.02 Å in the starting **19(a)** comparing with 2.08 Å for the remaining Li–N_{amido} contact while the newly formed imino nitrogen lies a distant 3.60 Å from the lithium

centre. Thus, in a complete reversal of roles from pathway (a), the zinc centre holds the (*i*Pr)N=CHCH₂N(*i*Pr) in place, remaining chelated by both of its nitrogen atoms. However, the developing asymmetric nature of this chelation (Zn–N_{amido} 1.96 Å, Zn–N_{imino} 2.12 Å) compared with that found within complex **19(a)** (Zn–N 1.99 Å and 2.04 Å) is a reflection of the reduced charge now found on the imino nitrogen atom in **19TS(b)**. Unlike the transformation of **19TS(a)** to the intermediate **19Int(a)**, the proposed intermediate **19Int(b)** entails a significant rearrangement with respect to **19TS(b)**. The most noteworthy change on moving from **19TS(b)** to **19Int(b)** is the relocation of the hydride ligand away from the (previously) ethylene bridge to allow the lithium to share its new highly anionic ligand with the Lewis acidic zinc centre. This results in zinc adopting a distorted tetrahedral geometry with a short Zn–H contact of 1.68 Å, marginally longer, and hence potentially more reactive, than that found within **19Int(a)** (Zn–H 1.62 Å). The sharing of the hydride ligand between both metal centres also results in a modest increase in the Li–H contact from 1.75 Å to 1.89 Å. To compensate for the weakening of the Li–H interaction, a strengthening of the Li–N_{amido} bond results in a short 1.96 Å separation. This is comparable to the value obtained experimentally for the alkyl amido zincate cocomplexation product **18** [1.993(3) Å]. These comparable separations betray a close structural relationship between **19Int(b)** and **18** owing to both complexes possessing an amido ligand bridging through a C₂ chain to a neutral nitrogen donor. However, the contrasting steric requirements and bridging ability of the *tert*-butyl ligand in **18**, compared with the hydride in **19Int(b)**, precludes a similar sharing of anionic ligands between both metal centres.

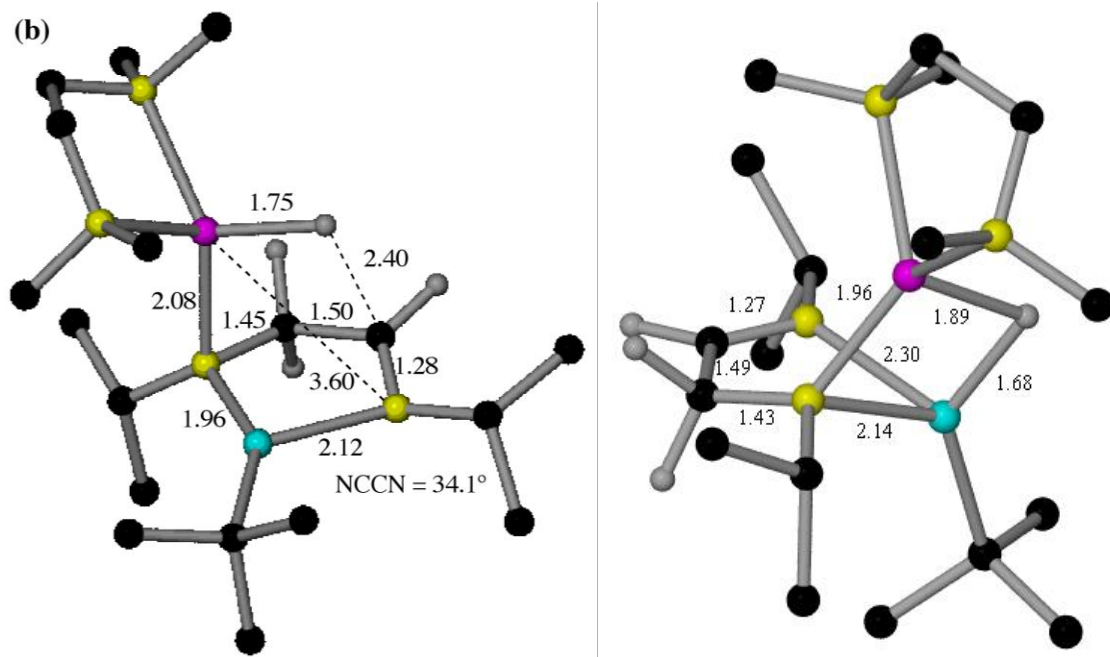


Figure 9.18: Optimised geometry for transition state 19TS(b) (left) and intermediate 19Int(b) (right) along the reaction pathway (b). All distances shown are in Å. All hydrogen atoms, except those involved in the reaction, omitted for clarity.

Now, examining the energetics of both pathway (a) and pathway (b), they are both found to be endothermic relative to **19(a)** (Figure 9.19). The zinc hydride species **19Int(a)** is found to be 14.7 kCal/mol less stable than **19(a)** while **19Int(b)** is found to be 8.6 kCal/mol less stable than the starting complex. Although the product of abstraction by lithium [pathway (b)] **19Int(b)** is more stable than the alternative zinc hydride species **19Int(a)** by 6.1 kCal/mol, this is insufficient to preclude **19Int(a)** as a viable reaction intermediate on route to eventual diazadiene formation. Indeed, inspecting the transition states for both pathways reveals a distinct kinetic preference for the formation of **19Int(a)** with an activation barrier of 23.2 kcal/mol for pathway (a) contrasting with 31.8 kCal/mol for pathway (b). However, 31.8 kCal/mol is still accessible under the reaction conditions used experimentally (refluxing hexane). Turning to the second step of the transformation, pathway (a) was completed in an exothermic reaction ($\Delta G = -13.2$ kCal/mol) to yield the diazadiene product **24(a)** and hydrogen gas. The transition state **19TS(a-2)** was successfully found for this transformation with a relatively modest energy barrier of 17.4 kCal/mol relative to **19Int(a)** or an overall activation energy of 32.1 kCal/mol relative to the starting diamide **19(a)**. Again these transformations are thus

within the limits of the experimental reaction conditions. Therefore, the overall transformation from the starting diamide **19(a)** to the diazadiene **24(a)** plus hydrogen gas is marginally endothermic ($\Delta G = 1.5$ kcal/mol), essentially thermo-neutral. It should also be noted that the determination that the initial hydride elimination is rate determining coupled with the relatively shallow energy well which **19Int(a)** represents (8.5 kcal/mol with respect to the reverse hydride addition) is consistent with the inability to observe imino products experimentally.

Examining the structural aspects of **19TS(a-2)** (Figure 9.20) it can be seen that the hydride ligand has significantly distanced itself from the zinc relative to **19Int(a)**, with a Zn–H separation of 1.94 Å compared to 1.62 Å. Indeed, the Zn–H distance to the protonic hydrogen (which it should be noted is being extracted from the same face of the (iPr)NCH₂CH₂N(iPr) ligand as the hydride was previously removed) of 2.29 Å, which is entering the range of Zn–H bond lengths listed within the CCDB [1.409 Å^[81]-2.167 Å^[82]

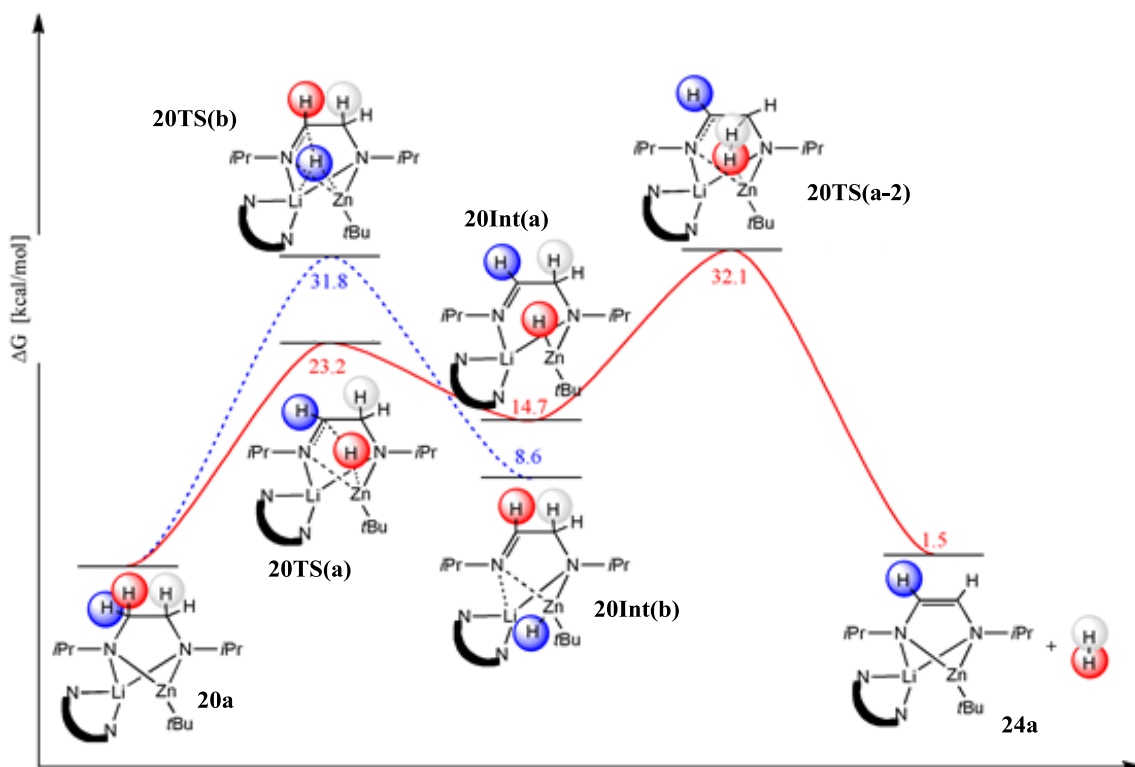


Figure 9.19: Free energy profile for the transformation of the diamide **19a** into the diazadiene species **24a**. Pathway (a) is in red while the dashed blue line refers to pathway (b).

Excluding an anomalously long contact within a zinc borohydride compound (2.409 Å)^[80], along with a H–H contact of 0.92 Å, could almost permit **19TS(a-2)** to be described as a dihydrogen complex, although the H–C distance of 1.55 Å demonstrates the deprotonation of the ligand backbone is not yet complete. Indeed, the C–C bond length (1.41 Å) and especially the C–N_{imino} bond distance (1.32 Å) are still somewhat short of their eventual shortening (1.37 Å) and lengthening (1.40 Å) respectively indicating the electronics of the NCCN bridge do not yet resemble the symmetric outcome of the diazadiene **24(a)**. However, the shortening of the Li–N_{imino} interaction from 2.03 Å in **19Int(a)** to 1.95 Å in **19TS(a-2)** suggests an increase in amido character. The complex still requires significant rearrangement to yield the final product, most noticeably the Zn–N_{imino} separation (4.31 Å) has actually increased dramatically from **19Int(a)** (3.65 Å) and must now close to 2.00 Å to give the essentially symmetrical chelate. Also, the lithium centre, which is currently being chelated by both pertinent nitrogen atoms, must now pass under the structure to achieve its final face capping role.

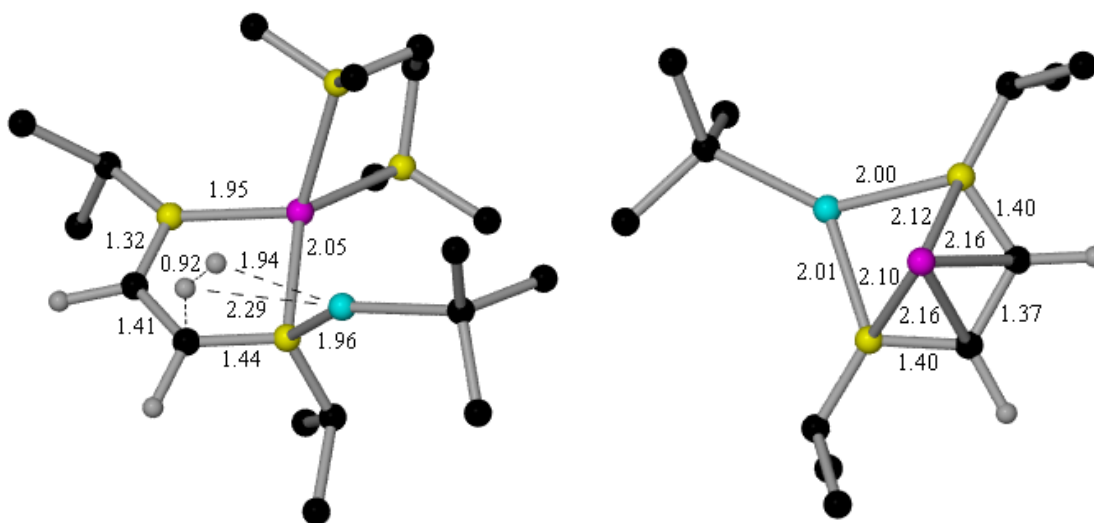


Figure 9.20: Optimised geometry for transition state **19TS(a-2) (left) and the final diazadiene product **24a** (right) along the reaction pathway (a). All distances shown are in Å. All hydrogen atoms, except those involved in the reaction, omitted for clarity as well as TMEDA from **24a**.**

Despite extensive investigations no transition state could be found corresponding to a transformation from **19Int(b)** to the diazadiene **24a**. This coupled with the kinetic

preference to form **19Int(a)** strongly suggests pathway (a) is the more likely mechanistic route. Scouring the reaction pathways investigated for examples of a synergic behaviour of the two metal centres provides some interesting examples. Perhaps the most pivotal example lies in the transition state of the rate determining step **19TS(a)**. As the hydrogen is transferred to the zinc the ligand is able to twist to expose its newly forming N=C π bond to a stabilising interaction with the lithium centre. This is most keenly evidenced by the significant increase in the N-C-C-N torsion angle from 31.4° [**19(a)**] to 56.3° and a shortening of the Li-N interaction from 2.02 Å to 1.98 Å. Turning to the deprotonation step, while the hydride ligand on the zinc is binding to the protonic hydrogen atom the lithium is again moving to stabilise the growing negative charge on the opposite nitrogen demonstrated by a shortening of the Li-N separation from 2.03 Å [**19Int(a)**] to 1.95 Å in **19TS(a-2)**. Also, although the formation of the hydride ligand requires the dissociation of the zinc from the newly formed imino nitrogen [**19Int(a)**], the presence of the lithium ion maintains the chelating mode of the ligand and hence imposes a level of rigidity on the system holding the proton to be removed in close proximity and perhaps having implications for the stereospecific nature of the reaction. Even examining the “failed” pathway (b) it can be seen that the sharing of the hydride ligand between both metal centres apparently leads to a more stable reaction intermediate [$\Delta G = 14.7$ kcal/mol **19Int(a)**] vs [$\Delta G = 8.6$ kcal/mol **19Int(b)**]. To obtain this stable configuration however, the hydride ligand must shift to the front of the complex which has a critical influence on the intermediates reactivity, apparently preventing any intramolecular deprotonation of the second proton.

We also decided to investigate the conversion of the dilithio zincate hydride species **26** to a diazadiene complex through DFT calculations. Experimentally the same reaction conditions that lead to the formation of the unsaturated **24** from the diamide **19** also succeed in producing **24** starting from the hydride species **26**. However, this is easily rationalised when it is considered that **26** appears to be in equilibrium with **19** and (TMEDA)LiH. Regardless, it was decided that a closer look at this tri-metallic complex could prove informative. The model complex **26a** was found to be in broad agreement with the data obtained experimentally (Figure 9.21, Table 9.1). The largest discrepancies

related to the positioning of the hydride ligand, though even these were not unworkable and could well be a result of the difficulties of locating hydrogen atoms crystallographically, rather than any failing of the level of theory employed.

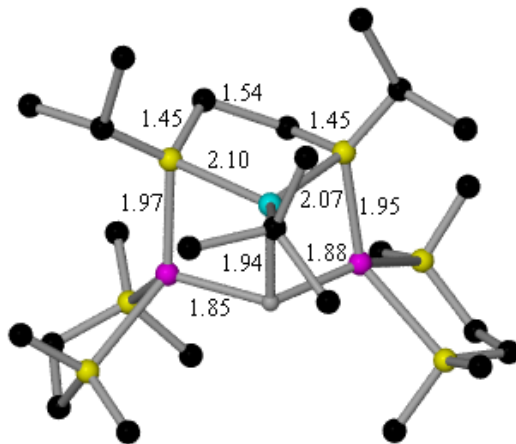


Figure 9.21: Optimized geometry of 26a with key distances shown in Å. All H atoms, except those involved in the reaction, are omitted for clarity.

Table 9.1: Comparison between the geometric parameters determined experimentally 26 and theoretically 26a for the dilithio zincate hydride species.

Bond Length	26	26a	Δ	Angles	26	26a	Δ
Li1 – H100	1.96(2)	1.85	-0.11	N1 – Zn1 – H100	92.8(6)	87.8	-5.0
Li2 – H100	2.07(2)	1.88	-0.19	N1 – Zn1 – N2	89.66(8)	88.2	-1.5
Zn1 – H100	2.14(2)	1.94	-0.20	N1 – Zn1 – C1	133.1(1)	137.3	4.2
Li1 – N2	1.979(4)	1.97	-0.01	N2 – Zn1 – C1	125.19(9)	126.2	1.0
Li2 – N1	1.989(4)	1.95	-0.04	N2 – Zn1 – H100	92.8(5)	90.8	-2.0
Zn1 – N1	2.043(2)	2.07	0.03	H100 – Zn1 – C1	113.0(6)	112.9	-0.1
Zn1 – N2	2.074(2)	2.10	0.03	N2 – Li1 – N5	121.8(2)	118.9	-2.9
Zn1 – C1	2.045(3)	2.05	0.00	N2 – Li1 – N6	129.6(2)	130.2	0.6
N1 – C9	1.481(3)	1.45	-0.03	N2 – Li1 – H100	101.5(6)	97.9	-3.6
N2 – C8	1.448(3)	1.45	0.00	N5 – Li1 – N6	85.7(6)	85.2	-0.5
C8 – C9	1.523(4)	1.54	0.02	N5 – Li1 – H100	115.9(6)	119.4	3.5
				N6 – Li1 – H100	101.6(6)	106.9	5.3

Analogous to the analysis of the transformation of the diamide **19a** to the diazadiene **24a**, we investigated extraction of the hydride by both the lithium [pathway (a)] and the zinc [pathway (b)]. Considering first pathway (a), **26TS(a)** shows both lithium centres play a role in the stabilisation of the newly forming hydride ligand with Li–H distances of 1.82 Å and 2.03 Å (Figure 9.22). The lithium attached to the newly forming imino nitrogen

begins to break away due to the decreasing electron density so that **26Int(a)** holds a more open structure with the imino nitrogen coordinated solely to the zinc and a tightly associated (TMEDA)LiH unit [Li–H 1.78 Å] moving to the periphery of the structure (Figure 9.22).

Considering now extraction by zinc [pathway (b)], a transition state **26TS(b)** and intermediate **26Int(b)** has been found that corresponds to such a transition (Figure 9.23). However, it requires a rearrangement of the complex, essentially switching the positions of the zinc with one of the lithium centres so that a lithium is now chelated by the ligand and the zinc is situated at the bottom of the structure. Now the hydride elimination can occur in a similar mode to pathway (a), assisted by the two non chelated metals, in this case a lithium and zinc centre. It is noteworthy that the hydrogen is removed from the lithium arm of this asymmetric complex in preference to that attached to zinc. The greater

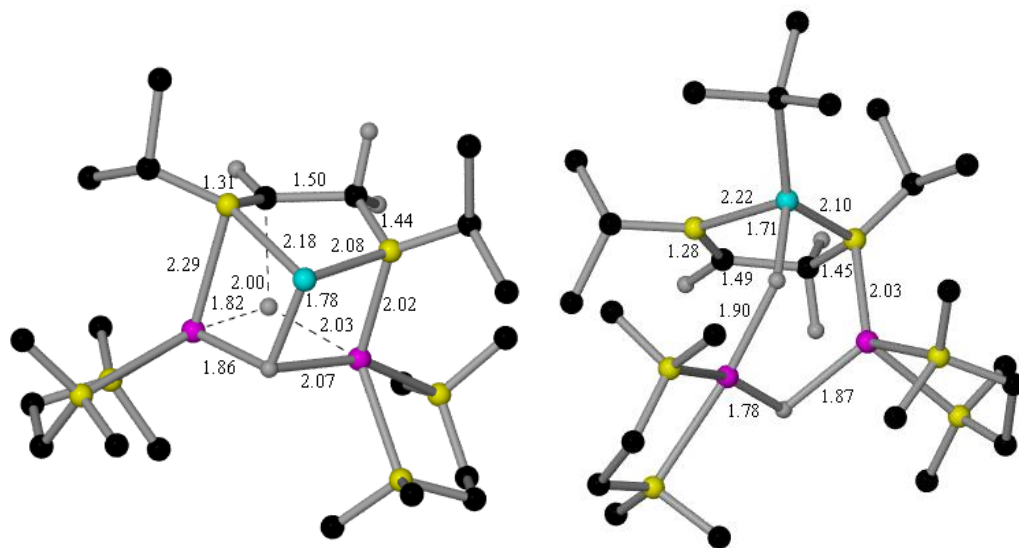


Figure 9.22: Optimised geometry for transition state 26TS(a) (left) and intermediate 26Int(a) (right) along the reaction pathway (a). All distances shown are in Å. All hydrogen atoms, except those involved in the reaction, omitted for clarity as well as the *tert*-butyl ligand from 26Int(a).

Lewis acidity of zinc compared with lithium is evident when comparing **26TS(a)** and **26TS(b)**. In **26TS(b)**, despite being the more distant partner in the removal of the hydrogen, the zinc quickly takes hold of the hydride ligand resulting in a more centralised extraction [Li–H 1.86 Å, Zn–H 1.95 Å] compared to **26TS(a)** [Li–H 1.82 Å and 2.03 Å].

Like **26Int(a)**, **26Int(b)** again appears to be struggling to maintain its integrity with a Li–N_{imino} separation of 2.49 Å.

Examining the energetics for the hydrogen extraction processes starting from the dilithio species **26a**, elimination to lithium [pathway (a)] proceeds with an activation energy of 30.1 kCal/mol to give **26Int(a)** which is 21.7 kCal/mol destabilised relative to **26a**. By comparison the formation of a zinc hydride [pathway (b)] has an energy barrier of 28.4 kCal/mol resulting in the slightly more stable **26Int(b)**, which is 21.1 kCal/mol destabilised relative to **26a** (Figure 9.26). Both of these processes are thus accessible within the experimental conditions employed and so neither pathway was ruled out at this stage.

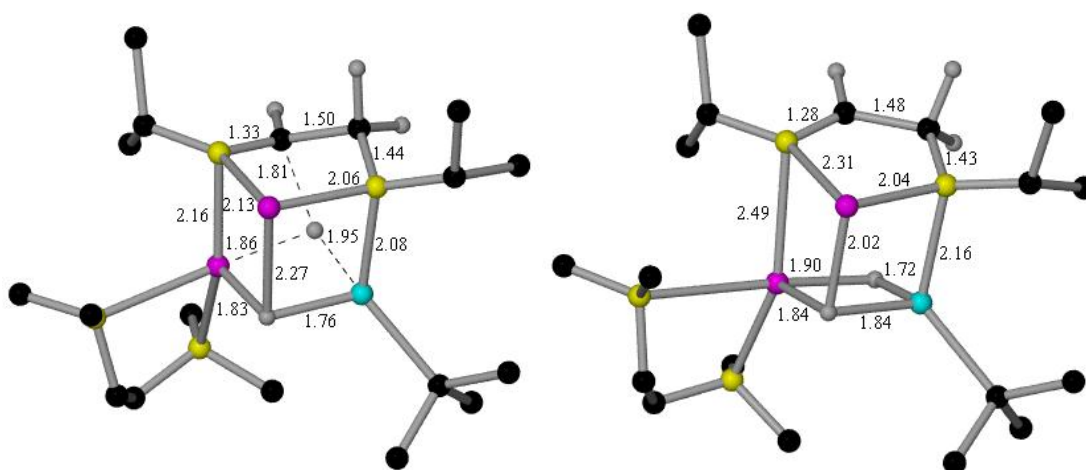


Figure 9.23: Optimised geometry for transition state **26TS(b)** (left) and intermediate **26Int(b)** (right) along the reaction pathway (b). All distances shown are in Å. All hydrogen atoms, except those involved in the reaction and TMEDA ligand, omitted for clarity.

A suitable transition state was found [**26TS(a-2)**] resulting in the formation of the diazadiene species [(TMEDA)Li]₂[(iPr)NCH=CHN(iPr)]Zn(*t*Bu)H **27a** from the intermediary **26Int(a)** (Figure 9.24). The hydride ligand remains supported by both lithium cations as it returns upward to form dihydrogen and complete the unsaturation process. At the same time the reformation of the second amido anion results in a tightening of the complex with the lithium that was essentially expelled from the imino functionality within **26Int(a)** returning to a Li–N separation of 1.97 Å in **27a**. A similar

process was found to facilitate the transformation of **26Int(b)** to the same diazadiene species **27a** via the transition state **26TS(b-2)** (Figure 9.25). The transition state still maintains the lithium in the chelated position so the required rearrangement to furnish **27a** must occur post transition state.

Again, investigating the energetics of both mechanisms, the deprotonation by **26Int(a)** to yield **27a** proceeds with an activation energy of 11.8 kcal/mol (**26TS(a-2)** is 33.5 kcal/mol less stable than **26a**) to yield the diazadiene complex **27a** in an exothermic reaction ($\Delta G = -16.7$ kcal/mol) (Figure 9.26). By comparison the transformation from the zinc hydride species **26Int(b)** proceeds through an activation barrier of 13.3 kcal/mol [**26TS(b-2)** is 34.4 kcal/mol destabilised relative to **26a**], again in an exothermic reaction

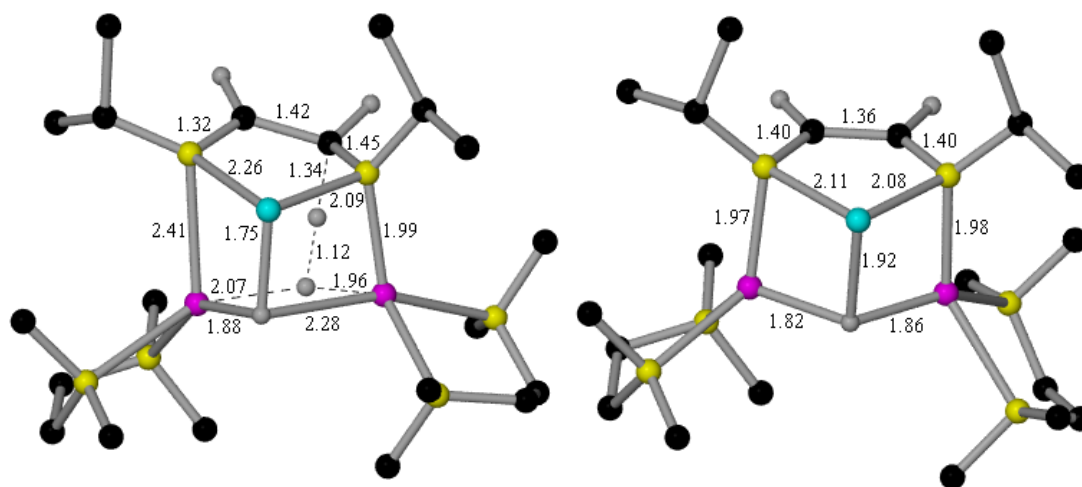


Figure 9.24: Optimised geometry for transition state **26TS(a-2)** (left) and final diazadiene product **27a** (right) along the reaction pathway (a). All distances shown are in Å. All hydrogen atoms, except those involved in the reaction, omitted for clarity as well as the *tert*-butyl ligand.

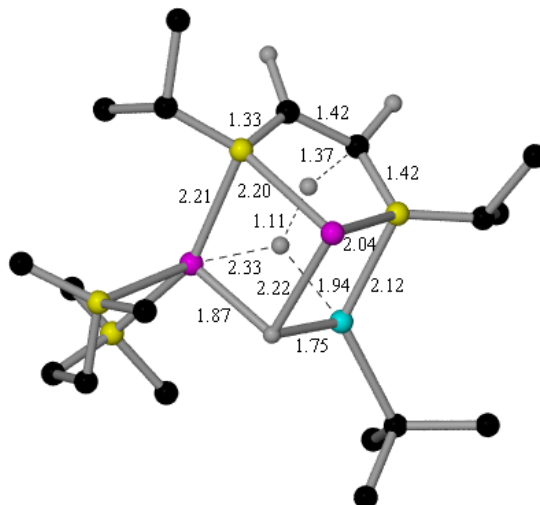


Figure 9.25: Optimised geometry for transition state 26TS(b-2) along the reaction pathway (b). All distances shown are in Å. All hydrogen atoms, except those involved in the reaction, and TMEDA ligand omitted for clarity.

($\Delta G = -16.1$ kcal/mol). This considerable hurdle for the synthesis of the diazadiene complex **27a** from **26Int(b)**, coupled with the much greater accessibility of the reverse reaction (**26Int(b)** to **26a** has an energy barrier of 7.3 kcal/mol) should lead to pathway (b) being disfavoured in preference to pathway (a). The comparable energies involved in the synthesis of **27** from the hydride **26** and of **24** from the diamide **19** should allow both mechanisms to be competitive when both **19** and **26** are present in solution i.e. the dissociation of (TMEDA)LiH from **26** is not required to achieve unsaturation. The energetics also reveal that the diamide complex **19** is more able to coordinate LiH than the diazadiene species **26**, but only by 3.5 kcal/mol. It may thus be thought surprising that only **25**, and not **27**, was obtained when starting from the hydride **26**. This may be explained by examining the structures of both **26Int(a)** and **26Int(b)**. In both cases it can be seen that the imino functionality is struggling to retain the coordinated (TMEDA)LiH. Dissociation of (TMEDA)LiH at this point could lead to the precipitation of LiH_∞ and a switching of reaction pathway from **26a** to **27a** to **19a** to **24a**.

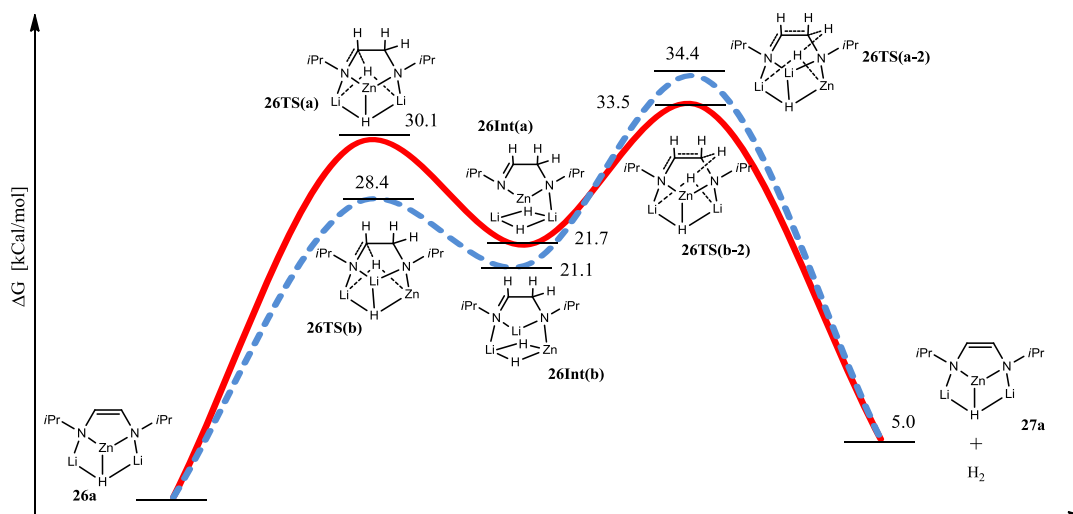


Figure 9.26: Free energy profile for the transformation of the dilithio zincate **26a** into the diazadiene species **27a**. Pathway (a) is in red while the dashed blue line refers to pathway (b). *Tert*-butyl and TMEDA ligands omitted for clarity.

9.4 Scope and limitations

Having discovered this surprising CH activation and investigated its potential synergic origins, we next looked to see how general it might be. First we wished to check the importance of the alkyl group on zinc. We investigated changing from the bulky *tert*-butyl ligand to the sterically benign methyl substituent. This would not only permit us to determine the importance of the sterics at zinc, but also, from a synthetic point of view, the use of Me_2Zn as opposed to $t\text{Bu}_2\text{Zn}$ would be preferable owing to the commercial availability of the former.

Taking a hexane solution of $\text{Li}[(i\text{Pr})\text{NCH}_2\text{CH}_2\text{NH}(i\text{Pr})]$ prepared *in situ* at 0°C and introducing sequentially Me_2Zn and TMEDA followed by a 1.5 hour reflux gave a bright orange solution indicative of diazadiene formation. Storage of the solution at -30°C furnished a crop of yellow crystals in a 44% yield suitable for X-ray diffraction analysis. The product was confirmed as the expected diazadiene species

(TMEDA)Li[(*i*Pr)NCH=CHN(*i*Pr)]Zn(Me) **28**. Furthermore, unlike in the case of the analogous *tert*-butyl species, the X-ray data was of sufficient quality to permit a detailed discussion of the complexes structural parameters. The overall structural motif is the same as that displayed by the *tert*-butyl analogue **24**, with a zinc centre chelated by a (*i*Pr)NCH=CHN(*i*Pr) ligand which also coordinates a (TMEDA)Li cation in a π -fashion (Figure 9.27). The chelation of the zinc is near symmetrical with Zn1–N1 and Zn1–N2 bond distances of 1.966(2) Å and 1.964(2) Å respectively and a bite angle N1–Zn1–N2 of 83.98(9) completing a distorted trigonal planar geometry [including the methyl ligand with a Zn1–C1 bond length of 1.956(3)]. The diazadiene ligand is essentially planar with a N1–C5–C6–N2 torsion angle of 2.2(4)°. The zinc centre lies just below (0.46 Å) the plane defined by the N1–C5–C6–N2 atoms. Apart from the planar nature of the diazadiene ligand, unsaturation can be confirmed by the average N–C and C5–C6 bond lengths of 1.400 Å and 1.349(3) Å respectively. Both isopropyl groups lie staggered with respect to the N1–C5–C6–N2 plane while the lithium sits 1.801(4) Å above it, off centre towards N1 [Li1–N1 2.165(4) Å, Li1–C5 2.235(4) Å, Li1–C6 2.286(4) Å, Li1–N2 2.301(4) Å].

Attempts were also made to vary the metals utilised in the synthesis of the diazadiene species. In an analogous procedure to the synthesis of the lithium zincates **24** and **28**, BuNa, (*i*Pr)N(H)CH₂CH₂NH(*i*Pr), *t*Bu₂Zn and TMEDA were combined sequentially in hexane solution at 0°C. Reflux for 30 minutes again resulted in the characteristic bright orange solution indicative of diazadiene formation. Concentration of the solution and storage at -30°C duly permitted the growth of an orange micro-crystalline material of (TMEDA)Na[(*i*Pr)NCH=CHN(*i*Pr)]Zn(*t*Bu) **29** in a 62% yield. Repeating the synthesis with three molar equivalents of THF in place of the diamine TMEDA allowed for the isolation of colourless crystals in a 26% yield which were suitable for X-ray diffraction

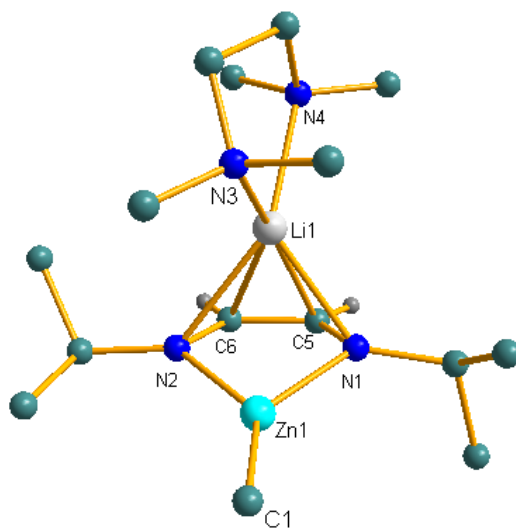


Figure 9.27: Molecular structure of the diazadiene complex **28** with hydrogen atoms, except those of C5 and C6, omitted for clarity. Selected bond lengths [Å] and angles [°]: Zn1-C1 1.956(3), Zn1-N1 1.966(2), Zn1-N2 1.964(2), Zn1-Li1 2.688(4), Li1-N1 2.165(4), Li1-N2 2.301(4), Li1-N3 2.145(4), Li1-N4 2.106(4), Li1-C5 2.235(4), Li1-C6 2.286(4), N1-C5 1.398(3), N2-C6 1.402(3), C5-C6 1.349(3), N1-C5 1.398(3); C-Zn1-N1 136.6(1), C1-Zn1-N2 138.69(9), N2-Zn1-N1 83.98(9), N2-Li1-N3 112.5(2), N4-Li1-N3 86.51(16), N4-Li1-N1 126.8(2), N3-Li1-N1 124.6(2), N4-Li1-N2 139.9(2), N1-Li1-N2 72.1(1).

and revealed the product to be the expected $(\text{THF})_3\text{Na}[(i\text{Pr})\text{NCH}=\text{CHN}(i\text{Pr})]\text{Zn}(t\text{Bu})$ **30**. Unsaturation of the diazadiene ligand is again confirmed by the planarity of the ligand with a N1-C8-C9-N2 torsion angle of $0.212(3)^\circ$. Comparing the C-N [1.398 Å (average)] and C-C [1.353(4) Å] bond distances of the diazadiene core with those found in the methyl lithium analogue **28** [1.400 (average) and 1.349(3) Å] indicates that the change in alkali metal has little effect on the diazadiene ligand. The zinc atom is again chelated essentially symmetrically [Zn-N bond distances 1.957(2) Å and 1.971(2) Å] by the diamide ligand, lying below the plane defined by the NCCN core of the diazadiene ligand by 0.413 Å, marginally less than in the lithium zincate **28** (0.46 Å). This slight discrepancy is most likely explained by the larger sodium cation, relative to lithium, lying further from the diazadiene ligand [Na1-(NCCN) 2.261(1) Å in complex **30** compared with Li1-(NCCN) 1.801(4) Å in the analogous **28**] resulting in reduced steric clashing between the alkylzinc cations and the ligands solvating the alkali metals. Three THF

molecules complete the coordination sphere of the sodium centre. The methine carbons of the isopropyl groups lie in the plane of the diazadiene ligand while their methyl groups protrude above and below this plane.

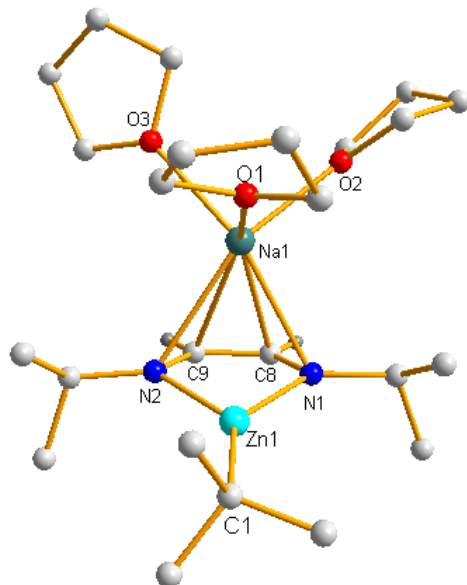


Figure 9.28 Molecular structure of the diazadiene sodium zincate $(\text{THF})_3\text{Na}[(i\text{Pr})\text{NCH}=\text{CHN}(i\text{Pr})]\text{Zn}(t\text{Bu})$ **30**. Hydrogen atoms (except those for C8 and C9) and minor disordered THF components have been omitted for clarity. Selected bond lengths [\AA] and angles [$^\circ$]: Na1–O1 2.350(2), Na1–O2 2.312(2), Na1–O3 2.312(2), Na1–N1 2.587(2), Na1–N2 2.662(2), Na1–C8 2.612(2), Na1–C9 2.649(2), Zn1–N1 1.957(2), Zn1–N2 1.971(2), Zn1–C1 2.009(2), N1–Na1–N2 60.81(6), N1–Zn1–N2 85.14(8), N1–Zn1–C1 139.88(10), N2–Zn1–C1 134.97(10).

Comparing the ^1H NMR spectra in C_6D_6 solution (the THF ligands of complex **30** prove volatile under vacuum and hence dissolution in C_6D_6 for NMR spectroscopic analysis was only achieved on addition of a drop of THF- D_8) of the four diazadiene complexes successfully synthesised thus far $\{(\text{TMEDA})\text{Li}[(i\text{Pr})\text{NCH}=\text{CHN}(i\text{Pr})]\text{Zn}(t\text{Bu})$ **24**, $(\text{TMEDA})\text{Li}[(i\text{Pr})\text{NCH}=\text{CHN}(i\text{Pr})]\text{Zn}(\text{Me})$ **28**, $(\text{TMEDA})\text{Na}[(i\text{Pr})\text{NCH}=\text{CHN}(i\text{Pr})]\text{Zn}(t\text{Bu})$ **29**, $(\text{THF})_3\text{Na}[(i\text{Pr})\text{NCH}=\text{CHN}(i\text{Pr})]\text{Zn}(t\text{Bu})$ **30} reveal some interesting and useful points. First and foremost, the formation of a diazadiene complex is clearly indicated by a diagnostic singlet near δ 6.0 attributable to the $\text{CH}=\text{CH}$ protons and simply distinguished from all other resonances belonging to both starting materials and products (Table 9.2). This provides a simple method for**

determining the success of any further syntheses. The most directly comparable data (lithium complex **24** CH=CH δ 5.83, sodium complex **29** CH=CH δ 6.06) indicates that the switch to the more polarised alkali metal gives rise to a small but rational down field shift of the diazadiene signals. Also, in both lithium species, the methyl signals of the isopropyl groups are split into two equal doublets. By comparison, the ^1H NMR spectra of both sodium complexes exhibit only one resonance for these same methyl groups (Table 9.2). This is indicative of hindered rotation of the isopropyl groups in the lithium complexes in solution due to steric clashing with the solvating diamine TMEDA. This obstruction of the isopropyl groups is lifted on switching to the larger sodium cation by increasing the distance to the solvating ligands on the alkali metal.

Table 9.2: Comparison of selected resonances of the four synthesised diazadiene complexes from ^1H NMR spectra in C_6D_6 .

	CH=CH	<i>i</i>Pr - Me
(TMEDA)Li[(<i>i</i> Pr)NCH=CHN(<i>i</i> Pr)]Zn(<i>t</i> Bu) 24	δ 5.83	δ 1.40, δ 1.32
(TMEDA)Li[(<i>i</i> Pr)NCH=CHN(<i>i</i> Pr)]Zn(Me) 28	δ 5.93	δ 1.42, δ 1.30
(TMEDA)Na[(<i>i</i> Pr)NCH=CHN(<i>i</i> Pr)]Zn(<i>t</i> Bu) 29	δ 6.06	δ 1.44
(THF) ₃ Na[(<i>i</i> Pr)NCH=CHN(<i>i</i> Pr)]Zn(<i>t</i> Bu) 30	δ 5.98*	δ 1.44*

* A drop of THF- D_8 was required to achieve dissolution.

As was achieved with the homologous synthesis of the lithium zincate complex **24**, we attempted to isolate reaction intermediates on route to diazadiene formation in the reaction producing **29**. Although the initial co-complexation adduct “(TMEDA)Na[(*i*Pr)NCH₂CH₂NH(*i*Pr)]Zn(*t*Bu)₂” with one N-H bond still remaining is apparently too short lived to isolate, when the reaction was carried out at 0 °C and the resulting solution stored at -30 °C, it was possible to isolate and fully characterise the dimeric species {(TMEDA)Na[(*i*Pr)NCH₂CH₂N(*i*Pr)]Zn(*t*Bu)}₂ **31** with no N-H bond but containing the saturated ethylene diamido backbone (Figure 9.29) which must exist further along the reaction pathway that ultimately produces **29**. Two independent centrosymmetric molecules of dimer **31** as well as a hexane molecule form the asymmetric unit. Sodium zincate **31** is constructed from a 5–4–5 fused ring system in a

distorted ladder conformation; the two ZnNCCN rings lie *anti* about the strictly planar central ZnN₂ZnN core. The N–C [1.452(6) Å and 1.463(6) Å] and C–C [1.494(7) Å] bond distances are indicative of a fully saturated bisamide. In contrast to in the lithium monomer **5**, the heavier alkali metal binds to only one of the available amido groups, with the core nitrogen atoms (N1, N1a) coordinating exclusively to zinc. Despite the variety of amide environments around zinc, the Zn–N bond distances show little variation (average 2.11 Å). Due to the narrow bite angle of the diamido ligand (85.9°) the zinc centre adopts a distorted tetrahedral geometry. A highly distorted tetrahedral geometry around sodium is also completed by a weak agostic interaction [2.977(6) Å] to a methyl arm of the tertiary butyl ligand on zinc. This is moderately longer than a similar interaction found in the bisalkyl-amido zincate (TMEDA)Na(TMP)Zn(*t*Bu)₂ (2.75 Å).^[25] 5–4–5 fused ring systems have been found before in metal ate complexes containing saturated NCCN diamido ligands. Examples include the lithium lanthanide complexes [(THF)₃Li[1,2-{N(SiMe₃)₂-C₆H₁₀]MCl₂]₂ (M = Nd, Yb)^[101] and the dimeric gallium species [{(Bz)NCH₂CH₂N(Bz)}Li{(Bz)NCH₂CH₂N(Bz)}GaO]₂ (Bz = benzyl, CH₂C₆H₅).^[102]

As well as efforts to change the alkali metal employed in the synthesis of diazadiene complexes, the effect of changing zinc for magnesium or the tri valent aluminium was also investigated. Reacting Na[N(*i*Pr)CH₂CH₂NH(*i*Pr)] with *n*Bu₂Mg in the presence of the bidentate donor TMEDA allowed the isolation and characterization of the fully saturated di-deprotonated {(TMEDA)Na[(*i*Pr)NCH₂CH₂N(*i*Pr)]Mg(*n*Bu)₂ **32** (Figure 9), which adopts a 5–4–5 fused ring distorted ladder structure analogous to the sodium zincate **31**. The ethylene bridges have C–C bond distances of 1.521(4) Å confirming that they remain saturated while the Mg–N bond lengths range from 2.080(2) Å–2.156(3) Å, differing little from the Zn–N bond lengths found in the analogous **31** (average Zn–N bond length 2.11 Å). A long range Na1–C1 [2.966(5)Å, comparable to the Na1–C4 in **31**, 2.977(6) Å] interaction completes a four membered NaNMgC ring. Including this long range contact, magnesiate **32** is thus constructed of a 4–5–4–5–4 fused ring system. Despite the structural similarities between the magnesiate **32** and the zincate **31**, even with extended reflux times of solutions of **32**, no significant levels of diazadiene formation could be detected, as evidenced by the absence of the diagnostic resonance at δ

6.0 in ^1H NMR spectra (Table 9.2). Given the structural resemblance between the magnesium and zinc species, it seems likely that the driving force between the reactivities of these two compounds may be predominantly electronic rather than steric.

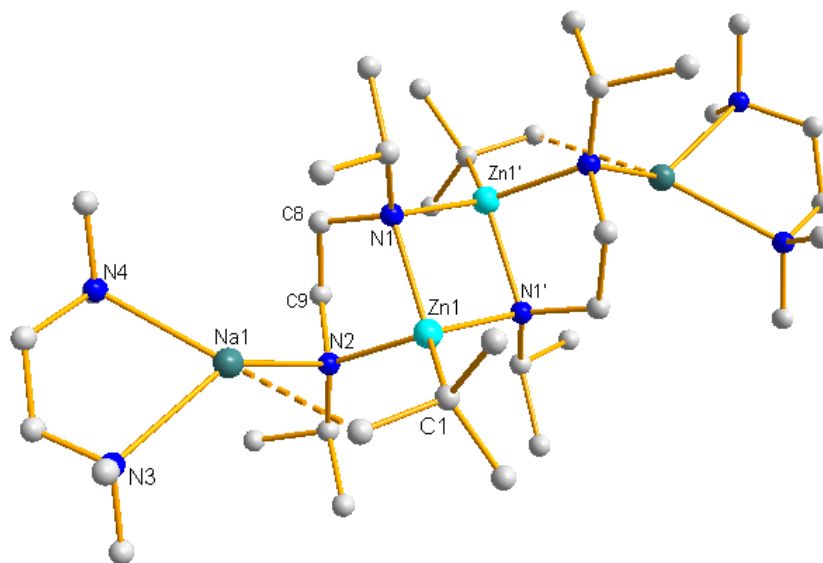


Figure 9.29: Molecular structure of one of the independent molecules of the dimeric sodium zincate $[(\text{TMEDA})\text{Na}[(i\text{Pr})\text{NCH}_2\text{CH}_2\text{N}(i\text{Pr})]\text{Zn}(i\text{Bu})_2]$ **31**. A weak agostic Na–C contact is denoted by a broken bond. Hydrogen atoms and disordered hexane of crystallization have been omitted for clarity. Symmetry operations to generate equivalent atoms: $-x, 1-y, 1-z$. Selected bond lengths [\AA] and angles [$^\circ$]: Na1–N1 3.720(4), Na2–N2 2.326(5), Na1–N3 2.490(6), Na1–N4 2.490(5), Na1–C4 2.977(6), Zn1–N1 2.105(4), Zn1–N2 2.103(4), Zn1–C1 2.072(5), Zn1–N1' 2.122(4), N1–C8 1.463(6), N2–C9 1.452(6), C8–C9 1.494(7), N4–Na1–N3 75.4(2), N4–Na1–N2 121.9(2), N4–Na1–C4 147.7(2), N3–Na1–N2 137.7(2), N3–Na1–C4 91.8(2), N2–Na1–C4 87.4(2), N2–Zn1–C1 117.1(2), N2–Zn1–N1 85.9(2), N2–Zn1–N1' 110.5(2), N1–Zn1–C1 127.6(2), N1–Zn1–N5 88.8(2), N5–Zn1–C1 120.0(2).

We also tried extending this chemistry to aluminium, encouraged by the richness and depth of aluminium hydride chemistry^[83, 86c, 86d, 103]. Thus $\text{Li}[\text{N}(i\text{Pr})\text{CH}_2\text{CH}_2\text{NH}(i\text{Pr})]$ was reacted with AlMe_3 in the presence of the Lewis base TMEDA, producing the monomeric lithium aluminate $(\text{TMEDA})\text{Li}[\text{N}(i\text{Pr})\text{CH}_2\text{CH}_2\text{N}(i\text{Pr})]\text{Al}(\text{Me})_2$ **33** (Figure 9.31) which crystallised at -30°C . In this structure the NCCN dianionic core of the amide ligand is locked in a planar conformation by its chelation of both $[(\text{TMEDA})\text{Li}]$ and $\text{Al}(\text{Me})_2$ cations which straddle this plane. The two metal cations have a symmetrical coordination to the nitrogen atoms of the ethylenediamide ligand. Both the Al and the Li

atoms adopt distorted tetrahedral geometries as a result of the ethylenediamide bite angles of $83.72(4)^\circ$ and $72.84(7)^\circ$ respectively.

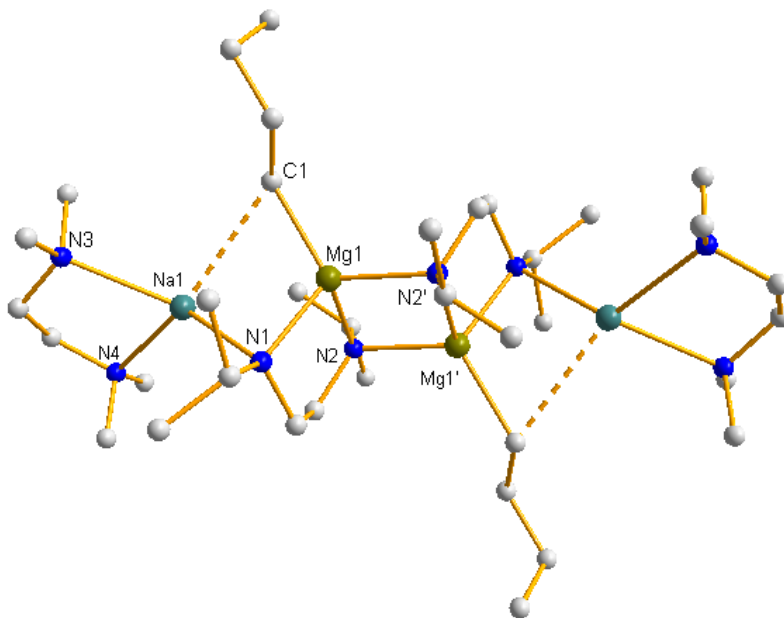


Figure 9.30: Molecular structure of the sodium magnesiate $\{(\text{TMEDA})\text{Na}[(i\text{Pr})\text{NCH}_2\text{CH}_2\text{N}(i\text{Pr})]\text{Mg}(n\text{Bu})\}_2 \cdot 32$. Symmetry operations to generate equivalent atoms: $2-x, -y, -z$. Selected bond lengths [\AA] and angles [$^\circ$]: Na1–N1 2.398(3), Na1–N3 2.469(3), Na1–N4 2.533(3), Na1–C1 2.966(5), Mg1–N1 2.080(2), Mg1–N2 2.156(3), Mg1–N2' 2.112(3), Mg1–C1 2.180(5), N1–C8 1.456(4), N2–C9 1.454(4), C8–C9 1.521(4), N1–Na1–N3 133.6(1), N1–Na1–N4 124.0(1), N1–Na1–C1 82.5(1), N3–Na1–N4 74.48(9), N3–Na1–C1 101.8(1), N4–Na1–C1 147.3(1), N1–Mg1–N2 85.1(1), N1–Mg1–N2' 118.2(1), N1–Mg1–C1 113.5(2), N2–Mg1–N2' 93.3(1), N2–Mg1–C1 120.1(2), N2'–Mg1–C1 119.9(2).

Refluxing hexane solutions of the aluminate complex **13** for two hours, mimicking the synthesis of the unsaturated zincocycle **1**, as with the magnesium compound, did not result in any significant levels of dehydrogenation of the CH_2CH_2 backbone. It is well known that the chemistry of hydride elimination is highly stereospecific. As such, the switch from divalent, tricoordinated zinc to trivalent, tetracoordinated aluminium may be a decisive factor in preventing, or at least slowing down, the reaction pathway which results in diazaethene **1**.

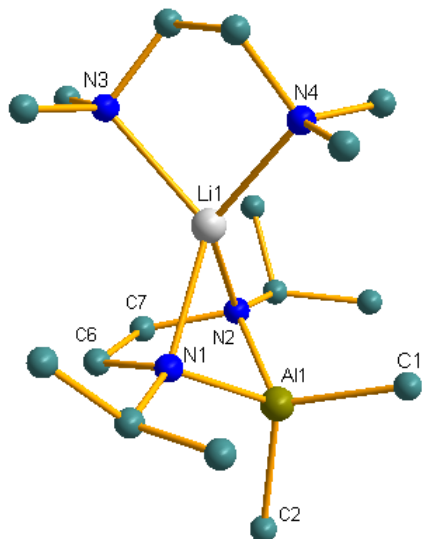
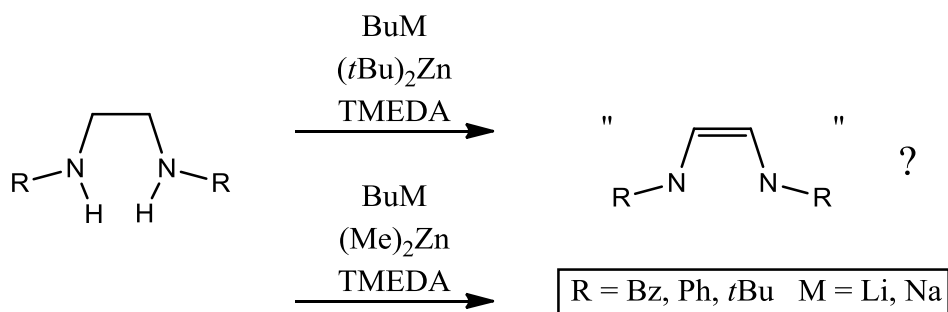


Figure 9.31: Molecular structure of the lithium aluminate (TMEDA)Li[(*i*Pr)NCH₂CH₂N(*i*Pr)]Al(Me)₂ **13**. Selected bond lengths [Å] and angles [°]: Al1–C1 1.976(1), Al1–C2 1.989(1), Al1–N1 1.905(1), Al1–N2 1.897(1), Li1–N1 2.099(2), Li1–N2 2.173(2), Li1–N3 2.220(2), Li1–N4 2.142(2), N1–C6 1.475(1), N2–C7 1.472(2), C6–C7 1.546(2), C1–Al1–C2 110.94(6), C1–Al1–N1 117.25(5), C1–Al1–N2 115.61(5), C2–Al1–N1 111.47(5), C2–Al1–N2 115.51(6), N1–Al1–N2 83.72(4), N1–Li1–N2 72.84(7), N1–Li1–N3 122.8(1), N1–Li1–N4 129.5(1), N2–Li1–N3 121.6(1), N2–Li1–N4 130.9(1), N3–Li1–N4 85.20(8).

Finally, we studied the effect of changing the sterics of the diamino ligand by varying the alkyl substituents on the nitrogen. First turning to the *tert*-butyl analogue (*t*Bu)N(H)CH₂CH₂NH(*t*Bu) extensively studied by Gardiner and Raston, repeating the synthesis that led to **24** with this more sterically demanding diamine resulted in a vibrant orange solution after reflux, characteristic of diazadiene formation. Concentration of the hexane solution followed by storage at -30°C resulted in the growth of long needle like colourless crystals. NMR spectroscopic analysis confirm the successful generation of a diazadiene species with a singlet in the ¹H NMR spectrum at 6.04 ppm, comparable to that seen in the other diazadiene complexes (Table 9.2), and also a comparable ⁷Li resonance of -2.50 ppm.

We also attempted the activation of both (Bz)N(H)CH₂CH₂NH(Bz) and (Ph)N(H)CH₂CH₂NH(Bz). It was reasoned that the phenyl groups may aid the formation of a diazadiene species by allowing for a delocalisation of charge and that such delocalisation could lead to interesting electronic properties within the new ligand. It was also envisaged that, in a reaction analogous to the aza-allyl formation discussed

previously (Figure 9.10), that there was potential for activation of the benzylic protons as well as of the ethylene backbone.



Scheme 9.10: Attempted extension of synergic CH activation to other diamines.

Both ligands were subjected to the conditions that led to the synthesis of the previous lithium and sodium diazadiene zincate complexes (Scheme 9.10). When sodium was employed along with Me_2Zn , after a two hour reflux and the addition of THF to achieve dissolution a crystalline solid could be isolated. X-ray diffraction studies revealed this compound to be the centrosymmetric dimeric $\{(\text{THF})_3\text{Na}[(\text{Bz})\text{NCH}_2\text{CH}_2\text{N}(\text{Bz})]\text{Zn}(\text{Me})_2\}_2$ **34** (Figure 9.32). The structure is highly reminiscent of its diisopropylethylenediamine / $t\text{Bu}_2\text{Zn}$ analogue **31**. Akin to the isopropyl substituted sodium diamide structures with zinc **31** and magnesium **32**, the benzyl substituted sodium diamido zincate **34** sits in a distorted ladder conformation constructed from a 5–4–5 fused ring system. It may thus be concluded that this is a particularly stable motif for divalent metal “ate” complexes incorporating diamides. The N–C [average 1.460 Å] and C8–C18 [1.524(3) Å] bond distances are indicative of a fully saturated diamide. The ladder motif results in two distinct amido environments; N2 contained within the central four membered ring and N1 completing the external five membered rings. Both coordinate to zinc with comparable Zn–N bond lengths [Zn1–N1 2.032(2) Å, Zn1–N2 2.118(1) Å, Zn1'–N2 2.068(1) Å]. The sodium cation coordinates to the exo amido N1 atom and is solvated by three THF molecules. Perhaps surprisingly, there is no apparent interaction between the sodium and the aromatic rings of the benzyl substituents. The lack of such an interaction is indicated by the sizable interatomic distance [Na1–C2 3.643(2) Å] and an interaction of this sort would be expected to be accompanied by a rotation of the aromatic ring to face the alkali metal. The shallow inter-

planar angle (C1C2C5)–(Na1C2C5) of 24.3(3)° indicates that this is not the case. However, a narrow Zn1–N1–Na1 angle of 89.04(5) may be indicative of a weak electrostatic interaction between the sodium and the methyl ligand [Na1–C20 3.187(2) Å]. This completes a distorted trigonal-bipyramidal geometry with terminal C20 and O1 atoms [C20–Na1–O1 169.04(6)°] and equatorial N1, O2 and O3 atoms (mean equatorial angle 119.1°).

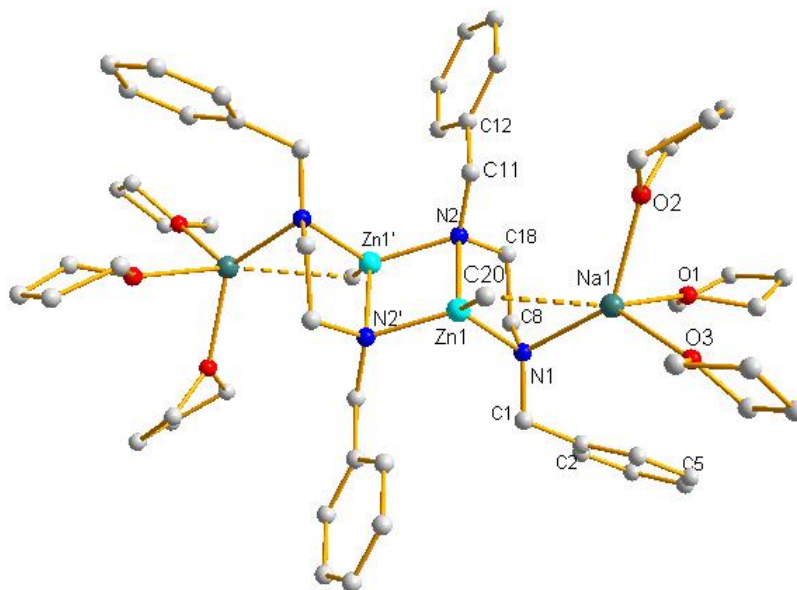


Figure 9.32: Molecular structure of the benzyl substituted sodium diamido zincate $\{(THF)_3Na[(Bz)NCH_2CH_2N(Bz)]Zn(Me)_2\}_2$ **34. Hydrogen atoms and minor disordered THF components have been omitted for clarity. Symmetry operations to generate equivalent atoms: 1-x, 1-y, 1-z. Selected bond lengths [Å] and angles [°]: Na1–O1 2.356(2), Na1–O2 2.379(2), Na1–O3 2.402(1), Na1–N1 2.413(2), Na1–C20 3.187(2), Zn1–N1 2.032(2), Zn1–N2 2.118(1), Zn1'–N2 2.068(1), Zn1–C20 2.011(3), N1–C8 1.453(2), N2–C18 1.467(2), C8–C18 1.524(3), N1–Na1–O1 103.11(5), N1–Na1–O2 134.23(6), N1–Na1–O3 128.43(6), O1–Na1–O2 85.87(6), O1–Na1–O3 94.52(5), O2–Na1–O3 94.60(6), C20–Na1–O1 169.04(6), C20–Na1–O2 88.23(6), C20–Na1–O3 95.16(6), C20–Na1–N1 74.67(6), N1–Zn1–C20 117.26(8), N1–Zn1–N2 86.31(6), N1–Zn1–N2' 111.53(6), C20–Zn1–N2 122.31(7), C20–Zn1–N2' 119.82(7), N2–Zn1–N2' 92.96(5), Na1–N1–Zn1 89.04(5).**

Also utilising the benzyl diamide ligand but with a lithium/ $(tBu)_2Zn$ combination, after a two hour reflux to encourage CH activation and addition of THF to achieve dissolution, the zinc rich zincate $(THF)Li[(Bz)N(H)CH_2CH_2N(Bz)]_2Zn_2[(Bz)NCH_2CH_2N(Bz)](tBu)$ **35** (Figure 9.33). This tri-metallic species adopts an arched 5–4–5–4–5 fused ring extended ladder motif with a Zn1–Zn2–Li1 angle of 137.3(1) and intermetallic

separations of Zn2–Zn1 2.891(1) Å and Zn1–Li1 2.632(5) Å. Each near planar four membered ring [Zn1–N2–Zn2–N3 -8.24(9), Zn2–N4–Li–N5 -12.2(2)] links two five membered rings in an *anti* fashion. Each metal centre is in a unique environment. The lithium centre is chelated by a mono-deprotonated diamide unit with the amino functionality adopting a terminal position. A single amido group of another diamido ligand also coordinates the lithium but, despite the varying oxidation states and coordination modes of the bound nitrogen atoms, the Li–N bond lengths differ little [Li1–N5 2.141(5) Å, Li1–N6 2.108(6) Å, Li1–N4 2.079(6) Å]. The distorted tetrahedral geometry around lithium is completed by a solvating molecule of THF. The central zinc atom is exposed entirely to amido ligands, unsymmetrically chelated by N3 and N4 [Zn2–N3 2.107(3) Å, Zn2–N4 2.053(2) Å] and bridging N2 and N5 [Zn2–N2 2.047(2) Å, Zn2–N5 2.008(2) Å]. Finally, the terminal zinc enjoys chelation by a second mono-deprotonated diamine ligand [Zn1–N1 2.176(6) Å, Zn1–N2 2.133(3) Å], coordination to one of the nitrogens of the central diamido ligand [Zn1–N3 2.046(2) Å], and is completed by a terminal *tert*-butyl anion [Zn1–C1 2.023(4) Å]. The unsymmetrical nature of **35** results in the complex incorporating an extraordinary nine formal chiral centres, including all three metal centres, although the syntheses from exclusively achiral materials requires that the bulk product is racemic and it is unclear how conformationally stable the complex may be.

Complex **35** is a rare example of an alkali metal zincate with a zinc rich constitution (LiZn₂) and was almost certainly generated as part of a disproportionation reaction likely also producing the tetra-alkyl zincate Li₂Zn(*t*Bu)₄ (Scheme 9.11). Such disproportionation processes are quite common within the remit of alkali metal zincates and are discussed in detail in chapter 10 “New alkyl amido zincates: a disproportionation reaction and novel stoichiometries”. The isolation of this aggregate also permits an extension of the earlier discussion on the synergic metallation of the second amino arm of a diamide (Scheme 9.3). We previously argued that the zincation of Li[(*i*Pr)NCH₂CH₂NH(*i*Pr)] by (TMEDA)Zn(*t*Bu)₂ proceeds with far greater efficiency than the analogous second lithiation by *n*BuLi because the formation of the co-complex (TMEDA)Li[(*i*Pr)NCH₂CH₂N(H)(*i*Pr)]Zn(*t*Bu)₂ **18** precludes the formation of higher oligomers. By contrast, a second lithiation allows the formation of the mixed aggregate

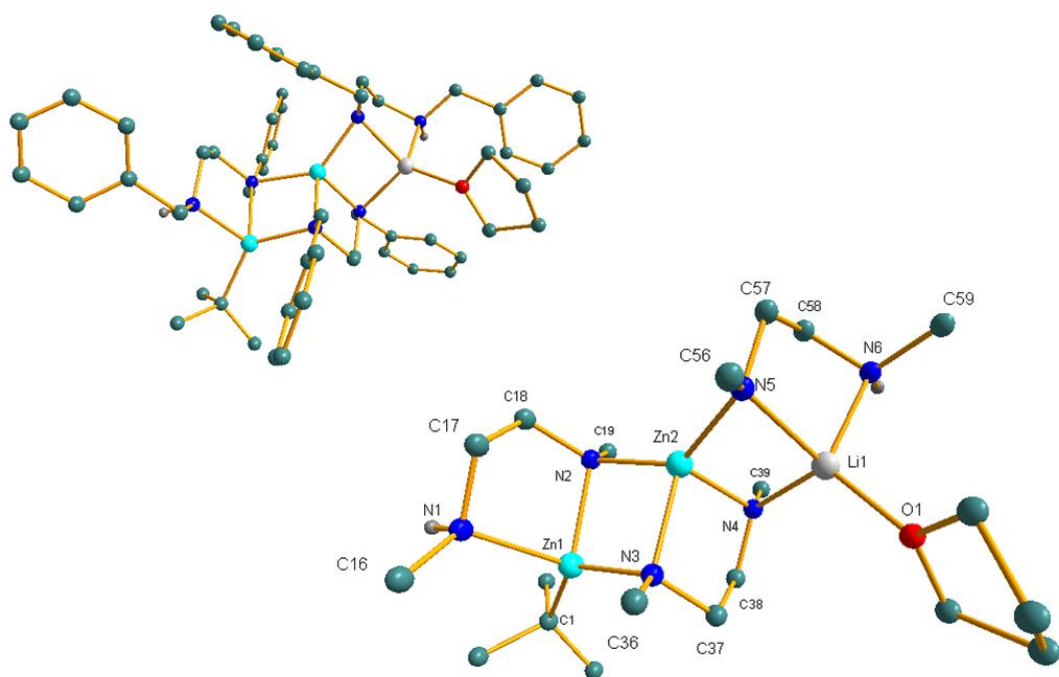
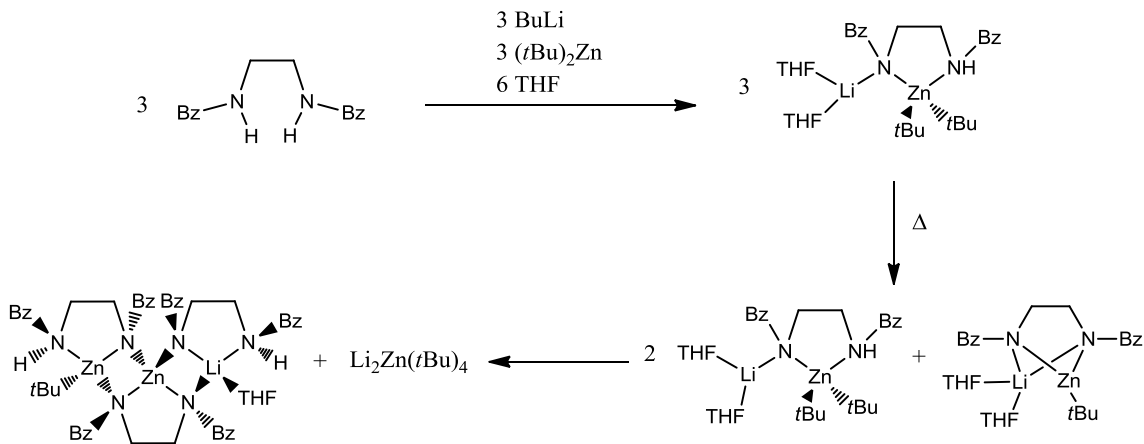


Figure 9.33: Molecular structure of the zinc rich diamido lithium zincate (THF)Li[(Bz)N(H)CH₂CH₂N(Bz)]₂Zn₂[(Bz)NCH₂CH₂N(Bz)](*t*Bu) **35**. Hydrogen atoms and minor disordered THF and benzyl components have been omitted for clarity (top left). Additionally, phenyl groups omitted (bottom right). Symmetry operations to generate equivalent atoms: 1-x, 1-y, 1-z. Selected bond lengths [Å] and angles [°]: Li1–N6 2.107(6), Li1–N5 2.141(5), Li1–N4 2.079(6), Li1–O1 1.983(6), Zn2–N5 2.008(2), Zn2–N4 2.053(2), Zn2–N3 2.107(3), Zn2–N2 2.047(2), Zn1–N3 2.046(2), Zn1–N2 2.133(3), Zn1–N1 2.176(3), Zn1–C1 2.023(4), O1–Li1–N6 113.7(3), O1–Li1–N5 120.1(2), O1–Li1–N4 1201.0(3), N6–Li1–N5 88.6(2), N6–Li1–N4 110.8(3), N5–Li1–N4 97.1(2), N5–Zn2–N4 102.30(9), N5–Zn2–N3 105.8(1), N5–Zn2–N2 135.67(9), N4–Zn2–N3 87.78(9), N4–Zn2–N2 113.28(9), N3–Zn2–N2 91.87(9), N3–Zn1–N2 91.14(9), N3–Zn1–N1 106.2(1), N3–Zn1–C1 132.4(1), N2–Zn1–N1 83.70(9), N2–Zn1–C1 124.5(1), N1–Zn1–C1 108.0(1).

{Li[N(*i*Pr)CH₂CH₂N(H)(*i*Pr)]Li}₂[N(*i*Pr)CH₂CH₂N(*i*Pr)], which is evidently a stable species and necessitates long reaction times or more forcing conditions to achieve complete metallation.^[51] The isolation of the mixed aggregate **35**, a zincate containing both mono and di-deprotonated diamide ligands, suggests that the reduction of steric bulk at nitrogen from isopropyl to benzyl substituents permits a greater level of aggregation within the formed zincate complexes and hence complete zincation becomes more challenging. However, the isolation of the sodium zincate **34** might suggest that switching to a more activated “ate” mixture can help mediate this complication.



Scheme 9.11: Plausible disproportionation mechanism leading to the zinc rich 35.

Unfortunately, a more definitive description of the nature of the bulk mixtures produced by all the attempted CH activations of the benzyl and phenyl substituted diamines was hampered by a series of complicated NMR spectra. Nevertheless, and importantly, the absence of any resonances 5-7 ppm excludes the possibility of successful CH activation leading to a diazadiene product. This in turn indicates the importance of the steric properties of the diamido ligand to achieve effective dehydrogenation through this synergic main group bi-metallic approach.

9.5 Conclusions and future work

This chapter has demonstrated that synergic mixed metal deprotonation can be widely applied to the metallation of diamines. The di-metallation of several diamines [(*i*Pr)N(H)CH₂CH₂NH(*i*Pr), (*t*Bu)N(H)CH₂CH₂NH(*t*Bu), (Ph)N(H)CH₂CH₂NH(Ph), (Bz)N(H)CH₂CH₂NH(Bz)] has been achieved most notably by zinc, but examples of magnesiation and alumination have also been established. Such direct metallation is not ordinarily available for metals such as zinc, which often exhibit kinetically challenged basicity. It has been demonstrated that zincation, via such a mixed Li metal approach, can actually lead to complete dimetallation of a diamino ligand with far greater efficiency than the corresponding di-lithiation, at least in some cases (Scheme 9.3), resulting from an enforced monomerisation of the reaction intermediates. This direct metallation,

utilising a mixed metal methodology, provides a new synthetic route to produce diamides of traditionally less reactive metals, such as zinc, to compliment more conventional techniques such as metathesis reactions starting from the appropriate metal chloride salt. Direct metallation could prove beneficial for applications in, for example, chemical vapour deposition, where it is desirable to avoid the incorporation of halide impurities in the film.^[104] It could also aid in the synthesis of diamides of metals that have poorly soluble halide salts, or when ethereal solvents, regularly a pre-requisite for efficient metathesis reactions, are prohibited.

The isolation of the dilithio zincate hydride **26** constitutes a rare example of a structurally characterised zincate hydride. Such reagents have already been shown to be highly selective reducing agents, often out competing more traditional reagents such as NaBH₄.^[93] The potential utility of hydrido zincate **26** as a reducing agent has been demonstrated by the successful test reaction with *t*Bu₂CO, yielding the lithium alkoxide [LiOCH(*t*Bu)₂]₄. A more detailed reactivity study is now required to determine the true utility of this new complex. Of particular interest would be the replacement of the diamine TMEDA for a chiral variant such as TMCDA (N,N,N',N'-(1*R*,2*R*)-Tetramethylcyclohexane-1,2-diamine) to potentially obtain a reagent capable of enantioselective reductions. Complex **26** also offered a rare opportunity to measure experimentally a ¹J_{Li-H} coupling constant. The continued discovery of further examples of lithium hydride coupling within fully characterised metal complexes is necessary to develop an understanding of what such data might indicate.

The most striking aspect of the extension of our mixed metal systems to diamines is of course the observed double CH activation leading to the formation of an unsaturated diazadiene ligand. While efficient transition metal catalytic systems have previously been developed that can selectively dehydrogenate a wide range of tertiary diamines^[72-73] there would be significant economic and environmental benefits if an alternative wide ranging efficient protocol could be developed utilising only main group metals. Unfortunately, although the work presented herein constitutes a novel synthetic route to give new diazadiene complexes, this mixed metal approach does not appear to deliver a general

method for the activation of a diverse array of ligand sets. The steric requirements for successful dehydrogenation under the conditions investigated appear to be quite specific. This is perhaps unsurprising given that, at the heart of this activation mechanism, the reaction relies upon an effective β -hydride elimination process; a process known to require a highly ordered transition state. Anticipating that further extension of this work to a broad range of diamines may prove less fruitful under the conditions investigated, developing a protocol utilising the heavier alkali metals (K, Rb, Cs) could provide a logical progression for this research. Not only does this provide an obvious polarising enhancement of reactivity but it is also well known that entropically demanding transition states can benefit from larger metal centres.^[105] It might thus be considered that a process such as β -hydride elimination, critical to the main group CH activation observed, could proceed in a greater number of cases if it were to take place on a larger, more diffuse, metal centre. A switch to the heavier alkali metals could potentially require a larger Lewis base than TMEDA to prevent oligomerization of the organometallic species. A potential substitute might be the tetradentate ligand Me₆-TREN {Tris[2-(dimethylamino)ethyl]amine} N[CH₂CH₂N(Me)₂]₃ that has already received attention within our research group.^[106]

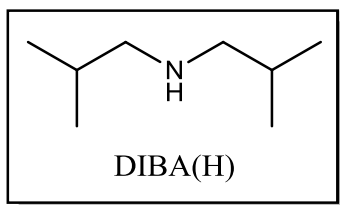
While the steric requirements of the β -hydride elimination are important for the generalisation of the double CH activation demonstrated in the synthesis of the zinc diazadiene complexes reported, critical even to the success with this one substrate is the ability of the mixed metal system to solubilise and prevent the aggregation of the metal hydride produced. Without this effective solvation of the metal hydride, it would be unlikely to achieve the final deprotonation that leads to diazadiene formation but would instead more likely result in the precipitation of a highly stable, unreactive ionic lattice. The use of bimetallic systems to achieve a greater solubility is not a new idea. For example Cahiez has been adding lithium bromide or chloride to suspensions of MnX₂ in THF for decades to produce the soluble “ate” species Li₂MnX₄ (X = Cl, Br) which prove much more efficient starting materials than the lone manganese salt in metathesis reactions with lithium or magnesium alkyls.^[107] More recently Knochel has successfully commercialised the mixed metal base TMPMgCl.LiCl.^[108] The novelty of this work is

that the solubility achieved for the hydride within the mixed metal framework permits its participation in further reactions. There is no reason to limit this concept to within the confines of β -hydride elimination. Many homo-metallic reactions which end with the precipitation of a highly ionic metal fragment could potentially exhibit further reactivity if a mixed metal approach was taken, which had the ability to prevent the polymerisation of the ionic metal fragment and, hence, activate it towards extending the reaction pathway. One potential avenue to explore is the chemistry of fluorination. The incorporation of fluorine into drug molecules can very often lead to drastic improvements in their pharmacokinetic and toxicological properties.^[109] The incorporation of ^{18}F is also important for the synthesis of radioactive tracer dyes for use in positron emission tomography (PET) imaging.^[110] Despite this however, the selective fluorination of functionalised small molecules remains a challenging undertaking and the development of new methodologies remains highly desirable.^[111] Alkali metal fluorides are already utilised as a convenient, non-toxic source of fluoride ions but, as with the analogous metal hydrides, they form highly stable, insoluble polymeric lattices.^[112] An *in situ* generated alkali metal fluoride, within a mixed metal scaffold, could result in a more soluble, and hence activated, source of fluoride.

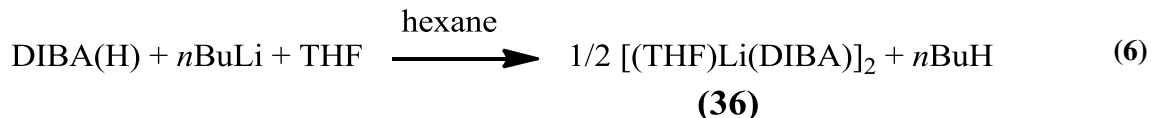
10 New alkyl amido zincates: a disproportionation reaction and novel stoichiometries

10.1 Introducing diisobutylamide and a new zinc rich zincate

Following on from the deliberate incorporation of diamide ligands into hetero-bimetallic systems (see chapter 9) our attention returned to the more conventional mono-amido chemistry. As stated previously, when research into mixed metal amido or alkyl amido bases has deviated from the sterically demanding TMP anion, other utility amides such as DA^[50] or HMDS^[49] have almost exclusively been chosen to deputise. It is surprising, given the great excitement generated by such mixed metal reagents in recent years, that amido ligands successfully incorporated into bimetallic bases belong to such an exclusive club. To expand on our knowledge of how the nature of the amido ligand affects the structural properties and reactivity of alkyl amido zincates we investigated the synthesis of a series of related complexes incorporating the diisobutylamide (DIBA) anion.



Diisobutylamine [DIBA(H)] is commercially available and significantly cheaper than the more sterically demanding TMP(H) [at the time of writing Aldrich sell 250 ml of DIBA(H) for £20.50 compared to £63.30 for 25g of TMP(H)]. However, despite being such an easily accessible ligand, the structural chemistry of the DIBA anion remained largely unexplored prior to the present work. The CCDB^[79] at the time of writing contains only three compounds containing a metallated DIBA unit: namely the zinc bisamide [(DIBA)₂Zn]₂,^[113] and the heteroleptic aluminium and gallium complexes [(DIBA)Al(Me)₂]₂^[114] and [(DIBA)Ga(Et)₂]₂.^[115] This paucity of structural information stimulated us to first examine the mono metallic chemistry of this ligand. The reaction of the amine DIBA(H) with *n*BuLi in hexane for one hour followed by the addition of one molar equivalent of the Lewis base THF and storage of the resulting solution at -30°C permitted the isolation of the lithium amide [(THF)Li(DIBA)]₂ **36** as a crop of colourless crystals suitable for X-ray diffraction studies.



In common with the THF solvates of the commonly utilised lithium amide reagents $[(\text{THF})\text{Li}(\text{DA})]_2$,^[116] $[(\text{THF})\text{Li}(\text{HMDS})]_2$,^[117] and the recently elucidated $[(\text{THF})\text{Li}(\text{TMP})]_2$,^[118] $[(\text{THF})\text{Li}(\text{DIBA})]_2$ also adopts a dimeric arrangement (Figure 10.1). The central rhombic Li–N–Li–N is strictly planar with near identical Li–N bond distances [Li1–N1 1.982(3) Å, Li1–N1' 2.004(3) Å] and average endocyclic bond angles Li–N–Li and N–Li–N of 73.3° and 106.7° respectively. The lithium's coordination sphere is completed by one molecule of the cyclic ether THF giving rise to a distorted trigonal planar geometry. Comparing the structures of the four THF solvated lithium amides, the average Li–N bond lengths increase marginally in the order DIBA < DA < HMDS < TMP from 1.993 Å to 2.055 Å (Table 10.1). Similarly, the N···N separations increase in the order DIBA < DA ≈ HMDS < TMP. These data are consistent with the intuitive assertion that the diisobutylamide anion is slightly less bulky than DA and HMDS anions while TMP is the most sterically demanding amido ligand.

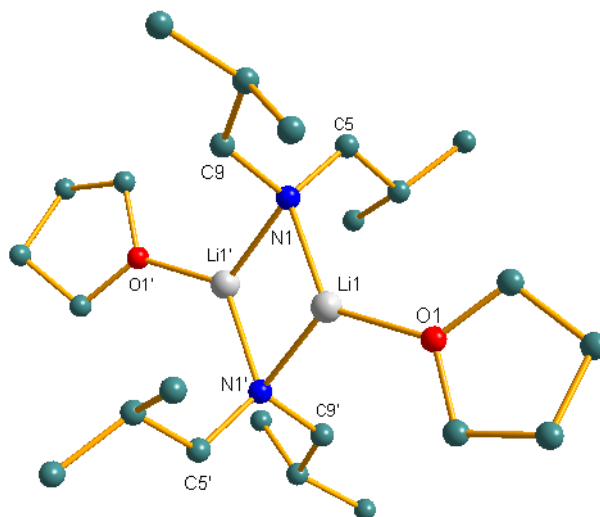


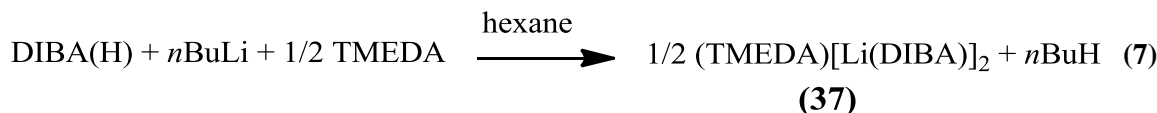
Figure 10.1: Molecular structure of one of the two centrosymmetric dimers of $[(\text{THF})\text{Li}(\text{DIBA})]_2$ 36 present within the unit cell. Hydrogen atoms and minor disordered THF components have been omitted for clarity. Symmetry operations to generate equivalent atoms: 1-x, 1-y, -z. Selected bond lengths [Å] and angles [°]: Li1–O1 1.927(3), Li1–N1 1.982(3), Li1–N1' 2.004(3), Li1···Li1' 2.380(5), O1–Li1–N1 130.2(1), O1–Li1–N1' 121.1(1), N1–Li1–N1' 106.7(1), Li1–N1–Li1' 73.3(1), Li1–N1–C5 118.9(1), Li1–N1–C9

121.7(1), Li1'-N1-C5 126.5(1), Li1'-N1 -C9 103.1(1), C5-N1-C9 109.4(1), Li1-N1-Li1'-N1' 0.0(3).

Table 10.1: Comparison of selected geometric parameters of the dimeric lithium amides [(THF)Li(DIBA)]₂, [(THF)Li(DA)]₂, [(THF)Li(HMDS)]₂, and [(THF)Li(TMP)]₂.

Bond/angle	Average bond length (Å) or angle (°)			
	DIBA	DA	HMDS	TMP
Li-N	1.99	2.01	2.02	2.06
N···N	3.20	3.24	3.24	3.36
Li-N-Li	73.3	72.05	73.6	70.1
N-Li-N	106.7	107.6	107.6	109.8

Reacting diisobutylamine with butyllithium in hexane followed by the addition of the neutral diamine TMEDA also allowed for the isolation of a crystalline solid. X-ray diffraction as well as NMR spectroscopic analysis revealed that the product is the polymeric complex {(TMEDA)[Li(DIBA)]₂}_∞ **37**.



The structure consists of a central (Li-N)₂ ring, much like that observed in the discrete molecular THF solvate [(THF)Li(DIBA)]₂, with an average Li-amide bond distance of 2.01 Å comparable to the THF solvate (1.99 Å). Presumably due to the sterically encumbered nature of the diisobutylamide anions, TMEDA is unable to chelate the lithium centres and instead each lithium cation receives only mono-solvation, with the bidentate ligand instead adopting a bridging arrangement between dimeric units, thus propagating the polymer. The average Li-N_(TMEDA) bond length (2.205 Å) is significantly longer than the Li-amide separations reflecting the difference in charge between the respective nitrogen atoms.

The TMEDA solvates of the lithium amides of DA^[119] and TMP^[120] share this same diamine:amide ratio of 1:2 although they do not both adopt the same structural motif. Deviating from this stoichiometry, the silylamide complex (TMEDA)Li(HMDS) is monomeric.^[121] The lithium diisopropylamide {(TMEDA)[Li(DA)]₂}_∞ adopts a

polymeric structure, akin to that in $\{(\text{TMEDA})[\text{Li}(\text{DIBA})]_2\}_\infty$, with the lithium centres

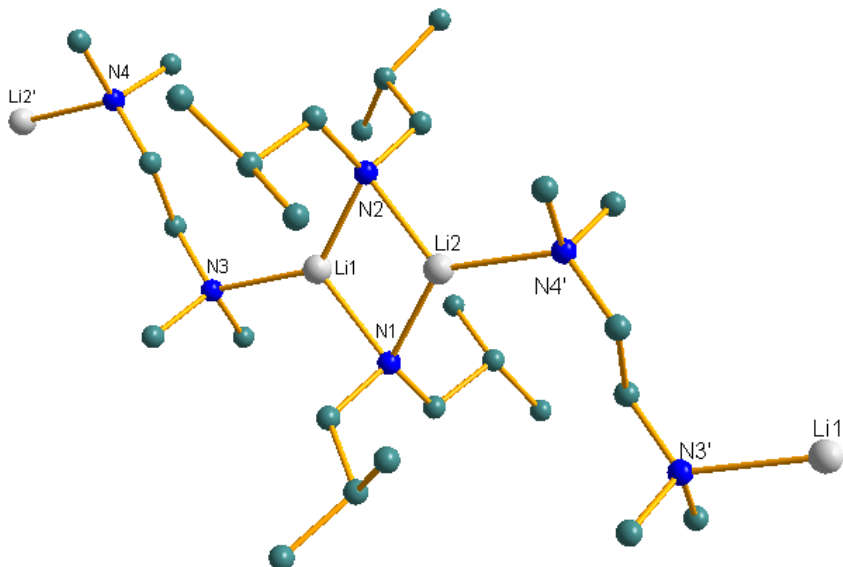


Figure 10.2: Section of the polymer of dimers of $\{(\text{TMEDA})[\text{Li}(\text{DIBA})]_2\}_\infty$ 37. Hydrogen atoms and minor disordered isobutyl components have been omitted for clarity. Symmetry operations to generate equivalent atoms: $-1+x, y, z$. Selected bond lengths [\AA] and angles [$^\circ$]: Li1–N1 2.030(3), Li1–N2 1.994(3), Li2–N1 1.981(3), Li2–N2 2.027(3), Li1–N3 2.217(3), Li2–N4 2.193(3), Li1–N1–Li2 75.2(1), Li1–N2–Li2 75.0(1), N1–Li1–N2 104.6(1), N1–Li1–N3 119.8(1), N2–Li1–N3 135.1(1), N1–Li2–N2 105.2(1), N1–Li2–N4' 132.6(1), N2–Li2–N4' 121.6(1).

each being solvated by one amino arm of the diamine TMEDA (Figure 9.3). By contrast, the TMEDA in $(\text{TMEDA})[\text{Li}(\text{TMP})]_2$ chelates to the lithium centre to which it is bound. This lithium atom is then bridged to a second lithium cation via the nitrogen centre of a TMP ligand and the second lithium centre is completed by a terminal TMP anion resulting in an asymmetrical “open dimer” motif (Figure 10.3). This unusual structure has been rationalised by the significant steric bulk of the TMP anions discouraging the closing of a Li–N–Li–N ring. The comparable structural motifs of the TMEDA solvates of lithium diisobutylamide and lithium diisopropylamide contrasting with the “open dimer” of the analogous TMP complex again suggests the steric requirements of the diisobutylamide anion are closely related to those of the diisopropylamido ligand and

distinct from that of the cyclic tetramethylpiperidide ligand with its four methyl substituents.

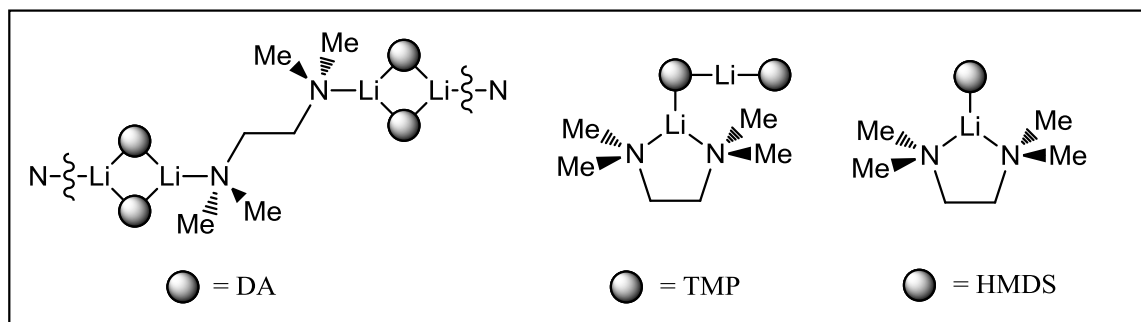
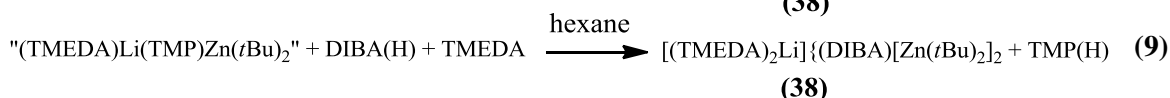
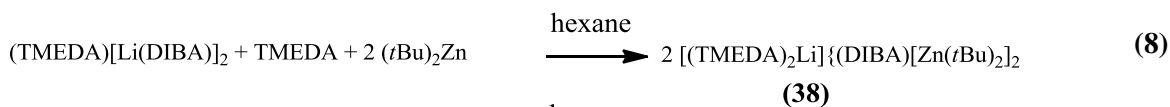


Figure 10.3: Contrasting structural motifs for the TMEDA solvates of LDA, LiHMDS and LiTMP.

The first bimetallic species incorporating a DIBA amide was synthesised on combining one molar equivalent of the dimer (TMEDA)[Li(DIBA)]₂ with one molar equivalent of the diamine TMEDA and two equivalents of freshly prepared (*t*Bu)₂Zn in hexane solution in an attempted synthesis of the putative heteroleptic “(TMEDA)Li(DIBA)Zn(*t*Bu)₂” (equation 8). This quickly gave rise to a white precipitate which was poorly soluble in hexane even on heating. An alternative synthesis, transamination of the structurally ill-defined lithium zincate “(TMEDA)Li(TMP)Zn(*t*Bu)₂” with the amine DIBA(H), sufficiently slowed the generation of the product to allow the precipitation of a crystalline material suitable for X-ray diffraction studies (equation 9). The product obtained was unexpected, namely the solvent separated zinc rich zincate [(TMEDA)₂Li]⁺{(*t*Bu)₂N[(Zn(*t*Bu)₂]₂}⁻ **38** (Figure 10.4). NMR spectroscopic analysis of a THF-D₈ solution confirmed that the white precipitate formed from the direct co-complexation was the same species crystallised through transamination.



Solvent separated zincate **38** contains two (*t*Bu)₂Zn molecules despite the reaction being carried out using equal stoichiometries of all reagents. The sole amido group bridges

between the two zincs to complete the complex anionic moiety. The bridging nitrogen has a distorted tetrahedral configuration, though it is much less distorted than the lithium amide dimer [(THF)Li(DIBA)]₂ (Figure 10.1), with the angles subtended at nitrogen ranging from 102.54(9)° to 113.2(2)° in **38** compared with 73.8(1)° to 126.4(1)° in the lithium amide. Both zinc atoms within the (tBu)₂Zn units adopt a trigonal planar geometry and bind the amido ligand near symmetrically with Zn–N bond distances of 2.077(2) Å and 2.090(2) Å. These bonds are marginally longer than the bridging interactions found within the homometallic zinc bisamide [(DIBA)₂Zn]₂ (average 2.00 Å). The cation, a lithium centre solvated tetrahedrally by two TMEDA ligands, is a common counter ion found in many solvent separated structures, including the three zincate complexes [(TMEDA)₂Li]{Zn[2,4,6-(iPr)₃C₆H₂]₃}, [(TMEDA)₂Li]{Me₂Zn[CH(Ph)(SiMe₃)]} and [(TMEDA)₂Li]{MeZn[CH(Ph)(SiMe₃)]₂}.^[122]

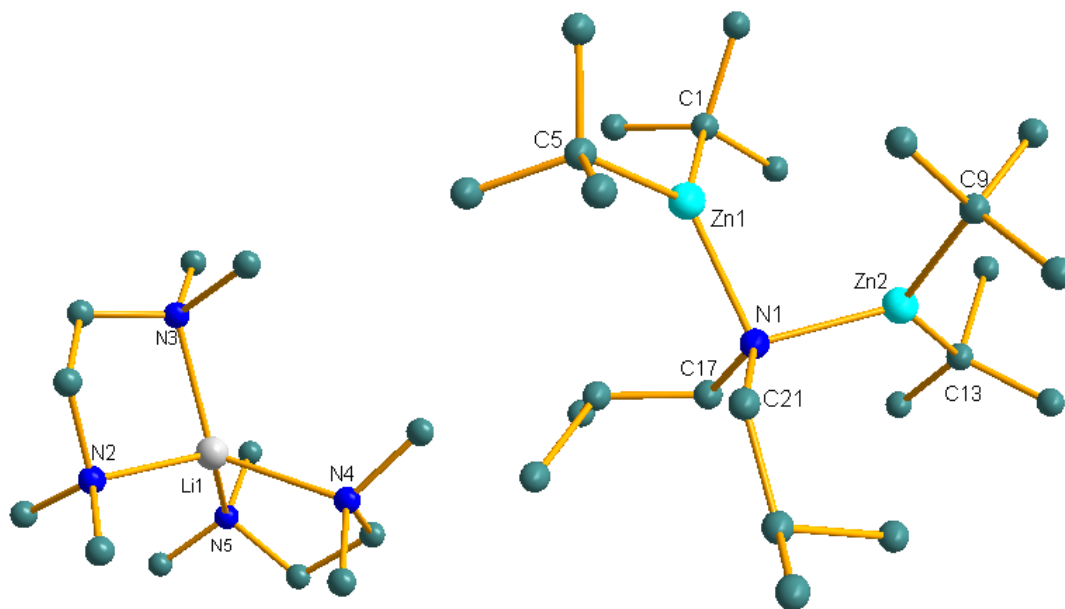


Figure 10.4: Structure of the solvent-separated zinc rich alkyl-amido zincate **38**, cation (LHS), anion (RHS). Hydrogen atoms and minor disordered TMEDA components have been omitted for clarity. Selected bond lengths [Å] and angles [°]: Zn1–C1 2.058(3), Zn1–C5 2.062(3), Zn2–C9 2.053(3), Zn2–C13 2.132(7), N1–Zn1 2.090(2), N1–Zn2 2.077(2), Li1–N2 2.128(5), Li1–N3 2.089(7), Li1–N4 2.137(6), Li1–N5 2.102(5), Zn1–N1–Zn2 102.54(9), Zn1–N1–C17 108.2(2), Zn1–N1–C21 108.4(2), Zn2–N1–C17 111.8(2), Zn2–N1–C21 112.1(2), C17–N1–C21 113.2(2), C1–Zn1–C5 123.4(1), C1–Zn1–N1 114.1(1), C5–Zn1–N1 121.7(1), C9–Zn2–C13 126.1(2), C9–Zn2–N1 112.5(1), C13–Zn2–N1 126.2(2), N2–Li1–N3 88.2(2),

N2–Li1–N4 122.2(3), N2–Li1–N5 120.9(3), N3–Li1–N4 116.9(3), N3–Li1–N5 125.6(3), N4–Li1–N5 87.0(2).

The mechanism by which this unexpected zinc rich solvent separated species is formed shall be discussed in conjunction with another zincate later (see chapter 10.2, page 106). The vast majority of structurally characterised zincates fit the general formula $AMZnR_3$ (where AM represents any alkali metal). A search of the CCDB^[79] for non-aqueous alkali metal zincates matching this formulation realised 109 hits. After this simple 1:1 stoichiometric ratio of the different metal centres, the next most common formulation for an alkali metal zincate is the “higher order” AM_2ZnR_4 . A search of the CCDB for this type of higher order zincate revealed 37 examples. By comparison, the zinc rich constitution $AMZn_2R_5$ is extremely rare, only recently emerging as a recognised member of the zincate family. A search of the CCDB for non-aqueous zinc rich alkali metal zincates $AMZn_2R_5$, found only ten hits,^[58, 123] five of which have been published in 2009 or later. Thus, the solvent separated complex **38**, as well as the diamido lithium zincate species **35** discussed previously (Figure 9.33, page 91), belong to an under represented class of zincate.

Of the ten published structurally characterised zinc rich zincates, alkyl amido **38** is quite distinct. There are only two examples of zinc rich zincates containing an amido ligand. The first, synthesised in 2006 by Lappert, is similar in construction, though synthesised through a different method, to that of diamido alkyl lithium zincate **35**. Thus a metathesis reaction between the lithium diamide $(NPPDA)Li_2$ ($NPPDA = NeoPentylPhenylDiAmide - Ph[1,2-N(CH_2^tBu)]_2$) with $ZnCl_2$ in ether at $-78^\circ C$ gave the dizincate $[(Et_2O)Li]_2[Zn_2(NPPDA)_3]$ with one bridging and two terminal NPPDA diamide ligands and two terminal $(Et_2O)Li$ cations (Figure 10.5),^[123b] analogous to the alkyl amido zincates discussed in the previous chapter (chapter 9), for example sodium zincates **31** and **34** or the analogous sodium magnesiate **32**. These complexes can be viewed as dimers of the common 1:1 $AMZnR_3$ zincate. Fortuitous partial hydrolysis of $[(Et_2O)Li]_2[Zn_2(NPPDA)_3]$ led to the isolation of the zinc rich zincate $[(Et_2O)Li]\{(NPPDA)_2Zn_2[NPPDA(H)]\}$, where one of the Li–N bonds has been replaced by a N–H bond (Figure 10.5). In common with the alkyl diamido **35**, Lappert’s complex

orders itself Zn···Zn···Li. However, its all amido constitution results in a different bridging mode for the diamido ligands; the terminal and partially hydrolysed examples chelating a zinc centre while the central diamide achieves a side on chelation of both zinc atoms, compared with the alkyl amido zincate **35**. In this case one terminal [(Bz)N(H)CH₂CH₂N(Bz)] ligand chelates a Zn(*t*Bu) cation while another chelates a lithium atom. Bridging between metal centres is only ever achieved by one of the two available nitrogen atoms of the [(Bz)NCH₂CH₂N(Bz)] unit; no chelating bridges such as seen in Lappert's complex is observed.

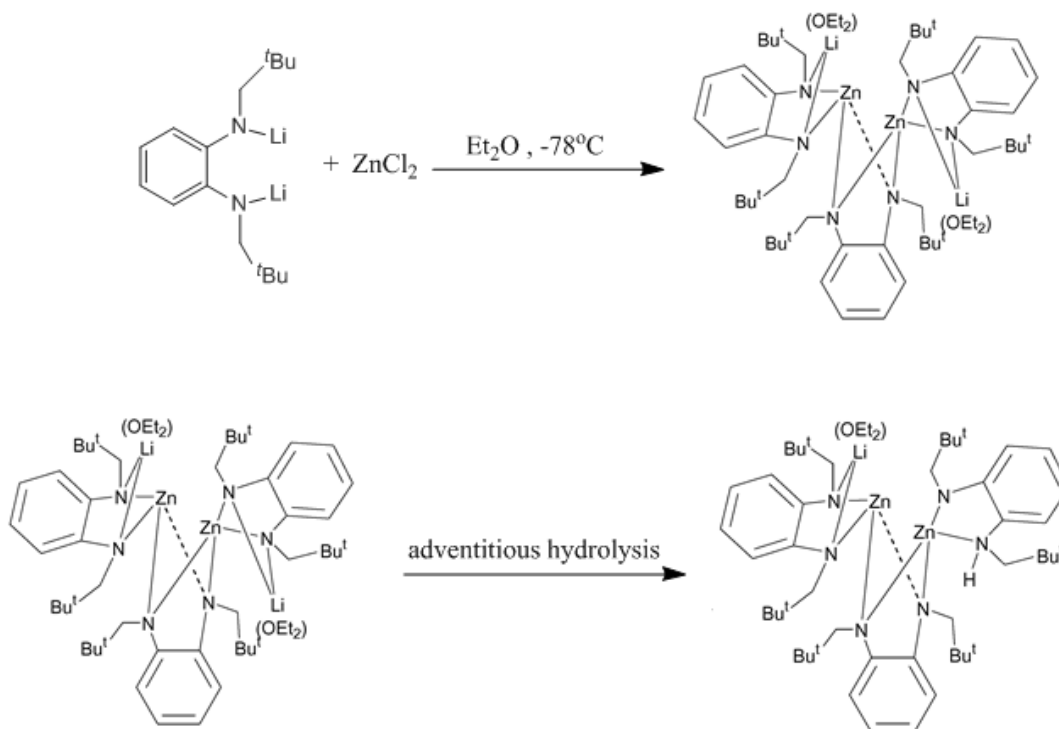


Figure 10.5: Reaction sequence that fortuitously formed a lithium dizincate.

The only previously reported zinc rich alkyl amido zincate was published in 2009 by our group, although it differs significantly from both the diamido **35** and the solvent separated **38**. Analogous to both **35** and **38**, (THF)₃Li[(Dipp)NH]Zn(Me)[(Dipp)NH]Zn(Me)₂ **39** was synthesised via a simple co-complexation of a lithium amide with a dialkylzinc followed by an unexpected disproportionation reaction. The zinc rich **39** is unique in having primary amido ligands. Indeed the three known alkyl amido zinc rich zincates each contain distinct classes of

amido ligand, with the solvent separated **38** possessing a bulky secondary amide and the extended ladder motif of **35** constructed from diamido ligands. The excellent bridging properties of the primary amide (Dipp)NH results in a contacted ion pair structure in **39**, akin to the diamido **35** but differing from the solvent separated **38**, again in the order $\text{Li}\cdots\text{Zn}\cdots\text{Zn}$. The alkyl to amido ratio is also different in **39** (3:2) compared with both solvent separated **38** (4:1 alkyl:amido) and diamido **35** (1:4 alkyl:amido). Thus, including Lappert's complex, there exists one example each of zinc rich zincates of formulation $\text{AMZn}_2\text{N}_x\text{C}_{5-x}$ (where N and C represent amido and alkyl ligands respectively) with $x = 1, 2, 4$ or 5 . Currently no known example exists where $x = 3$.

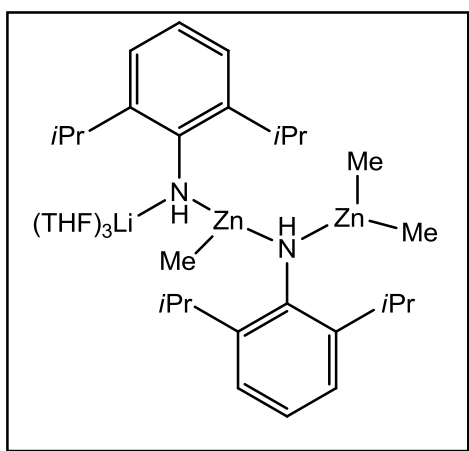
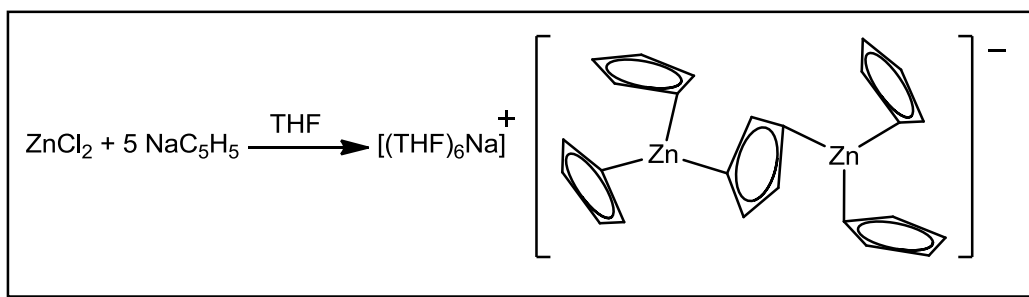


Figure 10.6: Structure of $(\text{THF})_3\text{Li}[(\text{Dipp})\text{NH}]\text{Zn}(\text{Me})[(\text{Dipp})\text{NH}]\text{Zn}(\text{Me})_2$ **39**, the only previously reported example of a zinc rich alkyl amido zincate.

A homoleptic carbanionic zinc rich zincate was prepared by Carmona in 2007. Thus the reaction of ZnCl_2 with five molar equivalents of sodium cyclopentadienyl in THF resulted in the sodium zincate $[(\text{THF})_6\text{Na}]^+[\text{Zn}_2(\text{C}_5\text{H}_5)_5]^-$ (Scheme 10.1).^[123d] It was first produced in a failed attempt to make a compound containing a Zn-Zn bond. Within this structure, each zinc centre is bound to three cyclopentadienyl ligands in a trigonal planar geometry. The zinc carbon bonding to the terminal ligands is stronger than that to the bridging Cp with bond distances of 2.08 Å compared to 2.17 Å. This is probably the closest structural analogy to the alkyl amido zincate **38**. It not only has a solvent separated construction, but the complex anion contains two terminal ZnR_2 units bridged by a final anionic ligand. However, although it has a similar solvent separated motif, its η^1 zinc-alkyl bonding is not directly comparable to the sigma bonding witnessed in **38**.



Scheme 10.1: Only example of a homoleptic carbanionic alkali metal zinc rich zincate.

Although the dizincate motif is highly unusual, neutral analogues have been known or inferred for a long time. Such species are believed to be responsible for the asymmetric addition of dialkylzinc reagents across aldehydes and ketones.^[124] An example of this synthetically important organic transformation has been well probed by Noyori.^[125] The catalysed addition of a zinc alkyl across benzaldehyde by the chiral amine DAIB [3-exo-(dimethylamino)isoborneol] begins with the alkylzinc reacting with the alcohol group of the DAIB to form an alkoxide. A second alkylzinc molecule then complexes to this alkoxide to form the dizinc complex which can then go on to add across the C=O bond of the aldehyde (Figure 10.7). The dizinc architecture has been inferred by the requirement for two equivalents of the alkylzinc as well as by various theoretical studies.^[125] The active species has been described as being ambifunctional because coordination of the incoming aldehyde to the monoalkylzinc activates it toward reaction while the complexation of the dialkylzinc also leads to an increase in the nucleophilic nature of its alkyl groups.^[126]

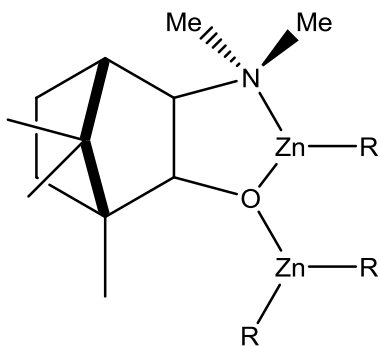


Figure 10.7: Proposed neutral dizinc complex responsible for various alkylation reactions.

10.2 The disproportionation reaction

Reaction of Na(DIBA) with $(t\text{Bu})_2\text{Zn}$ and TMEDA in a 1:2:2 ratio did not afford the sodium analogue of **38** but instead led to the bisamido-zincate (TMEDA)Na(DIBA) $_2$ Zn($t\text{Bu}$) **40** (Figure 10.8). This new complex has been characterized by multinuclear NMR spectroscopy and X-ray diffraction studies. It has been produced pure in a 31% crystalline yield. Its NMR spectroscopic data are discussed later. A contact ion pair structure, **40** consists of sodium and zinc centres bridged by two diisobutylamide ligands to produce an essentially planar Na–N–Zn–N core [torsion angle $0.86(1)^\circ$]. The nitrogen–zinc bonds (average 2.001 \AA) are significantly shorter compared with the average Na–N_(DIBA) bond distance of 2.445 \AA . Indeed the substantial zinc amide nature of the diisobutylamide ligands in **40** is indicated by the negligible difference of its Zn–N bonds compared with the bridging interactions found within the homometallic homoleptic [(DIBA) $_2$ Zn] $_2$ compound (average 2.00 \AA).^[113] The superior bridging ability of the electron rich amido ligands compared to the *tert*-butyl anion ensures that the distorted trigonal planar geometry around zinc (angles totalling 358.9°) is completed by a terminal *tert*-butyl ligand. Due largely to the narrow bite angle of the TMEDA ligand, the sodium centre adopts a distorted tetrahedral environment (angles totalling 664.1° , averaging 110.7°).

Comparable structures have been produced by other researchers in our laboratory using both sodium diisopropylamide^[127] and sodium (*cis*)-2,6-dimethylpiperidide (DMP)^[128].

The DMP analogue was synthesized by the co-complexation of Na(DMP), $(t\text{Bu})_2\text{Zn}$ and TMEDA, while the diisopropylamide example was created through transamination with sodium TMP zincate 2. Both of these methodologies have been successfully employed in the synthesis of **40**. All three structures have identical motifs. Unfortunately, the X-ray crystallographic data for $(\text{TMEDA})\text{Na}(\text{DMP})_2\text{Zn}(t\text{Bu})$ is not of sufficient quality to discuss bond lengths and angles. The diisopropylamide analogue has average $\text{Na}-\text{N}_{(\text{DMP})}$ and $\text{Zn}-\text{N}_{(\text{DMP})}$ bond distances of 2.419 Å and 2.020 Å respectively. These differ little with the 2.445 Å and 2.001 Å of the respective average bond lengths of **40**.

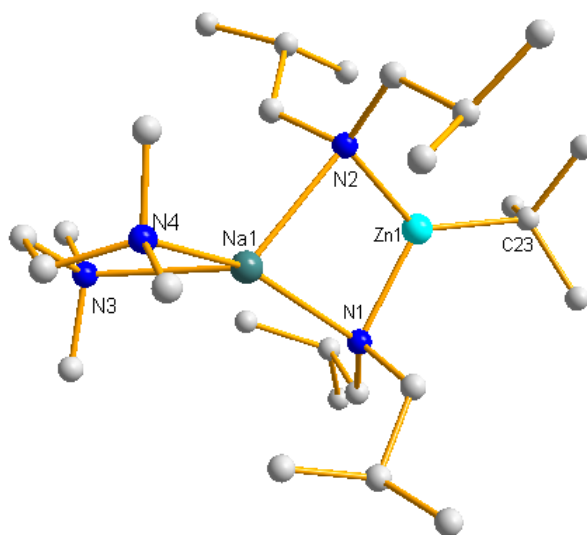


Figure 10.8: Molecular structure of bis-amido-zincate $(\text{TMEDA})\text{Na}(\text{DIBA})_2\text{Zn}(t\text{Bu})$ **40**. Hydrogen atoms have been omitted for clarity. Selected bond lengths [Å] and angles [°]: $\text{Na1}-\text{N1}$ 2.444(1), $\text{Na1}-\text{N2}$ 2.446(2), $\text{Zn1}-\text{N1}$ 2.028(1), $\text{Zn1}-\text{N2}$ 1.983(1), $\text{Zn1}-\text{C23}$ 2.033(2), $\text{Na1}-\text{N3}$ 2.554(2), $\text{Na1}-\text{N4}$ 2.593(2), $\text{Na1}-\text{N1}-\text{Zn1}$ 88.42(5), $\text{Na1}-\text{N2}-\text{Zn1}$ 9.41(5), $\text{N1}-\text{Zn1}-\text{N2}$ 102.58(6), $\text{N1}-\text{Zn1}-\text{C23}$ 123.83(6), $\text{N2}-\text{Zn1}-\text{C23}$ 132.44(6), $\text{N1}-\text{Na1}-\text{N2}$ 79.59(5), $\text{N1}-\text{Na1}-\text{N3}$ 123.56(5), $\text{N1}-\text{Na1}-\text{N4}$ 150.54(5), $\text{N2}-\text{Na1}-\text{N3}$ 125.04(5), $\text{N2}-\text{Na1}-\text{N4}$ 113.02(5), $\text{N3}-\text{Na1}-\text{N4}$ 72.35(5).

The formation of both $(\text{TMEDA})\text{Na}(\text{DMP})_2\text{Zn}(t\text{Bu})$ and $(\text{TMEDA})\text{Na}(\text{DA})_2\text{Zn}(t\text{Bu})$ have been rationalised in terms of a disproportionation mechanism. The first stage of this mechanism is proposed to be dimerization to give $[(\text{TMEDA})\text{Na}(\text{NR}_2)_2\text{Zn}(t\text{Bu})_2]_2$. Although no structures have formally been identified with this motif with amido substituents specifically, there have been similar structures produced with alkoxo bridges.^[129] The reaction of $\text{KO}t\text{Bu}$ and diethylzinc produced the related structure $[\text{K}(\text{O}t\text{Bu})\text{Zn}(\text{Et})_2]_2$ in toluene. The suspected $[(\text{TMEDA})\text{Na}(\text{NR}_2)\text{Zn}(t\text{Bu})_2]_2$ dimer is

then expected to break up unsymmetrically to form the bisamido-zincate and “(TMEDA)NaZn(*t*Bu)₃” (Figure 10.9). An examination of the filtrates of these reactions by NMR spectroscopy revealed resonances that could be attributed to this tris-alkyl zincate.

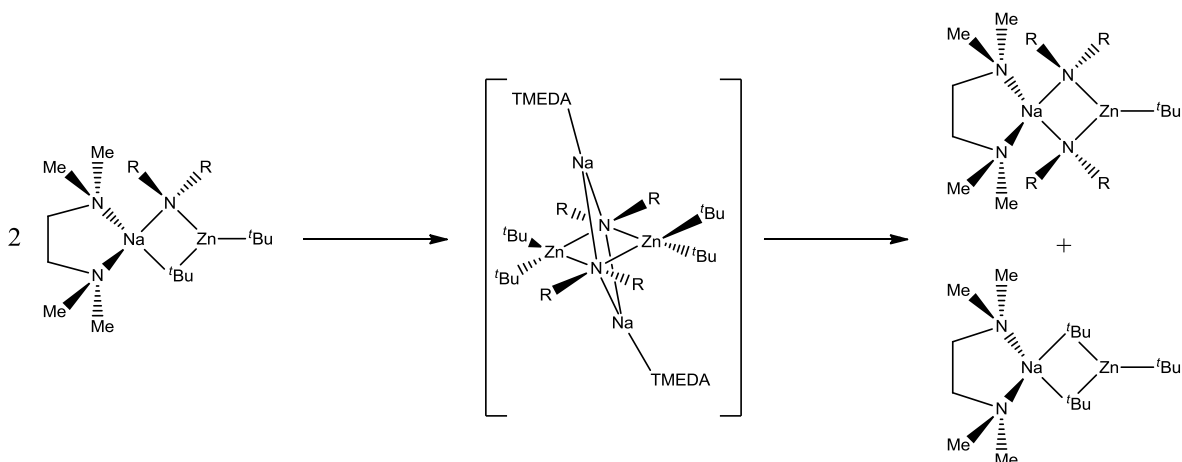


Figure 10.9: Typical disproportionation pathway exhibited by various alkylamido zincates.

The same mechanism can be used to explain the formation of the sodium diisobutyl amide zincate **40**. An adapted mechanism can also be used to explain the formation of the related solvent separated lithium zinc rich zincate **38**. It can be envisaged that the central dimer could disproportionate in different ways. If it were cleaved correctly then it could indeed form **38** and lithium diisopropylamide. It can also be supposed that the lithium dimer could still cleave in the analogous way to its sodium variant. In order to investigate further this complex solution chemistry an EXSY (exchange spectroscopy) NMR experiment was carried out. EXSY is a variant of two-dimensional NOESY (Nuclear Overhauser Effect Spectroscopy) NMR spectroscopy that detects exchange between species in solution.^[130]

The EXSY spectrum does indeed reveal equilibria between various species in solution. There are two exchange resonances between two different TMEDA states shown by the cross peaks of 2.14 ppm and 1.13 ppm (TMEDA CH₃) and 2.12 ppm and 1.45 ppm

(TMEDA CH_2). This observation is consistent with an exchange between solvent separated species and contact ion pairs. There is also an exchange detected between the *tert*-butyl signals at 1.67 ppm and 1.40 ppm. This is in agreement with an exchange between (TMEDA)Li(DIBA)Zn(*t*Bu)₂ and zinc rich **38**. The observation of cross peaks between the two different broad amido signals at 1.20 ppm and 1.05 ppm are also in accord with this exchange. The sharp resonances at 1.48 ppm and 1.37 ppm have been

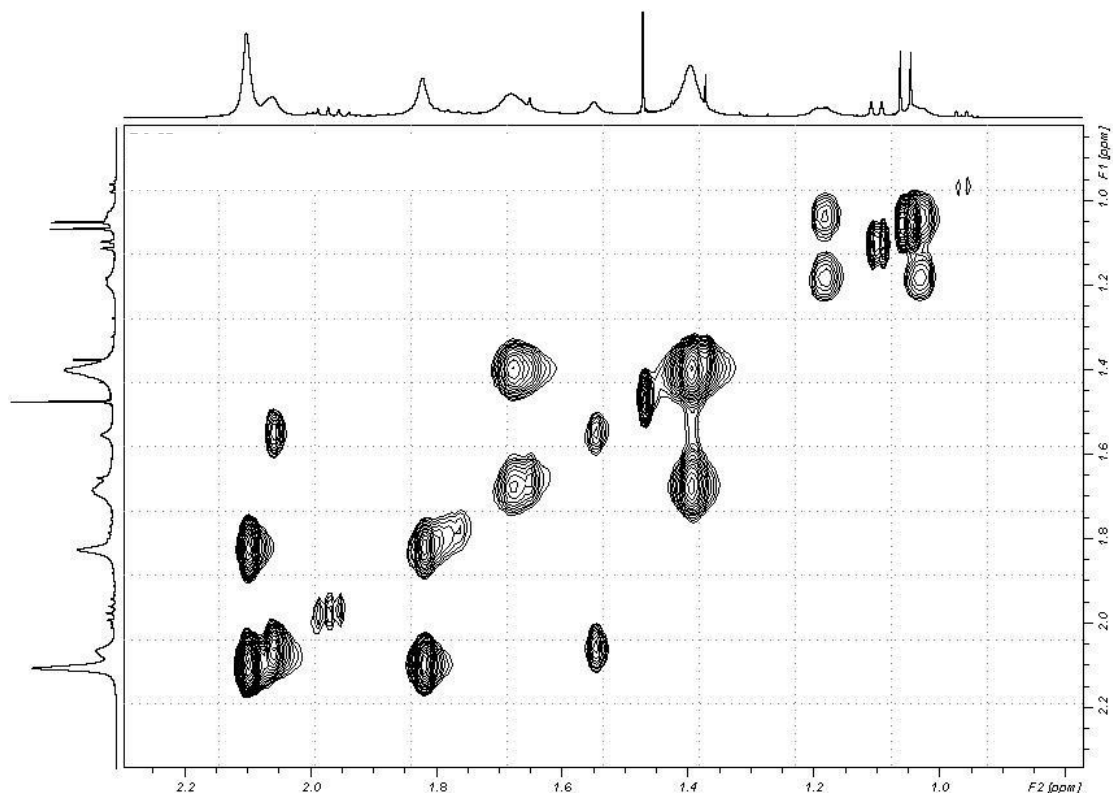
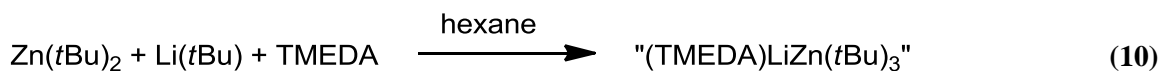


Figure 10.10: Exchange NMR spectrum showing the dynamic equilibrium present within the [(TMEDA)₂Li]{(*t*Bu)₂N[(Zn(*t*Bu)₂]₂} mixture in C₆D₆ solution.

identified as belonging to “(TMEDA)LiZn(*t*Bu)₃” by its independent synthesis and comparison with this authentic sample [equation (10)].



Recent work by Uchiyama, both theoretical and spectroscopic, has revealed that, in the presence of a donor, “LiZn(*t*Bu)₃” in fact exists as an equilibrium between bis-alkyl (*t*Bu)₂Zn and tetra-alkyl Li₂Zn(*t*Bu)₄.^[131] This is why it presents two signals in NMR

spectra when only one would be expected. Finally, a sharp resonance at 1.66 ppm, extruding from the aforementioned broad signal at 1.67 ppm, can be tentatively attributed to the presence of the bisamido-zincate (TMEDA)Li(DIBA)₂Zn(*t*Bu). The NMR analysis is therefore consistent with the scheme shown in Figure 10.11. Furthermore, the sharpness of the signals assigned to “LiZn(*t*Bu)₃” and (TMEDA)Li(DIBA)₂Zn(*t*Bu) suggest that their formation is not in equilibrium and is thus irreversible.

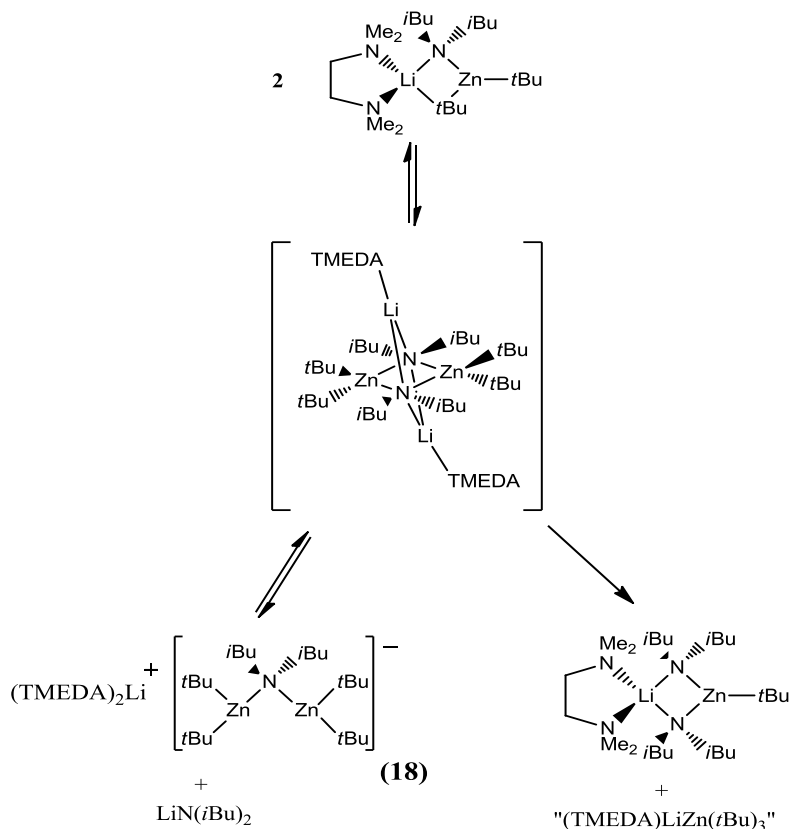


Figure 10.11: Proposed disproportionation mechanism for the formation of 38.

A similar dimerization followed by asymmetric cleavage was also intimated to explain the formation of the only other structurally characterised alkyl amido zinc rich zincate (THF)₃Li[(Dipp)NH]Zn(Me)[(Dipp)NH]Zn(Me)₂ **39** (Figure 10.6).^[123c] In this case the dissociation of the alkyl lithium MeLi in preference to a lithium amide gives rise to the greater amide incorporation in **39** compared with the solvent separated **38** (AMZn₂N_xC_{5-x}, X = 2 compared with X = 1). Also akin to the complex solution chemistry observed for the diisobutylamido zincate, The zinc rich primary amido zincate **39** can decompose to give rise to the bisamido zincate (THF)Li[(Dipp)NH]₂Zn(Me) and a homoleptic alkylzinc

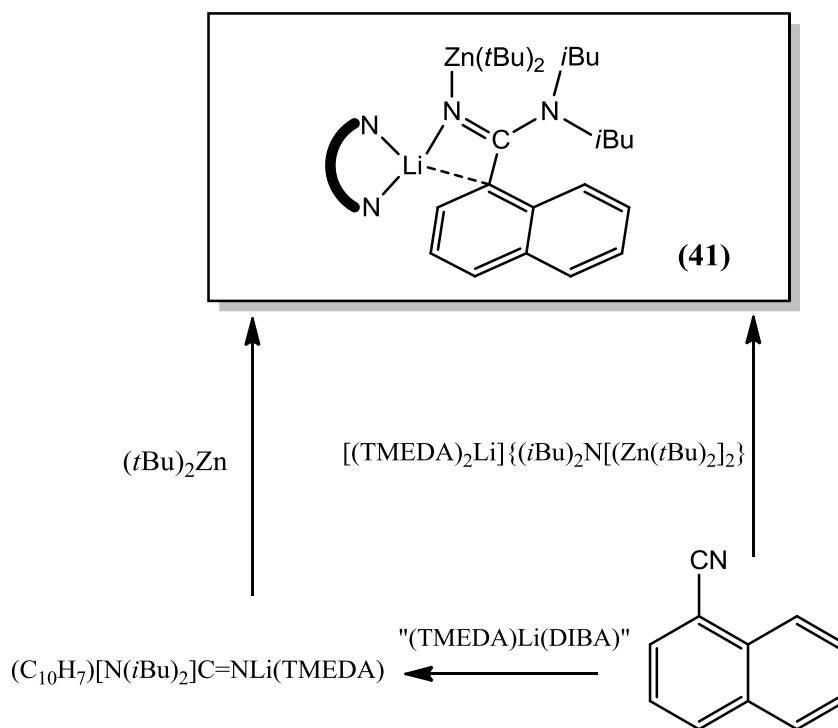
species. Apparently distinct from the diisobutylamide system however, the alkylzinc and bisamido zincate can recombine, and are in equilibrium with, the zinc rich **39**. Moreover, this equilibrium can be manipulated in a facile manner, to furnish exclusively the bisamido zincate (THF)Li[(Dipp)NH]₂Zn(Me), by taking advantage of the volatility of (THF)₂Zn(Me)₂ *in vacuo*.

Although a variable mixture of products does not appear the most desirable starting point for the development of new synthetically useful reagents it should be noted that a great deal of inorganic reagents are produced and utilized *in situ* without ever being thoroughly characterized. In any such cases the reagent may indeed be present as a mixture of different species. It cannot be predicted how reaction may affect the composition of the zincate mixture and as such the potential for relatively clean reactions still exists. This does however lead to ambiguity as to what the reactive species may be in any reaction and there is the possibility of the presence of several different active species which would likely lead to an undesirable mixture of products. Despite these obvious limitations the unusual stoichiometry of the zinc rich **38** provided the potential for new and novel molecular structures from its use. For this reason the zincate mixture was deployed with various substrates. The reactions of zincates with organic nitriles have already been shown to exhibit a rich structural chemistry (see chapter 8.2.1). For this reason they seemed an obvious place to begin in the search for novel molecular constructions.

10.3 New amidinato zincate compounds

A novel product can indeed be reported from the reaction of the zinc rich mixture resulting from **38** with 1-cyanonaphthalene in hexane solution. This produced a red solid that dissolved on heating. The large cubic orange crystals produced by slow cooling of this solution in a 20% yield were revealed, by X-ray diffraction and multinuclear NMR spectroscopic techniques, to be (C₁₀H₇)[N(*t*Bu)₂]C=N[Zn(*t*Bu)₂]Li(TMEDA) **41**. The same product was obtained on the reaction of “(TMEDA)Li(DIBA)” with 1-cyanonaphthalene followed by addition of one equivalent of (*t*Bu)₂Zn. This makes this

novel structure available without the complication of needing to use a complex zincate mixture in its synthesis (Scheme 10.2).



Scheme 10.2: Alternative syntheses of $(\text{C}_{10}\text{H}_7)[\text{N}(i\text{Bu})_2]\text{C}=\text{N}[\text{Zn}(t\text{Bu})_2]\text{Li}(\text{TMEDA})$ 41.

It can be seen that the diisobutylamido unit has added across the nitrile group producing a trigonal planar ketimido carbon atom. The negative charge on the former cyano nitrogen is now satisfied by both $(\text{TMEDA})\text{Li}$ and $\text{Zn}(t\text{Bu})_2$ cations. The C17-N2 bond distance [1.253(2) Å] is considerably shorter than that of the C17-N1 distance of 1.407(2) Å reflecting the distinct double and single bond character respectively. These bond lengths are comparable with those of the lithium amidinato complex $[\text{LiN}=\text{C}(\text{Ph})\text{NMe}_2]_6$ of 1.26 Å and 1.42 Å respectively.^[132] It can be observed, as is common place amongst aromatic zincates, that the lithium ion has a significant interaction with the naphthalene ring, judged by the short Li1-C18 distance [2.595(4) Å]. It has been previously noted that, within alkylamido zincate chemistry, a four-centred AM-N-Zn-C ring completed by an electrostatic interaction between an alkyl ligand and the alkali metal is a prominent, and thus presumably stable, motif (see chapter 8.2, page 12). While the potential for such a

closed ring structure exists in the amidinato **41**, it is clear that no electrostatic interaction exists between the lithium and *tert*-butyl ligands. This is evidenced by the shortest Li–MeC(Me₂)Zn distance of 4.087(3) Å being appreciably longer than the corresponding Li–MeC(Me₂)Zn distance [2.409(5) Å] found within the lithium zincate (THF)Li(TMP)Zn(*t*Bu)₂ 1.^[24] The Li1–N2–Zn1 bond angle [118.7(1)°] is also significantly greater than the more constrained Li–N–Zn angle within 1 [100.2(1)°]. The apparent inability to form an electrostatic interaction between the lithium and *tert*-butyl ligands in **41** may be rationalised by the need for a rotation around the N2–Zn1 bond, which would be expected to result in prohibitive steric clashing between the second *tert*-butyl anion and the diisobutylamine fragment of the amidinato ligand.

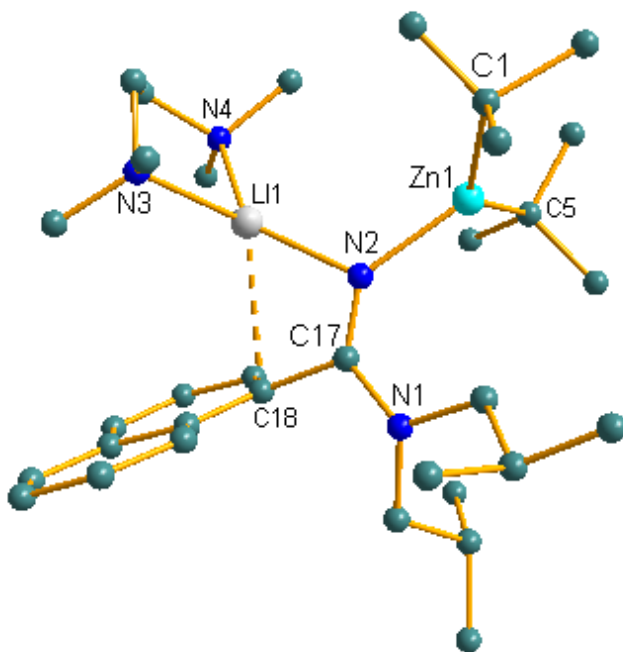


Figure 10.12: Molecular structure of (C₁₀H₇) [N(*i*Bu)₂]C=N[Zn(*t*Bu)₂]Li(TMEDA) **41**. Hydrogen atoms and minor disorder of a *tert*-butyl ligand omitted for clarity. Selected bond lengths [Å] and angles [°]: Li1–N2 1.947(4), Li1–C18 2.595(4), Zn1–N2 1.992(1), Zn1–C1 2.033(2), Zn1–C5 2.038(2), C17–N2 1.253(2), C17–N1 1.407(2), Li1–N2–Zn1 118.7(1), Li1–N2–C17 105.9(2), Zn1–N2–C17 135.1(1), N2–C17–N1 127.3(2), N2–C17–C18 117.6(2), N1–C17–C18 115.1(2), N2–Li1–N3 133.5(2), N2–Li1–N4 130.4(2), N2–Li1–C18 61.6(1), N3–Li1–N4 88.7(1), N3–Li1–C18 116.0(2), N4–Li1–C18 130.2(2).

Despite their extensive utility within transition metal chemistry,^[133] and the success of related β -diketiminato ligands within zinc chemistry,^[134] for example towards designing

effective precatalysts for the ring opening polymerisation of lactide,^[134d, 135] there are surprisingly few examples of amidinato ligands utilised within zincate chemistry. Moreover, the **41** is the first example of an alkyl amidinato zincate complex. It is also the first example of an amidinato zincate complex to contain an asymmetric amidinate ligand and thus the first to contain a ligand of form N=CNR₂ as opposed to RNCNR.

Two mixed amidinato halide lithium zincates have recently been synthesised by Schulz. The 1:1 reaction of Li{[N(Cy)]₂C(*t*Bu)} (Cy = cyclohexyl) with zinc bromide in diethylether solution produced the mixed lithium zincate {(*t*Bu)C[(Cy)N]₂}Zn(Br)₂Li(OEt)₂ (Figure 10.13).^[136] This species is structurally quite distinct from **41** in that the alkali metal has no interaction with the amidinato ligand but instead binds to two bromide ligands and two ether molecules. The symmetrical amidinato ligand {(*t*Bu)C[(Cy)N]₂} achieves chelation of zinc with an equal delocalisation of its negative charge between its two nitrogen atoms indicated by the similarity of its C–N bond lengths [1.342(3) Å and 1.326(3) Å] contrasting with the distinct double bond/single bond character observed in **41** [C–N 1.253(2) Å and 1.407(2) Å respectively]. The zinc rich amidinato species IZn{[N(*i*Pr)]₂C(Me)}₂Zn(I)₂Li(OEt)₂ was produced accidentally in low yield during iodolysis of Zn{[N(*i*Pr)]₂C(Me)}₂, successfully scavenging trace lithium iodide impurities from the starting materials (Figure 10.13).^[123a] Again, in this compound the lithium cation prefers to bind to halide anions than to interact with either amidinate ligand. In common with the previously discussed zinc rich zincates, IZn{[N(*i*Pr)]₂C(Me)}₂Zn(I)₂Li(OEt)₂ is ordered ZnZnLi as opposed to ZnLiZn. As well as being bound to two iodide anions, the central zinc is linked to both amidinato ligands, though only through one of their nitrogen atoms. One amidinate ligand, with distinct double and single bond character [C–N 1.283(4) Å and 1.406(4) Å], bridges the two zinc centres through its “amido” nitrogen while simultaneously chelating the terminal zinc atom. The second amidinate ligand, with a more evenly delocalised negative charge [C–N 1.323(4) Å and 1.334(4) Å], adopts a bridging Zn–N–C–N–Zn binding motif.

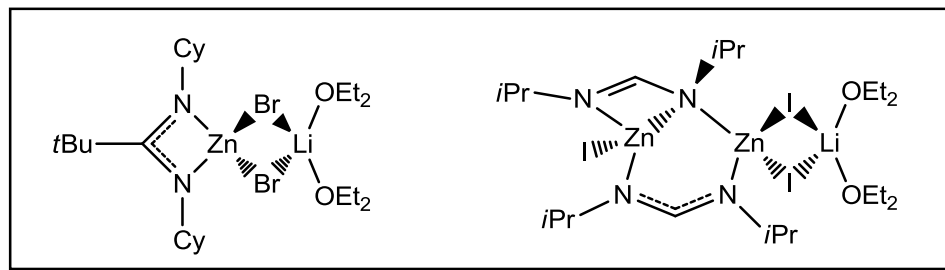


Figure 10.13: Rare examples of amidinato zincate complexes. $\{(t\text{Bu})\text{C}[(\text{Cy})\text{N}]_2\}\text{Zn}(\text{Br})_2\text{Li}(\text{OEt}_2)_2$ (LHS) and $\text{IZn}\{[\text{N}(i\text{Pr})]_2\text{C}(\text{Me})\}_2\text{Zn}(\text{I})_2\text{Li}(\text{OEt}_2)_2$ (RHS).

The three remaining amidinato zincate complexes are all lithium based inverse crowns, encapsulating either oxide or alkoxide anions. The first two examples were synthesised by Wheatley while investigating the zincate chemistry of the amidinato ligand $[\text{N}(\text{Ph})]_2\text{C}(\text{Ph})$. It was found that the 1:1 reaction of Me_2Zn with $\text{H}[\text{N}(\text{Ph})]_2\text{C}(\text{Ph})$ gave empirically “ $\text{MeZn}[\text{N}(\text{Ph})]_2\text{C}(\text{Ph})$ ” with loss of methane gas.^[137] Co-complexation of this amidinato zinc with $t\text{BuLi}$, followed by exposure to dry air, generated the hexanuclear oxo inverse crown $\{(\text{Ph})\text{C}[(\text{Ph})\text{N}]_2\}_6\text{Li}_4\text{Zn}_2\text{O}$, supported solely by amidinato ligands (Figure 10.14). If the same bimetallic mixture was exposed to dry air while in a THF solution, as opposed to toluene, then oxygen insertion into the methyl ligands on zinc resulted in tetranuclear $\{(\text{Ph})\text{C}[(\text{Ph})\text{N}]_2\}_4\text{Li}_2\text{Zn}_2(\text{OMe})_2$ (Figure 10.14).^[137] Finally, Junk investigated the incorporation of the amidinato ligand $[\text{N}(p\text{-Tol})]_2\text{CH}$ within zinc complexes. It was found that a constant impurity formed during the metathesis reaction of $\text{Li}[\text{N}(p\text{-Tol})]_2\text{CH}$ with zinc chloride in diethylether was the oxo inverse crown $[(p\text{-Tol})\text{NCHN}(p\text{-Tol})\text{O}]_6\text{Li}_2\text{Zn}_3$.^[138] This unusual species, only ever isolated in trace amounts, is presumed to form as a result of fortuitous ingress of oxygen contamination into the reaction media. These three examples suggest that amidinato ligands have a significant propensity towards inverse crown formation.

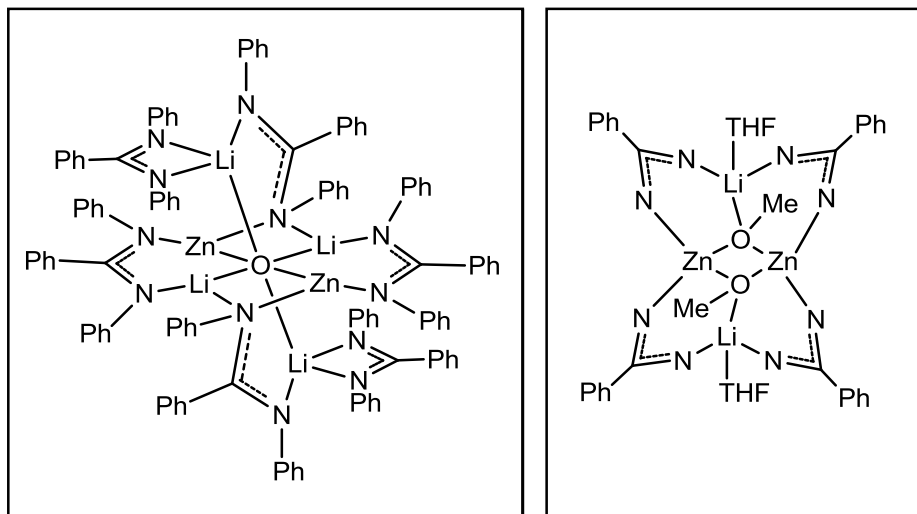
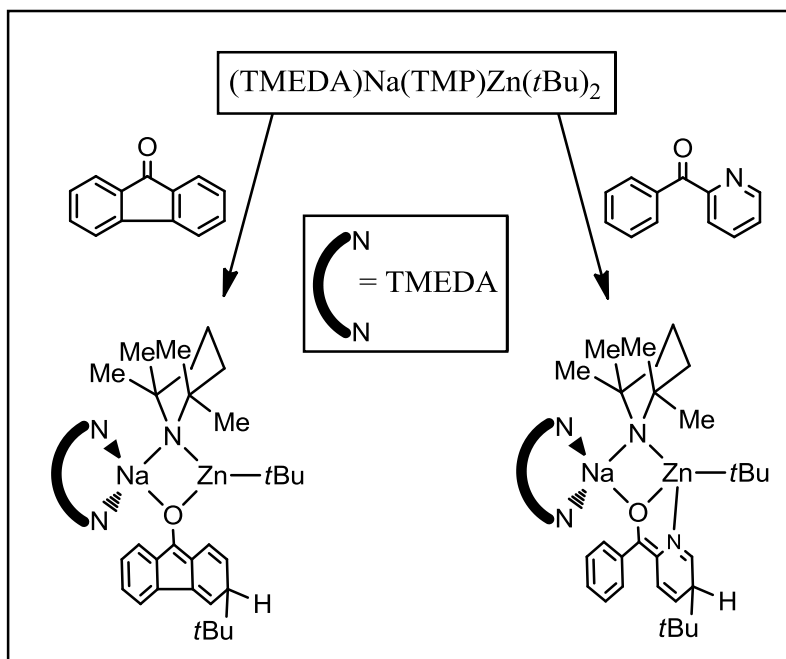


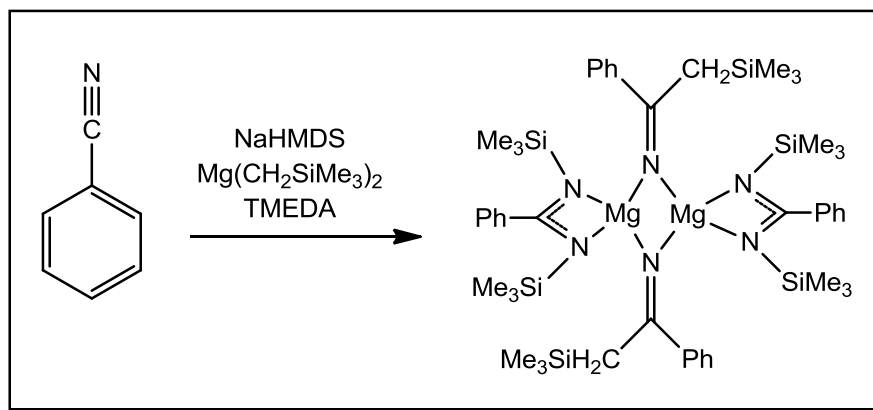
Figure 10.14: Structures of oxo and alkoxy zincate inverse crowns supported by the amidinato $(\text{Ph})\text{C}[(\text{Ph})\text{N}]_2$ ligand.

That the amidinato complex **41**, the amido addition product of an alkyl amido zincate mixture, is the favoured result is highly unusual. There are few examples of alkyl amido zincates engaging in addition reactions. Sodium TMP zincate **2**, which acts as an efficient Brønsted base towards 1-cyanonaphthalene, performs an unusual 1,6-addition of a *tert*-butyl anion to benzophenone.^[139] More recently, the same reagent performed 1,6-additions to fluorenone and 2-benzoylpyridine, establishing that this unusual mode of addition may be general for this TMP zincate towards benzoyl, or related heterocyclic functionalities (Scheme 10.3).^[140] The difference in selectivity between the TMP zincate **2** and the zinc rich **38** towards 1-cyanonaphthalene [**2** induces *ortho* deprotonation, **38** performs amido addition] is noteworthy and is most likely a result of the different steric demands of the different amido ligands. In the reaction between the TMP zincate **2** and 1-cyanonaphthalene, addition of the TMP anion across the nitrile functionality, analogous to the DIBA addition observed when zinc rich **38** is employed, should be severely hindered by the greater steric demands of TMP. This greater steric bulk, and therefore reduced nucleophilicity, relative to DIBA may also explain why TMP zincate **2**, when engaged in addition reactions, chemoselectively results in alkyl addition while in forming amidinato complex **41**, the DIBA zincate **38** produces the amido addition product.



Scheme 10.3: Unusual 1,6-alkylation of fluorenone and 2-benzoylpyridine performed by TMP zincate 2.

The reaction of the bimetallic mixture of NaHMDS and $\text{Mg}(\text{CH}_2\text{SiMe}_3)_2$ and one molar equivalent of TMEDA with benzonitrile provides another example of an alkyl amido ate addition reaction. When the organometallic species were pre-mixed with TMEDA before benzonitrile addition the symmetrical amidinato homometallic $(\{\text{Ph}\}\text{C}[\{\text{Ph}\}\text{N}]_2)\text{Mg}[\text{N}=\text{C}(\text{CH}_2\text{SiMe}_3)\text{Ph}]_2$ was produced (Scheme 10.4).^[141] As in the case of the synthesis of **41**, the exact nature of the organometallics responsible for this transformation remains uncertain. What is certain is that the bimetallic mixture has performed both an alkylation reaction and an amination within this one pot synthesis. Amination of benzonitrile by HMDS giving $\text{N}=\text{C}[\text{N}(\text{SiMe}_3)_2]\text{Ph}$ is followed by a 1,3-sigmatropic shift of a trimethylsilyl group to yield the final symmetrical amidinato ligand $[\text{N}(\text{SiMe}_3)_2]\text{C}(\text{Ph})$. The homometallic reagents have both demonstrated that they can perform the required addition reactions towards benzonitrile, independently of the other metal centre to furnish the same result.



Scheme 10.4: Combination of alkyl and amido addition exhibited by a Na/Mg bimetallic mixture.

10.4 α -Nitriles, a potential new area for zincates

Reaction of zinc rich zincate **38** with the *iso*-propylcyanide produced a second novel zincate reagent in $\{(TMEDA)Li[NCC(Me)_2Zn(tBu)_2]\}_2$ **42** (

Figure 10.15). A small crop of colourless crystals were grown at -30°C . The structure was confirmed by NMR spectroscopic analysis and X-ray diffraction techniques. Unfortunately the X-ray analysis was only sufficient to determine the basic molecular structure which negates discussion of geometrical data. In this example the *iso*-propyl methine proton is removed instead of nucleophilic addition across the nitrile. The zincated Me_2CCN units coordinate through the electronegative nitrogen atom to $\text{Li}(TMEDA)$ cations which dimerise to form a $(TMEDA)Li(\mu\text{-N}\equiv\text{CR})_2Li(TMEDA)$ ring.

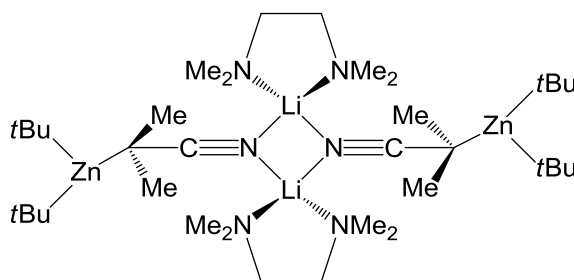
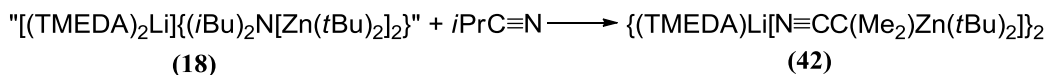


Figure 10.15: Synthesis of zincated nitrile complex **42** and its molecular structure.

There are currently only seven structures in the CCDB^[79] with a four-membered (MN)₂ ring (where M = any alkali metal and N belongs to N≡C) with “organic” nitrile species and a further eleven with “inorganic” nitrile ligands. A family of lithiated α -amino nitriles accounts for three of the organic nitrile compounds.^[142] α -Amino nitriles are important and versatile substrates in organic synthesis. A metallated α -amino nitrile can be thought of as a masked acyl anion and they have thus found utility in asymmetric nucleophilic acylation (Figure 10.16).^[143]

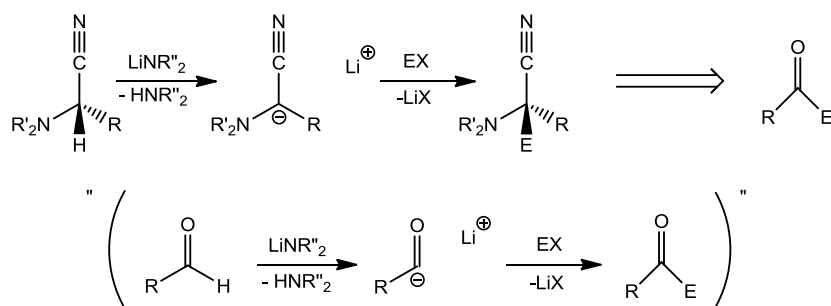


Figure 10.16: Illustration of the link between α -amino nitriles and acyl anions.

When the amino group of the α -amino nitrile is a chiral amine auxiliary then enantioselective Michael additions are possible and have shown in selective cases to exhibit high *ee* values. When quenching the Michael adduct by α -alkylation the two reactions in tandem produce two new chiral centres (Figure 10.17).^[144]

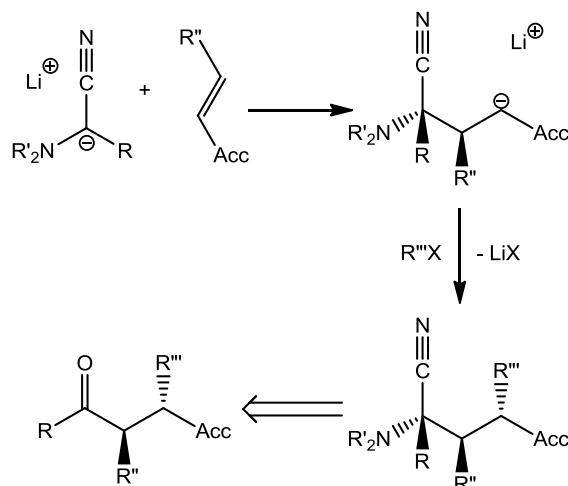
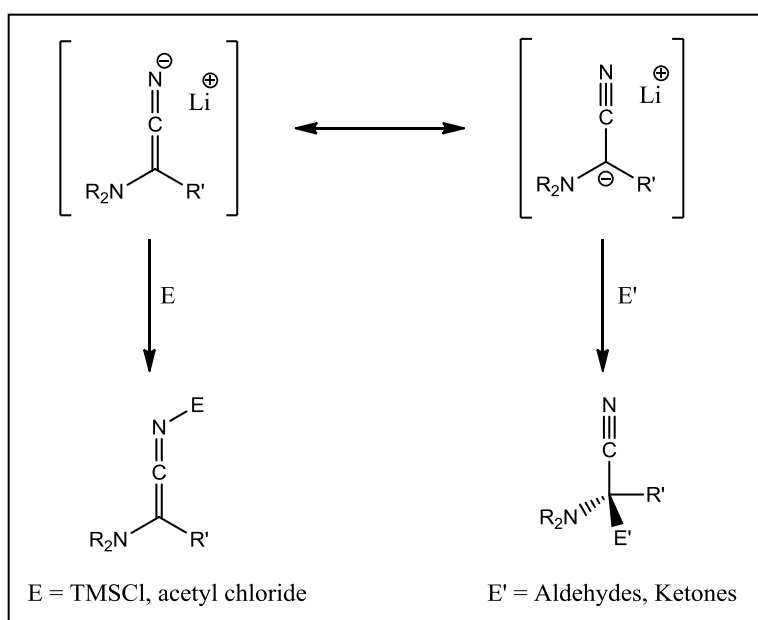


Figure 10.17: Michael addition of an α -amino nitrile producing two new chiral centres.

The quenching of metallated α -amino nitriles with electrophiles is complicated by their ability to behave as either nitrogen or carbon nucleophiles (Scheme 10.5).^[145] In order to treat these metallated species as a potential synthon for an acyl anion, and in order to take advantage of the enantioselectivity that a chiral amino auxiliary can induce, the metallated nitrile must act as a carbon nucleophile. Indeed, soft electrophiles such as aldehydes or ketones tend to promote exclusive carbo-nucleophilic addition of the metallated nitrile. By contrast, harder electrophiles such as acetyl chloride or trimethylsilyl chloride are more liable to produce an imine as a result of the metallated nitrile acting as a nitrogen nucleophile.



Scheme 10.5: Depiction of how a lithiated α -amino nitrile can act as both a carbon or nitrogen nucleophile.

Various α -proton α -amino nitrile compounds were metallated by lithium diethylamide and crystals amenable to X-ray diffraction studies were grown.^[142] All three of the produced lithiated nitriles had dimeric structures akin to that of **42** (Figure 10.18). Rather than bind to the deprotonated carbon, the lithium cation is situated on the cyano nitrogen in a bonding mode analogous to that seen in metal enolates. Bond lengths within these structures suggest a delocalised $C \text{---} C \equiv N$ system.

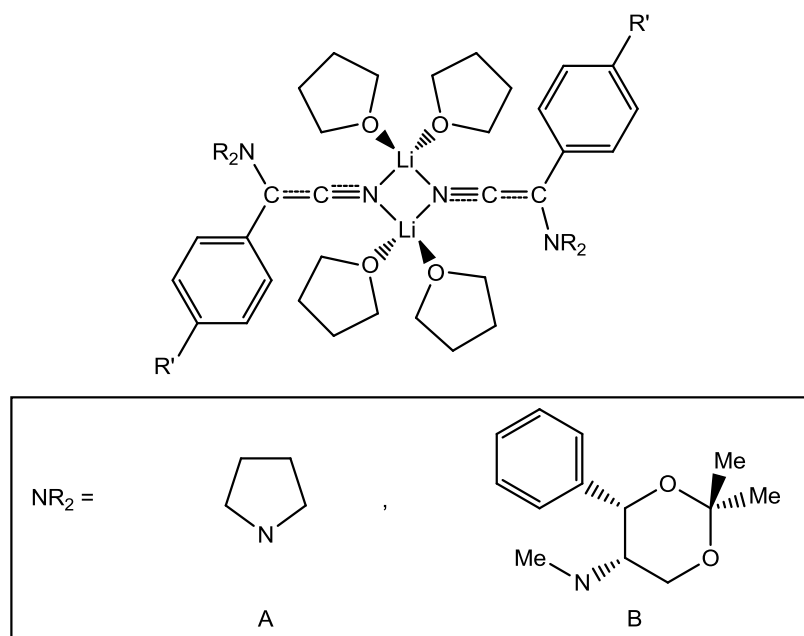


Figure 10.18: A general structure of α -amino nitriles.

The structure of **42** reveals that if the α -amino nitriles were metallated by a zincate reagent, or if the lithiated nitriles were subsequently complexed with a dialkylzinc reagent, then the substrates are liable to be simultaneously N and C metallated. This could be used to greatly alter both the sterics and the electronics of these important intermediates. This could potentially be used to control whether the metallated nitrile behaves as a nitrogen or a carbon nucleophile.

There is currently only one example in the CCDB^[79] of a nitrile that has been α -deprotonated and resides in a zincate complex, namely the supramolecular $[Li(THF)][Zn_3(CH_2C\equiv N)_3(LiBr)(NPM_e_3)_4]$.^[146] Its deprotonated acetonitrile units, in keeping with the theme of **42**, are N lithiated and C zincated (Figure 10.19). However, the complex is radically different to **42** in other respects. It is a polymer of asymmetric cubanes made up of three zinc and one lithium centres and four nitrogen centres of $N=PMe_3$. The cubanes are linked via lithium cations, which bridge three separate cubanes through nitrile nitrogen atoms, to form a 3-d network.

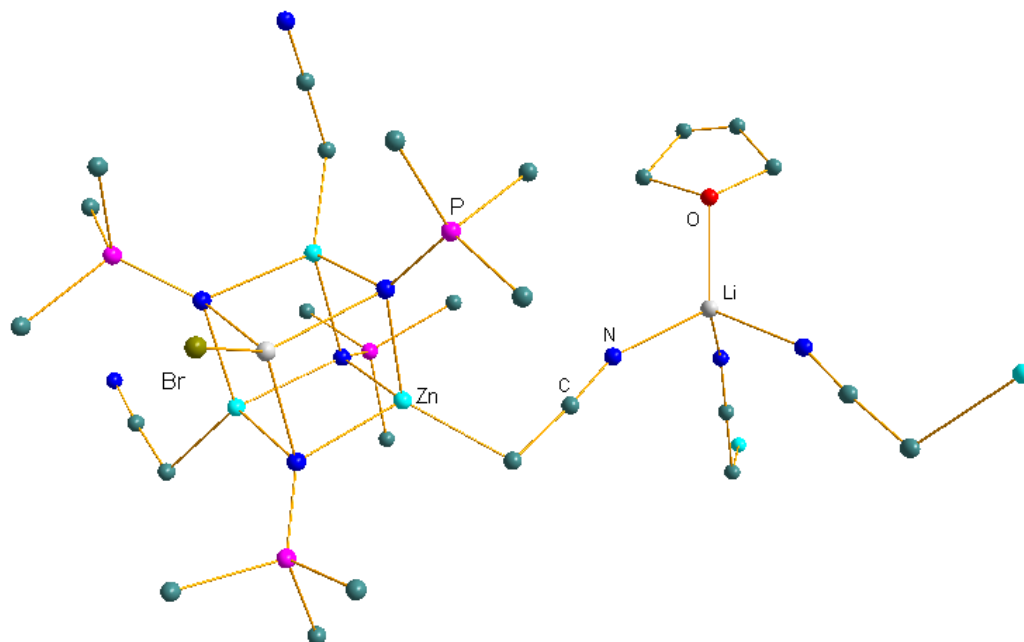


Figure 10.19: Monomeric unit of the supramolecular $[\text{Li}(\text{THF})][\text{Zn}_3(\text{CH}_2\text{CN})_3(\text{LiBr})(\text{NPMe}_3)_4]$ containing α -metallated acetonitrile units.

The aforementioned structures with a four-membered $\text{M}(\mu\text{-N}\equiv\text{C})\text{M}(\mu\text{-N}\equiv\text{C})$ (M = any alkali metal) with “inorganic” nitriles all belong to another class of “ate” complex. The nitrile group was first utilised in cuprate chemistry by Lipschutz in an attempt to produce higher order species of empirical formulation “ $\text{Li}_2\text{R}_2\text{CuCN}$ ”.^[147] It has since been discovered that these Lipschutz reagents, which often exhibit enhanced reactivity over the standard Gilman reagent LiCuR_2 , are most probably best described as “ $\text{LiCuR}_2\cdot\text{LiCN}$ ”^[148] analogous to the addition of LiCl to Grignard reagents pioneered by Knochel.^[148] A striking example of these cuprate complexes is $(\text{TMP})_2\text{CuLi}\cdot\text{LiCN}$ which has been efficiently utilised in the directed *ortho* metallation of *N,N*-diisopropylbenzamide.^[149]

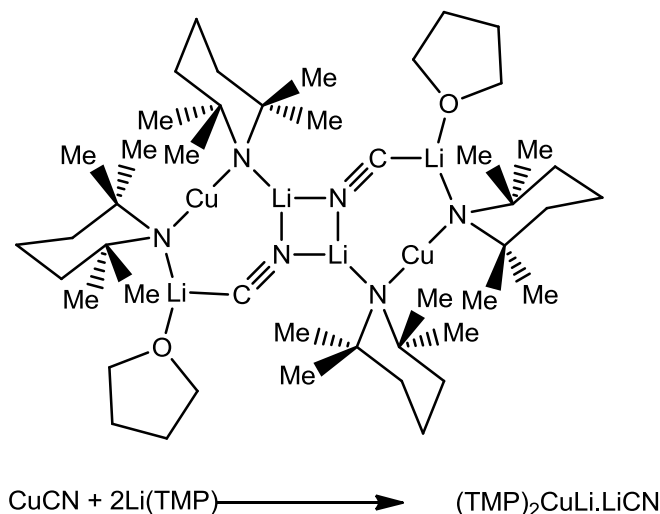


Figure 10.20: Example of a Lipschutz cuprate exhibiting a $[\text{Li}(\text{N}\equiv\text{C})]_2$ ring and its synthesis.

10.5 An expansion of zincate enolate chemistry

Another class of compound known to exhibit a high degree of structural diversity is metal enolates. For this reason 2,4,6-trimethylacetophenone was chosen as another substrate for zincation in the continuing search for novel molecular assemblies. The reaction of **38** was carried out in hexane solution producing luminous green crystals. X-ray diffraction revealed the product to be the monometallic zinc complex $(\text{TMEDA})\text{Zn}(t\text{Bu})\text{OC}(=\text{CH}_2)\text{Mes}$ **43** (Figure 10.21).

New zincate enolate **43** consists of a zinc centre in a distorted tetrahedral environment (angles totalling 644.51° , averaging 107.4°) involving the oxygen of the newly formed enolate anion [$\text{Zn1}-\text{O2}$ 1.933(2) Å], one *tert*-butyl ligand [$\text{Zn1}-\text{C1}$ 2.013(3) Å], and a TMEDA molecule [$\text{Zn1}-\text{N31}$ 2.175(3) Å, $\text{Zn1}-\text{N34}$ 2.176(3) Å]. Enolate formation can be inferred from the long C2–O2 bond length [1.318(4) Å], comparable to that in the zinc alkoxide $(\text{TMEDA})\text{Zn}(\text{Et})\text{OC}(\text{CF}_3)(\text{Et})\text{Ph}$ [C–O 1.362(6) Å], and the short C2–C20 bond length of 1.328(4) Å indicative of a C=C double bond.

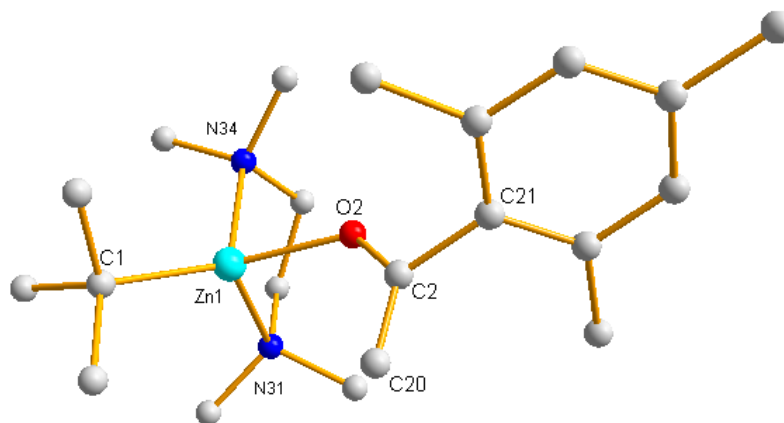


Figure 10.21: Molecular structure of (TMEDA)Zn(*t*-Bu)OC(=CH₂)Mes **43**. Hydrogen atoms omitted for clarity. Selected bond lengths [Å] and angles [°]: Zn1–O2 1.933(2), Zn1–C1 2.013(3), Zn1–N31 2.175(3), Zn1–N34 2.176(3), C2–O2 1.318(4), C2–C20 1.328(4), C2–C21 1.511(4), C1–Zn1–O2 130.0(1), C1–Zn1–N31 121.7(1), C1–Zn1–N34 119.6(1), O2–Zn1–N31 98.77(9), O2–Zn1–N34 90.46(9), N31–Zn1–N34 83.98(9), C20–C2–C21 119.6(3), C20–C2–O2 126.7(3), O2–C2–C21 113.7(3).

Examining the ¹H NMR spectrum for **43** in C₆D₆ solution reveals two signals at 4.00 ppm and 4.31 ppm confirming enolate formation. The presence of two distinct ethylene signals also establishes that these protons do not interchange on the NMR timescale. A fine coupling of these two vinylic protons is also observed with a ¹J_{H-H} coupling constant of 0.76 Hz. A singlet at 1.46 ppm corresponding to the *tert*-butyl anion integrates to nine relative to the vinylic proton signals, confirming a 1:1 ratio. Finally the resonances associated with TMEDA are highly broad, each spanning at least 0.25 ppm. This peak width is consistent with chelation of a heteroleptic zinc centre.^[140, 150] The presence of TMEDA was confirmed by characteristic resonances in the ¹³C NMR spectrum at 56.9 ppm and 47.1 ppm, and a ⁷Li NMR experiment was performed to confirm the absence of the alkali metal from the crystallised complex.

Investigations into the reactivity of the tris-amido zincate “LiZn(TMP)₃” and the dialkyl-amido zincate (TMEDA)Li(TMP)ZnMe₂ with 2,4,6-trimethylacetophenone have previously been reported.^[151] The latter was proposed to form the expected intermediate (TMEDA)Li[OC(=CH₂)Mes]ZnMe₂ before disproportionating to give the lithium enolate {(TMEDA)Li[OC(=CH₂)Mes]}₂ and (TMEDA)ZnMe₂ (Figure 10.22). This pathway was

evidenced by crystallisation of the lithium enolate and observation of $\text{Me}_2\text{Zn}(\text{TMEDA})$ and $\text{TMP}(\text{H})$ in the liquors by ^1H NMR spectroscopic studies.

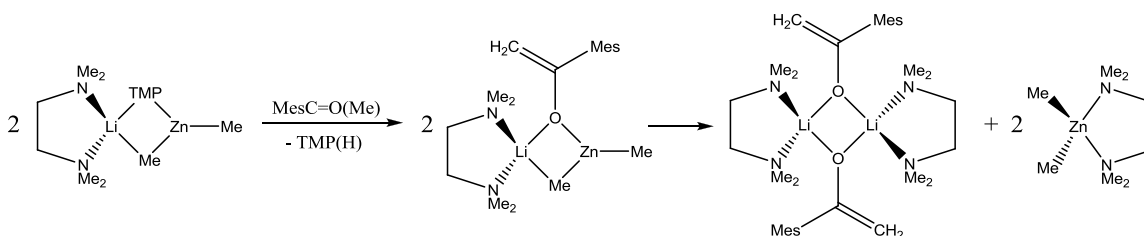


Figure 10.22: Proposed disproportionation pathway to explain the synthesis of $(\text{TMEDA})\text{Li}[\text{OC}(\text{=CH}_2)\text{Mes}]_2$ from $(\text{TMEDA})\text{Li}(\text{TMP})\text{ZnMe}_2$.

There are currently only seven examples of enolato zincate structures in the CCDB,^[79] the three products of 1,6-alkyl addition of the sodium zincate base **2** across bicyclic ketones discussed previously (Scheme 10.3), as well as $[\text{K}_2\text{Zn}_2\{\mu\text{-OC}(\text{=CH}_2)\text{-Mes}\}_6(\text{CH}_3\text{Ph})_2]$, $[\text{Na}_2\text{Zn}_2\{\mu\text{-OC}(\text{=CH}_2)\text{-Mes}\}_6\{\text{O}(\text{H})\text{C}(\text{CH}_3)\text{Mes}\}_2]$, $[(\text{TMEDA})_2\text{Na}_2\text{Zn}\{\mu\text{-OC}(\text{=CH}_2)\text{Mes}\}_4]$ and $[\{\text{Mes}(\text{CH}_3)\text{C}(\text{H})\text{O}\}_2\text{Na}_2\text{Zn}\{\mu\text{-OC}(\text{=CH}_2)\text{Mes}\}_4]$.^[151-152] These last four compounds were all prepared using homoleptic amido-zincates either $\text{MZn}(\text{HMDS})_3$ ($\text{M} = \text{Na}, \text{K}$)^[152] or $\text{LiZn}(\text{TMP})_3$.^[151] $\text{MZn}(\text{HMDS})_3$ produced an inverse crown type structure with a ring of two sodium or potassium cations, four enolate ligands and two zinc centres encapsulating two enolate guest anions. The sodium ions are solvated by non-deprotonated ketone while the potassium centres are solvated by toluene. $\text{LiZn}(\text{TMP})_3$ produced a linear tri-nuclear compound slightly reminiscent of that proposed in **35** (Figure 9.33, page 91). In this case however it is a symmetrical $\text{Li}\cdots\text{Zn}\cdots\text{Li}$ chain bridged by four enolate ligands. The lithium centres are capped by either TMEDA or $\text{TMP}(\text{H})$ depending on the reaction conditions.

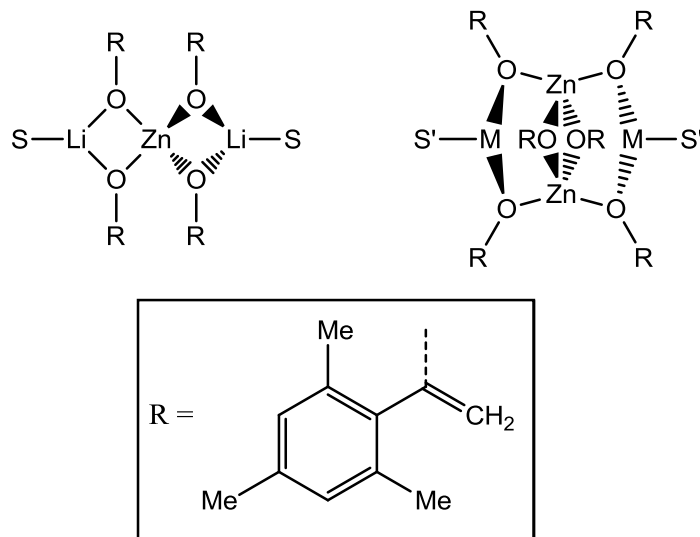


Figure 10.23: Enolatozincate structures derived from 2,4,6-trimethylacetophenone. **S** = TMEDA or TMP(H). **S'** = O=C(Me)Mes, **M** = Na; **S'** = toluene, **M** = K.

A monomeric zinc enolate, similar to **43** was prepared by direct deprotonation of two equivalents of 2,4,6-trimethylacetophenone using the bis-amide $\text{Zn}(\text{TMP})_2$.^[151] Crystallisation of the product was effected through the use of TMEDA as a donor solvent. It is interesting to note that while the lithium enolate exists as a dimer, **43** and $(\text{TMEDA})\text{Zn}[\text{OC}(\text{CH}_2)\text{Mes}]_2$ are both monomers. Recent studies by Henderson and Brown provided strong evidence in the case of magnesium enolates, that the stereoselectivity of enolate formation can be profoundly affected by the aggregation state in solution. $\text{Mg}(\text{HMDS})_2$ was reacted with half an equivalent of propiophenone in d_8 -toluene and the reaction monitored by ^1H NMR spectroscopy. This resulted in both the *E* and *Z* isomers of $(\text{HMDS})\text{Mg}(\mu\text{-HMDS})(\mu\text{-OR})\text{Mg}(\text{HMDS})$ [$\text{R} = \text{C}(\text{CH}_2\text{Me})\text{Ph}$] in a 74:26 ratio.^[153] The addition of THF- D_8 greatly altered the composition of the solution.^[154] There were now dimeric species present, $(\text{HMDS})(\text{THF})\text{Mg}(\mu\text{-OR})_2\text{Mg}(\text{THF})(\text{HMDS})$, in the three possible configurations *E/E*, *E/Z*, *Z/Z* as well as the *Z* monomer $\text{ROMg}(\text{THF})_2(\text{HMDS})$, however no *E* monomer was observed. DFT calculations confirmed that the *Z* monomer was 2.8 Kcal/mol more stable than the *E* monomer. This results in concentration having a profound influence on the total *E:Z* ratio in solution. The implication that the stability difference between *E* and *Z* isomers is more pronounced in the monomeric form than in higher oligomers suggests that monomeric

species analogous to **43**, if they fail to aggregate in solution, could lead to high levels of stereoselectivity.

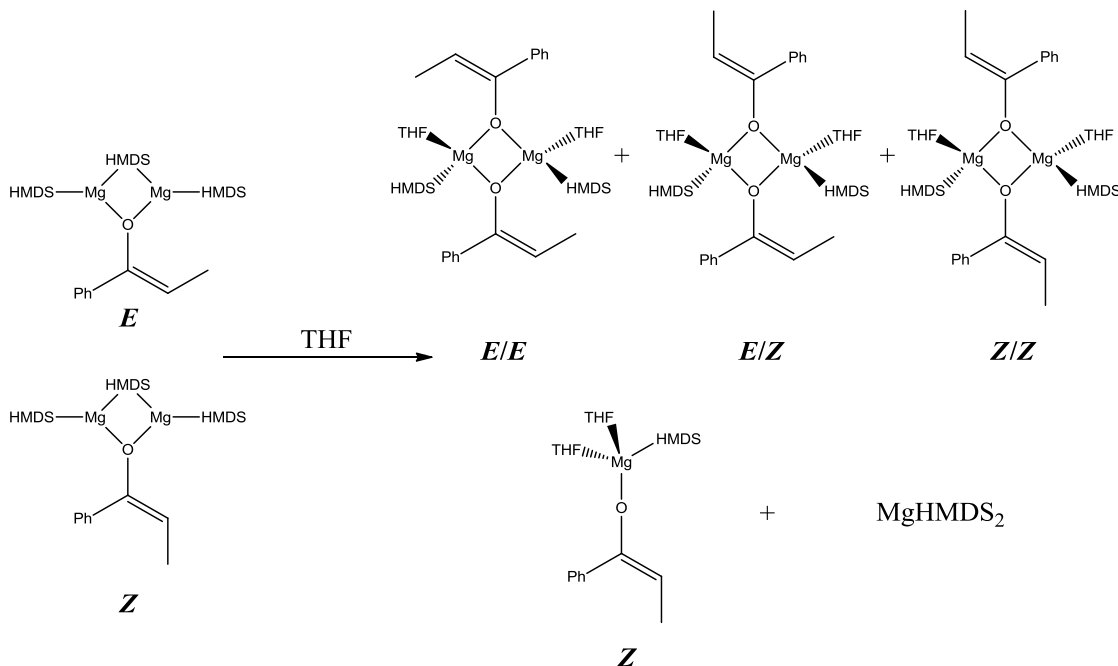


Figure 10.24: The different aggregation states of a magnesium enolate in THF solution.

10.6 Conclusions and future work

This chapter has focused on exploring the properties of the rarely studied amido ligand DIBA and utilising it to prepare novel zincate complexes. Of particular note is the solvent separated alkyl amido lithio dizincate **38**. A search of the CCDB^[79] revealed its composition to be significantly different to any of the other AMZn₂R₅ formulations (M = any alkali metal) previously reported. It was found however to resemble the motif of a neutral zinc complex proposed to be responsible for many alkylation reactions.

The formation of both the zinc rich **38** and the bisamido zincate **40** has been explained in terms of related disproportionation pathways. These are two further examples, combined with previous research investigating amido ligands such as DA, DMP and dimethylamide, which indicate that the integrity of alkyl amido zincates appears to be linked to the steric properties of the amido ligand. The sterically demanding TMP anion has an illustrious past in homometallic as well as in bimetallic metallation chemistry

owing to its high basicity yet low nucleophilicity. Specifically within a mixed metal context, as the complex nature of the zinc rich zincate's (**38**) solution chemistry demonstrates, a crucial yet underappreciated property of this amido ligand may also be its propensity to form constitutionally robust mixed metal species.

Despite the success of this investigation into the DIBA ligand to produce some interesting and novel structural chemistry its scope for success is limited, as has been alluded to previously, by the lack of control over the dizincate base. In order to produce a dizincate of synthetic utility new reagents will need to be designed that are reproducible without side products. A potential starting point is the dibenzofuran ligand set developed by Zsang^[155] and Hagadorn.^[156] The flexibility of this ligand set has been shown by the successful copper(I) catalysed coupling of various amino groups to 4,6-diiodobenzofuran. Even more encouraging is the successful clean and high yielding synthesis of various neutral dizinc complexes of general formula 4,6-[N(ZnR)CH₂CH₂NR'₂](C₁₂H₆O) where R = Me, Et, Ph and R' = Me, ⁱPr (Figure 10.25).^[124] It could be envisaged that further reaction of these or related neutral zinc complexes with two molar equivalents of M(TMP) (M = Li, Na, K) would bring about the synthesis of new dizincate reagents in a much more controlled process than in the synthesis of **38**. The diphenyl-dizinc complex 4,6-[N(ZnPh)CH₂CH₂NMe₂](C₁₂H₆O) tantalisingly demonstrates that the void between the two zinc centres is a good fit for 6-membered aromatic rings. New dizincate reagents built on this motif could theoretically be the key to di-metallations of substrates such as anisole. The formation of 4,6-{N[Al(Me)₂]CH₂CH₂NMe₂}(C₁₂H₆O)^[124] and related titanium complexes such as 4,6-{C[N(*i*Pr)]₂Ti(Me)₂Cp}Ar (Ar = 9-(Me₂)C₁₂H₆O)^[157] also highlights the potential to use different metal centres with this ligand set. Another potential avenue for further research is to utilise these dibenzofuran ligands to expand upon the growing area of alkali metal mediated transition metallation (AMMTM).

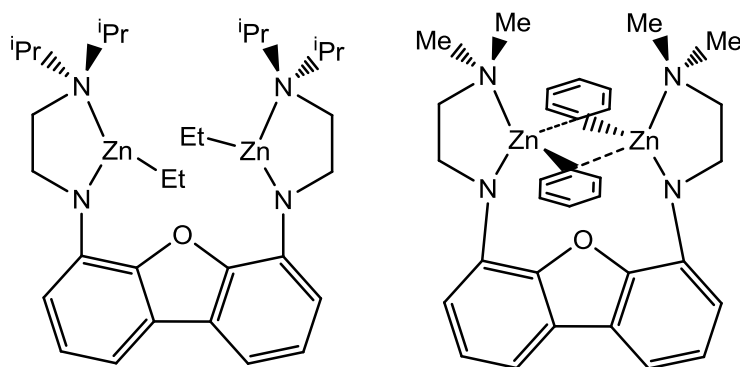


Figure 10.25: Examples of stable, neutral dizinc complexes (4,6-[N(ZnEt)CH₂CH₂N^{*i*}Pr₂](C₁₂H₆O) (LHS), 4,6-[N(ZnPh)CH₂CH₂NMe₂](C₁₂H₆O) (RHS)).

The synthesis of **41** has highlighted the paucity of research into alkali metal amidinatozincate chemistry. The limited literature known suggests that ligands of this class may be excellent constructors of inverse crown motifs. Since the coinage of the inverse crown concept in 2000, there have been some spectacular macromolecular constructs such as the 24 membered potassium magnesiate wheel containing 6 metallated tolyl anions,^[158] or more recently the trapping of a hexameric butyllithium fragment within a LiTMP/LiCp molecular square.^[159] One potential factor limiting access to greater numbers of inverse crowns, encapsulating a more diverse range of anions, under the synthetic methodologies employed thus far is the requirement of an amido ligand that can both perform an efficient metallation of a substrate to generate the desired anionic core and support the construction of the metallic crown. A new two phase synthetic strategy which utilises the TMP anions proven metallating prowess to generate the desired anion, followed by transamination (a concept already successfully demonstrated within TMP zincate chemistry)^[49c] for an amidinato ligand with their apparent innate ability to deliver inverse crown structures, might be envisioned to deliver a new wave of exciting and versatile macromolecular constructs.

After the synthesis of the α -zincated nitrile species **42**, one obvious route for further development of zinc chemistry is to investigate the metallations of various α -proton bearing nitrile compounds. This should be carried out both by well-defined zincate bases and by sequential lithiation followed by co-complexation via dialkyl-zinc reagents. Homometallic Zn(TMP)₂ could also prove synthetically useful in this field. If it proves

that the N-lithiated C-zincated motif of **42** is a recurring feature then judicious choice of metallating agent could permit a close tuning of the anionic properties of the metallated nitrile species. It should then prove interesting to exploit this new found control over the reaction intermediate in an attempt to dictate the outcome of electrophilic quench reactions.

11 Alkali metal control of the metal–metal bonding properties of the group VI metals

Metal-metal bonding has long been an area of special fascination to both synthetic and theoretical chemists. Recent achievements, including the first fully-characterised Mg–Mg^[160] and Zn–Zn^[161] bonds, as well as the first isolation of a stable quintuple metal–metal bond^[162] and subsequent probing of its chemistry,^[61, 163] demonstrate that this remains a topic that captures the imagination of researchers across the disciplines. The group VI metals have played a pivotal role in developing our understanding of the nature of metal–metal multiple bonding. It was this triad (Cr, Mo, W) that gave the first complete sets of homologous metal–metal quadruple bond containing compounds, such as the tris(cyclooctatetraene) species $M_2(C_8H_8)_3$ ^[164] and the tetralithium octamethylates $Li_4M_2Me_8$ ^[165] (M = Cr, Mo, W). While the metal–metal bonding interaction in the larger transition metal Mo and W octamethylates are assumed to be strong, the relevance of the Cr–Cr interaction to the stability of the octamethyl complex $Li_4Cr_2Me_8$ has been cast into doubt. This chapter aims to explore the chemistry of the octamethylates, in particular concentrating on the role of the alkali metal on the structure and stability of these complexes. To this end, the synthesis of sodium congeners to these classic lithium “ate” species has been attempted.

Lithium octamethylchromate $Li_4Cr_2Me_8$ was first synthesised by Krause in 1970 through the metathesis reaction of methyl lithium with chromium(II) chloride in diethylether.^[165c] After removal of the produced lithium chloride by simple filtration, the product could be isolated as the etherate $[(Et_2O)Li]_4Cr_2Me_8$ by crystallisation at $-30^\circ C$. If the reaction was repeated in an ether:THF, 90:10 solution then the THF solvate $[(THF)Li]_4Cr_2Me_8$ could be isolated, again by crystallisation at $-30^\circ C$ (Figure 11.1). Both compounds are yellow/orange in colour. X-ray diffraction data of the THF solvate unequivocally confirmed the compounds constitution and revealed that it contained a short Cr–Cr distance of $1.981(5) \text{ \AA}$. Analysis of either solvate by 1H NMR spectroscopy revealed sharp signals for the donor ligand (either THF or ether) and a sharp singlet for the methyl ligands, demonstrating that the complex is essentially diamagnetic. Thus, the four valence

d-electrons on each chromium centre are necessarily coupled, supporting the hypothesis that a strong Cr–Cr quadruple bond exists in these compounds.

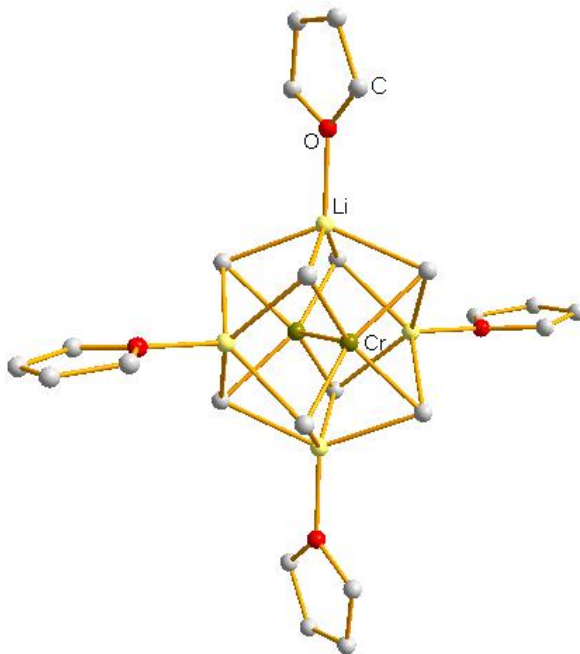


Figure 11.1: Molecular structure of the lithium octamethylchromate [(THF)Li]₄Cr₂Me₈.

Since the synthesis and structural elucidation of the octamethylate [(THF)Li]₄Cr₂Me₈, many other dimeric chromium(II) species have been identified containing a Cr–Cr interaction. The octamethylate is a highly unusual example of a compound containing such an interaction without the aid of ligands capable of bridging the two chromium centres. Also, puzzlingly, the observed chromium–chromium separation in the known chromium(II) dimers varies significantly. For example, the shortest known chromium(II) metal–metal separation is currently 1.773(1) Å, found within the paddlewheel complex [LCr(Me)]₂ {L = (HMDS)C[(Cy)N]₂}.^[166] By contrast, the closely related [(DMF)₆Li]₂[L'Cr(Cl)]₂ (L' = 7-azaindole) has a corresponding separation of 2.688(2) Å (Figure 11.2).^[167]

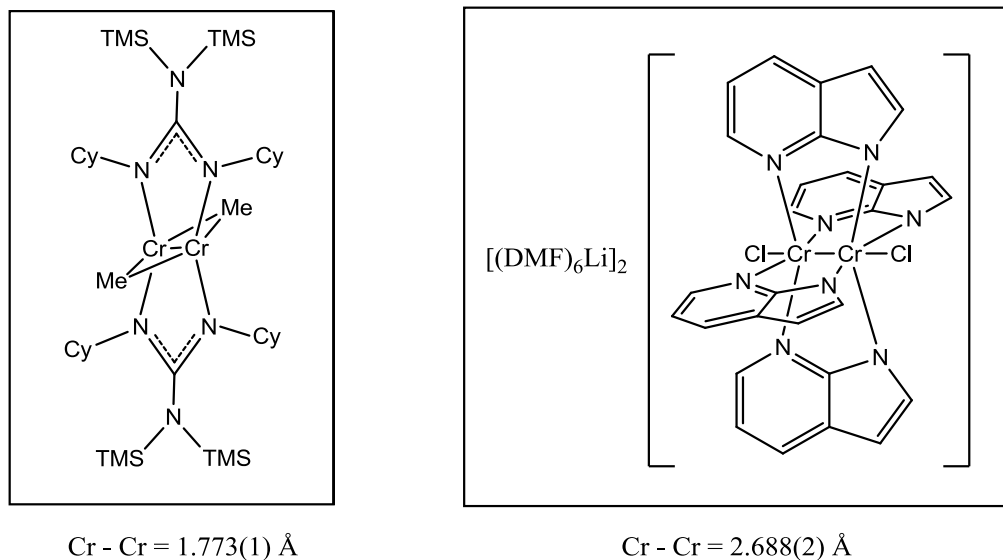
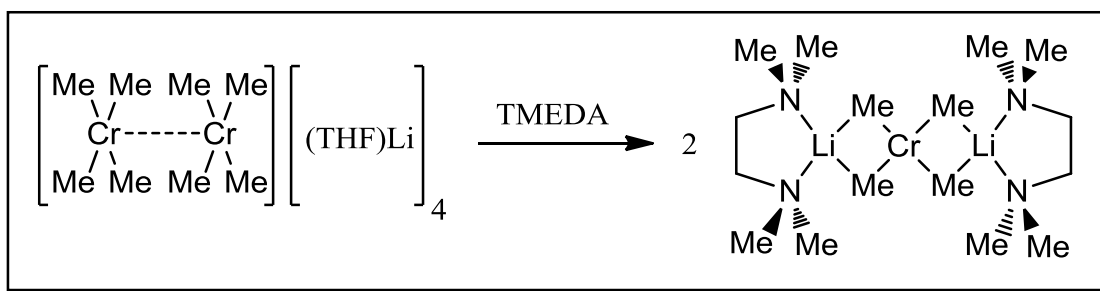


Figure 11.2: Cr–Cr separations in chromium(II) dimers varies greatly. For example $[\text{LCrMe}]_2$ (left) and $[(\text{DMF})_6\text{Li}]_2[\text{L}'\text{Cr}(\text{Cl})]_2$ (right).

In an authoritative review of the relevant literature,^[168] Gambarotta suggested that chromium(II) dimers do not contain strong metal–metal binding interactions, but instead the short Cr–Cr separations are an enforced artefact of the ligand set employed. This argument nicely explained the prominence of bridging ligands within known chromium(II) dimers and also the wide variation of the Cr–Cr “bond” lengths. He also elegantly used the monomeric nature of complexes such as $(\text{THF})_3\text{Cr}(\text{NC}_4\text{H}_4)_2$ and $(\text{Py})\text{Cr}[2-(\text{Me}_2\text{NCH}_2)-\text{C}_6\text{H}_4]_2$ (Py = pyridine) to argue that the chromium centres in such complexes must be electronically incapable of establishing a meaningful metal–metal bond, because there was no apparent steric hindrance that should prevent the formation of such a bond.

While Gambarotta’s reasoning made intuitive sense of the vast majority of known Cr–Cr interactions, the octamethylate $[(\text{THF})\text{Li}]_4\text{Cr}_2\text{Me}_8$ appeared to be an anomaly. There were surely no obvious bridging interactions within the Cr_2Me_8 tetra anion that could be said to enforce such a close Cr–Cr contact [1.981(5) Å]. It was again Gambarotta who discovered that reacting $[(\text{THF})\text{Li}]_4\text{Cr}_2\text{Me}_8$ with the diamine TMEDA resulted in homolytic cleavage to produce mono-nuclear $[(\text{TMEDA})\text{Li}]_2\text{CrMe}_4$ (Scheme 11.1).^[169] This severance of the formal Cr–Cr quadruple bond by the addition of a simple Lewis

base suggested that the metal–metal interaction must indeed be extremely weak. Gambarotta thus proposed that the octamethylate $[(\text{THF})\text{Li}]_4\text{Cr}_2\text{Me}_8$ was not being held together by an anomalously strong metal–metal interaction but instead through a series of Me–Li–Me bridges. It was this description of Krause’s classic complex that caught the attention of our group because it alluded to an alkali metal that was dictating the nature of a transition metal–metal bond.



Scheme 11.1: Cleavage of the lithium octamethylchromate dimer by the simple donor TMEDA.

11.1 Structural studies of sodium methylchromates

Turning to our own studies, given the apparent influential nature of the alkali metal in $[(\text{THF})\text{Li}]_4\text{Cr}_2\text{Me}_8$ we aimed to produce a sodium homologue. Therefore, to an ether solution of $[(\text{THF})\text{Li}]_4\text{Cr}_2\text{Me}_8$ at 0°C , prepared *in situ* by literature procedures,^[165c] was added four molar equivalents of sodium *tert*-butoxide. The solution colour changed from yellow/orange to green and was stirred for one hour, maintaining the temperature at 0°C . A crop of highly pyrophoric emerald green crystals could be isolated in a 51 % yield following the concentration of the solution and storage at -30°C overnight. X-ray diffraction data revealed the product to be the desired sodium chromate $[(\text{Et}_2\text{O})\text{Na}]_4\text{Cr}_2\text{Me}_8$ **44** (Figure 11.3). Even starting the synthesis from isolated crystalline material unambiguously confirmed to be the THF solvate $[(\text{THF})\text{Li}]_4\text{Cr}_2\text{Me}_8$, the product of reaction was always the diethylether solvate **44**.

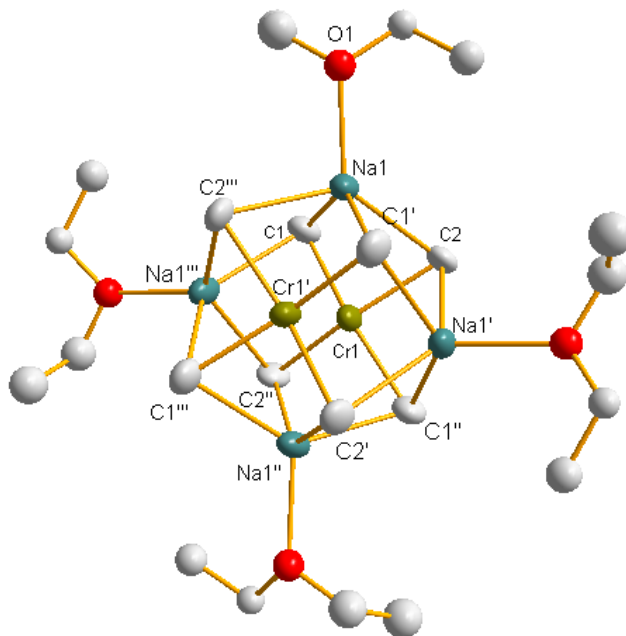


Figure 11.3: Molecular structure of sodium chromate $[(\text{Et}_2\text{O})\text{Na}]_4\text{Cr}_2\text{Me}_8$ 44. Thermal ellipsoids shown at the 50 % probability level. Hydrogen atoms and minor disorder of the ether molecules omitted for clarity. Symmetry operations to generate equivalent atoms: $y, 2-x, 2-z; 2-x, 2-y, z; 2-y, x, 2-z$. Selected bond lengths [\AA] and angles [$^\circ$]: Cr1–Cr1' 3.260(1), Cr1–C1 2.20(1), Cr1–C2 2.201(9), Na1–C1 2.68(1), Na1–C2 2.73(1), Na1–C1' 2.72(1), Na1–C2''' 2.68(1), Na1–O1 2.302(7), C1–Cr1–C2 87.8(4), C1–Cr1–C1'' 160.8(4), C1–Cr1–C2'' 89.0(4), C1–Na1–C1' 137.3(3), C1–Na1–C2 68.5(3), C1–Na1–C2''' 96.5(3), C1–Na1–O1 107.7(3).

The sodium methylchromate adopts a dimeric structure, similar to that observed for the lithium homologue. The high symmetry of the molecule (tetragonal) results in a unit cell containing only half an ether ligand, half a sodium atom, one methyl anion and a quarter of a chromium centre. The molecule, excluding the ether solvent molecules, exhibits D_{4h} symmetry. Chromium lies in a distorted square planar geometry with average chromium–methyl bond lengths of 2.20 \AA , the same as those observed within the lithium complex. The two CrMe_4 complex dianions sit in an eclipsed conformation relative to each other, with four sodium cations occupying the space between them, capping four-membered faces constructed out of two methyl ligands from each CrMe_4 dianion. The average Na–C bond distance is 2.73 \AA , considerably longer than the equivalent Li–C bond lengths observed within $[(\text{THF})\text{Li}]_4\text{Cr}_2\text{Me}_8$ (average 2.374 \AA) owing to the greater size of the sodium cations relative to their lithium counterparts. This increase in the alkali metal–

methyl bond length, when moving from the lithium to the sodium octamethylate, results in an increase in the distance between the two CrMe_4 dianions. As a result, the Cr–Cr separation has increased markedly relative to the lithium complex (Figure 11.4). The super short Cr–Cr “quadruple” bond distance in $[(\text{THF})\text{Li}]_4\text{Cr}_2\text{Me}_8$ [1.981(5) Å] has now been extended to 3.260(1) Å. Despite the large metal–metal separation, there remains tantalising structural evidence of a retention of a Cr–Cr interaction, albeit long range. The chromium centres in the CrMe_4 dianions lie displaced from the plane of the four methyl ligands, towards the centre of the cluster, by 0.369(1) Å. While perhaps indicative of a continued bonding interaction between the two chromium centres, this is surely a weakened interaction when compared to the lithium complex, as evidenced by the greater recession of the chromium atoms into the heart of the lithium complex, displaced by 0.641(1) Å from the plane of its four methyl ligands (Figure 11.4). Alvarez has previously demonstrated a relationship between the pyramidity of chromium within a dinuclear species and the Cr–Cr separation distance.^[170]

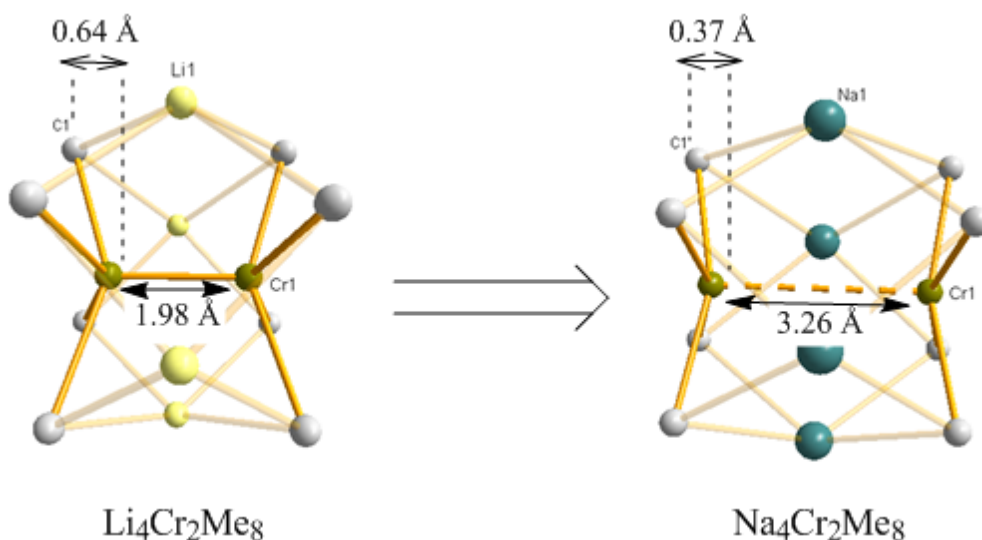


Figure 11.4: Illustration of the increase in the Cr–Cr separation, and the concomitant decrease in the distortion of the square planar geometry around chromium, when comparing lithium and sodium octamethylchromates.

We next set out to investigate how the sodium chromate might react towards the diamine TMEDA. Given the greater $\text{Cr}\cdots\text{Cr}$ separation in the sodium species, relative to its lithium congener, it might be expected that this dimeric species would cleave to produce

a mononuclear complex with even greater ease than observed by Gambarotta in the case of the lithium species $[(\text{Et}_2\text{O})\text{Li}]_4\text{Cr}_2\text{Me}_8$ (Scheme 11.1). Taking a pre-prepared ether solution of sodium chromate **44** and introducing four molar equivalents of TMEDA at -30°C gave a red/brown solution. A crop of intensely dark red crystals was produced on storage of the solution at -70°C . Single crystal X-ray diffraction analysis revealed surprisingly that the product was an unprecedented heptamethyl dichromate species of formula $[(\text{TMEDA})\text{Na}]_3\text{Cr}_2\text{Me}_7$ **45** (Figure 11.5). Within this structure, each Cr centre adopts a distorted trigonal bi-pyramidal geometry made up of four methyl ligands with the second Cr atom fulfilling the role of one of the equatorial constituents. Two methyl ligands occupy the remaining equatorial sites [Cr(1); C(1), C(5): Cr(2); C(2), C(6)] with a further two methyl ligands in axial positions [Cr(1); C(4), C(7): Cr(2); C(3), C(7)], including C(7), which acts as a bridge between the two Cr centres. The Cr to bridging methyl ligand bond distances are the longest in the complex with an average Cr–C_{bridging} bond length of 2.313 Å compared with Cr – C_{terminal} bond distances of 2.165 Å. The three sodium cations lie bridging the two Cr bi-pyramids, capping faces produced by the methyl ligands. Methyl carbons C(5), C(6) and C(7) constitute a fourth face that remains vacant. Na(2) and Na(3) both cap 4 methyl ligands which occupy a rectangular face while Na(1) caps an isosceles triangle of 3 methyl groups. Drawn in by the greater concentration of electron density, Na(1) is situated towards the bottom of the triangle; 2.554(2) Å from the bridging C(7), while only 1.824(1) Å from the mid point between C(1) and C(2). Na(3) sits essentially centrally upon its pyramid; 2.163(1) Å from the midpoint between C(1) and C(2) and 2.135(1) Å from the midpoint between C(3) and C(4). Finally Na(2) has been displaced from a central role to take advantage of the space provided by the vacant site, 2.310(1) Å from the midpoint between C(3) and C(4) and 1.966(1) Å from the midpoint between C(5) and C(6). These distortions create a significant difference in the separation distance between Na(1) and Na(3) [3.963(1) Å] and Na(2) and Na(3) [4.423(1) Å]. However, the most striking feature of **3** is the short Cr–Cr contact length of 1.9112(4) Å, which is comparable, but even shorter, than that within Krause's original lithium chromate species $[(\text{THF})\text{Li}]_4\text{Cr}_2\text{Me}_8$ [1.968(2) Å].^[169b]

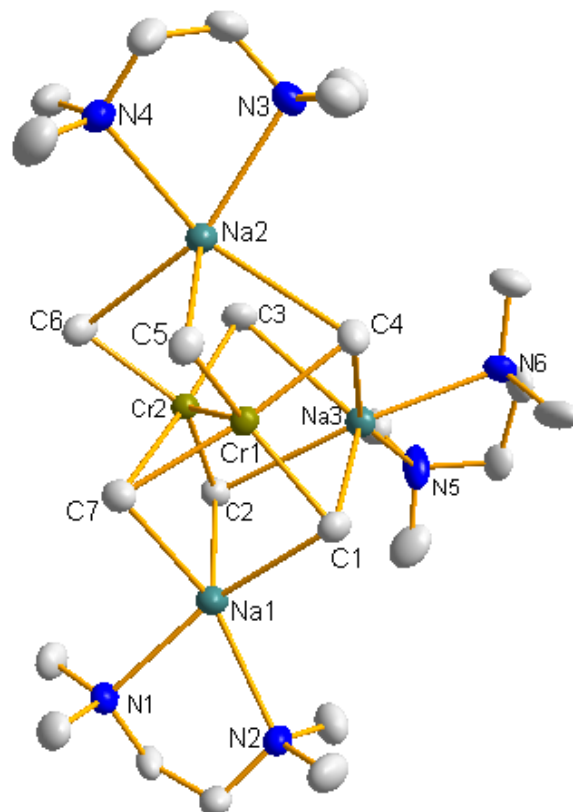
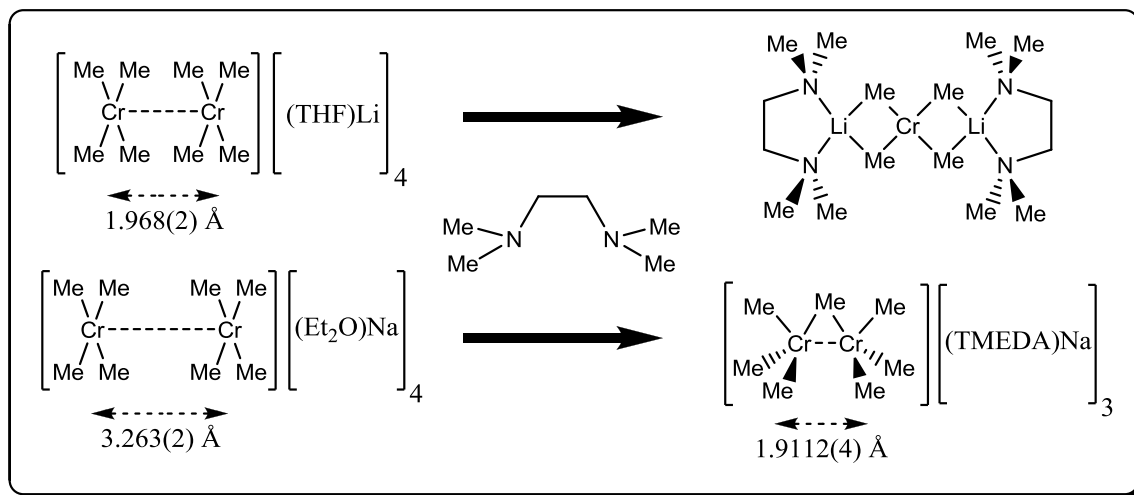


Figure 11.5: Molecular structure of [(TMEDA)Na]₃Cr₂Me₇ **45 with selected atom labelling. Hydrogen atoms and minor disorder in one of the TMEDA ligands omitted for clarity. Thermal ellipsoids are shown at the 50% probability level. Selected bond lengths and angles: Cr(1)–Cr(2) 1.9112(4), Cr(1)–C(1) 2.199(2), Cr(1)–C(4) 2.155(2), Cr(1)–C(5) 2.150(2), Cr(1)–C(7) 2.298(2), Na(1)–C(1) 2.567(2), Na(1)–C(2) 2.562(2), Na(1)–C(7) 2.554(2), Na(3)–C(1) 2.759(2), Na(3)–C(2) 2.870(2), Na(3)–C(3) 2.779(2), Na(3)–C(4) 2.739(2), Na(2)–C(3) 2.913(2), Na(2)–C(4) 2.879(2), Na(2)–C(5) 2.572(2), Na(2)–C(6) 2.692(2), Na(1)–N(1) 2.488(2), Na(1)–N(2) 2.513(2); C(1)–Cr(1)–C(4) 87.41(8), C(1)–Cr(1)–C(5) 134.84(7), C(1)–Cr(1)–C(7) 99.21(8), C(1)–Cr(1)–Cr(2) 111.88(5), C(4)–Cr(1)–C(5) 88.24(8), C(4)–Cr(1)–C(7) 173.35(7), C(4)–Cr(1)–Cr(2) 111.68(5), C(5)–Cr(1)–C(7) 86.69(7), C(5)–Cr(1)–Cr(2) 111.44(5), C(7)–Cr(1)–Cr(2) 66.43(5).**

The ¹H NMR spectrum of the heptamethyl chromium complex **45** in C₆D₆ solution consists of three broad singlets as might be expected if fluxional processes in solution were to average the methyl signals. The peak widths suggest the sample may exhibit some paramagnetic behaviour. Presumably due to the poor solubility of chromate **45** in C₆D₆, an excess of TMEDA is observed relative to that in the solid state structure. A ¹H NMR spectrum of **45** in the donor solvent THF-D₈ is devoid of any resonances indicating a cleavage of the Cr–Cr bond has resulted in a highly paramagnetic sample. This is

another example of how the presence of different donor ligands can profoundly alter the nature of Cr–Cr interactions.

Comparing the reactivities of the lithium and sodium octamethylates $[M]_4Cr_2Me_8$ $[M = (THF)Li, (Et_2O)Na]$ towards the Lewis base TMEDA provides another eye-catching example of the important role the alkali metals can play in dictating structural motifs within chromium species. While Gambarotta has demonstrated the symmetrical cleavage of the lithium species to give the mononuclear compound $[(TMEDA)Li]_2Cr_2Me_4$,^[169a] the sodium congener has favoured the formal elimination of a unit of $(TMEDA)NaMe$ to provide the dinuclear **45** (Scheme 11.2). Examining the transformation from the sodium octamethyl complex **44** to the TMEDA solvate **45** also reveals the vast potential provided by the subtleties of Cr(II) metal–metal bonding; the ability to profoundly alter the electronic and magnetic properties at the metal centre by the simple switching of the peripheral Lewis base. Dinuclear group VI metal species, including Cr, have already been demonstrated as useful catalysts.^[171] Indeed dinuclear Cr species have recently been implicated in the commercially highly significant selective tetramerisation of ethylene to 1-octene.^[172] One can envisage how sophisticated Cr based complexes could be designed in the future, taking advantage of the inherent lability of the Cr–Cr bond, to produce highly tuneable, potentially substrate-selective catalysis.



Scheme 11.2: Highlighting the stark contrast in reactivity between the lithium and sodium octamethyl complexes towards TMEDA.

To determine the generality of this surprising reaction we next turned to the closely related chiral diamine *N,N,N',N'*-tetramethylcyclohexanediamine (TMCD) to see how its different steric properties might affect the Cr environment. Again reaction of a preformed ethereal solution of the sodium chromate $[(\text{Et}_2\text{O})\text{Na}]_4\text{Cr}_2\text{Me}_8$ **44** with the new diamine produced crystals, on storage at -30°C , that were amenable to X-Ray diffraction studies. Formation of the dinuclear heptamethyl Cr species $[(\text{TMCD})\text{Na}]_3\text{Cr}_2\text{Me}_7$ **46** with the formal elimination of a NaMe unit was again the result. The Cr_2Me_7 core closely resembles that from the TMEDA solvate **45**, with similar Cr–C bond lengths [2.142(2) – 2.302(2) in **46**, 2.132(2) – 2.328(2) in **45**] and a Cr–Cr separation distance of 1.9136(4) Å [compared with 1.9112(4) in **45**]. Indeed, even the periphery has altered little, with the same pattern of sodium cations chasing electron density, or taking advantage of a void in steric protection, to provide similar distortions in the distances between sodium cations [Na(1)⋯Na(3), 4.044(1) Å; Na(1)⋯Na(2), 4.447(1) Å].

Attempts to synthesise and structurally determine sodium methylchromates with other Lewis bases have so far proved unsuccessful. As stated already while trying to prepare a THF solvate, displacement of the diethylether appears problematic. Other Lewis bases which have failed to displace diethylether (the solvent in which these reactions have been performed) and have led to the recrystallisation of **44** include the di-ether 1,2-dimethoxyethane, the tertiary amine triethylamine (in this case even when deployed as a bulk solvent) and the phosphine ligand triphenylphosphine. Using pyridine or the crown ether, 12-crown-4, immediately resulted in the formation of an insoluble precipitate which could not be crystallised. Introducing the tridentate PMDETA or the tetradentate $\text{Me}_6\text{-TREN}$ {Tris[2-(dimethylamino)ethyl]amine} allowed the growth of dark red/brown crystals when the ether solutions were left to stand at -30°C . Unfortunately, while a unit cell was obtained in both cases that suggested that a new compound had been prepared, despite repeated efforts crystals of suitable quality to permit a structural determination could not be obtained.

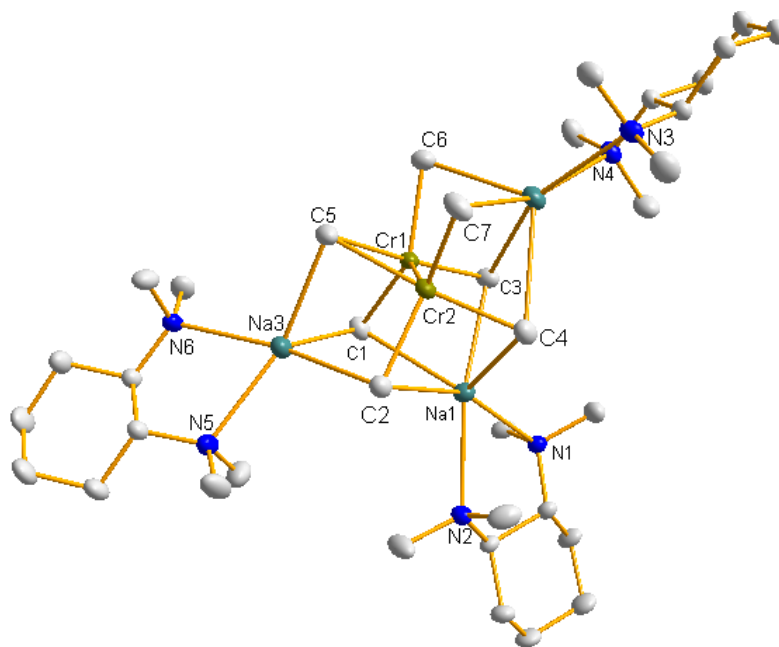


Figure 11.6: Molecular structure of [(TMCDA)Na]₃Cr₂Me₇ **46** with selected atom labelling. Hydrogen atoms have been omitted for clarity. Thermal ellipsoids are displayed at the 50% probability level. Selected bond lengths and angles: Cr(1)–Cr(2) 1.9136(4), Cr(1)–C(1) 2.205(2), Cr(1)–C(3) 2.160(2), Cr(1)–C(6) 2.160(2), Cr(1)–C(5) 2.302(2), Na(1)–C(1) 2.851(3), Na(1)–C(2) 2.899(3), Na(1)–C(3) 2.759(2), Na(1)–C(4) 2.769(3), Na(2)–C(3) 2.814(3), Na(2)–C(4) 2.993(2), Na(2)–C(6) 2.631(3), Na(2)–C(7) 2.786(3), Na(3)–C(1) 2.544(2), Na(3)–C(2) 2.634(3), Na(3)–C(5) 2.625(2), Na(1)–N(1) 2.609(2), Na(1)–N(2) 2.607(2); C(1)–Cr(1)–C(3) 87.49(9), C(1)–Cr(1)–C(5) 98.82(8), C(1)–Cr(1)–C(6) 134.03(8), C(1)–Cr(1)–Cr(2) 113.12(6), C(3)–Cr(1)–C(5) 173.27(9), C(3)–Cr(1)–C(6) 91.23(9), C(3)–Cr(1)–Cr(2) 110.50(6), C(5)–Cr(1)–C(6) 86.06(9), C(5)–Cr(1)–Cr(2) 64.92(6), C(6)–Cr(1)–Cr(2) 110.27(6).

11.2 Examining the electronic structures of the new chromium complexes

In order to gain a more informed understanding of the Cr–Cr interactions within **44** and **45**, a series of variable temperature magnetisation experiments, electron paramagnetic resonance (EPR) spectroscopic studies and DFT calculations have been performed. The magnetic susceptibility data for the sodium octamethylate **44** reveals that the four *d*-electrons formally residing on each Cr(II) centre are antiferromagnetically coupled with $S_1 = S_2 = 2$. Discounting a residual low value of χT at 2 K of $0.14 \text{ cm}^3 \text{ K mol}^{-1}$ as the result of trace Cr(III) impurities, **44** appears to have an $S = 0$ total spin ground state (Figure 10.7). Examining the Curie–Weiss plot, it can be observed that **44** does not obey

classical behaviour. A linear relationship is obtained between $1/\chi$ and T from approximately 60 – 300 K, however below 60 K this relationship is no longer observed (Figure 10.7). This is a consequence of low-lying excited states populated with increasing temperature, a natural consequence of the significant inter-nuclear Cr–Cr separation [3.263(2) Å]. At 300 K, the bulk molar susceptibility reaches $\sim 0.8 \text{ cm}^3 \text{ K mol}^{-1}$ which translates as an effective magnetic moment of $\sim 2.5 \mu_{\text{B}}$. This is substantially lower than the spin-only value expected for an $S_1 = S_2 = 2$ system, computed as $6.93 \mu_{\text{B}}$ via the spin only formula, $\mu_{\text{eff}} = g\{S_1(S_1 + 1) + S_2(S_2 + 1)\}^{1/2}$, where g is assumed to be 2. However, this discrepancy is consistent with antiferromagnetic coupling between the two chromium centres, with only the triplet excited state accessed at room temperature. Therein, a lower limit of 100 cm^{-1} can be derived for the isotropic exchange constant, J , defined as the energy gap between the $S = 0$ and $S = 1$ states. The exchange coupling while significantly smaller than that predicted for the TMEDA solvate **45** (-1860 cm^{-1} , see below), remains significantly larger than that determined for the chromium chloride dimer $\{[(\text{Dipp})\text{NCHCHN}(\text{Dipp})]\text{CrCl}\}_2$ (-17 cm^{-1})^[61] which has a similar Cr–Cr separation [3.431(1) Å]. This suggests that the chromium centres in **44**, despite the large separation, remain well primed to couple at least magnetically.

Turning to the EPR analysis of **44**, the data are in agreement with that of the magnetic susceptibility, consistent with an $S_1 = S_2 = 2$ system. The single resonance, which did not exhibit any hyperfine features due to the low natural abundance (9.51%) of ^{53}Cr isotope with nuclear spin, $I = 3/2$. The resonant field position of the signal corresponds to a g -value of 2 (Figure 10.8). The spectrum was simulated according to a spin-Hamiltonian for two coupled Cr(II) centres, equation 11, where the first term expresses the electron Zeeman interaction for each Cr(II) ion, while the second term encompasses the electron-electron interaction between the paramagnetic centres described by the interaction matrix **J**. The spin-spin interaction can be divided into its anisotropic and isotropic components, equation 12, where the last term involves the previously encountered exchange coupling

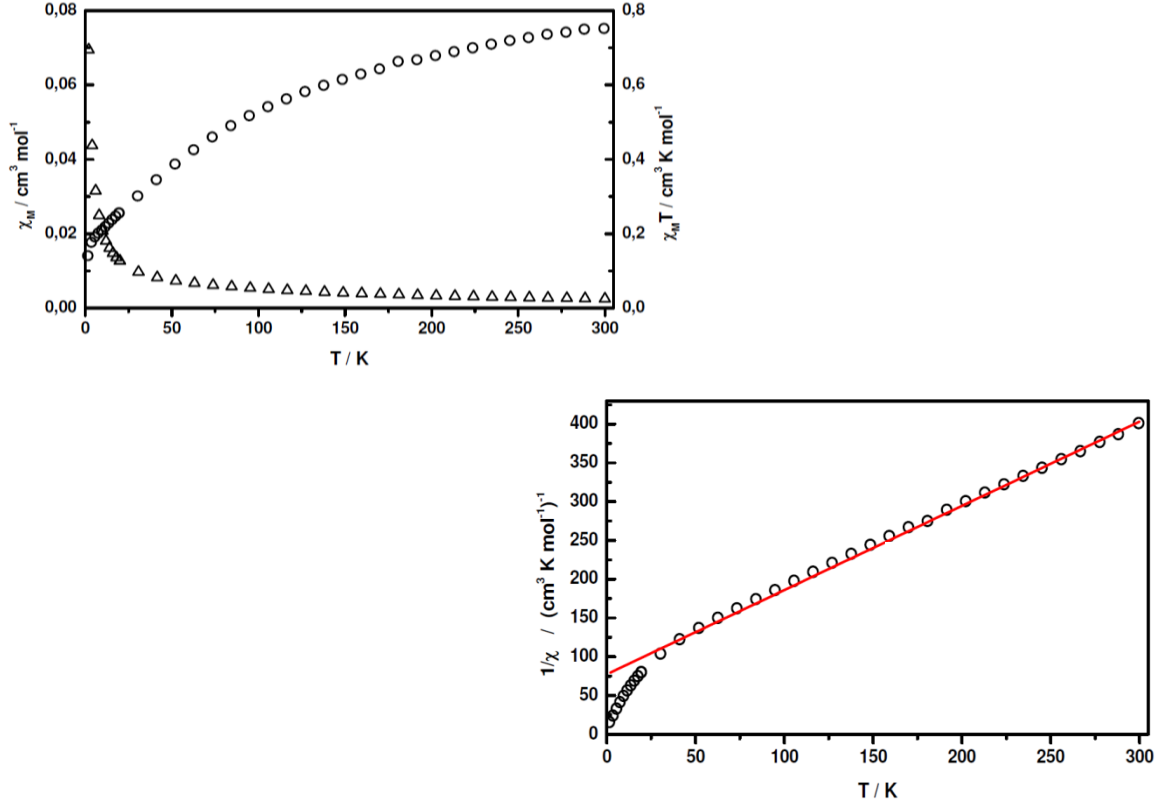


Figure 11.7: Magnetic susceptibility plot against temperature (top left) and Curie – Weiss plot (bottom right) for the sodium octamethylate **44**.

$$\hat{H} = \mu_B \sum \mathbf{S}_i \cdot \mathbf{g}_i \cdot \mathbf{B} + \mathbf{S}_1 \cdot \mathbf{J} \cdot \mathbf{S}_2 \quad (11)$$

$$\hat{H} = \mu_B \sum \mathbf{S}_i \cdot \mathbf{g}_i \cdot \mathbf{B} + \mathbf{S} \cdot \mathbf{D} \cdot \mathbf{S} - 2J(\mathbf{S}_1 \cdot \mathbf{S}_2) \quad (12)$$

constant whose lower limit was estimated at $\sim 100 \text{ cm}^{-1}$. The parameter determines the extent of mixing of excited states into the ground state for this $S_1 = S_2 = 2$ system. At this measurement temperature of 80 K, only the triplet and pentet states are contributing to the observed signal. The anisotropic component of the spin-spin interaction is defined by the D -tensor, often known as zero-field splitting, which as in equation 13 though, because of the four-fold symmetry inherent to **44**, there is no rhombicity ($E/D = 0$) in the spin-spin interaction, and therefore the spin-Hamiltonian can be simplified to give equation 14, where the g -values for each Cr(II) are the same.

$$\hat{H} = \mu_B \sum \mathbf{S}_i \cdot \mathbf{g}_i \cdot \mathbf{B} + D[\hat{S}_z^2 - 1/3S(S+1) + E/D(\hat{S}_x^2 + \hat{S}_y^2)] - 2J\mathbf{S}_1 \cdot \mathbf{S}_2 \quad (13)$$

$$\hat{H} = \mu_B \mathbf{B} \cdot \mathbf{g} \cdot \mathbf{S} + D[\hat{S}_z^2 - 1/3S(S+1)] - 2J\mathbf{S}_1 \cdot \mathbf{S}_2 \quad (14)$$

The spectral simulation depicted in Figure 10.8 was reached using $g = 2$ and $D = -0.13 \text{ cm}^{-1}$, with J fixed at -100 cm^{-1} . A larger exchange coupling constant would lead to inclusion of higher excited states leading to more pronounced spectral features which are clearly not seen experimentally, so the fixed value is in good agreement with the magnetochemical result. Despite being a Jahn-Teller ion, the very small zero-field splitting value is a consequence of the four very strong field ligands greatly destabilising the $d_{x^2-y^2}$ orbital relative to the four singly occupied d-orbitals for each Cr(II) d^4 ion. Thereby, the spin-conserving transitions within the d-orbital manifold that generate large D -values are nonexistent here.

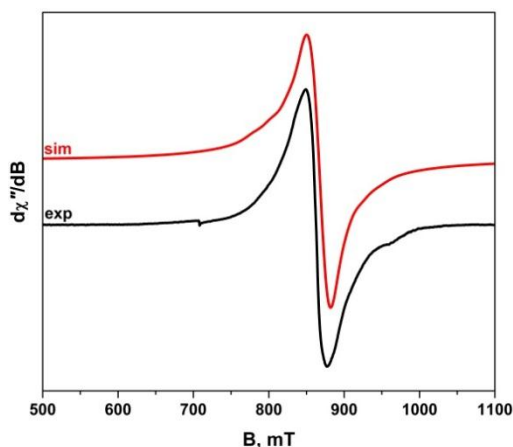


Figure 11.8: K-band EPR spectrum of polycrystalline 44 at 80 K . Experimental data shown in black; the simulation is depicted by the red trace.

Modelling the sodium octamethylate **44** through broken symmetry DFT calculations based on the solid state structure predicts four pairs of antiferromagnetically coupled d-based orbitals that give rise to an $S = 0$ spin ground state (Figure 10.9). The degree of overlap between the chromium-based ($>90\%$) singly occupied molecular orbitals (SOMO) is described by the integral overlap S , whose values range $0 \leq S \leq 1$ depending on the polarisation in the system. For $S = 1$, the coupling is Pauli and the MOs correspond to closed-shell – in essence a covalent bond. For $S < 1$, the MOs form the valence bond like overlapping magnetic pairs of the BS solutions. The calculated overlap integrals between magnetic pairs shown in Figure 10.9 are significantly less than unity. In one case, the d_{xy} MOs are essentially orthogonal with near-zero integral overlap. The high-spin $M_s = 9$ solution is slightly less favourable as represented by $J'_{\text{calcd}} = -194 \text{ cm}^{-1}$.

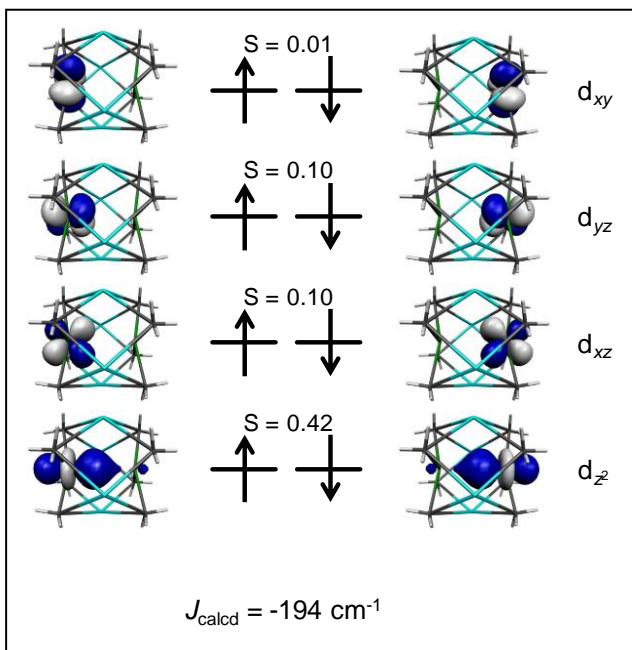


Figure 11.9: calculated magnetic orbitals as a result of overlap between the two Cr atoms of **44**.

arising from antiferromagnetic coupling between the Cr(II) ions at the expense of metal-metal bonding. A Mulliken spin population analysis shows four unpaired electrons reside on each chromium centre (Figure 10.10). Some spin polarisation of the CrMe₄ σ* MO elevates these spin densities above 4.

This energy gap represents $20J$ in terms of the spin ladder with total spins $S = 0, 1, 2, 3, 4$ for two coupled Cr(II) ions as described by the Heisenberg-Dirac-van Vleck Hamiltonian, $\hat{H}_{\text{HDvV}} = -2JS_1 \cdot S_2$, and therefore the calculated value is an order of magnitude less than the experimentally derived lower limit of $J > \sim 100 \text{ cm}^{-1}$. Nevertheless, the calculations are in agreement with the magnetic and EPR data, in that the total spin ground state of **44** is $S = 0$

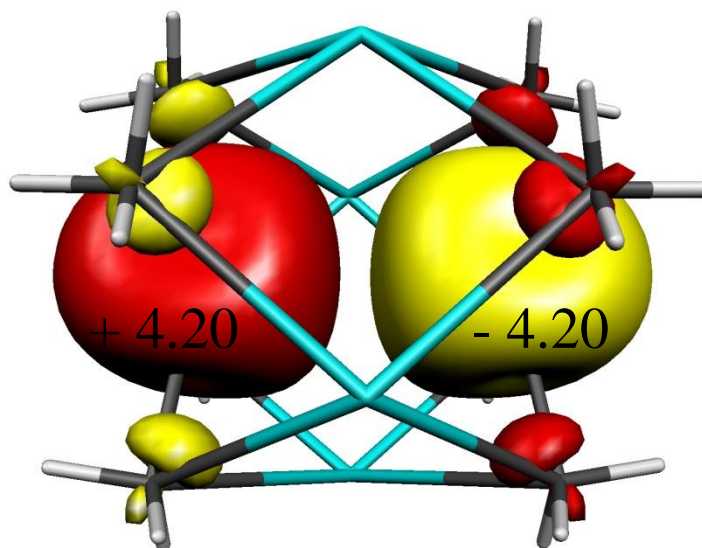


Figure 11.10: Mulliken spin density plot of **44**.

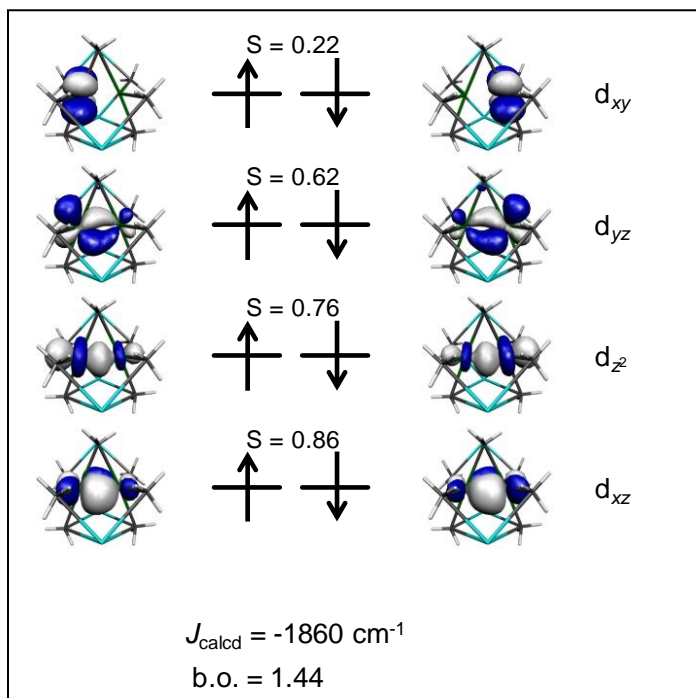


Figure 11.11: Molecular orbitals calculated between the Cr centres in 45.

(Figure 10.11). This is evident when examining the much greater exchange coupling ($J_{\text{calcd}} = -1860 \text{ cm}^{-1}$) which is a consequence of the $\mu\text{-Me}$ ligand that provides a short exchange pathway between the Cr(II) ions. Furthermore this indicates that higher

A sample of the TMEDA solvate **45** has been prepared and submitted for both magnetic susceptibility and EPR studies but, at the time of writing, these analyses have not yet been accomplished. However, the X-ray diffraction data has been used to permit the modelling of **45** by DFT calculations. As might be expected, the greatly reduced Cr–Cr separation [$1.9112(4) \text{ \AA}$] relative to that in **44** results in a far greater overlap between the chromium centres

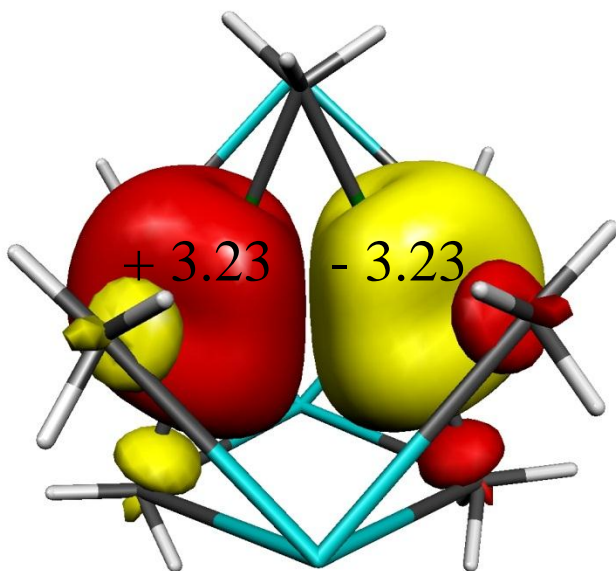


Figure 11.12: Mulliken spin density plot of 45.

temperatures will be needed to populate paramagnetic excited states to observe a response in magnetic susceptibility and EPR measurements. A bond order of 1.44 is calculated for the Cr–Cr unit in **45**, though noticeably and perhaps not surprisingly, short of an idealised formal quadruple bond. This is highlighted by the Mulliken spin density plot, where three unpaired electrons reside on each chromium centre despite the short inter-nuclear separation (Figure 10.12).

11.3 Synthesis of a sodium methylmolybdate

Next we decided to investigate the properties of the octamethylate complexes of the heavier group VI transition metals. Taking first molybdenum, its larger more diffuse *d* orbitals, relative to chromium, should lead to a better overlap between metal centres and hence a stronger bonding interaction. This may explain why Gambarotta failed to cleave $\text{Li}_4\text{Mo}_2\text{Me}_8$ with the diamine TMEDA in the same manner that was achieved with the chromium species.^[169b] The greater strength of Mo–Mo bonding interactions, relative to chromium, is also apparent through the greater prevalence of complexes such as $\{[(\text{H}_3\text{CC}\equiv\text{N})_4\text{Mo}]_2\}^+[\text{BF}_4]_4^-$ ^[173] and $[(\text{Me}_3\text{P})_2\text{Mo}(\text{Cl})_2]_2$,^[174] which sustain short metal–metal contacts without the aid of bridging ligands.

The synthesis of the sodium octamethyl molybdate was achieved via the metathetical reaction of $[(\text{Et}_2\text{O})\text{Li}]_4\text{Mo}_2\text{Me}_8$ in diethylether solution with four molar equivalents of $\text{NaO}t\text{Bu}$ producing a purple solution. From this solution a crop of red purple crystals suitable for X-ray diffraction studies could be isolated in a 35% yield following the addition of the diamine TMEDA and storage at -30°C . The product was revealed to be the sodium octamethyl molybdate $[(\text{TMEDA})\text{Na}]_4\text{Mo}_2\text{Me}_8$ **47**, which has a centrosymmetric dimeric structure. Analogous to that found in $[(\text{THF})\text{Li}]_4\text{Mo}_2\text{Me}_8$, the sodium molybdate's core consists of two Mo centres in identical square pyramidal coordination (including the axially-disposed Mo–Mo interaction) with four methyl ligands in an eclipsed conformation across the Mo–Mo bridge. The four $[(\text{TMEDA})\text{Na}]$

cations cap the bridging faces produced by the methyl ligands, occupying sites equidistant from the Mo centres. The Mo–Mo internuclear separation is 2.1403(2) Å, which is nearly identical to that of the lithium congener [(THF)Li]₄Mo₂Me₈ within experimental error [2.148(2) Å].^[165b] To accommodate the larger sodium cations, the alkali metals have been expelled from the core of the complex, the midpoint along the Mo–Mo short contact, by 0.46 Å relative to that in the lithium compound (Figure 11.14). These results confirm the intrinsic strength of the Mo–Mo quadruple bond while, at the same time, eliminating any inherent property of the octamethyl ligand set as being responsible for the significant elongation of the Cr–Cr separation within the sodium chromate [(Et₂O)Na]₄Cr₂Me₈ **44** when compared with the lithium species. It is also noteworthy that the sodium octamethylmolybdate **47** remained intact despite crystallising

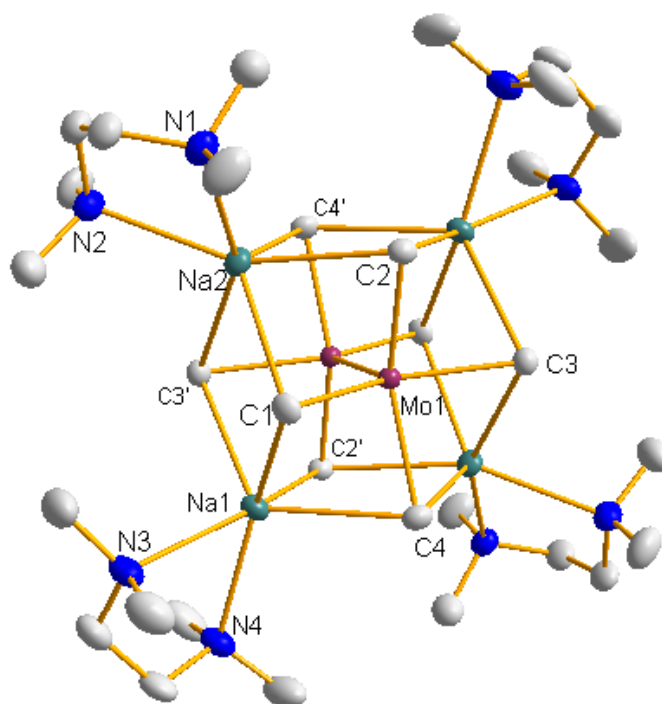


Figure 11.13: Molecular structure of [(TMEDA)Na]₄Mo₂Me₈ showing selected atom labelling. Hydrogen atoms are omitted for clarity and thermal ellipsoids are shown at the 50% probability level. Selected bond lengths and angles: Mo–Mo' 2.1402(2), Mo–C(1) 2.318(2), Mo–C(2) 2.305(2), Mo–C(3) 2.318(2), Mo–C(4) 2.324(2), Na(1)–C(1) 2.748(2), Na(1)–N(3) 2.614(2), Na(1)–N(4) 2.613(2); Mo'–Mo–C(1) 107.45(6), C(1)–Mo–C(3) 145.52(7), N(3)–Na(1)–N(4) 70.88(6).

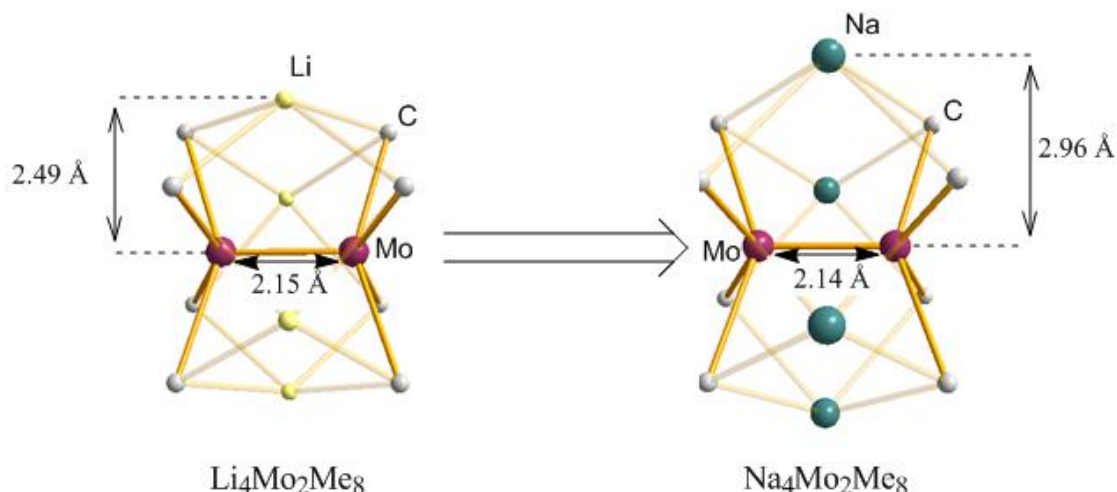


Figure 11.14: Depiction of how the Mo–Mo separation is unaffected by replacing lithium by sodium, but instead the heavier alkali metal is pushed further from the molybdate core.

as a TMEDA solvate. This is in contrast to the aforementioned cleavage of the lithium chromate $\text{Li}_4\text{Cr}_2\text{Me}_8$, or the formation of a heptamethyl species observed for the sodium chromate **44** in the presence of the diamine. ^1H and ^{13}C NMR analysis of molybdate **47** in both C_6D_6 and THF-D_8 reveal the presence of TMEDA and one sharp methyl signal. However, again presumably due to the poor solubility of **47** in C_6D_6 , analogous to the analysis of the heptamethyl chromate **45**, an excess of TMEDA is observed. This inconsistency is overcome by switching to THF-D_8 . The confirmation of the diamagnetic nature of **47**, even in the donor solvent THF-D_8 , infers the retention of the Mo–Mo quadruple bond.

11.4 Conclusions and future work

The family of alkali metal group VI methylates has been successfully extended to sodium for both chromium and molybdenum. The sodium chromates have given rise to as many structural and reactivity surprises as was delivered by previous research into their lithium congeners. While it had previously been asserted that the alkali metal plays a key role in supporting the short Cr–Cr contact in $[(\text{THF})\text{Li}]_4\text{Cr}_2\text{Me}_8$, the dramatic elongation of the Cr–Cr separation when moving from lithium to sodium constitutes the first direct experimental evidence of the defining influence of the alkali metal.

As well as this important structural difference between **44** and its lithium analogue, their contrasting reactivity towards Lewis bases has been investigated. While the neutral diamine TMEDA has been demonstrated to symmetrically cleave the lithium octamethylate, resulting in the mono-nuclear $[(\text{TMEDA})\text{Li}]_2\text{Cr}_2\text{Me}_4$, introducing TMEDA to **44** results in the asymmetric dinuclear **45** (Scheme 11.2). Analogous reactivity has also been demonstrated for the chiral diamine TMCDA. These highly unusual results point to a rich potential for the reactivity of **44** towards different donor ligands. Unfortunately further progress in this area has been frustrated by the apparent stability of the ether solvate, and by poorly diffracting crystalline material. However, future work in this area may still prove fruitful if suitable donor ligands can be found, or if analysis of the crystalline materials produced with PMDETA or $\text{Me}_6\text{-TREN}$ can be achieved, either by the growth of higher quality crystals or through access to more powerful diffraction techniques such as the synchrotron source.

While chromium alkyls are notoriously poor deprotonating agents, the polarising ability of sodium within **44** may deliver sufficient reactivity to at least attack relatively acidic protons. One potential utility might be an extension to the secondary diamine investigations discussed in chapter 9. Theopold has synthesised a remarkable dinuclear chromium species incorporating diazadiene ligands, with a super short metal–metal contact of $1.8028(9) \text{ \AA}$.^[61] The product, $\{[(\text{dipp})\text{NCHCHN}(\text{dipp})]\text{Cr}\}_2$, has an intermediary Cr–Cr bond order between four and five owing to the significant delocalisation of the electrons in the system. Indeed, $\{[(\text{dipp})\text{NCHCHN}(\text{dipp})]\text{Cr}\}_2$ can be viewed as an organometallic derivative of naphthalene. If **44** proved capable of similar CH activation to that observed with bi-metallic zinc complexes (chapter 9), then this could provide a novel route to a range of new diazadiene chromium complexes.

Preliminary investigations into the electronic make-up of **44**, by both experimental and theoretical techniques, have confirmed that no formal quadruple bond exists in this species. Currently, magnetic susceptibility and EPR data are being measured for the TMEDA solvate **45** and the lithium chromate $[(\text{Et}_2\text{O})\text{Li}]_4\text{Cr}_2\text{Me}_8$, as well as the sodium

molybdate **47**. This offers the opportunity to examine the effects of drastically altering the Cr–Cr separation without dramatically altering the ligand environment around chromium. The synthesis of the sodium molybdate **47**, in contrast to the chromium work, revealed little influence of the alkali metal on the metal–metal bond. Analysis of the molybdenum species should thus provide EPR and magnetic susceptibility data consistent with a true, strong quadruple bond supported by methyl ligands, even if the data simply confirms the diamagnetic nature of **47**. This can then be used to provide further context for the chromium results.

X-ray diffraction is an analytical technique for measuring the electron distribution of a compound within a single crystal. Typically these data are processed in such a way as to approximate the electron density distribution as a series of spherical points and, hence, locate the atomic positions within a molecule [the so called Independent Atom Molecule approach (IAM)]. In this way, standard structural determinations, such as those recorded within this thesis, are resolved. Hanson and Coppens pioneered a different processing technique [the Multipole Model (MM)] in which the electronic distribution data need not be approximated as a series of spherical points.^[175] In this way information about the electronic distribution about the bonds of a molecule can be investigated, not only the atomic positions. This is a technique that has recently been championed by Stalke,^[176] and used by to establish the non-bonding nature of two manganese centres that, nonetheless, lie close in space [Mn–Mn 2.78 Å].^[177] Such techniques could deliver direct experimental evidence of the bonding or non-bonding nature of the group VI methylates.

12 sp^3 C–H metallation mediated by synergic bimetallic aluminate bases

The replacement of sp^2 and sp C–H protons for a metal centre has been widely studied in both a homometallic and a synergic bimetallic context, and such transformations are of critical importance in organic synthesis.^[3b, 14, 22] By contrast, owing to their greater pK_a (lower acidity) (Table 8.1, page 4), the activation of sp^3 C–H bonds has proven more challenging. While transition metal complexes have been produced that are capable of delivering such results,^[178] there could be significant economic and environmental advantages to developing a main group approach. Due to the prohibitively high pK_a 's, the deprotonation at an sp^3 carbon generally requires activation via the inductive effect of an adjacent heteroatom, or unsaturated unit, to be a feasible transformation.^[179] While a heteroatom can provide an acidifying effect sufficient to permit metallation, it also provides lone pairs of electrons which engage in a repulsive interaction with the newly formed carbanion. This can often lead to decomposition of the metallated species. A classic example of such a reaction/degradation pathway is the lithiation and cleavage of the cyclic ether THF discussed previously (Scheme 8.15, page 30). Again as remarked upon in the introduction (8.2.2 Synergy in action: reactivity), the mixed metal sodium zincate base **13** as well as the synergic bimetallic mixture [LiTMP + (*i*Bu)₂Al(TMP)] **48** permit the deprotonation of THF while otherwise maintaining the cyclic ether's integrity.^[47] This unlikely result can be rationalised in both cases through the reduced polarity of the formed carbanion, relative to a lithiated species, and the occupation of the oxygen lone pairs by the alkali metal, resulting in a reduction of the repulsive interaction between these two entities (Scheme 8.15, page 30). After the successful sp^3 C–H activation observed within the diamido zincate complexes (9 Alkali-metal-mediated multiple main group C-H activation) it was decided to expand upon synergic aluminations as a promising route towards the challenge of sp^3 C–H activation.

As well as the deprotonation of THF, the synergic mixture **48**, together with the structurally defined aluminate (THF)Li(TMP)Al(*i*Bu)₃ **49**, have both achieved the selective intramolecular metallation of the di- and tri- tertiary amines TMEDA and PMDETA.^[180] The success of these transformations is presumably the result of a complex induced proximity effect as a consequence of chelation of the lithium ions by

the Lewis basic amines. This may also account for the greater regioselectivity of the aluminatation of the tridentate PMDETA, relative to lithiation, with complete discrimination in favour of the more available terminal methyl groups compared with the differing mixtures of terminal and central methyl deprotonation observed on lithiation depending on the conditions employed.^[181]

It was therefore decided that chelation of the aluminate base would increase the opportunity for successful metallation reactions. A number of bi- and tri- dentate substrates, incorporating in most cases a combination of nitrogen and oxygen heteroatoms, were selected to permit the systematic probing of the steric and electronic effects at work in such transformations (Figure 12.1). The reactivity of both the mono TMP aluminate base **49**, as well as its bis TMP analogue **48**, towards this diverse array of substrates was investigated.

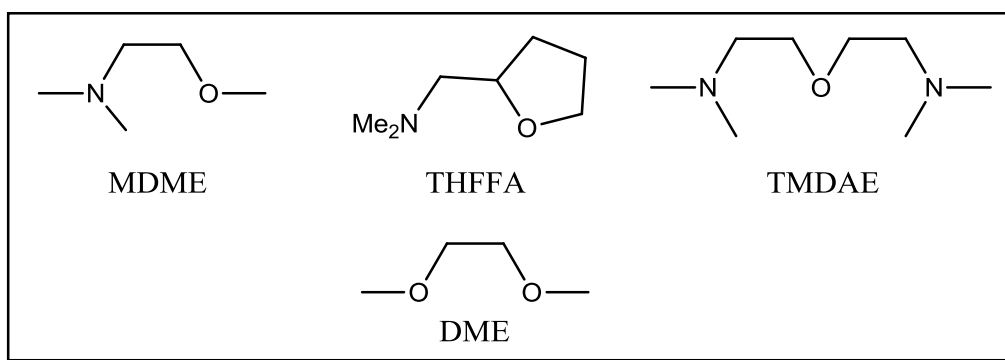
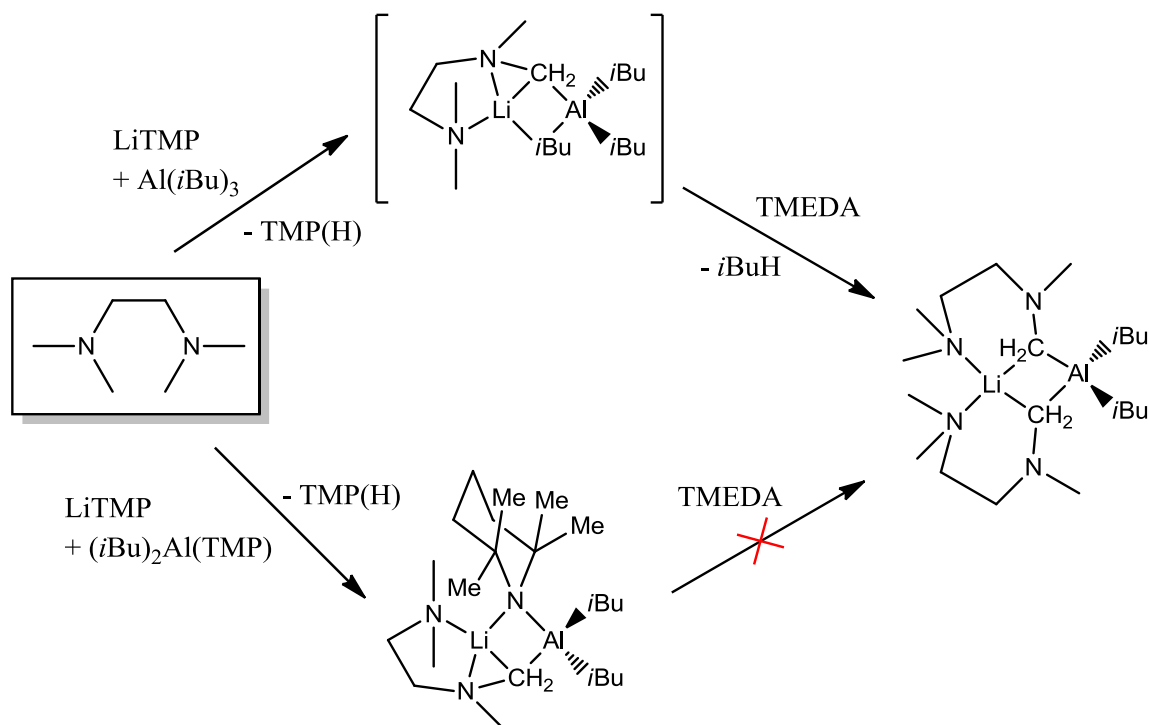


Figure 12.1: Homodentate and heterodentate substrates probed by both mono amido **49 and bis amido **48**.**

12.1 Reactions with the mono TMP aluminate base

Given its successful regioselective metallation of TMEDA and PMDETA the mono TMP aluminate **49** appears to be an ideal candidate for the deprotonation of the other substrates in Figure 12.1. Its advantages relative to the bisamido mixture **48** include a definitive structural determination and its facile one pot synthesis.^[182] The base not only achieved the deprotonation of a terminal methyl group of PMDETA, but also resulted in the metallation of two molecules of TMEDA per aluminium centres.^[180] This superior atom economic transformation is a rare example of an alkyl amido aluminate base exploiting

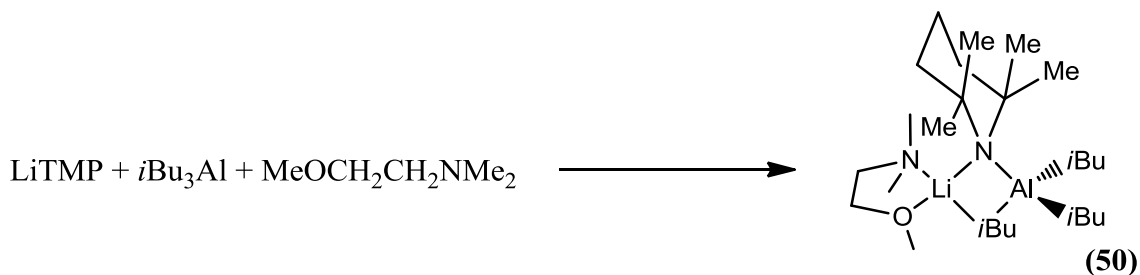
more than one of its basic arms and achieving alkyl, as well as amido, basicity. Comparison with the metallation of TMEDA by the synergic bisamido mixture confirms that metallation by the TMP aluminate of the diamine is first achieved by the amido anion. If alkyl basicity was exhibited first then the product would be the readily isolable and fully characterised $(\text{TMEDA}^*)\text{Li}(\text{TMP})\text{Al}(\text{iBu})_2$ [$\text{TMEDA}^* = \text{Me}_2\text{NCH}_2\text{CH}_2\text{N}(\text{Me})\text{CH}_2$] which is inert towards additional TMEDA ligands (Scheme 12.1).^[180]



Scheme 12.1: Contrasting TMEDA metallations pathways of TMEDA by the mono- and bis-TMP aluminates 49 and 48.

Bidentate 1-methoxy-2-dimethylaminoethane (MDME) is of a similar construction to the diamine TMEDA, except that one of its dimethylamino groups is replaced by a methoxy substituent. However, this leads to an unsymmetrical substrate and poses further questions over the selectivity of any potential metallation. Would deprotonation take place at the dimethylamino functionality, as in the metallation of TMEDA, or would deprotonation instead switch to the methoxy group, owing to the greater acidifying inductive effect of oxygen relative to nitrogen? Could a synergic aluminate base stabilise a methoxy deprotonation, as it managed to retain the cyclic integrity of a metallated THF,

or would this lead to decomposition of the metallated species? Could a base suitably discriminate between the nitrogen and oxygen activated hydrogen atoms or would a mixture of products result? To answer these questions, commercially available $\text{Al}(i\text{Bu})_3$ was added to a pre-prepared hexane solution of LiTMP followed by one molar equivalent of MDME (Scheme 12.2). This resulted in a pale yellow solution after stirring overnight. Concentration and storage of the solution at -30°C furnished a crop of colourless crystals suitable for X-ray crystallographic determination. The product was revealed to be the simple Lewis acid–Lewis base adduct $(\text{MDME})\text{Li}(\text{TMP})\text{Al}(i\text{Bu})_3$ **50**. Its asymmetric unit contains two near identical molecules of **50** of which for brevity only one will be discussed. The aluminium sits in a distorted tetrahedral geometry with three *iso*-butyl ligands possessing similar Al–C bond lengths as those within $(\text{THF})\text{Li}(\text{TMP})\text{Al}(i\text{Bu})_3$ with an average bond length of 2.043 Å compared to 2.035 Å for the THF solvate.^[182] Acting as a bridge to the alkali metal though situated closer to aluminium than lithium [Al1–N1 1.992(4) Å; Li1–N1 2.134(9) Å], the TMP ligand completes the aluminium coordination sphere. The TMP sits in a chair conformation overhanging the alkali metal. Lithium is also in a distorted tetrahedral environment. As well as bridging interactions with the TMP ligand and one *iso*-butyl anion, lithium is chelated by the MDME ligand with a tighter connection to the methoxy functionality relative to the dimethylamino group [Li1–N2 2.178(7) Å compared with Li1–O1 2.095(7) Å].



Scheme 12.2: coordination of MDME to the mono-TMP aluminate.

Attempting to rationalise why the combination of LiTMP and $\text{Al}(i\text{Bu})_3$ fails to deprotonate MDME, despite successfully metallating two molecules of TMEDA under the same ambient conditions it is prudent to reflect on the subtle steric and electronic differences between the two substrates. As stated already, the methoxy group would be expected to contain the more acidic protons due to the greater acidifying inductive effect

of oxygen relative to nitrogen. Thus, the difference in reactivity is presumably a result of the reduced steric cluttering of the MDME ligand, relative to TMEDA, owing to the reduced valency of oxygen compared to nitrogen. Again, as discussed already (Scheme 12.1), the TMP anion is expected to be the initial provider of any exhibited reactivity. As can be gleaned from the N1–Li1–N2 and N1–Li1–O1 angles [$137.4(3)^\circ$ and $135.8(3)^\circ$

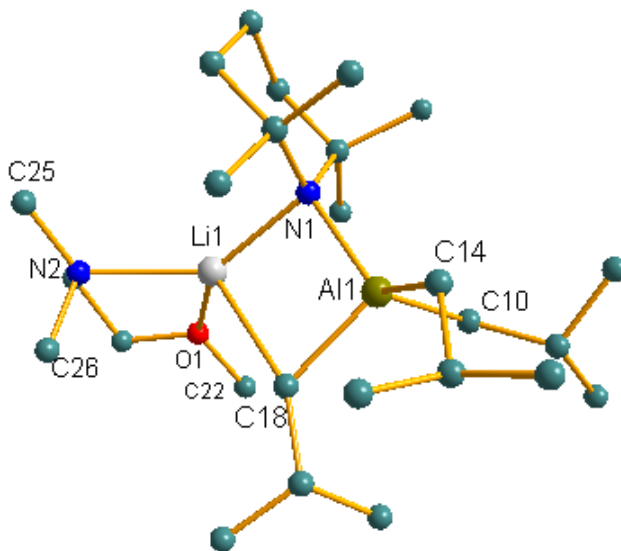


Figure 12.2: Molecular structure of the bifunctional chelate 50. Hydrogen atoms are omitted for clarity. Selected bond lengths [Å] and angles [°]: Li1–N1 2.134(9), Li1–C18 2.482(8), Li1–N2 2.178(7), Li1–O1 2.095(7), Al1–N1 1.992(4), Al1–C18 2.031(6), Al1–C10 2.054(3), Al1–C14 2.044(5), N1–Li1–N2 137.4(3), N1–Li1–O1 135.8(3), C18–Li1–N2 118.7(3), C18–Li1–O1 97.4(3), C18–Li1–N1 83.4(3), O1–Li1–N2 80.4(2), N1–Al1–C10 113.5(1), N1–Al1–C14 116.3(2), N1–Al1–C18 100.0(1), C10–Al1–C14 106.2(2), C10–Al1–C18 108.0(2), C14–Al1–C18 112.7(2).

respectively] relative to the C18–Li1–N2 and C18–Li1–O1 angles [$118.7(3)^\circ$ and $97.4(3)^\circ$], the substantial steric bulk of the TMP ligand forces the MDME towards the bridging alkyl ligand in a buttressing effect.^[183] Informatively, the methoxy functionality approaches significantly closer to the *iso*-butyl ligand than the nitrogen [O1...C18 3.450(4) Å, N2...C18 4.013(5) Å] (Figure 12.3). This suggests that the methoxy group can more easily approach the *iso*-butyl ligand than the dimethylamino group, presumably due to the reduced steric bulk around oxygen relative to nitrogen. The relative ease with which the methoxy group can encroach upon the *iso*-butyl ligand could potentially provide a greater amount of space for the dimethylamino functionality than would be

available to the diamino TMEDA. The resulting reduced steric strain may explain why the deprotonation of the MDME ligand is not forced in the same manner as that of TMEDA, despite containing hydrogen atoms of a slightly greater acidity.

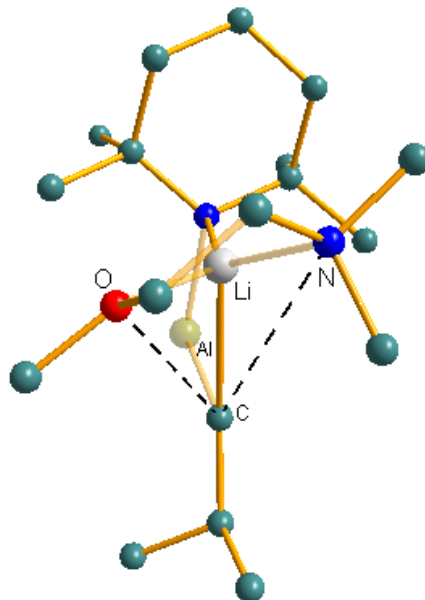


Figure 12.3: Depiction of how the reduced steric bulk around the oxygen permits it to get closer to the bridging *isobutyl* ligand compared to the nitrogen of the MDME ligand.

Considering now the substituted tetrahydrofuran *N,N*-dimethyltetrahydrofurfurylamine (THFFA) (Figure 12.1), the question posed was can the fused ring motif restrict the flexibility of the ether functionality sufficiently to prevent it from relieving the steric congestion around the alkali metal that could lead to metallation? Introducing the functionalised THF to a hexane solution of LiTMP and Al(*i*Bu)₃ resulted in a pale yellow solution which was stirred overnight. Concentration of this solution *in vacuo* and standing at -30°C resulted in the growth of colourless crystals suitable for X-ray diffraction studies. The product was again revealed to be a simple adduct (THFFA)Li(TMP)Al(*i*Bu)₃ **51** (Figure 12.4) with the donor unmetallated. Similar to that in the MDME and THF solvates **50** and **49**, the aluminium centre is in a distorted tetrahedral geometry made up of two terminal *iso*-butyl ligands, one bridging alkyl group and a bridging TMP anion. Again there is negligible difference in the Al–C bond lengths [average 2.035 Å] in **51** relative to those in the THF solvate **49** [average 2.035 Å]. The TMP ligand is in its familiar chair conformation overhanging the alkali metal but situated

closer to aluminium [Al–N1 1.987(1) Å, Li–N1 2.107(3) Å], completing a puckered four-atom, 4-element (Li–N–Al–C) ring [torsion angle 14.9(1)°]. The THFFA ligand successfully chelates the lithium centre, which binds more closely to the smaller oxygen than nitrogen [O1–Li1 1.981(3) Å, N2–Li1 2.206(4) Å].

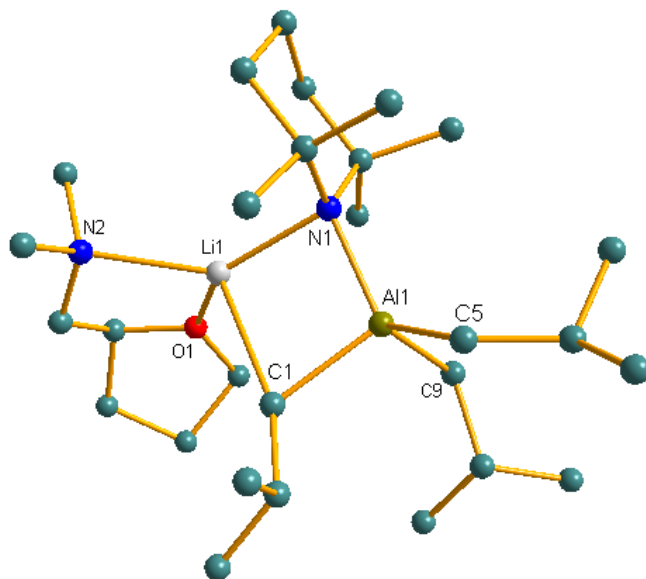


Figure 12.4: Molecular structure of the bifunctional chelate (THFFA)Li(TMP)Al(*i*Bu)₃. Hydrogen atoms and minor disorder of the THFFA ligand omitted for clarity. Selected bond lengths [Å] and angles [°]: Li1–N1 2.107(3), Li1–C1 2.471(4), Li1–N2 2.206(4), Li1–O1 1.981(3), Al–N1 1.987(1), Al–C1 2.051(2), Al–C5 2.028(2), Al–C9 2.025(2), N1–Li1–N2 136.8(2), N1–Li1–O1 133.1(2), C1–Li1–N2 118.1(1), C1–Li1–O1 96.8(1), C1–Li1–N1 86.5(1), O1–Li1–N2 81.9(1), N1–Al1–C1 102.44(7), N1–Al1–C5 117.76(7), N1–Al1–C9 117.17(7), C1–Al1–C5 110.10(8), C1–Al1–C9 105.68(8), C5–Al1–C9 103.15(8).

Posing again the question of why base **49** fails to deprotonate the bidentate substrate THFFA under the same conditions it metallates two molar equivalents of TMEDA, the answer once more appears to reside within the reduced steric congestion of the ether functionality relative to the dimethylamino group. As with the MDME ligand within chelate **50** the THFFA ligand once again attempts to retreat from the reactive, sterically demanding, TMP ligand resulting in very obtuse N1–Li1–N2 and N1–Li1–O1 bond angles of 136.8(2)° and 133.1(2)° compared with C1–Li1–N2 and C1–Li1–O1 of 118.1(2)° and 96.8(1)° respectively. As in the case with the MDME solvate though, the oxygen functionality encroaches significantly closer towards the *iso*-butyl ligand relative

to its nitrogen counterpart [O1...C1 3.344(2) Å, N2...C1 4.014(3) Å] providing steric relief to the amino group that would potentially not be so forthcoming to a diamino substrate (Figure 12.5).

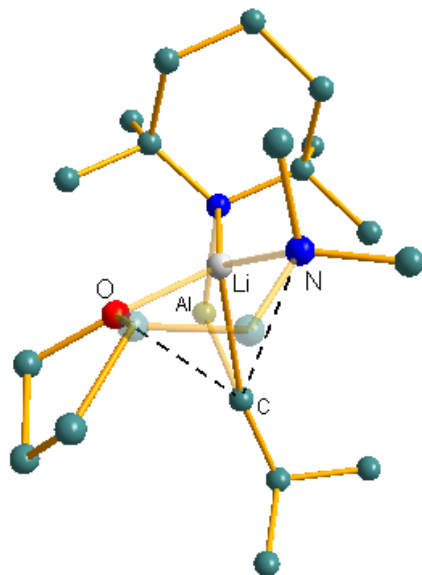


Figure 12.5: Depiction of how the reduced steric bulk around the oxygen permits it to get closer to the bridging *isobutyl* ligand compared to the nitrogen of the THFFA ligand within **51**.

Considering now the dioxygen substrate 1,2-dimethoxyethane (DME), in light of the aforementioned results with both MDME and THFFA it might well be thought unlikely that the mono amido aluminate should achieve metallation of this sterically compact diether. However, the successful aluminium of TMEDA, and the presence of now two oxygen atoms exerting a combined significantly acidifying inductive effect, meant that deprotonation of the DME remained a plausible outcome. To explore this, a hexane solution of the aluminium base **49** was taken to which was added one molar equivalent of DME resulting in a pale yellow solution. This was stirred overnight before being concentrated and left to stand at -30°C , resulting in the growth of colourless crystals suitable for X-ray diffraction. These crystals were revealed to be (DME)Li(TMP)Al(*i*Bu)₃ **52**. Thus, as with all of the oxygen substituted bidentate substrates explored thus far, the mono TMP aluminate fails to deprotonate DME under the reaction conditions employed and instead the Lewis acid-Lewis base product is the

result. In common with the THF, MDME and THFFA solvates, the DME complex has a distorted tetrahedral aluminium comprising three *iso*-butyl groups, two terminal and one bridging, and a TMP anion. The TMP anion lies again in a chair conformation overhanging the alkali metal. The lithium atoms coordination sphere is completed by a chelating DME molecule with near identical Li–O bond lengths [Li1–O1 2.023(5) Å, Li1–O2 2.052(5) Å]. Again in common with the bifunctional N, O solvates, the DME ligand distances itself from the bulky TMP ligand with N1–Li1–O1 and N1–Li1–O2 angles of 138.5(2)° and 132.4(2)° compared to those of C10–Li1–O1 and C10–Li1–O2 [99.9(2)° and 117.5(2)° respectively]. Reaffirming a preference for one functionality to approach closer to the bridging *iso*-butyl ligand than the other, the O1⋯C10 [3.536(4) Å] separation is considerably shorter than that of O2⋯C10 [3.960(4) Å]. Importantly, this confirms that the disparities observed in the D⋯C_{iBu} (D = donor atom) within the bifunctional chelates **50** and **51** are not solely a result of the different properties of the oxygen and nitrogen functional groups but that such an unsymmetrical arrangement is favoured, presumably for steric reasons.

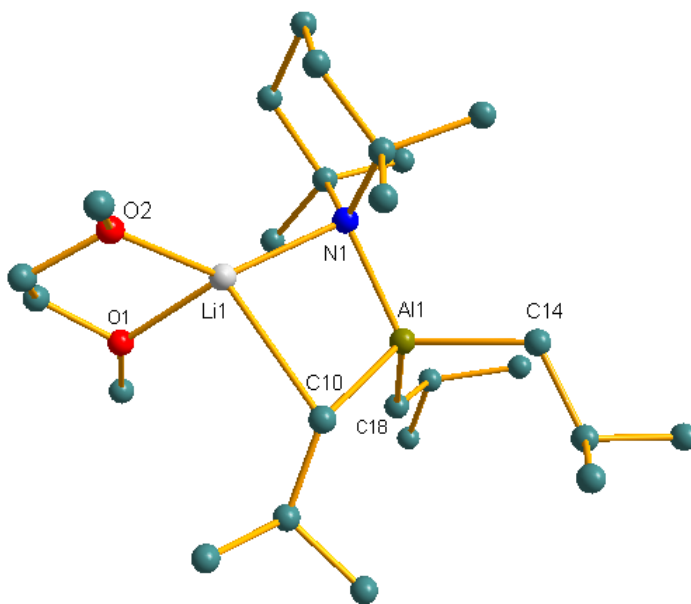


Figure 12.6: Molecular structure of DME solvate **52**. Hydrogen atoms are omitted for clarity. Selected bond lengths [Å] and angles [°]: N1–Li1 2.085(5), O1–Li1 2.023(5), O2–Li1 2.052(5), C10–Li1 2.570(5), N1–Al1 1.992(2), C10–Al1 2.070(3), C14–Al1 2.028(3), C18–Al1 2.030(3), N1–Al1–C10 102.9(1), N1–Al1–C14 114.1(1), N1–Al1–C18 118.6(1), C10–Al1–C14 110.5(1), C10–Al1–C18 105.0(1), C14–Al1–C18 105.4(1), N1–Li1–O1 138.5(2), N1–Li1–O2 132.4(2), C10–Li1–O1 99.9(2), C10–Li1–O2 117.5(2), C10–Li1–N1 85.4(2), O1–Li1–O2 81.4(2).

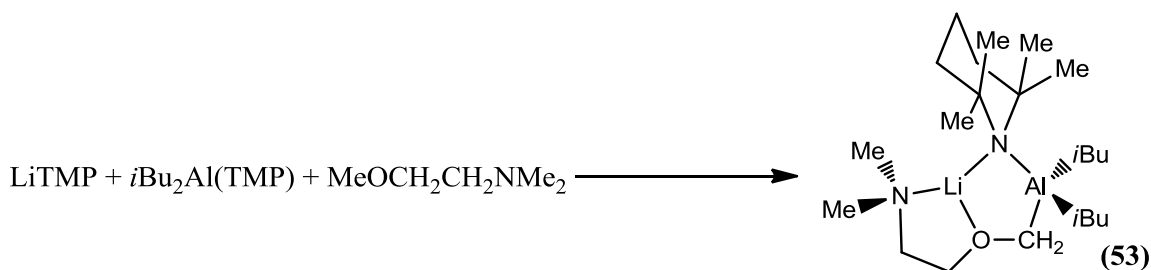
Having shown that the aluminium base struggles to metallate bi-dentate ligands we next investigated tridentate bifunctional bis[2-(N,N-dimethylamino)ethyl] ether (TMDAE – TetraMethylDiAminoEther). The increased size of the substrate, relative to the bidentate ligands discussed thus far, could result in TMDAE encroaching closer to the reactive TMP ligand, facilitating a clean deprotonation. The structural similarity between TMDAE and PMDETA, simply replacing the central methylamino functionality with an oxygen linker, also provides reason for optimism. Adding one molar equivalent of TMDAE to a pre-prepared hexane solution of LiTMP and tri-*iso*-butylaluminium instantly resulted in the formation of a yellow oil. No visual change was observed after stirring the mixture overnight. After storage at -30°C for several weeks a small crop of crystals amenable to X-ray diffraction were deposited. Unfortunately this analysis revealed these crystals to be LiTMP. Repeating the synthesis in toluene or methylcyclohexane did not prevent the precipitation of a yellow oil. Repeating the synthesis once more in hexane, stirring overnight, and quenching with D₂O resulted in no detectable deuteration of the TMDAE molecule. Therefore under these conditions it appears that TMDAE is inert towards **49**.

12.2 Reactions with the bis TMP aluminate base

Having established that sp³ metallation adjacent to a heteroatom of a chelating substrate by the mono TMP aluminate **49** is not a general reaction we turned our attentions to the bis TMP aluminate **48**. Reasoning that metallation of MDME, THFFA and DME by **49** failed as a result of the substrate successfully distancing itself from the reactive TMP anion by encroaching into the larger space provided by the bridging *iso*-butyl ligand, it seemed equally logical that changing the *iso*-butyl ligand for a second TMP anion might result in a sandwiching of the substrate between both reactive anions and thus enforce deprotonation.

To a mixture of LiTMP and (TMP)Al(*i*Bu)₂ in hexane was added the bifunctional MDME and the reaction stirred overnight to produce a pale yellow solution (Scheme

12.3). Concentration of this solution *in vacuo* and storage at -30°C resulted in the growth of colourless crystals suitable for X-ray diffraction analysis. This analysis revealed the product to be $(\text{MDME}^*)\text{Li}(\text{TMP})\text{Al}(\text{iBu})_2$ [$\text{MDME}^* = (\text{Me})_2\text{NCH}_2\text{CH}_2\text{OCH}_2$] **53** (Figure 12.7), where the OMe group has been deprotonated/aluminated to “OCH₂Al”. In the molecular structure, aluminium retains two terminal *iso*-butyl ligands and a TMP anion which bridges the aluminium to lithium. Comparable Al–C_(*i*Bu) and Al–N bond lengths are observed to those within the MDME solvate **50** [average Al–C_(terminal) 2.027 Å, Al–N1 1.990(2) Å compared with average Al–C_(terminal) 2.050 Å, Al–N1 1.992(4) Å], demonstrating little deviation between the common scaffolds of both complexes. However, the reduced steric bulk around lithium allows for a closer interaction with the TMP anion [Li1–N1 2.029(3) Å compared with Li1–N1 2.134(9) Å]. The bond distance between the carbanion belonging to the deprotonated MDME ligand and aluminium [C24–Al1 2.038(2) Å] is comparable to the average Al–C_(*i*Bu) bond length. This completes a puckered five atom, five element ring (Li–N–Al–C–O). Lithium’s coordination is completed by N, O chelation by the deprotonated MDME ligand [N–Li, 2.097(3) Å; O–Li, 1.841(4) Å; C–Li, 2.754(4) Å] and a long range interaction to C24 [2.754(4) Å]. The lithium centre is effectively in a distorted trigonal planar environment with the more distant coordination to the newly generated CH₂ anion essentially enforced due its obvious close proximity to the oxygen atom [angles totalling 357.9°]. However, the influence of the aluminium is clearly evident in the marked distortion of lithium’s coordination sphere [N1–Li1–N2 $163.4(2)^{\circ}$], an understandable consequence of the tethering of the deprotonated MDME ligand to the group XIII metal.



Scheme 12.3: Metallation of MDME by the bis-TMP aluminate.

Metallation of a methoxy group without resulting in the decomposition of the deprotonated substrate is a highly challenging transformation. To the best of our

knowledge, there are only four examples reported of structurally characterised products of methoxy deprotonation. All these metallations were carried out by complexes of expensive transition metals (Ce,^[184] Ir,^[185] Pt^[186]) and are hence unlikely to represent a suitable stoichiometric synthetic route towards this class of compound. By contrast, the bis TMP metallating agent **48**, which can be prepared in a one-pot synthesis from

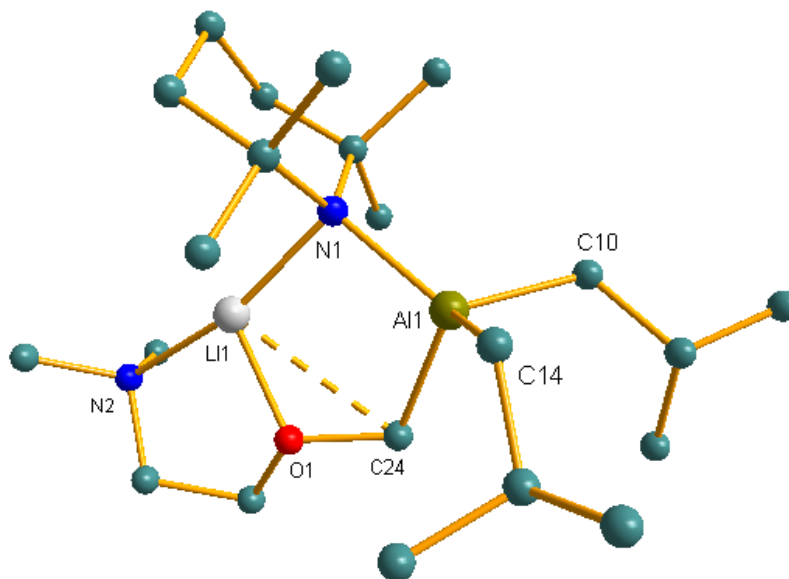
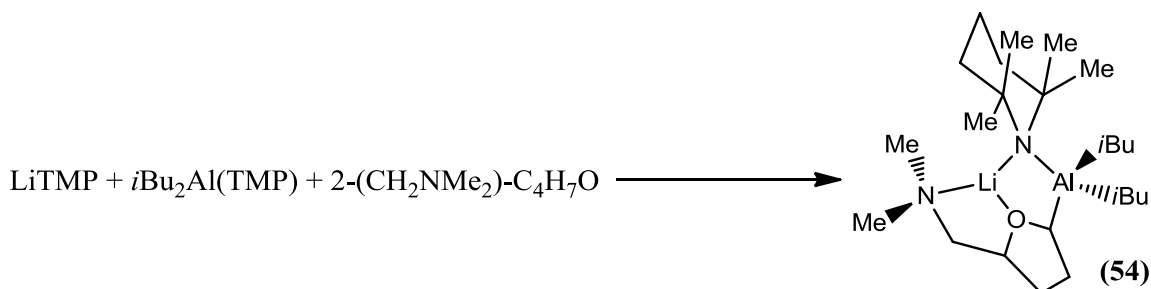


Figure 12.7: Molecular structure of the aluminated MDME-derived complex **53**. Hydrogen atoms omitted for clarity. Selected bond lengths [Å] and angles [°]: Li1–N1 2.029(3), Li1–N2 2.097(3), Li1–O1 1.841(4), Li1–C24 2.754(4), Al1–N1 1.990(2), Al1–C10 2.028(2), Al1–C14 2.025(2), Al1–C24 2.038(2), N1–Li1–N2 163.4(2), N1–Li1–O1 107.5(2), N2–Li1–O1 87.0(1), N1–Al1–C10 117.49(8), N1–Al1–C14 116.25(8), N1–Al1–C24 101.92(7), C10–Al1–C14 101.84(8), C10–Al1–C24 107.63(9), C14–Al1–C24 111.72(8).

relatively inexpensive commercially available starting materials, represents a much more economically viable method. Unfortunately, although **53** was the sole product isolated by crystallisation, NMR spectroscopic analysis of an aliquot of solution of the reaction between MDME and **48** reveals a complicated mixture of products of which **53** is only a minor component. Analysis of the reaction *in situ* is further complicated by the volatile nature of the MDME ligand, and the likely volatility of any decomposition product thereof, resulting in their absence from the NMR spectra. The major product of this reaction is yet to be identified.

Turning to the substituted tetrahydrofuran THFFA allows for a direct comparison with the remarkable aluminination of THF.^[48] This synthetic protocol would become much more attractive if it could be demonstrated to be a general transformation, and that it was compatible with more sophisticated, functionalised furan rings. While the THFFA used here is racemic, nevertheless its metallation would represent a rare opportunity to study the diastereoselectivity of a synergic bimetallic base. Combining LiTMP, (TMP)Al(*i*Bu)₂ and THFFA in hexane and stirring overnight produced a pale yellow solution (Scheme 12.4). Concentration of this solution *in vacuo* and storage at -30°C furnished a crop of colourless crystals suitable for X-ray diffraction in a 29% yield. The data are insufficiently accurate to permit a meaningful discussion of the bond lengths and angles. However, the product was unequivocally determined to be (THFFA*)Li(TMP)Al(*i*Bu)₂ {THFFA* = 5-[2-(Me)₂NCH₂-C₄H₆O]} **54**, the result of deprotonation of the substituted tetrahydrofuran (Figure 12.8). The structure is similar to that observed through deprotonation of other bidentate substrates such as the MDME complex **53** or the metallated TMEDA species (TMEDA*)Li(TMP)Al(*i*Bu)₂, with a core consisting of a TMP anion bridging lithium and aluminium which retains two terminal *iso*-butyl ligands. A new Al–C bond is formed with the deprotonated substrate and the lithium coordinates with the available heteroatoms to deliver a distorted trigonal planar geometry. Unlike the deprotonated THF product (THF)Li(TMP)(C₄H₇O)Al(*i*Bu)₂, **54** does not require a second donor molecule to solvate lithium but is instead satisfied by the amino arm of the deprotonated THFFA ligand. As with the MDME complex **53**, metallation has occurred adjacent to oxygen rather than nitrogen, deprotonating the furan in the previously unsubstituted C5 position.



Scheme 12.4: Metallation of THFFA by 48.

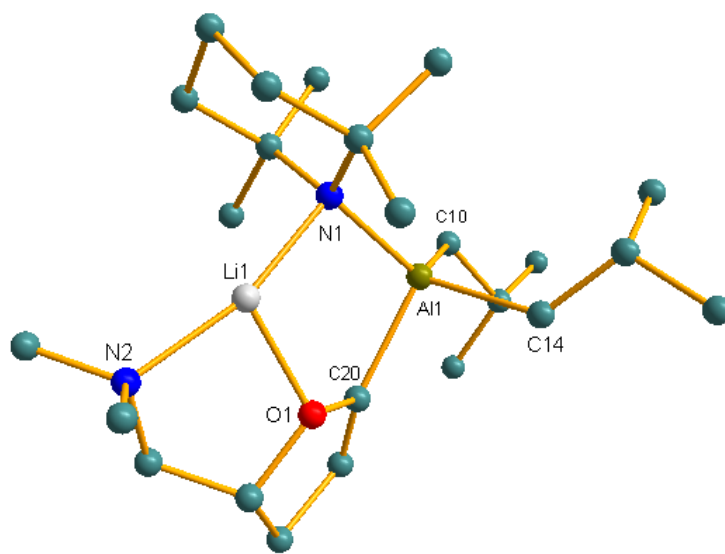
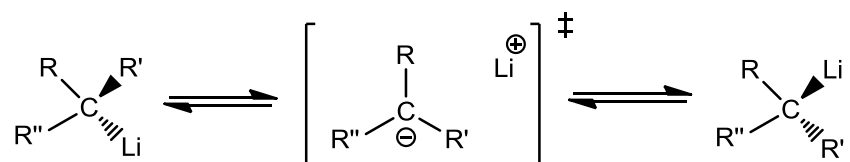


Figure 12.8: Molecular structure of (THFFA*)Li(TMP)Al(*i*Bu)₂ **54. Hydrogen atoms and disorder within the THFFA* ligand are omitted for clarity.**

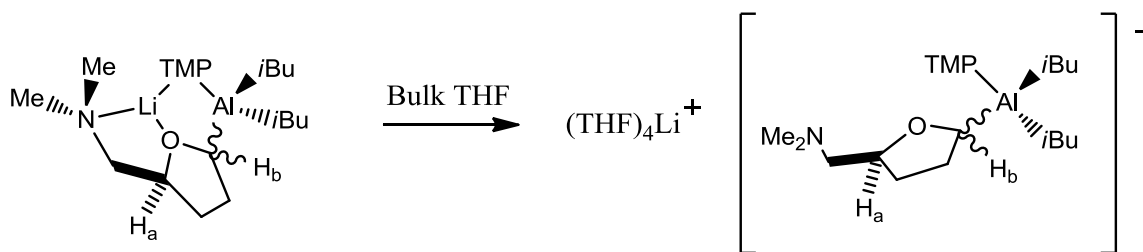
NMR spectroscopic analysis of an aliquot of solution of *in situ* generated **54** reveals that the consumption of THFFA is essentially quantitative. Furthermore, electrophilic quenching of the *in situ* generated **54** by deuterium oxide demonstrates that the deprotonation of THFFA is chemoselective, with no deuteration observed adjacent to nitrogen. In fact, the metallation also exhibits a degree of stereoselectivity, with deuteration exclusively at C5 of the furan ring at the expense of C2. As alluded to earlier, the formation of a bifunctionalised tetrahydrofuran potentially results in the formation of two diastereomers. This result is indeed realised, and its effects are felt both in the deuteration experiment and also in the analysis of the NMR spectroscopic data of the metallated species. Assignment of the ¹H NMR spectrum is complicated by the observation of both diastereomers at room temperature. The ⁷Li NMR spectrum of the metallated species in C₆D₆ contains two well resolved resonances in approximately a 2:1 ratio, fitting well with the observed diastereoselectivity of the deuterium oxide quench. The observation of two distinct diastereomers in the NMR spectra of the aluminated product indicates that any potential interconversion between the two must be slow on the NMR time scale. This is in stark contrast to lithiated diastereomers which, due to the greater ionic nature of their metal–carbon bonds, can rapidly interconvert via a trigonal

planar ion separated intermediate (Scheme 12.5). This rapid interconversion can result in the loss of diastereo or enantio selectivity of a lithiation reaction. The contrasting stability observed of the two diastereomers of **54** in solution exemplifies the potential of lithium aluminates to retain diastereo or enantio selectivity within deprotonation reactions, if appropriate ligand systems can be designed to induce the desired selectivity in the first place.



Scheme 12.5: Depiction of the racemisation of a lithiated carbon centre via an ion pair transition state. The aluminated THFFA **54** appears far less susceptible to such interconversion pathways.

Measuring the NMR spectra in the donor solvent THF-D₈, in place of C₆D₆, results in sharper, more defined resonances. Informatively, the ⁷Li NMR spectrum in THF-d₈ contains only one resonance intimating the formation of a solvent separated structure in solution as the fragmentation of **54** in the donor solvent would relieve the lithium cation from the influence of the different diastereomers of the THFFA* ligand. The ¹H NMR spectrum in THF-D₈ reveals that the two diastereomers are still present in approximately a 2:1 ratio and that any potential interchange between them remains slow on the NMR timescale even in donor media. The resonances for the TMP and *iso*-butyl ligands are also both clearly split by the influence of the diastereomeric nature of the THFFA* ligand, indicating that these remain in close proximity in solution. The apparent structural disparity of **54** in donating and non-donating media could prove important for the reactivity of the complex. Especially important could be how this affects the reactivity of **54** towards electrophiles. More generally, it implies that the parent bi-metallic bases may well be subject to the same structural variations when changing between donating and non-donating media. The diligent choice of solvent is always important for the success of any synthesis. This result contributes towards a rationale for different reactivity observed within mixed metal chemistry when changing from a donating to a non-donating solvent.



Scheme 12.6: The contact ion pair structure of **54** appears vulnerable to the donor solvent THF.

In an attempted repeat synthesis of **54** a trace amount of a crystalline material was produced at room temperature after THFFA addition. Given this uncharacteristic insolubility the crystals were analysed by X-ray diffraction and the compound was revealed to be the monometallic $\{(THFFA)[Li(TMP)]_2LiCl\}_2$ **55**. The unexpected lithium chloride is thought to have been carried over from the synthesis of $(TMP)Al(iBu)_2$ from $(iBu)_2AlCl$ and $LiTMP$, though this $LiCl$ is removed by filtration before the produced $(TMP)Al(iBu)_2$ is used in the synthesis of **48**. This structure can be described in several different ways. It can be thought of as an extended ladder motif consisting of five four membered fused rings, analogous to the zinc rich zincate $(THF)Li[(Bz)N(H)CH_2CH_2N(Bz)]_2Zn_2[(Bz)NCH_2CH_2N(Bz)](tBu)$ **35** with its 5-4-5-4-5 fused ring system. The core of this fused system is a $(LiCl)_2$ rhombus while the external heteroleptic $Li-N-Li-Cl$ rings at each end of the extended ladder are each capped by a neutral THFFA ligand. Alternatively a part of **55** can be likened to the “open dimer” structure of $(TMEDA)[Li(TMP)]_2$ discussed previously (Figure 10.3, page 100). In this case a $LiTMP$ “open dimer” unit constructed from $Li4-N2-Li3-N3$ has been capped by a THFFA ligand as opposed to $TMEDA$ and has also acquired a lithium chloride fragment $Li1-Cl1$. This $(THFFA)[Li(TMP)]_2LiCl$ moiety then dimerizes through the lithium chloride. The $Li-N$ bond lengths are comparable but on average slightly longer than those in the $TMEDA$ solvate $(TMEDA)[Li(TMP)]_2$ ^[120] [$Li4-N2$ 2.02(1) Å, $Li3-N2$ 2.021(8) Å, $Li3-N3$ 2.050(8) Å compared with 1.950(5) Å, 2.049(6) Å and 1.885(6) Å] although the complexation of lithium chloride results in a greater deviation from linearity of the $N_{(TMP)}-Li-N_{(TMP)}$ linkage [$N2-Li3-N3$ 160.1(5)° compared with 172.5(3)°].

Finally **55** can be considered an analogue to the recently coined Metal Anionic Crown (MAC) complexes.^[187] MAC complexes constitute a new lineage of the more widely studied inverse crown family. Inverse crowns, where a metal-ligand cationic framework encapsulates an anionic “guest”, are so termed by means of comparison with a crown ether solvate, where a Lewis basic framework encapsulates a Lewis acidic “guest”. Inverse crowns have been briefly discussed already (Figure 10.14, page 116; Figure 10.23, page 126). In contrast to the standard inverse crown, which are typically neutral organometallic molecules constructed from a mixture of mono- and di- valent metals, MACs have so far all been monometallic and, critically, the organometallic cycle possesses an overall negative charge. A typical example of a MAC complex is the mixed lithium amide lithium chloride adduct [(TMCD_A)₂Li][Li₅(HMDS)₅Cl]. The Li1–N3–Li3–N2–Li4 segment within **54** can be considered as half of a TMP analogue of this

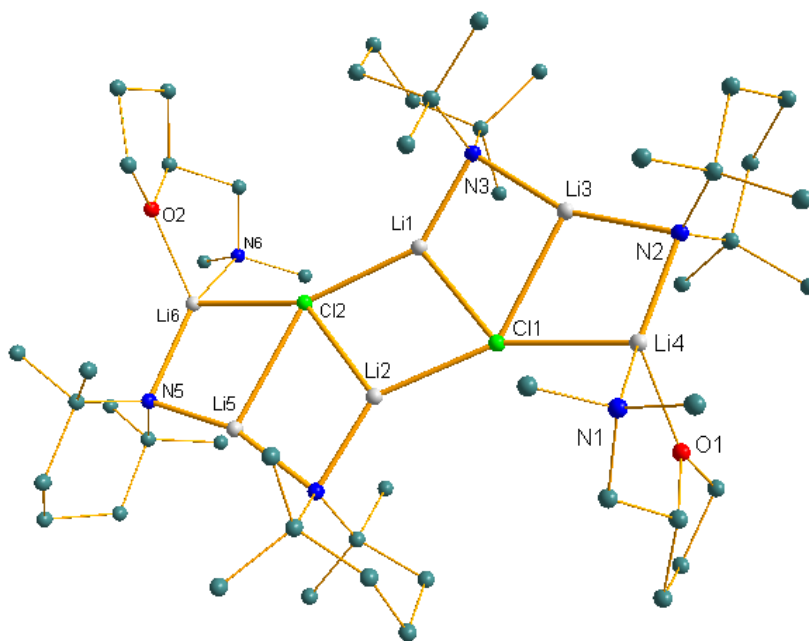


Figure 12.9: Molecular structure of the “turbo” lithium TMP complex {(THFFA)[Li(TMP)]₂LiCl}₂ **55** with emphasis of its extended ladder framework. Hydrogen atoms omitted for clarity. Selected bond lengths [Å] and angles [°]: Li1–N3 1.93(1), Li1–Cl1 2.349(8), Li1–Cl2 2.343(9), Li2–N4 1.94(1), Li2–Cl1 2.341(9), Li2–Cl2 2.325(9), Li3–N2 2.021(8), Li3–N3 2.050(8), Li3–Cl1 2.564(8), Li4–N2 2.02(1), Li4–Cl1 2.534(9), Li4–N1 2.25(1), Li4–O1 1.991(9), Li5–N4 2.037(9), Li5–N5 2.034(9), Li5–Cl2 2.617(9), Li6–N5 2.05(1), Li6–Cl2 2.554(8), Li6–N6 2.25(1), Li6–O2 1.972(8), N2–Li3–N3 160.1(5), N2–Li3–

Cl1–Li3–Cl1 102.4(3), N3–Li3–Cl1 97.3(3), Cl1–Li1–Cl2 105.4(4), Cl1–Li1–N3 108.6(4), Cl2–Li1–N3 144.9(5), N1–Li4–O1 82.8(5), N1–Li4–N2 132.5(6), N1–Li4–Cl1 99.4(4), O1–Li4–N2 129.2(6), O1–Li4–Cl1 104.2(4), N2–Li4–Cl1 103.5(4).

anionic crown, again constructed around a chloride anion, as demonstrated in Figure 12.10. Formation of a MAC motif in the case of **55** is precluded owing to its amide deficient, halide rich constitution relative to $[(\text{TMCD A})_2\text{Li}]^+[\text{Li}_5(\text{HMDS})_5\text{Cl}]^-$. However, it is interesting to note that the synthesis of the HMDS MAC complex was not sensitive to the stoichiometry employed, providing $[(\text{TMCD A})_2\text{Li}]^+[\text{Li}_5(\text{HMDS})_5\text{Cl}]^-$ even when the lithium amide and halide source were added in a 1:1 ratio. This could be construed to suggest that the differences in the structural motifs observed are as a result of the differing properties of the amide anions (and/or of the neutral donor ligands) in each case rather than as a result of differing synthetic protocols.

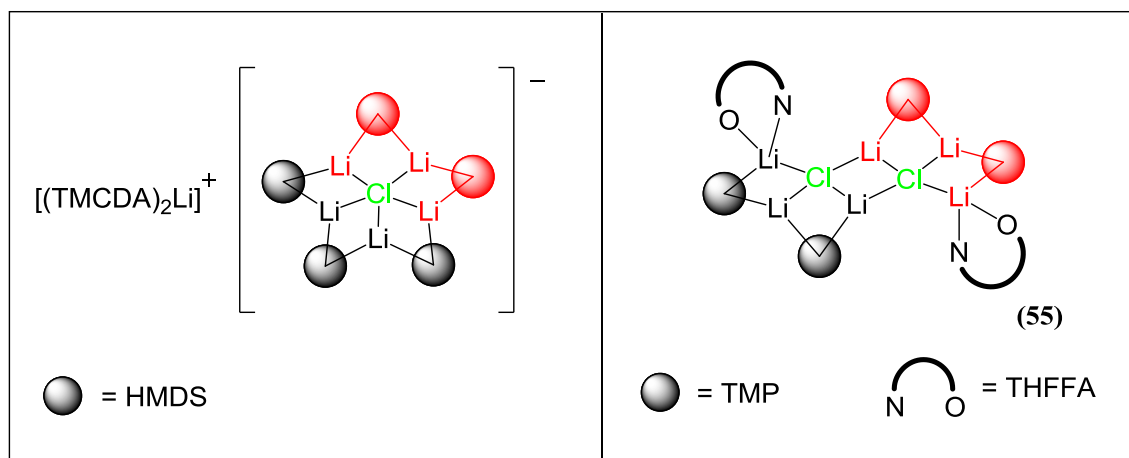


Figure 12.10: Depiction of MAC complex $[(\text{TMCD A})_2\text{Li}][\text{Li}_5(\text{HMDS})_5\text{Cl}]$ (LHS) and TMP complex **55** (RHS) with a segment of common architecture between the two complexes highlighted in red.

Recently a significant level of interest has been shown in the incorporation of metal salts, in particular lithium chloride, into organometallic chemistry.^[188] Especially prolific has been the group of Knochel, who have demonstrated that bimetallic “turbo” Grignards or Hauser bases such as “(TMP)MgCl.LiCl” can exhibit enhanced reactivity towards metallation chemistry relative to monometallic (TMP)MgCl.^[108] Detailed structural studies of “(TMP)MgCl.LiCl”, both in the solid state^[189] as well as in THF solution,^[190] have been carried out by our own group. NMR studies reveal that the lithium chloride salt

is not ordinarily coordinated to the magnesium amide in solution. However, the solid state structure $(\text{THF})\text{Li}(\text{Cl})_2\text{Mg}(\text{TMP})(\text{THF})$ suggests that, on the occurrence of any transient co-complexation of the Hauser base $[(\text{TMP})\text{MgCl}]_2$ with lithium chloride the effect is twofold. Firstly, the lithium chloride adduct $(\text{THF})\text{Li}(\text{Cl})_2\text{Mg}(\text{TMP})(\text{THF})$ is monomeric and the breaking down of organometallic aggregates has long been considered integral to increasing their reactivity. Secondly, the magnesium atom is now solvated by a potentially labile THF ligand intimating a potential docking site for incoming substrates unavailable to the monometallic species. Analogous to the reagents of Knochel, **55** could be considered a “turbo” lithiating agent. Salt effects have also been exploited within the field of lithium amide chemistry. Collum has previously demonstrated that the presence of as little as >0.5 mol% lithium chloride in a reaction mixture can provide significant enhancements in reaction rate (as much as one hundredfold acceleration).^[191] This opens the possibility that many “salt free” protocols could be affected by unforeseen trace salt impurities (indeed the unintended synthesis of **55** is a case in point). In fact, through a battery of NMR studies, utilising ^6Li and ^{15}N enriched material, the monomeric lithium amide complex $[\text{Li}(\text{TMP})]_2\text{LiCl}$ has been detected in equilibrium with the 1:1 species $\text{Li}(\text{TMP})\text{LiCl}$.^[192] Recent NMR studies in this group have also implicated a mixed lithium amide/lithium chloride complex as the true reactive species in the heavily utilised TMP zincate complex “ $\text{LiZn}(\text{TMP})_3$ ” (which is synthesised *in situ* by the metathesis reaction of LiTMP and zinc chloride in THF).^[193] As a result, the ready synthesis and isolation of a structurally determined “turbo” LiTMP complex could provide the ideal platform from which to expand our knowledge of these already synthetically significant (although this significance remains often underappreciated) reagents.

Turning now to the bidentate ether DME, we pondered if the reduced steric bulk relative to that of MDME or THFFA might prevent metallation, as in the case with the mono TMP aluminate base **49**, or whether we might add to our repertoire of successful methoxy deprotonations. So experimentally, as with the synthesis of **53** and **54**, one molar equivalent of DME was introduced to a pre-prepared hexane solution of LiTMP and $(i\text{Bu})_2\text{Al}(\text{TMP})$. The solution was stirred overnight, concentrated *in vacuo* and left to

stand at -30°C resulting in the growth of colourless crystals. While the quality of these crystals proved insufficient for analysis by X-ray diffraction they did permit the measurement of clean NMR spectra. The ^7Li NMR spectrum confirmed the presence of the alkali metal, exhibiting one sharp resonance at 0.77 ppm. The ^1H NMR spectrum (Figure 12.11) contained signals for *iso*-butyl ligands (CH_2 0.48 ppm and 0.65 ppm, CH 2.36 ppm and HCMe_2 1.35 ppm and 1.40 ppm) and TMP anions (TMP-*Me* 1.41 ppm) in a 2:1 ratio. In the window from 2.5 ppm to 3.5 ppm, this spectrum showed signals attributable to two distinct DME species, namely two sets of triplets at 2.63 ppm and 3.97 ppm, each integrating to two, which correspond to a DME ethylene backbone that has lost its symmetry (as a result of the symmetry exhibited in free DME its ^1H NMR spectrum consists of one singlet for the ethylene backbone and one singlet for the methoxy groups in a 2:3 ratio). This loss of symmetry is consistent with deprotonation of one methoxy group. There are then two singlets at 2.58 ppm and 3.01 ppm which both integrate to three and two singlets at 3.05 ppm and 3.36 which both integrate to two. This is therefore consistent with one DME ligand deprotonated at the methoxy group and half a DME ligand solvating the complex. On this basis, and consistent with the NMR analysis, we suggest that the crystalline product is methoxy deprotonated product $(\text{DME})[(\text{DME}^*)\text{Li}(\text{TMP})\text{Al}(\text{iBu})_2]_2$ **56** ($\text{DME}^* = \text{CH}_2\text{OCH}_2\text{CH}_2\text{OMe}$) (Figure 12.12). These crystals have been isolated in up to a 64% yield indicating that the bis TMP aluminate base **48** can deliver substantial methoxy deprotonation, and can sustain this useful synthon within a synergic mixed metal complex.

The final substrate to introduce to the bis TMP base again offers the potential for selectivity issues. While **48** has thus far acted chemoselectively, deprotonating adjacent to oxygen and avoiding substitution adjacent to nitrogen, the dimethylamino functional group of TMDAE is presumably more sterically exposed than the hydrogens adjacent to oxygen on the ligands ethylene backbone. This assertion is in line with the only other previously reported metallation of a tridentate ligand by this base. Triamine PMDETA was cleanly metallated at its terminal dimethylamino functionality with no deprotonation observed at either the central methyl group or the ethylene bridges.^[180] The introduction of TMDAE to the aluminium base in hexane solution instantly resulted in the formation

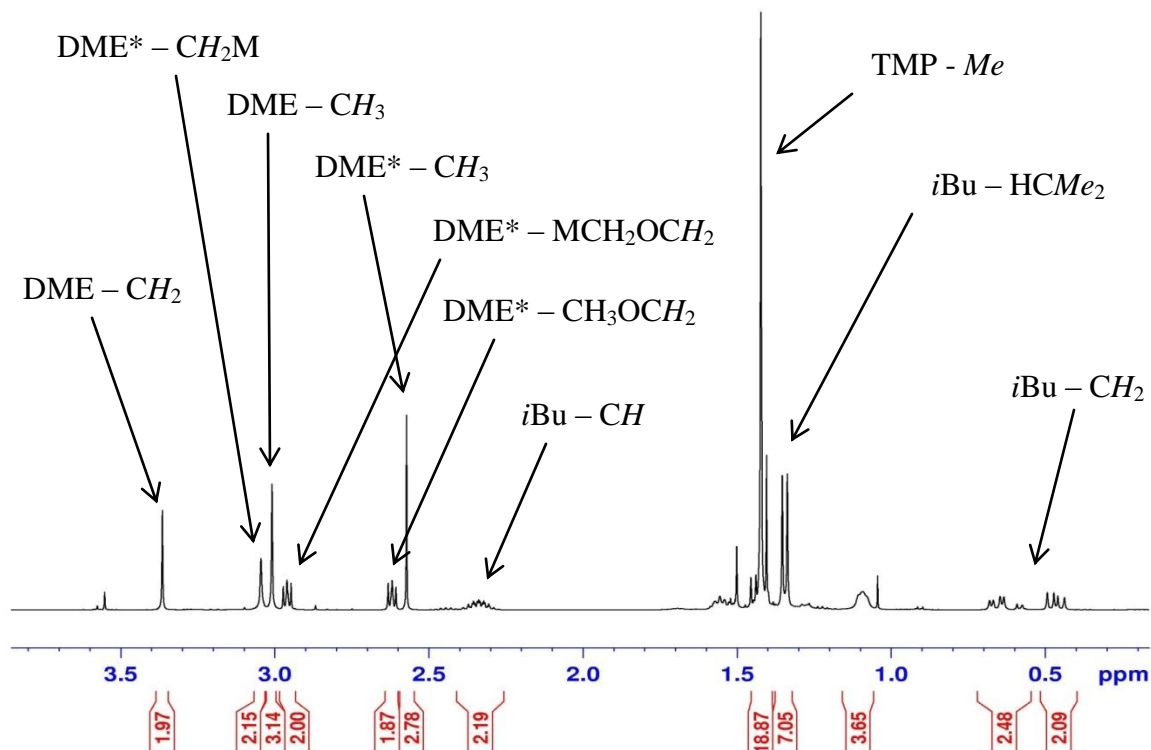


Figure 12.11: Assigned ^1H NMR spectrum of putative deprotonated DME complex $(\text{DME})[(\text{DME}^*)\text{Li}(\text{TMP})\text{Al}(\text{iBu})_2]$ **56**.

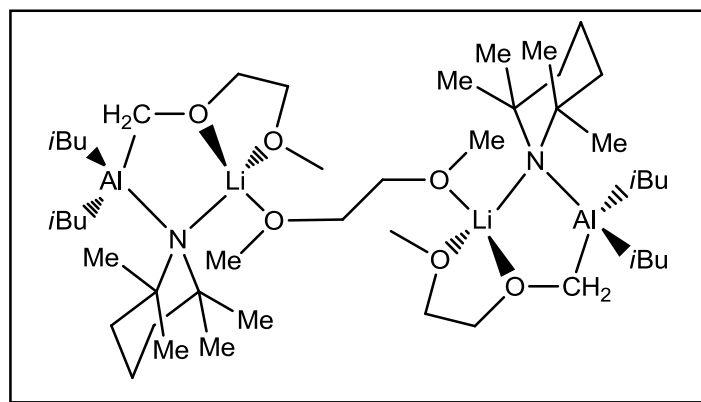


Figure 12.12: Proposed structure of putative $(\text{DME})[(\text{DME}^*)\text{Li}(\text{TMP})\text{Al}(\text{iBu})_2]$ **56**.

of a white precipitate. Gentle heating achieved the dissolution of this precipitate and X-ray quality crystals were grown on standing the solution at room temperature overnight in a 42% yield. The product was revealed to be the deprotonated TMDAE species $(\text{TMDAE}^*)\text{Li}(\text{TMP})\text{Al}(\text{iBu})_2$ **57** [$\text{TMDAE}^* = \text{CH}(\text{CH}_2\text{NMe}_2)\text{OCH}_2\text{CH}_2\text{NMe}_2$] (Figure

12.13). The X-ray data are of insufficient quality to permit a meaningful discussion of the metric parameters of **57** but the connectivity is definite. A mirror plane exists through the centre of **57**, cutting through Al1 and N2. The asymmetric unit contains a lithium and half an aluminium atom, half a TMP anion and one *iso*-butyl ligand. All of the TMDAE* ligand is present in the asymmetric unit except half of the N2 atom and one of its methyl groups. All other atoms are symmetry generated including disorder of the TMDAE* ligand and of the lithium position. In accordance with the general structural motif observed for metallated MDME and THFFA complexes **53** and **54**, aluminium is in a distorted tetrahedral environment coordinated to two terminal *iso*-butyl ligands, the metallated substrate TMDAE* and a TMP ligand. The TMP anion bridges the aluminium and lithium atoms and sits in its familiar chair conformation overhanging the alkali metal. Metallation has occurred on the ethylene backbone of the TMDAE adjacent to oxygen. This has left a terminal dimethylamino functionality floating free, unable to chelate either the lithium or aluminium atoms. That this available Lewis basic site remains vacant, avoiding both intra and inter coordination of the aluminate, indicates that both metal centres within **57** are effectively coordinatively saturated, unlike in the DME complex **56**.

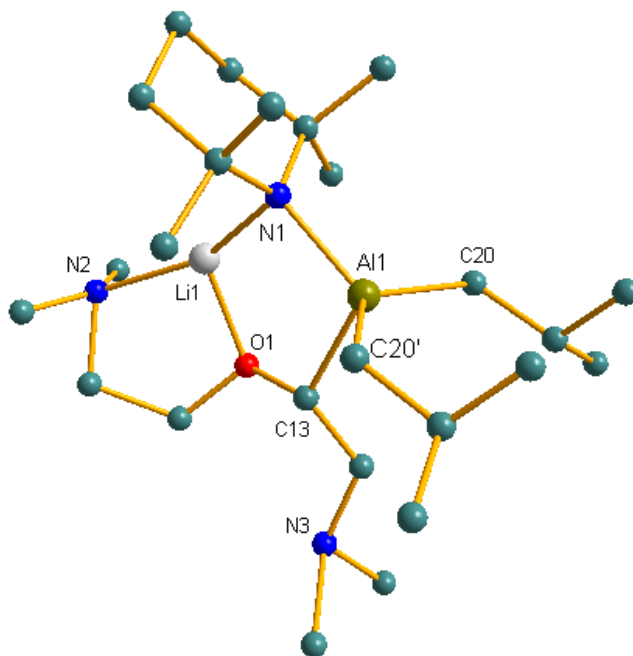


Figure 12.13: Molecular structure of (TMDAE*)Li(TMP)Al(*i*Bu)₂ **57. Hydrogen atoms and disorder within TMDAE* and *iso*-butyl groups are omitted for clarity.**

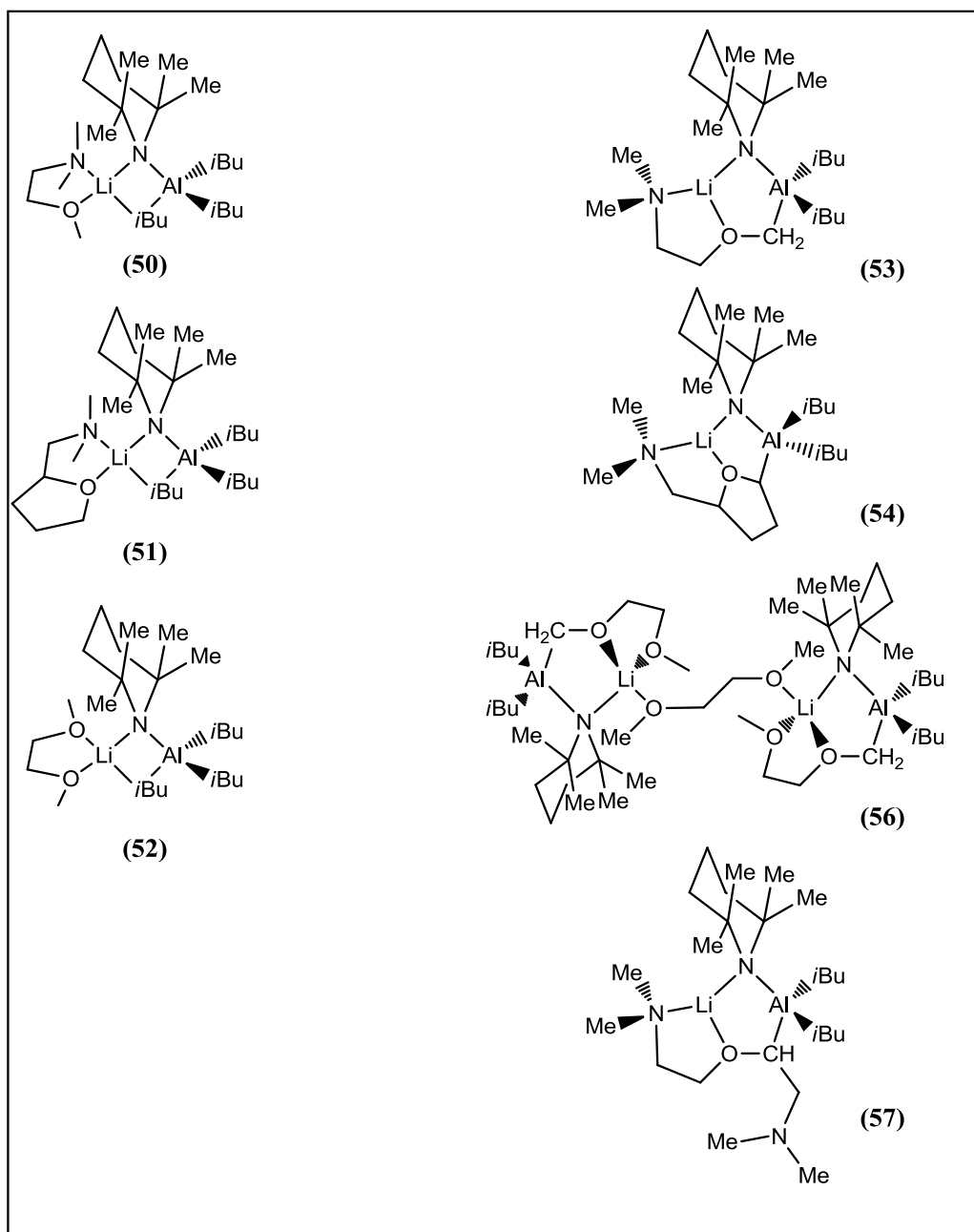


Figure 12.14: Summary of the aluminium species discussed in this chapter.

Given the metallation pattern observed and the structural similarity between **57** and **53**, TMDAE is best considered in this case as a substituted variant of the MDMAE ligand. As a result of the additional functionalization of the TMDAE ligand, relative to MDMAE, its aluminium results in the formation of a chiral (racemic) carbon centre. Analysis of the ^1H NMR spectrum reveals that each of the ethylene protons of the spine of the TMDAE

ligand give distinct resonances indicating, as in the case of the aluminated THFFA, that the newly formed Al–C bond is significantly covalent and that any interchange between enantiomers is slow on the NMR timescale. It also points to significantly hindered rotation of the “free” CH₂NMe₂ unit. This might be thought unusual when considering the structure in the solid state. In solution it may be possible that the terminal amino functionality is participating in some sort of either intra or inter molecular coordination. This could in turn result in a greater degree of conformational stability of the TMDAE* ligand.

12.3 Conclusions and future work

We have demonstrated that, despite its early results being extremely promising, the mono TMP aluminate base does not provide α -metallation for a series of bi and tri-dentate substrates. The failure to deprotonate ethereal substrates has been rationalised, at least in part, by the reduced steric requirements of an ether functionality, relative to a tertiary amino group, resulting in a more comfortable fit and thus higher activation energy towards metallation for the chelating ligand relative to a di- or tri-amine. This increased stability for ethereal bidentate ligands has allowed for the synthesis of the first chelated complexes of **49**. Of particular note is the complex of the bifunctional THFFA ligand **51**. While the THFFA utilised in these studies was racemic, the primary amine from which it was synthesised is also commercially available enantiomerically pure in either its *R* or *S* form. Aluminate **51** could thus be used as a model compound towards developing a new enantioselective base. If it was found to be sufficiently reactive towards suitable substrates then the racemic THFFA could be replaced with the more expensive enantiomerically pure form in the hope of inducing either enantioselective metallations or quenches.

Unlike the reactions of the mono TMP base **49**, the bis TMP mixture **48** has been demonstrated to be quite adept at α -metallation of chelating substrates. Rare examples of stable methoxy metallation products have been isolated and structurally characterised. In each case **48** has demonstrated complete chemoselectivity for hydrogens adjacent to

oxygen, with no detectable metallation α to nitrogen. Recent advances in THF metallation have been expanded upon to include the functionalised furan THFFA, which is metallated regioselectively and also exhibits a modest diastereo excess (*de* 33%). The presence of two different diastereomers of complex **54** permitted a more detailed study of its solution state chemistry. It became evident from the ^7Li NMR spectra of **54** that, in C_6D_6 solution the contact ion pair motif is maintained, while in THF- D_8 , the lithium is no longer influenced by the THFFA* ligand, intimating a solvent separated species. Although we have successfully, and significantly, expanded the scope of sp^3 metallation using the aluminium base **48**, there remains a great deal of exploration required to determine the limits of such a protocol. As well as deploying **48** in reactions with increasingly sophisticated and sterically challenging substrates, reaction of different heteroatoms must also be explored. Metallation adjacent to sulphur has already been achieved with the successful deprotonation of tetrahydrothiophene, but little is known of how the presence of a sulphur atom within a multi-functional substrate might affect the chemoselectivity of such a reaction. Given the importance of phosphine ligands in developing new ligands for transition metal catalysis an expansion into phosphorus chemistry could prove highly rewarding. The base has also been demonstrated to deprotonate aromatic rings, even when substituted with halogens (Cl, Br, I). However, halogens have not been explored within sp^3 hybridised systems. Perhaps most interestingly of all from a mechanistic point of view would be an investigation into how **48** might be utilised within silicon chemistry. A silyl group is capable of activating adjacent hydrogens towards metallation but, uniquely, is unlikely to act as a donor towards the aluminate base.

The isolation and structural characterisation of the first “turbo” LiTMP structure is a particularly exciting find. However, to progress further with this complex it is imperative that a rational and reproducible synthesis is devised. This would then permit a DOSY NMR study into the behaviour of a structurally determined lithium chloride adduct of LiTMP. A screening progress of “turbo” LiTMP towards various substrates could then ensue, again, importantly, starting from a well understood reagent. Of particular interest might be the wealth of substrates already investigated with respect to the “ $\text{LiZn}(\text{TMP})_3$ ”

reagent. While it is highly reasonable to believe that transmetallation for zinc in this system should deliver an increased stability for the deprotonated species, is this stability always required and/or may it be replicated, at least in part, by the incorporation of the lithium chloride salt.

Finally, the free amino arm of the TMDAE* ligand in **57** is an unusual example of a vacant Lewis basic site within a bimetallic reagent. It is highly tempting to introduce additional organometallics in an attempt to gain access to a family of rationally prepared tri-metallic clusters. The apparent vacant site may also be able to be exploited by a second equivalent of the aluminate base to yield a second metallation. Could this aluminium system successfully stabilise a dianion and prevent the cleavage of such a potentially energetic intermediate? This question is one to be answered by future studies.

13 Experimental

13.1 General procedures

13.1.1 Schlenk Techniques

Many of the reactants and products routinely encountered throughout the course of this project are both air and moisture sensitive thus the use of a Schlenk line (Figure 13.1) and Schlenk techniques are essential. All reactions were carried out under a protective blanket of argon on a standard vacuum / argon double manifold.

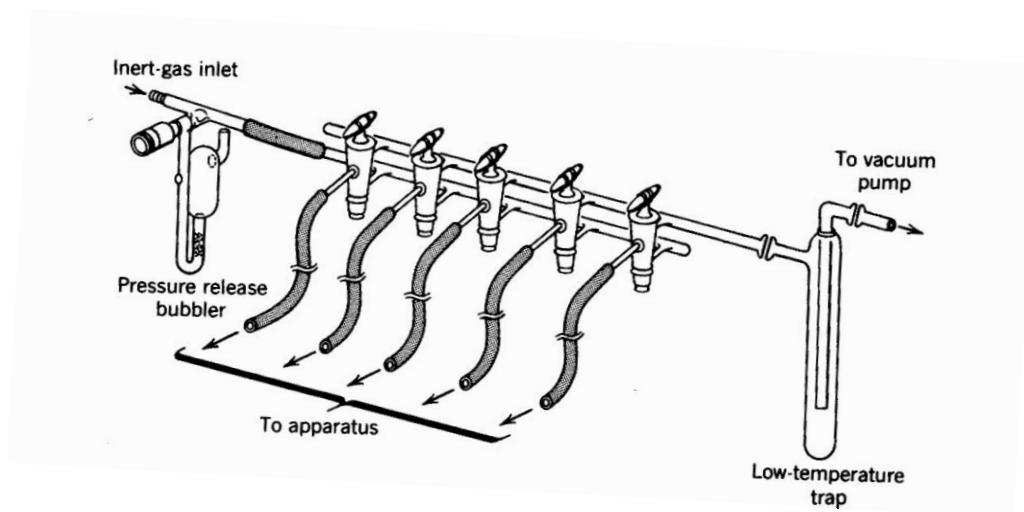


Figure 13.1: Diagram of a typical Schlenk line.

The Schlenk line comprises two separate channels – one which is connected to a high vacuum pump and the other connected to dry, oxygen free argon. At each of five positions on the line, a two way tap (coated with high vacuum grease) can be adjusted to expose the system to either vacuum or argon. To eliminate air and moisture from the system, the Schlenk tubes are evacuated and refilled with argon. This process is repeated three times. To ensure no pressure build up, an oil-filled pressure release bubbler is used. Finally, a solvent trap (contained in a Dewar flask of liquid nitrogen) is included before the line reaches the pump to condense volatile substances and prevent them from reaching and damaging the pump.

13.1.2 Use of a Glove Box

A glove box is vital for the manipulation of solid materials to prevent their decomposition. Solid reactants (as well as deuterated solvents) can be taken into the box by evacuating (for a minimum of 10 minutes) and flushing the port with argon three times. After the port is filled with argon, the gas supply continues to flow and the door is opened enough to place the reagents inside. The door is then closed, but not sealed, and the flow of argon maintained for around 10 minutes. The door can then be sealed and the gas flow stopped and the reagents taken into the box through the inner door. Solids can be removed from the glove box by placing clean, dry and greased glassware into the port (with taps open) and repeating the evacuation / argon flush procedure three times. The items can then be taken into the glove box and used in a dry and oxygen free argon atmosphere. Solid products that have been isolated via filtration can be taken into the box under vacuum. Providing all joints are well greased, the vacuum inside the vessel will be maintained until it is inside the box, where it can be opened to the argon atmosphere. Preparation of IR or NMR spectroscopic samples is also carried out in the glove box.

13.1.3 Solvents and Liquid Reagents

As many commercial solvents contain trace amounts of moisture and dissolved oxygen, these must be dried and degassed before use. All solvents were distilled over sodium / benzophenone under a nitrogen atmosphere. Sodium reacts with benzophenone to form an intensely blue ketyl radical which reacts rapidly in the presence of oxygen or water to give colourless or yellow products thus acting as a self-indicating desiccant. The dried solvent is then stored in a round-bottomed flask over 4A molecular sieves (previously dried for 12 hours at 130°C) and under argon or nitrogen. The round bottomed flask was sealed with a subseal maintaining the oxygen-free environment during storage. Solvent can be removed using a glass syringe and needle which has previously been flushed three times with argon. A volume of argon must be injected into the solvent flask before withdrawing solvent to ensure a negative pressure does not develop – this may lead to

diffusion of air through the subseal as the pressure gradient tries to re-equilibrate thus contaminating the solvent.

Where necessary, solvents were de-gassed using the freeze-pump-thaw method.^[194] This involves freezing the solvent (whilst under argon) using a liquid nitrogen bath. As soon as the solvent is frozen, a vacuum is applied to the flask removing the most volatile components of the mixture (the dissolved gases). The solvent is then allowed to fully thaw (under argon). The process is repeated in triplicate.

NMR solvents and reagents such as the amine TMPH were dried using oven-dried 4A molecular sieves which are added around 12 hours before use.

13.1.4 Reagents Used

The majority of reagents used were purchased from the Aldrich Chemical Company including: *n*BuLi (1.6M in hexane), *t*BuLi (1.7M in pentane) and ZnCl₂ (1.0M in diethylether). NaO^tBu and TMEDA were purchased from Lancaster Chemicals and TMPH from Acros Organics.

13.1.5 Standardisation of Reagents

Alkyl lithium solutions react with air and moisture causing decomposition. This decreases the molarity of the solution and so the reagents must be standardised to establish the actual molarity and ensure the correct stoichiometry is used. This can be achieved by titration of the alkyl lithium with salicylaldehyde phenylhydrazone in dry THF.^[195] The yellow solution formed turns red when the end point is reached.

13.1.6 Preparation of Salicylaldehyde Phenylhydrazone

Phenylhydrazine (100mmol, 9.85ml) is dissolved in ethanol (20ml) with stirring. Salicylaldehyde (100mmol, 10.67ml) is dissolved separately in ethanol (30ml) and then added to the phenylhydrazine solution. The resultant mixture is then stirred for 30 minutes at -15°C (in an ice / NaCl bath). The creamy, yellow precipitate formed is

filtered and dried under vacuum producing a powdery, yellow solid which is stored in a dessicator.

13.1.7 Standardisation of Alkylolithium Compounds

Salicylaldehyde phenylhydrazone (approximately 0.6 g) is weighed accurately into a Schlenk tube (**X** g) and dried under vacuum. Dry THF (10 ml) is added to form a translucent, yellow solution. The solution is titrated against *t*BuLi (in pentane) or *n*BuLi (in hexane) until the yellow colour is replaced by a permanent red indicating the end-point (**Y** ml).

The molarity of the solution can then be calculated:

$$\text{Moles of salicylaldehyde phenylhydrazone (Z)} = (\mathbf{X}) / 212.25$$

1 mole indicator reacts with 1 mole alkylolithium:

$$\text{Molarity of solution (mol l}^{-1}\text{)} = (\mathbf{Z}) / (\mathbf{Y}) \times 1000$$

13.2 Preparation of Starting Materials

The preparations of BuNa and *t*Bu₂Zn will be detailed in this section. These preparations were carried out numerous times throughout the duration of the project.

13.2.1 Preparation of BuNa

BuNa was prepared according to the method of Schleyer.^[196] Thus, NaO*t*Bu (40 mmol, 3.84 g) was added to a Schlenk tube in the glove box. Upon removal, 30 ml dried hexane was added. The suspension was placed in a sonic bath for around 10 minutes to give a fine, white dispersion. The suspension was then cooled in an ice bath while BuLi (40 mmol, 25 ml) was added dropwise. The resulting thick, white suspension was allowed to stir overnight. Filtration of the suspension yielded a white solid (BuNa) which was washed with hexane (~50 ml) before being dried under vacuum and transferred for storage in the glove box. It was assumed that this solid was pure BuNa

13.2.2 Preparation of $t\text{Bu}_2\text{Zn}$

ZnCl_2 (20 mmol, 20 ml) was added to a Schlenk tube (previously evacuated and flushed with argon). To this, diethylether (10 ml) was added and the solution cooled to 0°C in an ice bath. $t\text{BuLi}$ (20 mmol, 24 ml) was introduced dropwise to the cooled solution forming a white precipitate. The Schlenk tube was covered with black plastic (as the solution is light sensitive) and the solution allowed to stir for around 3 hours. Filtration through Celite and glass wool yielded a translucent, colourless solution which was transferred to the prepared sublimator via cannula. The solvent was removed from the solution under vacuum but before the volatile $t\text{Bu}_2\text{Zn}$ was removed, the cold finger was filled with a methanol/liquid nitrogen mixture (-20°C lowering to -50°C as reaction proceeded) causing the pure $t\text{Bu}_2\text{Zn}$ to solidify on the cold finger. After approximately one hour, the coolant was removed and the sublimator transferred under vacuum to the glove box where the pure $t\text{Bu}_2\text{Zn}$ was scraped from the cold finger (a white crystalline product produced consistently in yields as high as 80 %) and weighed into a Schlenk tube.

13.3 Instrumentation

NMR spectra were recorded on a Bruker AVANCE 400 NMR spectrometer, operating at 400.13 MHz for ^1H , 155.50 MHz for ^7Li and 100.62 MHz for ^{13}C . Data for X-ray crystal structure determination were obtained with an Oxford Diffraction Gemini diffractometer using MoK α ($\lambda = 0.71073 \text{ \AA}$) and CuK α ($\lambda = 1.54180 \text{ \AA}$) graphite-monochromated radiations. The K-band EPR spectrum was recorded on a Bruker ELEXSYS E500 spectrometer operating at a frequency of 24.1787 GHz, 0.1 mW and a modulation of 1.8 mT and simulated with XSophe distributed by Bruker Biospin GmbH.

13.4 Synthesis for chapter 9

13.4.1 Synthesis of $\{\text{Li}[\text{N}(\text{iPr})\text{CH}_2\text{CH}_2\text{N}(\text{H})(\text{iPr})]\}_2$ **17**

3.75 mL (6 mmol) BuLi was added dropwise to a solution of 1.08 mL (6 mmol) DPEDA(H₂) in 20 mL of hexane at 0 °C giving a pale yellow solution. This solution was allowed to warm to room temperature and was stirred for 1 h. The solution was concentrated and stored at -30 °C giving a crop of colourless crystals (0.71g, 79% yield). ¹H NMR (400.13 MHz, C₆D₆, 300 K): δ(ppm) = 3.6-2.4 (br, 6 H, CH and NCH₂), 1.6-0.7 (br, 12 H, CH₃, iPr), 0.6-0.3 (m, br, 1 H, NH). ⁷Li (155.50 MHz, C₆D₆, 300 K): δ(ppm) = 2.4 (br).

13.4.2 Synthesis of (TMEDA)Li[(iPr)NCH₂CH₂N(H)(iPr)]Zn(tBu)₂ **18**

1.25 mL (2 mmol) *n*BuLi was added dropwise to a solution of 0.36 mL (2 mmol) DPEDA(H₂) in 10 mL hexane at 0 °C. This temperature was maintained as 0.3 mL (2 mmol) TMEDA and a solution of 0.36 g (2 mmol) *t*Bu₂Zn in 10 mL hexane were added giving a pale yellow solution with some white solid. This solution was stored immediately at -27 °C giving a crop of colourless crystals suitable for X-ray crystallographic analysis corresponding to complex **18**. Attempts to characterise by NMR spectroscopy the kinetic product **18** were unsuccessful due to its high thermal instability.

13.4.3 Synthesis of [(iPr)N(H)CH₂CH₂N(H)(iPr)]Zn(tBu)₂ **20**

A Schlenk tube was charged with 4 mmol (0.72 g) of Zn^{*t*}Bu₂ which was dissolved in 20 mL of hexane and one equivalent of DPEDA(H₂) (4 mmol, 0.72 mL) was added via syringe. The resultant colourless solution was allowed to stir overnight at RT and heated at reflux temperature for 10 min. To aid crystallisation the solution was concentrated under reduced pressure to a final volume of 2-3 mL and, after standing overnight -27 °C, colourless crystals of **1** (suitable for X-ray crystallographic analysis) were obtained (0.20 g, 15 %). The low crystalline yield obtained for **1** is just a reflection of its high solubility, as the overall reaction yield was almost quantitative as determined by NMR

spectroscopic analyses of both **20** and reaction filtrates. ^1H NMR (400.13 MHz, C_6D_6 , 293 K): δ = 2.62 (m, 2 H, CH, *i*Pr), 2.02 (m, 4 H, CH_2), 1.34 (s, 18 H, CH_3 , *t*Bu), 0.90 (d, J = 5,2 Hz, 12 H, CH_3 , *i*Pr), 0.85 (s, br, 2 H, NH). $^{13}\text{C}\{^1\text{H}\}$ NMR (100.62 MHz, C_6D_6 , 293 K): δ = 49.5 (CH, *i*Pr), 47.2 (CH_2), 35.8 (CH_3 , *t*Bu), 23.1 (CH_3 , *i*Pr), 19.9 ($\text{C}(\text{CH}_3)$, *i*Pr).

13.4.4 Synthesis of (TMEDA)Li[(*i*Pr)NCH₂CH₂CH₂N(*i*Pr)]Zn(*t*Bu) **21**

1.25 ml (2 mmol) *n*BuLi was added dropwise to a solution of 0.39 ml (2 mmol) (*i*Pr)NHCH₂CH₂CH₂NH(*i*Pr) in 10 ml hexane at 0 °C. This temperature was maintained as 0.30 ml (2 mmol) TMEDA and a solution of 0.36 g (2 mmol) (*t*Bu)₂Zn in 10 ml hexane were added giving a pale yellow solution and a sticky white powder. This solution was refluxed for 2 hours producing a clear yellow solution. Storing the solution at -30 °C gave a crop of colourless crystals which were isolated in a 50% (0.40 g) yield. ^1H NMR (400.13 MHz, C_6D_6 , 300 K): δ (ppm) = 3.34 (m, 2 H, CH_2 , NCH₂CH₂CH₂N), 3.29 (m, 2H, CH, *i*Pr), 2.93 (m, 2 H, CH_2 , NCH₂CH₂CH₂N), 1.95 (m, 2H, CH_2 , NCH₂CH₂CH₂N), 1.90 (s, 12H, CH_3 , TMEDA), 1.72 (s, 4H, CH_2 , TMEDA), 1.59 (s, 9H, CH_3 , *t*Bu), 1.35 (d, $^3J_{\text{H-H}}$ = 6.4 Hz, 6H, CH_3 , *i*Pr), 1.18 (d, $^3J_{\text{H-H}}$ = 6.4 Hz, 6H, CH_3 , *i*Pr). $^{13}\text{C}\{^1\text{H}\}$ NMR (100.62 MHz, C_6D_6 , 300 K): δ (ppm) = 55.97 (CH_2 , TMEDA), 50.39 (CH_2 , NCH₂CH₂CH₂N), 46.12 (CH_3 , TMEDA), 38.82 (CH_2 , NCH₂CH₂CH₂N), 34.81 (CH_3 , *t*Bu), 21.60 (CCH_3 , *t*Bu). ^7Li (155.50 MHz, C_6D_6 , 300 K): δ (ppm) = 0.75.

13.4.5 Synthesis of {(THF)Li[(*i*Pr)NCH₂CH₂N(*i*Pr)]Zn(*t*Bu)}₂ **22**

To a solution of 0.36 g (2 mmol) (*t*Bu)₂Zn in 20 ml of hexane was added 0.30 ml (4 mmol) THF and 2.35 ml (4 mmol) *t*BuLi. To this was added 0.36 ml (2 mmol) (*i*Pr)NHCH₂CH₂NH(*i*Pr) which gave a bright green solution with a green oil. The oil dissolved after a 30 minute stir and the resulting solution was concentrated *in vacuo* and stored at 0 °C overnight giving colourless crystals in a 0.30 g (43%) yield. ^1H NMR (400.13 MHz, C_6D_6 , 300 K): δ (ppm) = 3.47 (m, 4H, THF), 3.23 (bs, 2 H, CH_2 , NCH₂CH₂CH₂N), 3.11 (bs, 2H, CH, *i*Pr), 2.81 (bs, 2 H, CH_2 , NCH₂CH₂CH₂N), 1.51 (s, 9H, CH_3 , *t*Bu), 1.31 (m, 4H, THF), 1.21 (bs, 12H, CH_3 , *i*Pr). $^{13}\text{C}\{^1\text{H}\}$ NMR (100.62 MHz, C_6D_6 , 300 K): δ (ppm) = 68.31 (THF), 55.05 (CH_2 , NCH₂CH₂CH₂N), 52.70 (CH, *i*Pr),

34.30 (CH₃, *t*Bu), 26.91 (CH₃, *i*Pr), 26.44 (CH₃, *i*Pr), 20.81 (CCH₃, *t*Bu). ⁷Li (155.50 MHz, C₆D₆, 300 K): δ(ppm) = 1.21.

13.4.6 Synthesis of (TMEDA)Li[(*i*Pr)NCH=CHN(*i*Pr)]Zn(*t*Bu) 24

1.25 mL (2 mmol) *n*BuLi was added dropwise to a solution of 0.36 mL (2 mmol) DPEDA(H₂) in 10 mL hexane at 0 °C. This temperature was maintained as 0.3 mL (2 mmol) TMEDA and a solution of 0.36 g (2 mmol) *t*Bu₂Zn in 10 mL hexane were added giving a pale yellow solution with some white solid. This solution was refluxed for 2 hours producing a bright orange solution. Storing the solution at -70 °C gave a crop of yellow crystals which were isolated in a 38.9% (0.30g) crystalline yield. ¹H NMR (400.13 MHz, C₆D₆, 300 K): δ(ppm) = 5.83 (s, 2 H, CH, CH=CH), 3.48 (m, 2 H, CH, *i*Pr), 1.81 (s, 12 H, CH₃, TMEDA), 1.60 (s, 9 H, CH₃, *t*Bu), 1.58 (s, 4 H, CH₂, TMEDA), 1.40 (d, *J* = 6.3 Hz, 6 H, CH₃, *i*Pr), 1.32 (d, *J* = 6.3 Hz, 6 H, CH₃, *i*Pr). ¹³C{¹H} NMR (100.62 MHz, C₆D₆, 300 K): δ(ppm) = 116.3 (CH, CH=CH), 56.0 (CH₂, TMEDA), 52.7 (CH, *i*Pr), 45.6 (CH₃, TMEDA), 35.4 (CH₃, *t*Bu), 28.6 (CH₃, *i*Pr), 28.0 (CH₃, *i*Pr), 20.6 (C(CH₃), *t*Bu). ⁷Li (155.50 MHz, C₆D₆, 300 K): δ(ppm) = -2.40.

13.4.7 Synthesis of [(TMEDA)Li(*i*Pr)NCH₂CH₂N(*i*Pr)Li]₂ 25

An evacuated Schlenk tube was charged with 20 ml hexane and 0.36 ml (2 mmol) (*i*Pr)NHCH₂CH₂NH(*i*Pr). To this colourless solution 3.75 ml (6 mmol) *n*BuLi was added dropwise by syringe. The addition of 0.90 ml (6 mmol) TMEDA was followed by a two hour reflux giving a vibrant red solution which was concentrated *in vacuo* and stored at -30 °C overnight producing colourless crystals in a 32% (0.17 g) yield. ¹H NMR spectra reveal the presence of complex dynamics in solution. Gardener and Raston have previously discussed in depth the kinds of processes likely to be taking place.^[51]

13.4.8 Synthesis of [(TMEDA)Li]₂[(*i*Pr)NCH₂CH₂N(*i*Pr)]Zn(*t*Bu)H 26

1.25 ml (2 mmol) *n*BuLi was added dropwise to a solution of 0.36 ml (2 mmol) (*i*Pr)NHCH₂CH₂CH₂NH(*i*Pr) in 10 ml hexane at 0 °C. This temperature was maintained as 0.60 ml (4 mmol) TMEDA and a solution of 0.36 g (2 mmol) (*t*Bu)₂Zn in 10 ml hexane were added giving a pale yellow solution with some white solid. To this solution

a further 1.25 ml (2 mmol) *n*BuLi was added producing a white precipitate. A 5 min reflux produced a vibrant red solution with some white solid remaining. This was stored at -30 °C giving a crop of colourless crystals in a 35% (0.35 g) yield. ¹H NMR (400.13 MHz, C₆D₆, 300 K): δ(ppm) = 3.48 (m, 2H, CH, *i*Pr), 3.26 (m, 2H, CH₂, NCH₂CH₂N), 2.96 (m, 2H, CH₂, NCH₂CH₂N), 2.05 (s, CH₃, TMEDA), 1.88 (bs, CH₂, TMEDA), 1.74 (s, 9H, CH₃, *t*Bu), 1.53 (d, ³J_{H-H} = 6.1 Hz, 6H, CH₃, *i*Pr), 1.45 (d, ³J_{H-H} = 6.3 Hz, 6H, CH₃, *i*Pr). ¹³C{¹H} NMR (100.62 MHz, C₆D₆, 300 K): δ(ppm) = 57.15 (CH₂, TMEDA), 55.91 (CH₂, NCH₂CH₂CH₂N), 54.43 (CH, *i*Pr), 37.44 (CH₃, *t*Bu), 27.25 (CH₃, *i*Pr), 26.83 (CH₃, *i*Pr), 17.91 (CCH₃, *t*Bu). ⁷Li (155.50 MHz, C₆D₆, 300 K): δ(ppm) = 0.90 (d, ¹J_{Li-H} = 13.3 Hz).

13.4.9 Synthesis of [LiOCH(*t*Bu)₂]₄

After the *in situ* preparation of 2 mmol of the hydride species **26**, the ketone ^tBu₂CO (0.35 ml, 2 mmol) was added and the solution stirred for one hour. Concentration of the solution *in vacuo* and storage at -30 °C facilitated the growth of colourless crystals in a 60 % yield (0.18 g). ¹H NMR (400.13 MHz, C₆D₆, 300 K): δ(ppm) = 3.30 (s, 1 H, CH), 1.12 (s, 18 H, CH₃). ¹³C{¹H} NMR (100.62 MHz, C₆D₆, 300 K): δ(ppm) = 89.6 (CH), 38.8 (C(CH₃)₃), 30.1 (CH₃). ⁷Li (155.50MHz, C₆D₆, 300 K): δ(ppm) = 1.12.

13.4.10 Synthesis of (TMEDA)Li[(*i*Pr)NCH=CHN(*i*Pr)]Zn(Me) **28**

1.25 mL (2 mmol) BuLi was added dropwise to a solution of 0.36 mL (2 mmol) DPEDA(H₂) in 20 mL hexane at 0 °C. This temperature was maintained as 0.3 mL (2 mmol) TMEDA and 2 mL (2mmol) of 1M Me₂Zn in heptane were added giving a pale yellow solution. This solution was refluxed for 1.5 hours producing a bright orange solution. Storing the solution at -30°C gave a crop of yellow crystals (suitable for X-ray crystallographic analysis) which were isolated in a 43.7% (0.30 g) crystalline yield. ¹H NMR (400.13 MHz, C₆D₆, 300 K): δ(ppm) = 5.93 (s, 2 H, CH, CH=CH), 3.54 (m, 2 H, CH, *i*Pr), 1.83 (s, br, 12 H, CH₃, TMEDA), 1.60 (s, br, 4 H, CH₂, TMEDA), 1.42 (d, *J* = 6.1 Hz, 6 H, CH₃, *i*Pr), 1.30 (d, *J* = 6.2 Hz, 6 H, CH₃, *i*Pr), -0.02 (s, 3 H, CH₃, ZnCH₃). ¹³C{¹H} NMR (100.62 MHz, C₆D₆, 300 K): δ(ppm) = 116.9 (CH, CH=CH), 56.1 (CH₂,

TMEDA), 52.5 (CH, *i*Pr), 45.6 (CH₃, TMEDA), 28.7 (CH₃, *i*Pr), 27.7 (CH₃, *i*Pr), -11.6 (CH₃, *ZnMe*). ⁷Li (155.50MHz, C₆D₆, 300 K): δ(ppm) = -2.34.

13.4.11 Synthesis of (TMEDA)Na[(*i*Pr)NCH=CHN(*i*Pr)]Zn(*t*Bu) 29

A Schlenk tube was charged with 0.32 g of *n*BuNa (4 mmol) and suspended in 20 mL of hexane, the resultant suspension was cooled down to 0 °C and 0.60 ml TMEDA (4 mmol), followed by 0.72 ml of (*i*Pr)NHCH₂CH₂CH₂NH(*i*Pr) (4 mmol), were added via syringe. The resultant colourless solution was allowed to stir at 0 °C for 5 min. In a separate Schlenk tube 0.72 g of (*t*Bu)₂Zn (4 mmol) was dissolved in 20 mL of hexane, cooled down to 0 °C, and added to the previous solution. The resultant colourless solution was heated to reflux for 30 min obtaining a bright yellow orange suspension. The suspension was filtered off separating a white solid (0.04 g; which proved to be non soluble in common organic solvents and exhibited gas and heat release when treated with acetone) and a bright yellow orange solution. Standing the solution overnight at -27 °C afforded a flaky bright yellow orange solid corresponding to (TMEDA)Na[(*i*Pr)NCH=CHN(*i*Pr)]Zn(*t*Bu) (1.00 g, 62%). ¹H NMR (400.13 MHz, C₆D₆, 300 K): δ(ppm) = 6.06 (s, 2 H, CH, CH=CH), 3.70 (sept, ³J_{H-H} = 6.3 Hz, 2 H, CH, *i*Pr), 1.72 (s, 12 H, CH₃, TMEDA), 1.65 (s, 9 H, CH₃, *t*Bu), 1.54 (s, 4 H, CH₂, TMEDA), 1.44 (d, ³J_{H-H} = 6.4 Hz, 6 H, CH₃, *i*Pr), 1.32 (d, ³J_{H-H} = 6.3 Hz, 6 H, CH₃, *i*Pr). ¹³C{¹H} NMR (100.62 MHz, C₆D₆, 300 K): δ(ppm) = 118.6 (CH, CH=CH), 56.2 (CH₂, TMEDA), 53.6 (CH, *i*Pr), 45.1 (CH₃, TMEDA), 35.8 (CH₃, *t*Bu), 29.1 (CH₃, *i*Pr), 20.8 (C(CH₃), *t*Bu).

13.4.12 Synthesis of (THF)₃Na[(*i*Pr)NCH=CHN(*i*Pr)]Zn(*t*Bu) 30

A Schlenk tube was charged with 0.08 g of *n*BuNa (1 mmol) which was suspended in 10 ml of hexane. This suspension was subsequently cooled to 0 °C before 0.18 ml of (*i*Pr)NHCH₂CH₂NH(*i*Pr) (1 mmol) was added producing a pale yellow solution. The addition of a freshly prepared solution of 1 mmol (*t*Bu)₂Zn in 5 ml hexane gave a pale pink oil which dissolved on the addition of 0.22 ml (3 mmol) THF. The resulting solution was allowed to warm to room temperature before being refluxed for 30 minutes, producing a bright orange solution. Concentrating this solution in vacuo and storing at -

27 °C over night resulted in the growth of colourless crystals (0.13 g, 26% yield). Dissolution for NMR spectroscopic analysis was achieved in C₆D₆ with the addition of a drop of THF-D₈. ¹H NMR (400.13 MHz, C₆D₆, 300 K): δ(ppm) = 5.98 (s, 2 H, CH, CH=CH), 3.67 (sept, 3JH-H = 6.3 Hz, 2 H, CH, *i*Pr), 1.59 (s, 9 H, CH₃, *t*Bu), 1.44 (d, 3JH-H = 6.4 Hz, 6 H, CH₃, *i*Pr). ¹³C{¹H} NMR (100.62 MHz, C₆D₆, 300 K): δ(ppm) = 118.3 (CH, CH=CH), 53.8 (CH, *i*Pr), 35.9 (CH₃, *t*Bu), 29.0 (CH₃, *i*Pr), 20.4 (C(CH₃), *t*Bu).

13.4.13 Synthesis of {(TMEDA)Na[(*i*Pr)NCH₂CH₂N(*i*Pr)]Zn(*t*Bu)}₂ 31

A Schlenk tube was charged with 0.32 g of *n*BuNa (4 mmol) and suspended in 30 mL of hexane, the resultant suspension was cooled down to 0 °C and 0.60 ml TMEDA (4 mmol), followed by 0.72 ml of (*i*Pr)NHCH₂CH₂CH₂NH(*i*Pr) (4 mmol), were added via syringe. The resultant colourless solution was allowed to stir at 0 °C for 5 min. In a separate Schlenk tube 0.72g of (*t*Bu)₂Zn (4 mmol) was dissolved in 30 mL of hexane, cooled down to 0 °C, and added to the previous solution. The resultant colourless solution was stirred for 5 min at 0 °C and cooled immediately to -27 °C. Standing the solution overnight at -27 °C afforded colourless crystals of {(TMEDA)Na[(*i*Pr)NCH₂CH₂N(*i*Pr)]Zn(*t*Bu)}₂ (1.20 g, 71%, considering in the calculation half a molecule of hexane of crystallisation). ¹H NMR (400.13 MHz, C₆D₆, 300 K): δ(ppm) = 3.47 (m, 8H, CH₂, NCH₂CH₂N), 3.34 (m, 4H, CH, *i*Pr), 1.75 (s, 24H, CH₃, TMEDA), 1.62 (s, 8H, CH₂, TMEDA), 1.59 (s, 9H, CH₃, *t*Bu), 1.37 (m, 24H, CH₃, *i*Pr). ¹³C{¹H} NMR (100.62 MHz, C₆D₆, 300 K): δ(ppm) = 56.6 (CH₂, TMEDA), 55.3 (CH₂, NCH₂CH₂CH₂N), 54.0 (CH, *i*Pr), 45.3 (CH₃, TMEDA), 35.4 (CH₃, *t*Bu), 27.3 (CH₃, *i*Pr), 23.1 (C(CH₃), *t*Bu).

13.4.14 Synthesis of {(TMEDA)Na[(*i*Pr)NCH₂CH₂N(*i*Pr)]Mg(*n*Bu)}₂ 32

A Schlenk tube was charged with 2 mmol (0.16 g) of BuNa which was suspended in 10 mL of hexane and at 0 °C a molar equivalent of TMEDA (2 mmol, 0.30 mL) was added via syringe obtaining a yellowish suspension. This was followed by the addition at 0 °C of 1 mmol of (*i*Pr)(H)NCH₂CH₂CH₂N(H)*i*Pr (0.18 mL) and 1 mmol of Bu₂Mg (1 mL of 1.0 M solution in heptane) and the resultant white suspension was heated to reflux for 1 h

obtaining a clear yellowish solution. Standing the solution at $-27\text{ }^{\circ}\text{C}$ afforded colourless crystals of $\{(\text{TMEDA})\text{Na}[(i\text{Pr})\text{NCH}_2\text{CH}_2\text{N}(i\text{Pr})]\text{Mg}(n\text{Bu})\}_2$, which were suitable for X-ray crystallographic analysis. NMR analysis of the crystals and of the filtrate showed a complex mixture which does not clearly fit with the solid state composition and no resonances in the aromatic region were observed.

13.4.15 Synthesis of $(\text{TMEDA})\text{Li}[(i\text{Pr})\text{NCH}_2\text{CH}_2\text{N}(i\text{Pr})]\text{Al}(\text{Me})_2$ 33

A Schlenk tube was charged with 2 mmol (0.16 g) of BuLi which was suspended in 10 mL of hexane and at $0\text{ }^{\circ}\text{C}$ and a molar equivalent of TMEDA (2 mmol, 0.30 mL) was added via syringe obtaining a pale yellow solution. This was followed by the addition at $0\text{ }^{\circ}\text{C}$ of 2 mmol of $i\text{Pr}(\text{H})\text{NCH}_2\text{CH}_2\text{CH}_2\text{N}(\text{H})i\text{Pr}$ (0.36 ml) and 2 mmol of Me_3Al (1 mL of a 2.0 M solution in hexane) and the resultant solution was heated to reflux for 2 h obtaining a yellow suspension. The solid dissolved on addition of 4 ml toluene. Standing the solution at $-27\text{ }^{\circ}\text{C}$ afforded colourless crystals of $(\text{TMEDA})\text{Li}[(i\text{Pr})\text{NCH}_2\text{CH}_2\text{N}(i\text{Pr})]\text{Al}(\text{Me})_2$ in a 20% yield (0.13 g), which were suitable for X-ray crystallographic analysis. ^1H NMR (400.13 MHz, C_6D_6 , 300 K): $\delta(\text{ppm}) = 3.25$ (m, 4H, CH_2 , $\text{NCH}_2\text{CH}_2\text{N}$), 3.02 (m, 2H, CH , $i\text{Pr}$), 2.37 (m, 2H, CH , $i\text{Pr}$), 1.87 (s, 12H, CH_3 , TMEDA), 1.66 (s, 4H, CH_2 , TMEDA), 1.35 (m, 12H, CH_3 , $i\text{Pr}$), -0.33 (bs, 3H, AlCH_3), -0.44 (bs, 3H, AlCH_3). ^7Li (155.50MHz, C_6D_6 , 300 K): $\delta(\text{ppm}) = 0.46$.

13.5 Synthesis for chapter 10

13.5.1 Synthesis of $(\text{TMEDA})[\text{Li}(\text{DIBA})]_2$ 37

A Schlenk tube with a magnetic stirrer bar was flushed with argon three times (10 minute evacuations). To this Schlenk was added 20 ml hexane, 12.5 ml (20 mmol) BuLi (1.6 M in pentane), 3.3 ml (20 mmol) $(i\text{Bu})_2\text{NH}$ and 1.5 ml (10 mmol) TMEDA producing a yellow/green solution that was stirred overnight producing a white precipitate. This white powder was collected in a 38% (1.45 g) yield. Upon repeating the reaction, heating the suspension produced a solution, which after slow cooling in a Dewar flask filled with hot water produced clear colourless crystals suitable for XRD. ^1H NMR (400.13 MHz, C_6D_6 ,

300 K): $\delta(\text{ppm}) = 2.63$ (d, 4H, CH_2 , *i*Bu), 2.30 (s, 2H, CH_2 , TMEDA), 2.15 (s, 6H, CH_3 , TMEDA), 1.80 (m, 2H, CH , *i*Bu), 1.61 (m, 2H, CH , *i*Bu), 0.83 (d, 12H, CH_3 , *i*Bu). ^{13}C (100.62MHz, C_6D_6 , 300K): $\delta(\text{ppm}) = 68.7$ (CH_2 , *i*Bu), 58.9 (CH_2 , TMEDA), 46.2 (CH_3 , TMEDA), 30.6 (CH , *i*Bu), 22.4 (CH_3 , *i*Bu). ^7Li (155.50 MHz, C_6D_6 , 300 K): $\delta(\text{ppm}) = -0.31$.

13.5.2 Synthesis of $[(\text{TMEDA})_2\text{Li}]\{(\text{DIBA})[\text{Zn}(\text{tBu})_2]_2\}$ 38

A Schlenk tube with a magnetic stirrer bar was flushed with argon three times (10 minute evacuations) before 4 mmol (0.77 g) $(\text{TMEDA})[\text{Li}(\text{DIBA})]_2$ was added and dissolved in 10 ml hexane to produce a pale yellow solution. 6 mmol (0.9 ml) TMEDA was then introduced followed by 4 mmol of $(\text{tBu})_2\text{Zn}$ (1.44 g in 10 ml hexane). Upon the addition of the $(\text{tBu})_2\text{Zn}$ a white precipitate was formed instantly. The produced suspension was stirred overnight and 1.4 g of a white powder was isolated. ^1H NMR (400.13 MHz, THF-D_8 , 300 K): $\delta(\text{ppm}) = [(\text{TMEDA})_2\text{Li}]\{(\text{DIBA})[\text{Zn}(\text{tBu})_2]_2\}$: 3.00 (bs, 3H, CH_2 , *i*Bu), 2.32 (s, 8H + 3.94H, CH_2 , TMEDA), 2.17 (s, 24H + 10.99H, CH_3 , TMEDA), 1.87 (m, 2H, CH , *i*Bu), 0.98 (s, 36H, *t*Bu), 0.93 (m, 12H + 12.58H, CH_3 , *i*Bu). $[(\text{TMEDA})_2\text{Li}][\text{Zn}(\text{tBu})_3]$: 0.92 (s, 12.58H + 12H, *t*Bu). $(\text{TMEDA})[\text{Li}(\text{DIBA})]_2$: 2.67 (d, 1.1H, CH_2 , *i*Bu), 1.65 (m, 0.5H, CH , *i*Bu), 0.88 (d, 1.5H, CH_3 , *i*Bu). $''(\text{TMEDA})\text{Li}(\text{DIBA})\text{Zn}(\text{tBu})_2''$: (δ 2.79, d), (δ 1.65, m), (δ 1.03, s).

13.5.3 Alternative synthesis of $[(\text{TMEDA})_2\text{Li}]\{(\text{DIBA})[\text{Zn}(\text{tBu})_2]_2\}$ 38

A Schlenk tube with a magnetic stirrer bar was flushed with argon three times (10 minute evacuations). 10 ml hexane was added followed by 1.25 ml (2 mmol) BuLi (1.6 M in pentane) and 0.34 ml (2 mmol) TMP(H). This yellow solution was stirred for 1 hour before 0.3 ml (2 mmol) TMEDA and 2 mmol of a $(\text{tBu})_2\text{Zn}$ solution (0.36 g in 10 ml hexane) were introduced producing a white suspension. After 1 hour, 0.3 ml (2 mmol) TMEDA and 0.33 ml (2 mmol) $(\text{iBu})_2\text{NH}$ were added. With stirring, overnight the white suspension dissolved producing a yellow solution. This was concentrated until there was a slight precipitation of an oil which re-dissolved on mixing. This solution yielded 0.22 g of clear colourless crystals on standing at 0°C overnight.

13.5.4 Synthesis of [(TMEDA)₂Li][Zn(*t*Bu)₃]

A Schlenk tube with a magnetic stirrer bar was flushed with argon three times (10 minute evacuations). To this Schlenk was added 1 mmol (0.18 g) (*t*Bu)₂Zn in 10 ml of hexane and 0.59 ml (1 mmol) (*t*Bu)Li (1.7 M in pentane). This solution instantly produced a white precipitate on the addition of 0.3 ml (2 mmol) TMEDA. This white precipitate was isolated by filtration in a 53% yield (0.17 g). ¹H (400.13 MHz, THF-D₈, 300 K): δ(ppm) = 2.30 (s, 8H, CH₂, TMEDA), 2.15 (s, 24H, CH₃, TMEDA), 0.92 (s, 27H, *t*Bu).

13.5.5 Synthesis of (TMEDA)Na(DIBA)₂Zn(*t*Bu) 40

0.32 g of BuNa was suspended in 10 ml of hexane to produce an off-white suspension. To this was added 1.32 ml (8 mmol) (*i*Bu)₂NH and 0.6 ml TMEDA, producing a clear orange solution after a 1 hour stir. A solution of 4mmol of ^tBu₂Zn (0.72g in 10ml hexane) was added by cannula to the reaction mixture and allowed to stir overnight. The solvent level was reduced producing a white powder in a 31% (0.65g) yield. ¹H NMR (400.13 MHz, C₆D₆, 300 K): δ(ppm) = 2.93 (d, 8H, CH₂, *i*Bu), 1.90 (m, 4H, CH, *i*Bu), 1.86 (s, 12H, CH₃, TMEDA), 1.75 (s, 4H, CH₂, TMEDA), 1.64 (s, 9H, *t*Bu), 1.05 (d, 24H, CH₃, *i*Bu). ¹³C NMR (100.62 MHz, C₆D₆, 300 K): δ(ppm) = 67.5 (CH₂, *i*Bu), 57.2 (CH₂, TMEDA), 45.7 (CH₃, TMEDA), 35.2 (*t*Bu), 31.2 (CH, *i*Bu), 22.2 (CH₃, *i*Bu).

13.5.6 Synthesis of (C₁₀H₇)C[N(*i*Bu)₂]₂N[Zn(*t*Bu)₂]₂Li(TMEDA) 41

A Schlenk tube with a magnetic stirrer bar was flushed with argon three times (10 minute evacuations). In this was placed 0.45 g (0.5 mmol) of **38** and 10 ml hexane. To this white suspension 0.08 g (0.5 mmol) 2-cyanonaphthalene was introduced. This instantly produced a bright yellow suspension which became red over a 2 hour stir. 40 ml hexane was added and the solution was heated until the suspension dissolved producing a red solution. This was left to stand at 0°C producing large orange plates in a 20% (0.06 g) yield. ¹H NMR (400.13 MHz, C₆D₆, 300 K): δ(ppm) = 8.53 (m, 1H, C₁₀H₇, 8'), 7.52 (m, 1H, C₁₀H₇, 5'), 7.41 (m, 2H, C₁₀H₇, 2' and 4'), 7.29 (m, 1H, C₁₀H₇, 7'), 7.19 (m, 1H, C₁₀H₇, 6'), 7.11 (m, 1H, C₁₀H₇, 3'), 3.25 (bs, 2H, CH₂, *i*Bu), 3.00 (m, 2H, CH₂, *i*Bu), 2.00 (m, 2H, CH, *i*Bu), 1.67 (s, 18H, *t*Bu), 1.03 (d, 6H, CH₃, *i*Bu), 0.91 (d, 6H, CH₃, *i*Bu). ¹³C

(100.62 MHz, C₆D₆, 300 K): $\delta(\text{ppm}) = [155.0, 144.4, 134.3, 131.3, 128.1, 127.1, 126.5, 126.4, 125.7, 125.0]$ (C₁₀H₇), 56.0 (CH₂, TMEDA), 35.8 (CH₃, TMEDA), 26.6 (*t*Bu), 21.8 (CH₂, *i*Bu), 21.1 (CH, *i*Bu), 20.8 (CH₃, *i*Bu). ⁷Li (155.50 MHz, C₆D₆, 300 K): $\delta(\text{ppm}) = 0.85$.

13.5.7 Synthesis of {(TMEDA)Li[NCC(Me)₂Zn(*t*Bu)₂]}₂ 42

A Schlenk tube with a magnetic stirrer bar was flushed with argon three times (10 minute evacuations). To this was added 0.40 g (0.5 mmol) of **38** and 10 ml hexane producing a white suspension. 0.05 ml (0.5 mmol) (*i*Pr)CN was then introduced giving a clear colourless solution over 2 hours. The solvent level was reduced *in vacuo* and the Schlenk left to stand at -30°C. A small crop of clear colourless crystals was produced (0.03g, 8%). ¹H NMR (400.1MHz, C₆D₆, 300K): $\delta(\text{ppm}) = 1.96$ (bs, 12H, CH₃, TMEDA), 1.81 (bs, 4H, CH₂, TMEDA), 1.54 (s, 6H, CH₃, Me₂CCN), 1.36 (s, 18H, *t*Bu).

13.5.8 Synthesis of (TMEDA)Zn(*t*Bu)OC(=CH₂)Mes 43

A Schlenk tube with a magnetic stirrer bar was flushed with argon three times (10 minute evacuations). The addition of 0.40 g (0.5 mmol) of **38** and 10 ml hexane produced a white suspension. 0.09 ml (0.5 mmol) 2,4,6-trimethylacetophenone was introduced instantly giving a pale yellow solution which was allowed to stir for 2 hours. The solvent level was reduced by half *in vacuo* and the solution left overnight to crystallise. Small yellow green crystals were produced in a yield of 45% (0.09 g). ¹H (400.13 MHz, C₆D₆, 300 K): $\delta(\text{ppm}) = 6.93$ (s, 4H, CH, Mes), 4.31 (s, 1H, CH₂, (CH₂=)CO), 4.01 (s, 1H, CH₂, (CH₂=)CO), 2.73 (s, 6H, CH₃, Mes), 2.24 (s, 3H, CH₃, Mes), 1.46 (s, 18H, *t*Bu). ¹³C (100.62 MHz, C₆D₆, 300 K): $\delta(\text{ppm}) = 167.4$ (CO), [143.8, 134.9, 134.4, 128.0] (Ar, Mes), 82.0 (CH₂, (CH₂=)CO), 56.9 (CH₂, TMEDA), 47.0 (CH₃, TMEDA), 34.8 (*t*Bu), 21.2 (CH₃, Mes), 20.8 (CH₃, Mes).

13.6 Synthesis for chapter 11

13.6.1 Synthesis of $[\text{Na}(\text{OEt}_2)]_4\text{Cr}_2\text{Me}_8$ **44**

A slurry of 0.98 g of CrCl_2 (8 mmol) in 80 ml of ether was cooled below -30°C , and the dropwise addition of MeLi (20 ml, 32 mmol of a 1.6 M solution in ether) produced a yellow suspension. This mixture was stirred for 5 h while slowly warming to 0°C . The precipitated LiCl was then removed by filtration and washed with 10 mL of ether while maintaining the temperature of the filtrate at 0°C . Upon the addition of 1.54 g (16 mmol) of NaOtBu , a green solution was obtained. This solution was stirred for 1 h at 0°C before being concentrated *in vacuo* and stored overnight at -27°C . A crop of emerald-green crystals of **44** could then be isolated in 51% yield (1.25 g).

13.6.2 Synthesis of $[(\text{TMEDA})\text{Na}]_3\text{Cr}_2\text{Me}_7$ **45**

0.31 g (0.5 mmol) $[(\text{Et}_2\text{O})\text{Na}]\text{Cr}_2\text{Me}_8$ was dissolved in 20 ml diethyl ether and the green solution was cooled to -30°C . The subsequent addition of 0.30 ml (2 mmol) of TMEDA produced a red brown solution which was stirred for 1 h. After concentration *in vacuo* the solution was stored at -70°C giving intensely dark red crystals in a 48 % (0.15 g) yield. ^1H NMR (400.13 MHz, C_6D_6 , 300 K): $\delta(\text{ppm}) = 2.19$ (bs, 62-X H, CH_3 , TMEDA), 2.00 (bs, X H, CH_3 , TMEDA), -0.24 (bs, 21 H, CH_3 , Me). $^{13}\text{C}\{^1\text{H}\}$ NMR (100.62 MHz, C_6D_6 , 300 K): $\delta(\text{ppm}) = 57.35$ (CH_2 , TMEDA), 46.23 (CH_3 , TMEDA).

13.6.3 Synthesis of $[(\text{TMEDA})\text{Na}]_3\text{Cr}_2\text{Me}_7$ **46**

Following the procedure used to prepare **44**, 0.31 g (0.5 mmol) $[(\text{Et}_2\text{O})\text{Na}]\text{Cr}_2\text{Me}_8$ was dissolved in 20 ml of diethyl ether and the solution was cooled to -30°C . The addition of 0.38 ml (2 mmol) TMCDA produced a red brown solution which was stirred for 1 h. After concentration *in vacuo* the solution was stored at -30°C giving yellow green crystals in a 38% (0.15 g) yield. ^1H NMR (400.13 MHz, C_6D_6 , 300 K): $\delta(\text{ppm}) = 2.29$ (bs, 12H, NMe_2 , TMCDA), 2.12 (bs, 2H, Me_2NCH , TMCDA), 1.51 (bm, 4H, CHCH_2 , TMCDA), 0.80 (bs, 4H, CHCH_2CH_2 , TMCDA). $^{13}\text{C}\{^1\text{H}\}$ NMR (100.62 MHz, C_6D_6 , 300 K): $\delta(\text{ppm}) = 63.7$ (NMe_2 , TMCDA), 40.8 (CH , TMCDA), 25.4 (CHCH_2 , TMCDA), 22.5 (CHCH_2CH_2 , TMCDA).

13.6.4 Synthesis of [(TMEDA)Na]₄Mo₂Me₈ 47

0.43 g (1 mmol) of [Mo(O₂CCH₃)₂]₂ was suspended in 30 ml of diethyl ether and the mixture was cooled to 0°C. A purple colour became apparent on the dropwise introduction of MeLi [5 mL of a 1.6 M solution in diethyl ether (8 mmol)]. The resulting suspension was stirred for 18 h whilst maintaining the temperature at 0°C before the solids were removed by filtration and washed with a further 10 ml of diethyl ether. The purple solution was then re-cooled to 0°C at which point 0.38 g (4 mmol) of NaO*t*Bu and 0.60 ml TMEDA were added. The resulting solution was stirred for 1 h, concentrated *in vacuo* and stored at -30°C overnight yielding a crop of red crystals (0.30 g, 35 % yield). ¹H NMR (400.13 MHz, THF-D₈, 300 K): δ(ppm) = 2.31 (s, 4 H, CH₂, TMEDA), 2.16 (s, 12 H, CH₃, TMEDA), -1.11 (s, 6H, CH₃, Me). ¹³C{¹H} NMR (100.62 MHz, THF-D₈, 300 K): δ(ppm) = 58.91 (CH₂, TMEDA), 46.25 (CH₃, TMEDA), 2.98 (CH₃, Me). ¹H NMR (400.13 MHz, C₆D₆, 300 K): δ(ppm) = 2.23 (s, 34 H, TMEDA), -0.40 (s, 6 H, CH₃, Me). ¹³C{¹H} NMR (100.62 MHz, C₆D₆, 300 K): δ(ppm) = 58.10 (CH₂, TMEDA), 46.29 (CH₃, TMEDA), 4.32 (CH₃, Me).

13.7 Synthesis for chapter 12

13.7.1 Synthesis of (MDME)Li(TMP)Al(*i*Bu)₃ 50

To an argon filled Schlenk tube was added 10 ml hexane, 0.17 ml (1 mmol) TMP(H) and 0.63 ml (1 mmol, 1.6 M solution in hexane) *n*BuLi. The resulting yellow solution was stirred for 1 h before the addition of 1ml (1 mmol, 1.0 M solution in hexane) (*i*Bu)₃Al and 0.13 ml (1 mmol) MDME. After stirring for 15 h, the solution was concentrated *in vacuo* and left to stand at -30°C. After 24 h clear colourless crystals of (MDME)Li(TMP)Al(*i*Bu)₃ were produced in an 18% yield (0.08 g). ¹H (400.13 MHz, C₆D₆, 300 K): δ(ppm) = 2.93 (s, 3H, OCH₃, MDME), 2.64 (s, 2H, OCH₂, MDME), 2.43 (m, 3H, CH, *i*Bu), 1.76 (t, ³J_{H-H} = 5.18 Hz, 2H, NCH₂, MDME), 1.70 (s, 6H, NCH₃, MDME), 1.50 (bs, 12H, CH₃, TMP), 1.46 (d, ³J_{H-H} = 6.50 Hz, 3H, CH₃, *i*Bu), 1.42 (d, ³J_{H-H} = 6.50 Hz, 15H, CH₃, *i*Bu), 1.40 (m, 2H, CH₂, TMP), 0.27 (d, ³J_{H-H} = 6.50 Hz, 6H, CH₂, *i*Bu). ¹³C (100.62 MHz, C₆D₆, 300 K): δ(ppm) = 68.2 (OCH₂, MDME), 59.4

(OCH₃, MDME), 57.8 (NCH₂, MDME), 52.8 (α -CMe₂, TMP), 45.1 (NCH₃, MDME), 45.0 (β -CH₂, TMP), 29.9 (CH₂, *i*Bu), 29.7 (CH₃, *i*Bu), 29.4 (Me, TMP), 28.6 (Me, TMP), 27.8 (CH₂, TMP), 27.7 (CH, *i*Bu), 18.8 (γ -CH₂, TMP). ⁷Li (155.50 MHz, C₆D₆, 300 K): δ (ppm) = - 0.34.

13.7.2 Synthesis of (THFFA)Li(TMP)Al(*i*Bu)₃ 51

To an argon filled Schlenk tube was added 10 ml hexane, 0.17 ml (1 mmol) TMP(H) and 0.63 ml (1 mmol, 1.6 M solution in hexane) *n*BuLi. The resulting yellow solution was stirred for 1 h before the addition of 1ml (1 mmol, 1.0 M solution in hexane) (*i*Bu)₃Al and 0.14 ml (1 mmol) THFFA. After stirring for 15 h, the solution was concentrated *in vacuo* and left to stand at -30°C. After 24 h clear colourless crystals of (THFFA)Li(TMP)Al(*i*Bu)₃ were produced in a 61% yield (0.29 g). ¹H (400.13 MHz, THF-D₈, 300 K): δ (ppm) = 3.90 (m, 1H, α -CH, THFFA), 3.78 (m, 1H, α -CH₂, THFFA), 3.64 (m, 1H, α -CH₂, THFFA), 2.30 (m, 2H, CH₂NMe₂, THFFA), 2.20 (s, 6H, NCH₃, THFFA), 1.93 (m, 1H, OCHCH₂, THFFA), 1.89 (m, 3H, CH, *i*Bu), 1.81 (m, 2H, OCH₂CH₂, THFFA), 1.54 (m, 1H, OCHCH₂, THFFA), 1.52 (m, 2H, γ -CH₂, TMP), 1.22 (s, 12H, CH₃, TMP), 1.22 (m, 4H, β -CH₂, TMP), 0.89 (d, ³J_{H-H} = 6.4 Hz, 3H, CH₃, *i*Bu), 0.84 (d, ³J_{H-H} = 6.4 Hz, 15H, CH₃, *i*Bu), -0.20 (d, ³J_{H-H} = 6.3 Hz, 5H, CH₂, *i*Bu), -0.34 (m, 1H, CH₂, *i*Bu). ¹³C (100.62 MHz, THF-D₈, 300 K): δ (ppm) = 78.7 (OCH, THFFA), 68.4 (OCH₂, THFFA), 64.8 (CH₂NMe₂, THFFA), 52.5 (CMe₂, TMP), 46.5 (NMe₂, THFFA), 45.3 (β -CH₂, TMP), 34.6 (Me, TMP), 30.8 (OCHCH₂, THFFA), 30.2 (CH₃, *i*Bu), 28.7 (CH, *i*Bu), 30.0 (CH₂, *i*Bu), 26.2 (OCH₂CH₂, THFFA), 20.2 (γ -CH₂, TMP). ⁷Li (155.50 MHz, THF-D₈, 300 K): δ (ppm) = - 0.43.

13.7.3 Synthesis of (DME)Li(TMP)Al(*i*Bu)₃ 52

To an argon filled Schlenk tube was added 10 ml hexane, 0.34 ml (2 mmol) TMP(H) and 1.25 ml (2 mmol, 1.6 M solution in hexane) *n*BuLi. The resulting yellow solution was stirred for 1 h before the addition of 2 ml (2 mmol, 1.0 M solution in hexane) (*i*Bu)₃Al and 0.21 ml (2 mmol) DME. After stirring for 15 h, the solution was concentrated *in vacuo* and left to stand at 0°C. After 24 h clear colourless crystals of (DME)Li(TMP)Al(*i*Bu)₃ were produced. ¹H (400.13 MHz, C₆D₆, 300 K): δ (ppm) = 2.86

(s, 6H, CH₃, DME), 2.68 (s, 4H, CH₂, DME), 2.40 (m, 3H, CH, *i*Bu), 1.52 (bs, 12H, CH₃, TMP), 1.40 (d, ³J_{H-H} = 6.6 Hz, 18H, CH₃, *i*Bu), 0.29 (d, ³J_{H-H} = 6.1 Hz, 5H, CH₂, *i*Bu), 0.21 (m, 5H, CH₂, *i*Bu). ¹³C (100.62 MHz, C₆D₆, 300 K): δ(ppm) = 69.7 (CH₂, DME), 59.0 (CH₃, DME), 52.8 (CMe₂, TMP), 44.8 (β-CH₂, TMP), 29.7 (CH₃, TMP), 27.8 (CH, *i*Bu), 27.8 (CH₃, *i*Bu), 18.9 (γ-CH₂, TMP).

13.7.4 Synthesis of (MDME*)Li(TMP)Al(*i*Bu)₂ 53

A Schlenk tube was charged with 0.15 g (1 mmol) LiTMP and 0.28 g (1 mmol) of (TMP)Al(*i*Bu)₂. 20 ml hexane were added to produce a pale yellow solution. After the addition of 0.13 ml (1 mmol) MDME the solution was stirred for 15 h. Concentration of the solution *in vacuo* and storage at -30°C resulted in the growth of colourless crystals of (MDME*)Li(TMP)Al(*i*Bu)₂ in a 15% (0.06 g) yield. ¹H (400.13 MHz, THF-D₈, 300 K): δ(ppm) = 3.57 (m, 2H, AlCH₂OCH₂, MDME*), 3.20 (s, 2H, AlCH₂, MDME*), 2.46 (m, 2H, Me₂NCH₂, MDME*), 2.26 (s, 6H, Me₂N, MDME*), 1.86 (m, 2H, CH, *i*Bu), 1.59 (m, 2H, γ-CH₂, TMP), 1.25 (s, 12H, CH₃, TMP), 1.25 (m, 4H, β-CH₂, TMP), 0.90 (d, ³J_{H-H} = 6.4 Hz, 6H, CH₃, *i*Bu), 0.88 (d, ³J_{H-H} = 6.4 Hz, 6H, CH₃, *i*Bu), -0.12 (m, 4H, CH₂, *i*Bu). ¹³C (100.62 MHz, THF-D₈, 300 K): δ(ppm) = 78.0 (AlCH₂, MDME*), 71.7 (AlCH₂OCH₂, MDME*), 60.0 (Me₂NCH₂, MDME*), 52.6 (CMe₂, TMP), 45.5 (Me₂N, MDME*), 45.0 (β-CH₂, TMP), 33.9 (Me, TMP), 30.8 (CH₂, *i*Bu), 30.0 (CH₃, *i*Bu), 29.2 (CH₃, *i*Bu), 28.3 (CH, *i*Bu), 19.6 (γ-CH₂, TMP). ⁷Li (155.50 MHz, THF-D₈, 300 K): δ(ppm) = 0.19.

13.7.5 Synthesis of (THFFA*)Li(TMP)Al(*i*Bu)₂ 54

A Schlenk tube was charged with 0.30 g (2 mmol) LiTMP and 0.56 g (2 mmol) of (TMP)Al(*i*Bu)₂. 20 ml of hexane were added to produce a pale yellow solution. After the addition of 0.28 ml (2 mmol) THFFA the solution was stirred for 15 h. Concentration of the solution *in vacuo* and storage at -30°C resulted in the growth of colourless crystals of (THFFA*)Li(TMP)Al(*i*Bu)₂ in a 29% (0.24 g) yield. ¹H (400.13 MHz, THF-D₈, 300 K): δ(ppm) = Diastereomer A/Diastereomer B 2:1; Diastereomer A [3.94 (m, 1H, CHCH₂N, THFFA*), 3.26 (dd, ³J_{H-H} = 13.0 Hz, ³J_{H-H} = 5.9 Hz, 1H, AlCH, THFFA*), 2.33 (m, 1H, CH₂NMe₂, THFFA*), 2.24 (s, 6H, CH₃, THFFA*), 2.06 (m, 1H, CH₂NMe₂, THFFA*),

1.92 (m, 1H, AlCHCH₂, THFFA*), 1.90 (m, 2H, CH₂CH, *i*Bu), 1.79 (m, 1H, AlCHCH₂CH₂, THFFA*), 1.64 (m, 1H, γ-CH₂, TMP), 1.51 (m, 1H, AlCHCH₂CH₂, THFFA*), 1.30 (s, 6H, CH₃, TMP), 1.27 (m, 1H, AlCHCH₂, THFFA*), 1.25 (s, 6H, CH₃, TMP), 1.23 (m, 1H, γ-CH₂, TMP), 0.92 (m, 12H, CH₂, *i*Bu), -0.08 (d, ³J_{H-H} = 6.3, 3H, CH₂, *i*Bu), -0.17 (d, ³J_{H-H} = 6.5 Hz, 1H, CH₂, *i*Bu)], Diastereomer B [3.98 (m, 1H, CHCH₂N, THFFA*), 3.37 (dd, ³J_{H-H} = 12.6 Hz, ³J_{H-H} = 5.8 Hz, 1H, AlCH, THFFA*), 2.43 (m, 1H, CH₂NMe₂, THFFA*), 2.23 (s, 6H, CH₃, THFFA*), 2.17 (m, 1H, CH₂NMe₂, THFFA*), 2.05 (m, 1H, AlCHCH₂, THFFA*), 1.95 (m, 1H, AlCHCH₂CH₂, THFFA*), 1.85 (m, 2H, CH₂CH, *i*Bu), 1.58 (m, 1H, γ-CH₂, TMP), 1.29 (m, 1H, AlCHCH₂, THFFA*), 1.28 (m, 1H, AlCHCH₂CH₂, THFFA*), 1.27 (m, 1H, γ-CH₂, TMP), 1.24 (s, 6H, CH₃, TMP), 1.22 (s, 6H, CH₃, TMP), 0.89 (m, 12H, CH₂, *i*Bu), 0.00 (m, 4 H, CH₂, *i*Bu)]. ¹³C (100.62 MHz, THF-D₈, 300 K): δ(ppm) = Diastereomer A [84.3 (AlCH, THFFA*), 76.1 (CHCH₂NMe₂, THFFA*), 66.7 (CHCH₂NMe₂, THFFA*), 52.7 (CMe₂, TMP), 46.3 (CH₃, THFFA*), 44.6 (AlCHCH₂, THFFA*), 33.7 (CH₃, TMP), 32.8 (AlCHCH₂CH₂, THFFA*), 28.1 (CH, *i*Bu), 28.0 (CH, *i*Bu), 19.2 (γ-CH₂, TMP). Diastereomer B: [84.5 (AlCH, THFFA*), 76.5 (CHCH₂NMe₂, THFFA*), 65.8 (CHCH₂NMe₂, THFFA*), 52.5 (CMe₂, TMP), 46.1 (CH₃, THFFA*), 44.2 (AlCHCH₂, THFFA*), 34.6 (CH₃, TMP), 34.4 (CH₃, TMP), 33.0 (AlCHCH₂, THFFA*), 28.3 (CH, *i*Bu), 28.2 (CH, *i*Bu), 19.6 (γ-CH₂, TMP). Diastereomer A/B 30.4 (CH₂, *i*Bu), 29.9 (CH₂, *i*Bu), 29.0 (CH₂, *i*Bu), 28.7 (CH₂, *i*Bu) [31.2, 30.1, 29.7, 29.4]. ⁷Li (155.50 MHz, THF-D₈, 300 K): δ(ppm) = 0.33.

13.7.6 Synthesis of (DME)[(DME*)Li(TMP)Al(*i*Bu)₂]₂ 56

A Schlenk tube was charged with 0.30 g (2 mmol) LiTMP and 0.56 g (2 mmol) of (TMP)Al(*i*Bu)₂. 20 ml hexane were added to produce a pale yellow solution. After the addition of 0.21 ml (2 mmol) DME the solution was stirred for 15 h. Concentration of the solution *in vacuo* and storage at -30°C resulted in the growth of colourless crystals of (DME)[(DME*)Li(TMP)Al(*i*Bu)₂]₂ in a 64% (0.45 g) yield. (400.13 MHz, C₆D₆, 300 K): δ(ppm) = 3.36 (s, 2H, AlCH₂, DME*), 3.06 (s, 2H, CH₂, DME), 3.01 (s, 3H, CH₃, DME), 2.96 (m, 2H, CH₂, DME*), 2.62 (m, 2H, CH₂, DME*), 2.57 (s, 3H, CH₃, DME*), 2.34

(m, 2H, CH, *i*Bu), 1.56 (m, 2H, γ -CH₂, TMP), 1.42 (s, 12H, CH₃, TMP), 1.41 (d, 6H, CH₃, *i*Bu), 1.34 (d, 6H, CH₃, *i*Bu), 1.09 (m, 4H, β -CH₂, TMP), 0.65 (m, 2H, CH₂, *i*Bu), 0.46 (m, 2H, CH₂, *i*Bu). ⁷Li (155.50 MHz, THF-D₈, 300 K): δ (ppm) = 0.77.

13.7.7 Synthesis of (TMDAE*)Li(TMP)Al(*i*Bu)₂ 57

A Schlenk tube was charged with 0.30 g (2 mmol) LiTMP and 0.56 g (2 mmol) of (TMP)Al(*i*Bu)₂. 20 ml hexane were added to produce a pale yellow solution. After the addition of 0.38 ml (2 mmol) TMDAE a white precipitate was formed. The precipitate dissolved on gentle heating and colourless crystals of (TMDAE*)Li(TMP)Al(*i*Bu)₂ were grown upon standing the Schlenk in a Dewar of hot water overnight in a 42% (0.38 g) yield. ¹H (400.13 MHz, C₆D₆, 300 K): δ (ppm) = 4.48 (m, 1H, OCH₂, TMDAE*), 3.50 (d, J = 11.1 Hz, OCHCH₂, TMDAE*), 3.28 (m, 1H, OCH, TMDAE*), 3.15 (m, 1H, OCH₂, TMDAE*), 2.66 (d, ³J_{H-H} = 14.4 Hz, 1H, OCHCH₂, TMDAE*), 2.35 (m, 2H, CH, *i*Bu), 2.25 (s, 6H, CH₃, TMDAE*), 2.02 (m, 1H, OCH₂CH₂, TMDAE*), 1.84 (m, 1H, γ -CH₂, TMP), 1.60 (s, 6H, CH₃, TMDAE*) 1.55 (m, 1H, OCH₂CH₂, TMDAE*), 1.51 (bs, 12H, CH₃, TMP), 1.36-1.46 (m, 12H, CH₃, *i*Bu), 1.34 (m, 1H, γ -CH₂, TMP), 0.48-0.54 (m, 4H, CH₂, *i*Bu). ¹³C (100.62 MHz, C₆D₆, 300 K): δ (ppm) = 82.0 (OCH, TMDAE), 69.7 (OCH₂, TMDAE*), 68.2 (OCHCH₂, TMDAE*), 60.1 (OCH₂CH₂, TMDAE*), 46.12 (CH₃, TMDAE*), 45.4 (CH₃, TMDAE*), 43.2 (CH₃, TMDAE*), 35.7 (CH₃, TMP), 30.2 (CH₃, *i*Bu), 29.6 (CH₃, *i*Bu), 29.4 (CH₃, *i*Bu), 29.0 (bs, CH₂, *i*Bu), 28.6 (CH₃, *i*Bu), 27.8 (CH, *i*Bu), 27.6 (CH, *i*Bu), 18.3 (γ -CH₂, TMP). ⁷Li (155.50 MHz, C₆D₆, 300 K): δ (ppm) = 1.34.

14 References

- [1] W. Schlenk, J. Holtz, *Ber. Dtsch. Chem. Ges.* **1917**, *50*, 262-274.
- [2] D. B. Collum, *Acc. Chem. Res.* **1993**, *26*, 227-234.
- [3] a) M. Schlosser, Second Edition ed., John Wiley & Sons, LTD, **2004**; b) H. Yamamoto, K. Oshima, *Vol. 1*, Wiley-VCH, **2004**.
- [4] a) J. F. Garst, *Acc. Chem. Res.* **1971**, *4*, 400; b) J. F. Garst, F. E. Barton, *J. Am. Chem. Soc.* **1974**, *96*, 523; c) T. Cohen, J. P. Sherbine, J. R. Matz, R. R. Hutchins, B. M. McHenry, P. R. Willey, *J. Am. Chem. Soc.* **1984**, *106*, 3245; d) P. K. Freman, L. L. Hutchinson, *J. Org. Chem.* **1980**, *45*, 1924.
- [5] M. Yus, *Chem. Soc. Rev.* **1996**, 155.
- [6] F. G. Bordwell, *Acc. Chem. Res.* **1988**, *21*, 456-463.
- [7] R. W. Taft, F. G. Bordwell, *Acc. Chem. Res.* **1988**, *21*, 463-469.
- [8] M. B. Smith, J. March, Sixth edition ed., John Wiley & Sons, Hoboken, **2007**.
- [9] K. Shen, Y. Fu, J.-N. Li, L. Liu, Q.-X. Guo, *Tetrahedron* **2007**, *63*, 1568-1576.
- [10] M. C. Whisler, S. MacNeil, V. Snieckus, P. Beak, *Angew. Chem. Int. Ed.* **2004**, *43*, 2206-2225.
- [11] A. Carpita, R. Rossi, C. A. Veracini, *Tetrahedron* **1985**, *41*, 1919.
- [12] Y. S. Park, G. A. Weisenburger, P. Beak, *J. Am. Chem. Soc.* **1997**, *119*, 10537.
- [13] D. J. Gallagher, P. Beak, *J. Org. Chem.* **1995**, *60*, 7092.
- [14] J. Clayden, in *Tetrahedron Organic Chemistry Series, Vol. 23*, first edition ed. (Eds.: J. E. Baldwin, R. M. Williams), Pergamon, **2002**.
- [15] N. S. Narasimhan, R. S. Mali, *Synthesis* **1983**, 957.
- [16] a) D. Seyferth, R. L. Lambert, *J. Organomet. Chem.* **1973**, *54*, 123; b) D. Seebach, R. Hässig, J. Gabriel, *Helv. Chim. Acta* **1983**, *66*, 308; c) M. D. Rausch, F. E. Tibbetts, H. B. Gorden, *J. Organomet. Chem.* **1966**, *67*, 321; d) N. J. Foulger, B. J. Wakefield, *J. Organomet. Chem.* **1974**, *69*, 321; e) E. T. McBee, R. A. Sanford, *J. Am. Chem. Soc.* **1950**, *72*, 5574.
- [17] a) H. J. Reich, I. L. Reich, N. H. Phillips, *J. Am. Chem. Soc.* **1985**, *107*, 4101; b) H. J. Reich, N. H. Phillips, *J. Am. Chem. Soc.* **1986**, *108*, 2102; c) G. Wittig, U. Schollkopf, *Tetrahedron* **1958**, *3*, 91.
- [18] H. J. Reich, D. Patrick Green, N. H. Phillips, *J. Am. Chem. Soc.* **1989**, *111*, 3444-3445.
- [19] W. B. Farnham, J. C. Calabrese, *J. Am. Chem. Soc.* **1986**, *108*, 2451-2453.
- [20] a) A. Varvoglis, *Tetrahedron* **1997**, *53*, 1179-1255; b) J. P. Brand, D. F. Gonzalez, S. Nicolai, J. Waser, *Chem. Commun.* **2011**, *47*, 102-115; c) K. Niedermann, N. Früh, E. Vinogradova, M. S. Wiehn, A. Moreno, A. Togni, *Angew. Chem. Int. Ed.* **2011**, *50*; d) M. Uyanik, T. Yasui, K. Ishhara, *Angew. Chem. Int. Ed.* **2010**, *49*, 2175-2177; e) R. Koller, K. Stanek, D. Stolz, R. Aardoom, K. Niedermann, A. Togni, *Angew. Chem. Int. Ed.* **2009**, *48*, 4332-4336.
- [21] L. Pauling, Cornell University Press, Ithaca N. Y., **1960**.

- [22] a) R. E. Mulvey, *Acc. Chem. Res.* **2008**, *42*, 743-755; b) R. E. Mulvey, *Organometallics* **2006**, *25*, 1060-1075; c) R. E. Mulvey, F. Mongin, M. Uchiyama, Y. Kondo, *Angew. Chem. Int. Ed.* **2007**, *46*, 3802.
- [23] Y. Kondo, M. Shilai, M. Uchiyama, T. Sakamoto, *J. Am. Chem. Soc.* **1999**, *121*, 3539-3540.
- [24] W. Clegg, S. H. Dale, E. Hevia, G. W. Honeyman, R. E. Mulvey, *Angew. Chem. Int. Ed.* **2006**, *45*, 2370.
- [25] P. C. Andrikopoulos, D. R. Armstrong, H. R. L. Barley, W. Clegg, S. H. Dale, E. Hevia, G. W. Honeyman, A. R. Kennedy, R. E. Mulvey, *J. Am. Chem. Soc.* **2005**, *127*, 6184.
- [26] W. Clegg, S. H. Dale, A. M. Drummond, E. Hevia, G. W. Honeyman, R. E. Mulvey, *J. Am. Chem. Soc.* **2006**, *128*, 7434-7435.
- [27] E. Hevia, A. R. Kennedy, J. Klett, M. D. McCall, *Chem. Commun.* **2009**, 3240.
- [28] W. Clegg, S. H. Dale, R. W. Harrington, E. Hevia, G. W. Honeyman, R. E. Mulvey, *Angew. Chem. Int. Ed.* **2006**, *45*, 2374-2377.
- [29] D. R. Armstrong, W. Clegg, S. H. Dale, E. Hevia, L. M. Hogg, G. W. Honeyman, R. E. Mulvey, *Angew. Chem. Int. Ed.* **2006**, *45*, 3775-3778.
- [30] *Unpublished results.*
- [31] D. R. Armstrong, J. Garcia-Alvarez, D. V. Graham, G. W. Honeyman, E. Hevia, A. R. Kennedy, R. E. Mulvey, *Chem. Eur. J.* **2009**, *2009*, 3800-3807.
- [32] W. Clegg, S. H. Dale, A. M. Drummond, E. Hevia, *J. Am. Chem. Soc.* **2006**, *128*, 7434.
- [33] L. Balloch, A. R. Kennedy, R. E. Mulvey, T. Rantanen, S. D. Robertson, V. Snieckus, *Organometallics* **2011**, *30*, 145.
- [34] N. Daisuke, M. Uchiyama, *J. Org. Chem.* **2008**, *73*, 1117-1120.
- [35] D. R. Armstrong, C. Dougan, D. V. Graham, E. Hevia, A. R. Kennedy, *Organometallics* **2008**, *27*, 6063-6070.
- [36] W. Clegg, B. Conway, E. Hevia, M. D. McCall, L. Russo, R. E. Mulvey, *J. Am. Chem. Soc.* **2009**, *131*, 2375-2384.
- [37] W. Clegg, S. H. Dale, E. Hevia, L. M. Hogg, G. W. Honeyman, R. E. Mulvey, C. T. O'Hara, L. Russo, *Angew. Chem. Int. Ed.* **2008**, *47*, 731-734.
- [38] D. R. Armstrong, L. Balloch, E. Hevia, A. R. Kennedy, R. E. Mulvey, C. T. O'Hara, S. D. Robertson, *Beilstein J. Org. Chem.* **2011**, *7*, 1234-1248.
- [39] D. R. Armstrong, V. L. Blair, W. Clegg, S. H. Dale, J. Garcia-Alvarez, G. W. Honeyman, E. Hevia, R. E. Mulvey, L. Russo, *J. Am. Chem. Soc.* **2010**, *132*, 9480-9487.
- [40] L. Balloch, A. R. Kennedy, J. Klett, R. E. Mulvey, C. T. O'Hara, *Chem. Commun.* **2010**, *46*, 2319-2321.
- [41] U. Azzena, L. Pilo, A. Sechi, *Tetrahedron* **1998**, *54*, 12389.
- [42] E. Hevia, A. R. Kennedy, J. Klett, M. D. McCall, *Chem. Commun.* **2009**, 3240-3242.
- [43] T. H. Chan, D. Wang, *Chem. Rev.* **1995**, *95*, 1279.
- [44] T. F. Bates, S. A. Dandekar, J. L. Longlet, K. A. Wood, R. D. Thomas, *J. Organomet. Chem.* **2000**, *595*, 87.
- [45] a) J. Clayden, S. A. Yasin, *N. J. Chem.* **2002**, *26*, 191; b) A. Maercker, *Angew. Chem. Int. Ed. Engl.* **1987**, *26*, 972.

- [46] R. B. Bates, L. M. Kroposki, D. E. Potter, *J. Org. Chem.* **1972**, *37*, 560.
- [47] A. R. Kennedy, J. Klett, R. E. Mulvey, D. S. Wright, *Science* **2009**, *326*, 706.
- [48] E. Crosbie, P. Garcia-Alvarez, A. R. Kennedy, J. Klett, R. E. Mulvey, S. D. Robertson, *Angew. Chem. Int. Ed.* **2010**, *49*, 9388-9391.
- [49] a) X. He, B. C. Noll, A. Beatty, R. E. Mulvey, K. W. Henderson, *J. Am. Chem. Soc.* **2004**, *126*, 7444; b) A. R. Kennedy, J. Klett, R. E. Mulvey, S. Newton, D. S. Wright, *Chem. Commun.* **2008**, 308; c) D. R. Armstrong, W. Clegg, S. H. Dale, J. Garcia-Alvarez, R. W. Harrington, E. Hevia, G. W. Honeyman, A. R. Kennedy, R. E. Mulvey, C. T. O'Hara, *Chem. Commun.* **2008**, 187; d) E. Hevia, G. W. Honeyman, A. R. Kennedy, R. E. Mulvey, D. C. Sherrington, *Angew. Chem. Int. Ed.* **2005**, *44*, 68; e) D. V. Graham, E. Hevia, A. R. Kennedy, R. E. Mulvey, *Organometallics* **2006**, *25*, 3297; f) G. W. Honeyman, A. R. Kennedy, R. E. Mulvey, D. C. Sherrington, *Organometallics* **2004**, *23*, 1197; g) J. J. Morris, B. C. Noll, G. W. Honeyman, C. T. O'Hara, A. R. Kennedy, R. E. Mulvey, K. W. Henderson, *Chem. Eur. J.* **2007**, *13*, 4418; h) G. C. Forbes, A. R. Kennedy, R. E. Mulvey, B. A. Roberts, R. B. Rowlings, *Organometallics* **2002**, *21*, 5115; i) A. R. Kennedy, R. E. Mulvey, R. B. Rowlings, *J. Am. Chem. Soc.* **1998**, *120*, 7816; j) B. Conway, P. Garcia-Alvarez, A. R. Kennedy, J. Klett, R. E. Mulvey, S. D. Robertson, *N. J. Chem.* **2010**, *34*, 1707; k) A. R. Kennedy, R. E. Mulvey, R. B. Rowlings, *J. Organomet. Chem.* **2002**, *648*, 288; l) G. C. Forbes, A. R. Kennedy, R. E. Mulvey, P. J. A. Rodger, R. B. Rowlings, *J. Chem. Soc., Dalton Trans.* **2001**, 1477; m) G. C. Forbes, A. R. Kennedy, R. E. Mulvey, P. J. A. Rodger, *Chem. Commun.* **2001**, 1400; n) P. C. Andrikopoulos, D. R. Armstrong, A. R. Kennedy, R. E. Mulvey, C. T. O'Hara, R. B. Rowlings, S. Weatherstone, *Inorg. Chim. Acta* **2007**, *360*, 1370; o) A. R. Kennedy, R. E. Mulvey, R. B. Rowlings, *Angew. Chem. Int. Ed.* **1998**, *37*, 3180; p) L. M. Carrella, C. Forster, A. R. Kennedy, J. Klett, R. E. Mulvey, E. Rentschler, *Organometallics* **2010**, *29*, 4756; q) W. Clegg, G. C. Forbes, A. R. Kennedy, R. E. Mulvey, S. T. Liddle, *Chem. Commun.* **2003**, 406; r) L. Barr, A. R. Kennedy, J. G. MacLellan, J. H. Moir, R. E. Mulvey, P. J. A. Rodger, *Chem. Commun.* **2000**, 1757; s) G. C. Forbes, A. R. Kennedy, R. E. Mulvey, R. B. Rowlings, W. Clegg, S. T. Liddle, C. C. Wilson, *Chem. Commun.* **2000**, 1759.
- [50] a) W. Clegg, K. W. Henderson, A. R. Kennedy, R. E. Mulvey, C. T. O'Hara, R. B. Rowlings, D. M. Tooke, *Angew. Chem. Int. Ed.* **2001**, *40*, 3902; b) D. J. Gallagher, K. W. Henderson, A. R. Kennedy, C. T. O'Hara, R. E. Mulvey, R. B. Rowlings, *Chem. Commun.* **2002**, 376; c) P. C. Andrikopoulos, D. R. Armstrong, W. Clegg, C. J. Gilfillan, E. Hevia, A. R. Kennedy, R. E. Mulvey, C. T. O'Hara, J. A. Parkinson, D. M. Tooke, *J. Am. Chem. Soc.* **2004**, *126*, 11612; d) D. V. Graham, A. R. Kennedy, R. E. Mulvey, C. T. O'Hara, *Acta Crystallogr., Sect. C: Cryst. Struct. Commun.* **2006**, *62*, m366; e) J. Garcia-Alvarez, D. V. Graham, E. Hevia, A. R. Kennedy, R. E. Mulvey, *Dalton Trans.* **2008**, 1481; f) P. C. Andrikopoulos, D. R. Armstrong, A. R. Kennedy, R. E. Mulvey, C. T. O'Hara, R. B. Rowlings, *Eur. J. Inorg. Chem.* **2003**, 3354; g) D. R. Armstrong, P. Garcia-Alvarez, A. R. Kennedy, R. E. Mulvey, J. A. Parkinson, *Angew. Chem. Int. Ed.* **2010**, *49*, 3185; h) E. Hevia, F. R. Kenley, A. R. Kennedy, R. E. Mulvey, R. B. Rowlings, *Eur. J. Inorg. Chem.* **2003**, 3347; i) D. R. Armstrong, W. Clegg,

- S. H. Dale, J. Garcia-Alvarez, R. W. Harrington, E. Hevia, G. W. Honeyman, A. R. Kennedy, R. E. Mulvey, C. T. O'Hara, *Chem. Commun.* **2008**, 187; j) W. Clegg, J. Garcia-Alvarez, P. Garcia-Alvarez, D. V. Graham, R. W. Harrington, E. Hevia, A. R. Kennedy, R. E. Mulvey, L. Russo, *Organometallics* **2008**, *27*, 2654.
- [51] M. G. Gardiner, C. L. Raston, *Inorg. Chem.* **1996**, *35*, 4047-4059.
- [52] M. Uchiyama, Y. Matsumoto, D. Nobuto, T. Furuyama, K. Yamaguchi, K. Morokuma, *J. Am. Chem. Soc.* **2006**, *128*, 8748-8750.
- [53] K. Snegaroff, S. Komagawa, M. Yonehara, F. Chevallier, P. C. Gros, M. Uchiyama, F. Mongin, *J. Org. Chem.* **2010**, *75*, 3117-3120.
- [54] H. Mimoun, J. Y. de Saint Laumer, L. Giannini, R. Scopelliti, C. Floriani, *J. Am. Chem. Soc.* **1999**, *121*, 6158.
- [55] C. E. MacBeth, P. L. Larsen, T. N. Sorrell, D. Powell, A. S. Borovik, *Inorg. Chim. Acta* **2002**, *341*, 77-84.
- [56] B. S. Hammes, D. Ramos-Maldonado, G. P. A. Yap, L. Liable-Sands, A. L. Rheingold, V. G. Young, Jr., A. S. Borovik, *Inorg. Chem.* **1997**, *36*, 3210-3211.
- [57] C. E. MacBeth, B. S. Hammes, V. G. Young, Jr., A. S. Borovik, *Inorg. Chem.* **2001**, *40*, 4733-4741.
- [58] A. M. J. Devoille, P. Richardson, N. L. Bill, J. L. Sessler, J. B. Love, *Inorg. Chem.* **2011**, *50*, 3116.
- [59] R. J. Baker, R. D. Farley, C. Jones, M. Kloth, D. M. Murphy, *Chem. Commun.* **2002**, 1196-1197.
- [60] R. J. Baker, R. D. Farley, C. Jones, D. P. Mills, M. Kloth, D. M. Murphy, *Chem. Eur. J.* **2005**, *11*, 2972-2982.
- [61] K. A. Kreisel, G. P. A. Yap, O. Dmitrenko, C. R. Landis, K. H. Theopold, *J. Am. Chem. Soc.* **2007**, *129*, 14162-14163.
- [62] P. Yang, X.-J. Yang, J. Yu, Y. Liu, C. Zhang, Y.-H. Deng, B. Wu, *Dalton Trans.* **2009**, 5773.
- [63] X.-J. Yang, J. Yu, Y. Liu, Y. Xie, H. F. Schaefer, Y. Liang, B. Wu, *Chem. Commun.* **2007**, 2363.
- [64] J. Yu, X.-J. Yang, Y. Liu, Z. Pu, Q.-S. Li, Y. Xie, H. F. Schaefer, B. Wu, *Organometallics* **2008**, *27*, 5800.
- [65] E. Rijnberg, J. Boersma, J. T. B. H. Jastrzebski, M. T. Lakin, A. L. Spek, G. v. Koten, *Organometallics* **1997**, *16*, 3158.
- [66] E. Rijnberg, J. Boersma, J. T. B. H. Jastrzebski, M. T. Lakin, A. L. Spek, G. v. Koten, *Chem. Commun.* **1995**, 1839.
- [67] E. Rijnberg, B. Richter, K.-H. Thiele, J. Boersma, N. Veldman, A. L. Spek, G. v. Koten, *Inorg. Chem.* **1998**, *37*, 56.
- [68] Y. Liu, S. Li, X.-J. Yang, P. Yang, B. Wu, *J. Am. Chem. Soc.* **2009**, *131*, 4210.
- [69] E. S. Schmidt, N. W. Mitzel, H. Schmidbaur, *Z. Naturforsch. B* **2001**, *56*, 937.
- [70] S. Aldridge, R. J. Baker, N. D. Coombs, C. Jones, R. P. Rose, A. Rossin, D. J. Willock, *Dalton Trans.* **2006**, 3313.
- [71] M. Veith, B. Schillo, V. Huch, *Angew. Chem. Int. Ed.* **1999**, *38*, 182-184.
- [72] A. D. Bolig, M. Brookhart, *J. Am. Chem. Soc.* **2007**, *129*, 14544-14545.
- [73] X. Zhang, A. Fried, S. Knapp, A. S. Goldman, *Chem. Commun.* **2003**, 2060-2061.
- [74] X.-Q. Gu, W. Chen, D. Morales-Morales, C. M. Jensen, *J. Mol. Catal. A.* **2002**, *189*, 119.

- [75] (Ed.: A. Aesar), Heysham, **2011-13**.
- [76] a) P. C. Andrews, D. R. Armstrong, D. R. Baker, R. E. Mulvey, W. Clegg, L. Horsburgh, P. A. O'Neil, D. Reed, *Organometallics* **1995**, *14*, 427; b) P. C. Andrews, P. J. Duggan, G. D. Fallon, T. D. McCarthy, A. C. Peatt, *J. Chem. Soc., Dalton Trans.* **2000**, 2505; c) P. C. Andrews, P. J. Duggan, M. Maguire, P. J. Nichols, *Chem. Commun.* **2001**, 53; d) P. C. Andrews, D. R. Armstrong, R. E. Mulvey, D. Reed, *J. Am. Chem. Soc.* **1988**, *110*, 5235; e) P. C. Andrews, R. E. Mulvey, W. Clegg, D. Reed, *J. Organomet. Chem.* **1990**, 386, 287.
- [77] a) P. J. Davidson, M. F. Lappert, R. Pearce, *Chem. Rev.* **1976**, *76*, 219; b) W. H. Glaze, J. Lin, E. G. Felton, *J. Org. Chem.* **1966**, *31*, 2643; c) K. N. Houk, N. G. Rondan, P. v. R. Schleyer, E. Kaufmann, T. Clark, *J. Am. Chem. Soc.* **1985**, *107*, 2821.
- [78] J. A. Garden, A. R. Kennedy, R. E. Mulvey, S. D. Robertson, *Dalton Trans.* **2011**, *40*, 11945-11954.
- [79] F. H. Allen, *Acta Cryst. B.* **2002**, *58*, 380.
- [80] P. Ghosh, T. Hascall, C. Dowling, G. Parkin, *J. Chem. Soc., Dalton Trans.* **1998**, 3355.
- [81] W. Marciniak, K. Merz, M. Moreno, M. Driess, *Organometallics* **2006**, *25*, 4931.
- [82] D. Ravensbaek, Y. Filinchuk, Y. Cerenius, H. J. Jakobsen, F. Besenbacher, J. Skibsted, T. R. Jensen, *Angew. Chem. Int. Ed.* **2009**, *48*, 6659.
- [83] M. Veith, P. Konig, A. Rammo, V. Huch, *Angew. Chem. Int. Ed.* **2005**, *44*, 5968.
- [84] N. S. Hosmane, Y. Wang, H. Zhang, J. A. Maguire, M. McInnis, T. G. Gray, J. D. Collins, R. K. Kremer, H. Binder, E. Waldhor, W. Kaim, *Organometallics* **1996**, *15*, 1006.
- [85] a) W. Uhl, H. R. Bock, M. Claesener, M. Layh, I. Tiesmeyer, E.-U. Wurthwein, *Chem. Eur. J.* **2008**, *14*, 11557; b) W. Uhl, M. R. Halvagar, M. Claesener, *Chem. Eur. J.* **2009**, *15*, 11298.
- [86] a) M. G. Gardiner, S. M. Lawrence, C. L. Raston, *Inorg. Chem.* **1995**, *34*, 4652; b) C. Eaborn, S. M. El-Hamruni, M. S. Hill, P. B. Hitchcock, M. Hopman, A. L. Gouic, J. D. Smith, *J. Organomet. Chem.* **2000**, 597, 3; c) G. Linti, W. Kostler, A. Rodig, *Z. Anorg. Allg. Chem.* **2002**, 628, 1319; d) W. Uhl, *Z. Anorg. Allg. Chem.* **1989**, 570, 37.
- [87] a) D. Jacoby, S. Isoz, C. Floriani, A. Chiesi-Villa, C. Rizzoli, *J. Am. Chem. Soc.* **1995**, *117*, 2805; b) N. Etkin, A. J. Hoskin, D. W. Stephan, *J. Am. Chem. Soc.* **1997**, *119*, 11420; c) A. J. Hoskin, D. W. Stephan, *Organometallics* **2000**, *19*, 2621.
- [88] a) A. Berry, M. L. H. Green, J. A. Bandy, K. Prout, *J. Chem. Soc., Dalton Trans.* **1991**, 2185; b) P. M. Morse, Q. D. Shelby, D. Y. Kim, G. S. Girolami, *Organometallics* **2008**, *27*, 984.
- [89] T. A. Bazhenova, L. M. Kachapina, A. E. Shilov, M. Y. Antipin, Y. T. Struchkov, *J. Organomet. Chem.* **1992**, 428, 107.
- [90] a) T. Dube, S. Gambarotta, G. P. A. Yap, *Organometallics* **2000**, *19*, 817; b) T. Dube, S. Gambarotta, G. P. A. Yap, *Organometallics* **2000**, *19*, 121.
- [91] F. Rioux, *J. Chem. Ed.* **1977**, *54*, 555-556.
- [92] a) R. J. Baker, C. Jones, P. C. Junk, M. Kloth, *Angew. Chem. Int. Ed.* **2004**, *43*, 3852-3855; b) J. A. R. Schmidt, J. Arnold, *Organometallics* **2002**, *21*, 3426-3433;

- c) G. T. DeLong, D. Hoffmann, H. D. Nguyen, R. D. Thomas, *J. Am. Chem. Soc.* **1997**, *119*, 11998-11999; d) A. Heine, D. Stalke, *Angew. Chem. Int. Ed.* **1992**, *31*, 854-855; e) T. M. Gilbert, R. G. Bergman, *J. Am. Chem. Soc.* **1985**, *107*, 6391-6393.
- [93] a) T. Aida, N. Kuboki, K. Kato, W. Uchikawa, C. Matsuno, S. Okamoto, *Tetrahedron Lett.* **2005**, *46*, 1667; b) H. Mimoun, J. Y. de Laumer, L. Giannini, R. Scopelliti, C. Floriani, *J. Am. Chem. Soc.* **1999**, *121*, 6158; c) M. Uchiyama, S. Furumoto, M. Saito, Y. Kondo, T. Sakamoto, *J. Am. Chem. Soc.* **1997**, *119*, 11425; d) T. Ohkuma, S. Hashiguchi, R. Noyori, *J. Org. Chem.* **1994**, *59*, 217.
- [94] Z. Zhu, R. J. Wright, M. M. Olmstead, E. Rivard, M. Brynda, P. P. Power, *Angew. Chem. Int. Ed.* **2006**, *45*, 5807-5810.
- [95] W. Marciniak, K. Merz, M. Moreno, M. Driess, *Organometallics* **2006**, *25*, 4931-4933.
- [96] A. Lennartson, M. Håkansson, S. Jagner, *Angew. Chem. Int. Ed.* **2007**, *46*, 6678-6680.
- [97] a) T. J. Boyle, T. M. Alam, K. P. Peters, M. A. Rodriguez, *Inorg. Chem.* **2001**, *40*, 6281; b) J. Adamchuk, R. R. Schrock, Z. J. Tonzetich, P. Müller, *Organometallics* **2006**, *25*, 2364; c) P. G. Williard, J. M. Salvino, *Tetrahedron Lett.* **1985**, *26*, 3931; d) R. Campbell, P. Garcia-Alvarez, A. R. Kennedy, R. E. Mulvey, *Chem. Eur. J.* **2010**, *16*, 9964; e) L. O. Müller, R. Scopelliti, I. Krossing, *Chimia* **2006**, *60*, 220; f) M. A. Nichols, A. T. McPhail, E. M. Arnett, *J. Am. Chem. Soc.* **1991**, *113*, 6222; g) U. Piarulli, D. N. Williams, C. Floriani, G. Gervasio, D. Viterbo, *Chem. Commun.* **1994**, 1409; h) P. C. Andrews, S. D. Bull, M. Koutsaplis, *New J.Chem.* **2010**, *34*, 1678; i) A. Reisinger, N. Trapp, I. Krossing, *Organometallics* **2007**, *26*, 2096; j) E. M. Arnett, M. A. Nichols, A. T. McPhail, *J. Am. Chem. Soc.* **1990**, *112*, 7059.
- [98] Y. Zhao, D. G. Truhlar, *J. Chem. Phys.* **2006**, *125*, 194101.
- [99] a) P. C. Hariharan, J. A. Pople, *Theor. Chim. Acta* **1973**, *58*, 1200; b) R. Krishnan, J. S. Binkley, R. Seeger, J. A. Pople, *J. Chem. Phys.* **1980**, *72*, 650.
- [100] M. J. Frisch, G. W. Trucks, H. B. Schlegel, G. E. Scuseria, M. A. Robb, J. R. Cheeseman, G. Scalmani, V. Barone, B. Mennucci, G. A. Petersson, H. Nakatsuji, M. Caricato, X. Li, H. P. Hratchian, A. F. Izmaylov, J. Bloino, G. Zheng, J. L. Sonnenberg, M. Hada, M. Ehara, K. Toyota, R. Fukuda, J. Hasegawa, M. Ishida, T. Nakajima, Y. Honda, O. Kitao, H. Nakai, T. Vreven, J. Montgomery, J. A. J. E. Peralta, F. Ogliaro, M. Bearpark, J. J. Heyd, E. Brothers, K. N. Kudin, V. N. Staroverov, R. Kobayashi, J. Normand, K. Raghavachari, A. Rendell, J. C. Burant, S. S. Iyengar, J. Tomasi, M. Cossi, N. Rega, J. M. Millam, M. Klene, J. E. Knox, J. B. Cross, V. Bakken, C. Adamo, J. Jaramillo, R. Gomperts, R. E. Stratmann, O. Yazyev, A. J. Austin, R. Cammi, C. Pomelli, J. W. Ochterski, R. L. Martin, K. Morokuma, V. G. Zakrzewski, G. A. Voth, P. Salvador, J. J. Dannenberg, S. Dapprich, A. D. Daniels, O. Farkas, J. B. Foresman, J. V. Ortiz, J. Cioslowski, D. J. Fox, A.02 ed., Gaussian, Inc., Wallingford, CT, **2009**.
- [101] C.-R. Lu, H.-H. Li, B. Zhao, Q. Shen, Y.-M. Yao, Y. Zhang, *Chin. J. Chem.* **2007**, *25*, 1588-1592.
- [102] E. S. Schmidt, N. W. Mitzel, H. Schmidbaur, *Personal Communication to CCDB* **2004**.

- [103] a) A. Heine, D. Stalke, *Angew. Chem. Int. Ed.* **1992**, *31*, 854; b) W. Uhl, A. Vester, *Chem. Ber.* **1993**, *126*, 941; c) H. Noth, A. Schlegel, J. Knizek, I. Krossing, W. Ponikwar, T. Seifert, *Chem. Eur. J.* **1998**, *4*, 2191; d) H. Noth, T. Seifert, *Eur. J. Inorg. Chem.* **1998**, 1931; e) J. Pauls, B. Neumuller, *Inorg. Chem.* **2001**, *40*, 121; f) M. G. Gardiner, S. M. Lawrence, C. L. Raston, *Inorg. Chem.* **1999**, *38*, 4467; g) N. Srivastava, A. Kumar, *J. Indian Counc. Chem.* **1995**, *11*, 62-84; h) J. L. Atwood, D. C. Hrcncir, R. D. Rogers, J. A. K. Howard, *J. Am. Chem. Soc.* **1981**, *103*, 6787; i) A. G. Avent, C. Eaborn, I. B. Gorrell, P. B. Hitchcock, J. D. Smith, *J. Chem. Soc., Dalton Trans.* **2002**, 3971; j) M. M. Andrianarison, A. G. Avent, M. C. Ellerby, I. B. Gorrell, P. B. Hitchcock, J. D. Smith, D. R. Stanley, *J. Chem. Soc., Dalton Trans.* **1998**, 249; k) S. S. Al-Juaid, C. Eaborn, I. B. Gorrell, S. A. Hawkes, P. B. Hitchcock, J. D. Smith, *J. Chem. Soc., Dalton Trans.* **1998**, 2411; l) G. Hencken, E. Weiss, *J. Organomet. Chem.* **1974**, *73*, 35; m) C. Eaborn, P. B. Hitchcock, J. D. Smith, S. E. Sozerli, *Organometallics* **1998**, *17*, 4322; n) K. Goto, J. Kobayashi, R. Okazaki, *Organometallics* **1999**, *18*, 1357; o) N. M. Yoon, *Pure Appl. Chem.* **1996**, *68*, 843-848; p) W. Uhl, E. Schnepf, J. Wagner, *Z. Anorg. Allg. Chem.* **1992**, *613*, 67; q) W. Uhl, J. E. O. Schnepf, *Z. Anorg. Allg. Chem.* **1991**, *595*, 225; r) G. Linti, H. Noth, P. Rahm, *Z. Naturforsch., B: Chem. Sci.* **1988**, *43*, 1101.
- [104] S. E. Potts, C. J. Carmalt, C. S. Blackman, T. Leese, H. O. Davies, *Dalton Trans.* **2008**, 5730-5736.
- [105] C. Brinkmann, A. G. M. Barrett, M. S. Hill, P. A. Procopiou, *Angew. Chem. Int. Ed.* **2012**, 10.1021/ja209135t.
- [106] M. G. Davidson, D. Garcia-Vivo, A. R. Kennedy, R. E. Mulvey, S. D. Robertson, *Chem. Eur. J.* **2011**, *17*, 3364-3369.
- [107] a) G. Cahiez, B. Laboue, *Tetrahedron Lett.* **1989**, *30*, 3545; b) G. Cahiez, C. Duplais, J. Buendia, *Chem. Rev.* **2009**, *109*, 1434-1476.
- [108] B. Haag, M. Mosrin, H. Ila, V. Malakhov, P. Knochel, *Angew. Chem. Int. Ed.* **2011**, *50*, 9794-9824.
- [109] K. Müller, C. Faeh, F. Diederich, *Science* **2007**, *317*, 1881-1886.
- [110] V. Gouverneur, *Science* **2009**, *325*, 1630-1631.
- [111] J. S. Carey, D. Laffan, C. Thomson, M. T. Williams, *Org. Biomol. Chem.* **2006**, *4*, 2337-2347.
- [112] D. A. Watson, M. Su, G. Teveroskiy, Y. Zhang, J. Garcia-Fortanet, T. Kinzel, S. L. Buchwald, *Science* **2009**, *325*, 1661-1664.
- [113] H. Schumann, J. Gottfriedsen, F. Girgsdies, *Z. Anorg. Allg. Chem.* **1997**, *623*, 1881.
- [114] D. C. Bradley, I. S. Harding, I. A. Maia, M. Motevalli, *J. Chem. Soc., Dalton Trans.* **1997**, 2969.
- [115] W. R. Nutt, K. J. Murray, J. M. Gulick, J. D. Odom, Y. Ding, L. Lebioda, *Organometallics* **1996**, *15*, 1728.
- [116] P. G. Williard, J. M. Salvino, *J. Org. Chem.* **1993**, *58*, 1.
- [117] L. M. Engelhardt, B. S. Jolly, P. C. Junk, C. L. Raston, B. W. Skelton, A. H. White, *Aust. J. Chem.* **1986**, *39*, 1337.

- [118] D. R. Armstrong, J. Garcia-Alvarez, A. R. Kennedy, R. E. Mulvey, S. D. Robertson, *Chem. Eur. J.* **2011**, *17*, 6725.
- [119] M. P. Bernstein, F. E. Romesberg, D. J. Fuller, A. T. Harrison, D. B. Collum, Q.-Y. Liu, P. G. Williard, *J. Am. Chem. Soc.* **1992**, *114*, 5100.
- [120] P. G. Williard, Q.-Y. Liu, *J. Am. Chem. Soc.* **1993**, *115*, 3380.
- [121] K. W. Henderson, A. E. Dorigo, Q.-Y. Liu, P. G. Williard, *J. Am. Chem. Soc.* **1997**, *119*, 11855.
- [122] a) K. Thiele, H. Gorls, W. Seidel, *Z. Anorg. Allg. Chem.* **1998**, *624*, 555; b) M. Westerhausen, M. Wieneke, W. Ponikwar, H. Noth, W. Schwartz, *Organometallics* **1998**, *17*, 1438.
- [123] a) S. Schmidt, S. Schulz, D. Blaser, R. Boese, M. Bolte, *Organometallics* **2010**, *29*, 6097; b) P. B. Hitchcock, M. F. Lappert, X.-H. Wei, *Dalton Trans.* **2006**, 1181; c) W. Clegg, D. V. Graham, E. Herd, E. Hevia, A. R. Kennedy, M. D. McCall, L. Russo, *Inorg. Chem.* **2009**, *48*, 5320; d) E. Alvarez, A. Girrane, I. Resa, D. del Rio, A. Rodriguez, E. Carmona, *Angew. Chem. Int. Ed.* **2007**, *46*, 1296; e) D. J. Darensbourg, J. C. Yoder, G. E. Struck, M. W. Holtcamp, J. D. Draper, J. H. Reibenspies, *Inorg. Chim. Acta* **1998**, *274*, 115; f) W. Gaderbauer, I. Balatoni, H. Wagner, J. Baumgartner, C. Marschner, *Dalton Trans.* **2010**, *39*, 1598; g) R. W. Saalfank, N. Mooren, A. Scheurer, H. Maid, F. W. Heinemann, F. Hampel, W. Bauer, *Eur. J. Inorg. Chem.* **2007**, 4815.
- [124] M. L. Hlavinka, J. R. Hagadorn, *Organometallics* **2005**, *24*, 5335-5341.
- [125] M. Yamakawa, R. Noyori, *J. Am. Chem. Soc.* **1995**, *117*, 6327-6335.
- [126] G. Rowlands, *Tetrahedron* **2001**, *57*, 1865-1882.
- [127] D. R. Armstrong, W. Clegg, S. H. Dale, J. Garcia-Alvarez, R. W. Harrington, E. Hevia, G. W. Honeyman, A. R. Kennedy, R. E. Mulvey, C. T. O'Hara, *Chem. Commun.* **2008**, 187-189.
- [128] R. Campbell, B. Conway, G. S. Fairweather, P. Garcia-Alvarez, A. R. Kennedy, J. Klett, R. E. Mulvey, C. T. O'Hara, G. M. Robertson, *Dalton Trans.* **2009**.
- [129] R. M. Fabicon, M. Parvez, H. G. Richey, *J. Am. Chem. Soc.* **1991**, *113*, 1412.
- [130] J. Jeneer, B. H. Meier, P. Bachmann, R. R. Ernst, *J. Chem. Phys.* **1979**, *71*, 4546-4553.
- [131] T. Furuyama, M. Yonehara, S. Arimoto, M. Kobayashi, Y. Matsumoto, M. Uchiyama, *Chem. Eur. J.* **2008**, *14*, 10348-10356.
- [132] D. Barr, W. Clegg, R. E. Mulvey, R. Snaith, K. Wade, *Chem. Commun.* **1986**, 295.
- [133] a) F. T. Edelman, *Adv. Organomet. Chem.* **2008**, *57*, 133-352; b) F. T. Edelman, *Chem. Soc. Rev.* **2009**, *38*, 2253-2268; c) J. Barker, M. Kilner, *Coord. Chem. Rev.* **1994**, *133*, 219-300.
- [134] a) J. Prust, A. Stasch, W. Zheng, H. W. Roesky, E. Alexopoulos, I. Uson, D. Böhler, T. Schuchardt, *Organometallics* **2001**, *20*, 3825-3828; b) J. Prust, H. Hohmeister, A. Stasch, H. W. Roesky, J. Magull, E. Alexopoulos, I. Uson, H.-G. Schmidt, M. Noltemeyer, *Eur. J. Inorg. Chem.* **2002**, 2157-2162; c) S. Aboukacem, W. Tyrra, I. Pantenburg, *Z. Anorg. Allg. Chem.* **2003**, *629*, 1569-1574; d) S. D. Allen, D. R. Moore, E. B. Lobkovsky, G. W. Coates, *J. Am. Chem. Soc.* **2002**, *124*, 14284-14285; e) B. W. Liu, C. Y. Tian, L. Zhang, W. D. Yan, W. J. Zhang, *J. Polym. Sci. Part A: Polym. Chem.* **2006**, *44*, 6243-6251; f) M.

- Kröger, C. Folli, O. Walter, M. Döring, *Adv. Synth. Cat.* **2006**, *348*, 1908-1918; g) M. Cheng, D. R. Moore, J. J. Reczek, B. M. Chamberlain, E. B. Lobkovsky, G. W. Coates, *J. Am. Chem. Soc.* **2001**, *123*, 8738-8749.
- [135] a) M. Cheng, A. B. Attygalle, E. B. Lobkovsky, G. W. Coates, *J. Am. Chem. Soc.* **1999**, *121*, 11583-11584; b) B. M. Chamberlain, M. Cheng, D. R. Moore, T. M. Ovitt, E. B. Lobkovsky, G. W. Coates, *J. Am. Chem. Soc.* **2001**, *123*, 3229-3238; c) M. H. Chisholm, J. C. Huffman, K. Phomphrai, M. Cheng, A. B. Attygalle, E. B. Lobkovsky, G. W. Coates, *J. Chem. Soc., Dalton Trans.* **1999**, 222-224; d) S. D. Allen, D. R. Moore, E. B. Lobkovsky, G. W. Coates, *J. Organomet. Chem.* **2003**, *683*, 137-148; e) M. H. Chisholm, J. C. Gallucci, K. Phomphrai, *Inorg. Chem.* **2005**, *44*, 8004-8010.
- [136] C. Jones, L. Furness, S. Nembenna, R. P. Rose, S. Aldridge, A. Stasch, *Dalton Trans.* **2010**, *39*, 8788.
- [137] A. D. Bond, D. J. Linton, P. Schooler, A. E. H. Wheatley, *J. Chem. Soc., Dalton Trans.* **2001**, 3173.
- [138] M. L. Cole, D. J. Evans, P. C. Junk, L. M. Louis, *N. J. Chem.* **2002**, *26*, 1015.
- [139] E. Hevia, G. W. Honeyman, A. R. Kennedy, R. E. Mulvey, *J. Am. Chem. Soc.* **2005**, *127*, 13106.
- [140] J. J. Crawford, B. J. Fleming, A. R. Kennedy, J. Klett, C. T. O'Hara, S. A. Orr, *Chem. Commun.* **2011**, *47*, 3772-3774.
- [141] R. Forret, A. R. Kennedy, J. Klett, R. E. Mulvey, S. D. Robertson, *Organometallics* **2010**, *29*, 1436-1442.
- [142] D. Enders, J. Kirchoff, P. Gerdes, D. Mannes, G. Raabe, J. Runsink, G. Boche, M. Marsch, H. Albrecht, H. Sommer, *Eur. J. Org. Chem.* **1998**, 63.
- [143] M. C. Roux, J. Seyden-Penne, L. Wartski, G. H. Posner, M. Nierlich, D. Vigner, M. Lance, *J. Org. Chem.* **1993**, *58*, 3969-3973.
- [144] D. Enders, H. Lotter, N. Maignot, J. P. Mazaleyrat, Z. Welvart, *Nouv. J. Chim.* **1984**, *8*, 747-750.
- [145] a) J. D. Albright, *Tetrahedron* **1983**, *39*, 3207-3233; b) M. Zervos, L. Wartski, *Tetrahedron Lett.* **1984**, *25*, 4641-4644; c) M. Zervos, L. Wartski, J. Seyden-Penne, *Tetrahedron* **1986**, *42*, 4963-4973; d) D. Enders, P. Gerdes, H. Kipphardt, *Angew. Chem. Int. Ed.* **1990**, *29*, 179-181; e) M. C. Roux, L. Wartski, M. Nierlich, M. Lance, *Tetrahedron* **1996**, *10083-10094*.
- [146] M. Krieger, R. O. Gould, K. Dehnicke, *Z. Anorg. Allg. Chem.* **2002**, *628*, 1289.
- [147] a) B. H. Lipshutz, K. Siegmann, E. Garcia, F. Kayser, *J. Am. Chem. Soc.* **1993**, *115*, 9276-9282; b) B. H. Lipshutz, R. S. Wilhelm, D. M. Floyd, *J. Am. Chem. Soc.* **1981**, *103*, 7672-7674.
- [148] E. Nakamura, N. Yoshikai, *Bull. Chem. Soc. Jpn.* **2004**, *77*, 1-12.
- [149] a) S. Usui, Y. Hashimoto, J. V. Morey, A. E. H. Wheatley, M. Uchiyama, *J. Am. Chem. Soc.* **2007**, *129*, 15102-15103; b) J. Haywood, J. V. Morey, A. E. H. Wheatley, C.-Y. Liu, S. Yasuike, J. Kurita, M. Uchiyama, P. R. Raithby, *Organometallics* **2009**, *28*, 38.
- [150] E. Hevia, A. R. Kennedy, J. Klett, Z. Livingstone, M. D. McCall, *Dalton Trans.* **2010**, *39*, 520-526.
- [151] D. R. Armstrong, A. M. Drummond, L. Balloch, D. V. Graham, E. Hevia, A. R. Kennedy, *Organometallics* **2008**, *27*, 5860-5866.

- [152] S. E. Baillie, E. Hevia, A. R. Kennedy, R. E. Mulvey, *Organometallics* **2007**, *26*, 204-209.
- [153] X. He, J. Morris, B. C. Noll, S. N. Brown, K. W. Henderson, *J. Am. Chem. Soc.* **2004**, *128*, 13599.
- [154] E. R. Hurley, X. He, S. N. Brown, K. W. Henderson, *J. Am. Chem. Soc.* **2009**, *131*, 6056-6057.
- [155] K. Y. Tsang, H. Diaz, N. Graciani, J. W. Kelly, *J. Am. Chem. Soc.* **1994**, *116*, 3988-4005.
- [156] M. L. Hlavinka, J. R. Hagadorn, *Chem. Commun.* **2003**, 2686-2687.
- [157] J. R. Hagadorn, M. J. McNevin, *Organometallics* **2003**, *22*, 609.
- [158] P. C. Andrews, A. R. Kennedy, R. E. Mulvey, C. L. Raston, B. A. Roberts, R. B. Rowlings, *Angew. Chem. Int. Ed.* **2000**, *39*, 1960.
- [159] A. A. Fyfe, A. R. Kennedy, J. Klett, R. E. Mulvey, *Angew. Chem. Int. Ed.* **2011**, *50*, 7776-7780.
- [160] S. P. Green, C. Jones, A. Stasch, *Science* **2007**, *318*, 1754-1757.
- [161] I. Resa, E. Carmona, E. Gutierrez-Puebla, A. Monge, *Science* **2004**, *305*, 1136-1138.
- [162] T. Nguyen, A. D. Sutton, M. Brynda, J. C. Fettinger, G. J. Long, P. P. Power, *Science* **2005**, *310*, 844.
- [163] a) A. Noor, F. R. Wagner, R. Kempe, *Angew. Chem. Int. Ed.* **2008**, *47*, 7246-7249; b) A. Noor, G. Glatz, R. Müller, M. Kaupp, S. Demeshhko, R. Kempe, *Nat. Chem.* **2009**, *1*, 323; c) C.-W. Hsu, J.-S. K. Yu, C.-H. Yen, G.-H. Lee, Y. Wang, Y.-C. Tsai, *Angew. Chem. Int. Ed.* **2008**, *47*, 9933-9936; d) Y.-C. Tsai, C.-W. Hsu, J.-S. K. Yu, G.-H. Lee, Y. Wang, T.-S. Kuo, *Angew. Chem. Int. Ed.* **2008**, *47*, 7250-7253.
- [164] a) D. J. Brauer, C. Krüger, *Inorg. Chem.* **1976**, *15*, 2511; b) F. A. Cotton, S. Koch, A. J. Schultz, J. H. Williams, *Inorg. Chem.* **1978**, *17*, 2093-2098.
- [165] a) F. A. Cotton, S. Koch, K. Mertis, M. Millar, G. Wilkinson, *J. Am. Chem. Soc.* **1977**, *99*, 4989-4992; b) F. A. Cotton, J. M. Troup, T. R. Webb, D. H. Williamson, G. Wilkinson, *J. Am. Chem. Soc.* **1974**, *96*, 3824-3828; c) J. Krausse, G. Marx, J. Schodl, *J. Organomet. Chem.* **1970**, *21*, 159.
- [166] S. Horvath, S. I. Gorelsky, S. Gambarotta, I. Korobkov, *Angew. Chem. Int. Ed.* **2008**, *47*, 9937-9940.
- [167] F. A. Cotton, C. A. Murillo, H.-C. Zhou, *Inorg. Chem.* **2000**, *39*, 3728-3730.
- [168] J. J. H. Edema, S. Gambarotta, *Coments. Inorg. Chem.* **1991**, *11*, 195-214.
- [169] a) S. Hao, S. Gambarotta, C. Bensimon, *J. Am. Chem. Soc.* **1992**, *114*, 3556-3557; b) S. Hao, J.-I. Song, P. Berno, S. Gambarotta, *Organometallics* **1994**, *13*, 1326-1335.
- [170] J. Losada, S. Alvarez, J. J. Novoa, F. Mota, *J. Am. Chem. Soc.* **1990**, *112*, 8998-9000.
- [171] a) T. Susuki, T. Jiro, *J. Org. Chem.* **1970**, *35*, 2982-2986; b) R. C. Kerber, B. R. Waldbaur, *J. Organomet. Chem.* **1996**, *513*, 277-280; c) H. Tsurugi, K. Yamada, M. Majumdar, Y. Sugino, A. Hayakawa, K. Mashima, *Dalton. Trans.* **2011**, DOI: 10.1039/c1031dt11129a; d) P. W. Jolly, *Acc. Chem. Res.* **1996**, *29*, 544-551.
- [172] a) S. Licciulli, I. Thapa, K. Albahily, I. Korobkov, S. Gambarotta, R. Duchateau, R. Chevalier, K. Schuhen, *Angew. Chem. Int. Ed.* **2010**, *49*, 9225-9228; b) S.

- Peitz, B. R. Aluri, N. Peulecke, B. H. Müller, A. Wöhl, W. Müller, M. H. Al-Hazmi, F. M. Mosa, U. Rosenthal, *Chem. Eur. J.* **2010**, *16*, 7670-7676; c) A. Bollmann, K. Blann, J. T. Dixon, F. M. Hess, E. Killian, H. Maumela, D. S. McGuinness, D. H. Morgan, A. Neveling, S. Otto, M. Overset, A. M. Z. Slawin, P. Wasserschied, S. Kuhlmann, *J. Am. Chem. Soc.* **2004**, *126*, 14712-14713.
- [173] F. A. Cotton, K. J. Wiesinger, *Inorg. Chem.* **1991**, *30*, 871.
- [174] F. A. Cotton, M. W. Extine, T. R. Felthouse, B. W. S. Kolthammer, D. G. Lay, *J. Am. Chem. Soc.* **1981**, *103*, 4040.
- [175] N. K. Hansen, P. Coppens, *Acta Crystallogr. Sect. A* **1978**, *34*, 909-921.
- [176] D. Stalke, *Chem. Eur. J.* **2011**, *17*, 9264-9278.
- [177] U. Flierler, M. Burzler, D. Leusser, J. Henn, H. Ott, H. Braunschweig, D. Stalke, *Angew. Chem. Int. Ed.* **2008**, *47*, 4321-4325.
- [178] a) A. N. Vedernikov, *Curr. Org. Chem.* **2007**, *11*, 1401-1416; b) R. A. Periana, G. Bhalla, W. J. Tenn, K. J. H. Young, X. Y. Liu, O. Mironov, C. Jones, V. R. Ziatdinov, *J. Mol. Catal. A Chem.* **2004**, *220*, 7-25; c) R. H. Crabtree, *J. Organomet. Chem.* **2004**, *689*, 4083-4091; d) R. H. Crabtree, *Pure Appl. Chem.* **2003**, *75*, 435-443; e) R. A. Baillie, T. Tran, K. M. Lalonde, J. Y. K. Tsang, M. E. Thibault, B. O. Patrick, P. Legzdins, *Organometallics* **2012**, *31*, 1055-1067; f) S. P. Semproni, P. M. Graham, M. S. A. Buschhaus, B. O. Patrick, P. Legzdins, *Organometallics* **2009**, *28*, 4480-4490; g) S. P. Semproni, P. Legzdins, *Organometallics* **2009**, *28*, 6139-6141; h) J. A. Cabeza, P. Garcia-Alvarez, D. Polo, *Inorg. Chem.* **2012**, *51*, 2569-2576; i) J. A. Cabeza, M. Damonte, P. Garcia-Alvarez, M. G. Hernandez-Cruz, A. R. Kennedy, *Organometallics* **2012**, *31*, 327-334; j) J. A. Cabeza, P. Garcia-Alvarez, V. Pruneda, *Organometallics* **2012**, *31*, 941-946.
- [179] S. V. Kessar, P. Singh, *Chem. Rev.* **1997**, *97*, 721-737.
- [180] B. Conway, J. Garcia-Alvarez, E. Hevia, A. R. Kennedy, R. E. Mulvey, S. D. Robertson, *Organometallics* **2009**, *28*, 6462-6468.
- [181] C. Strohmam, V. H. Gessner, *Angew. Chem. Int. Ed.* **2007**, *46*, 4566-4569.
- [182] H. Naka, M. Uchiyama, Y. Matsumoto, A. E. H. Wheatley, M. McPartlin, J. V. Morey, Y. Kondo, *J. Am. Chem. Soc.* **2007**, *129*, 1921.
- [183] a) R. Adams, H. C. Yuan, *Chem. Rev.* **1933**, *12*, 261-338; b) J. Gorecka, C. Heiss, R. Scopelliti, M. Schlosser, *Org. Lett.* **2004**, *6*, 4591-4593.
- [184] E. L. Werkema, R. A. Andersen, A. Yahia, L. Maron, O. Eisenstein, *Organometallics* **2009**, *28*, 3173-3185.
- [185] a) H. Werner, M. Schulz, B. Windmüller, *Organometallics* **1995**, *14*, 3659-3668; b) J. Choi, Y. Choliy, X. Zhang, T. J. Emge, K. Krogh-Jespersen, A. S. Goldman, *J. Am. Chem. Soc.* **2009**, *131*, 15627-15629.
- [186] P. Leoni, L. Marchetti, V. Bonuccelli, S. K. Mohapatra, A. Albinati, S. Rizzato, *Chem. Eur. J.* **2010**, *16*, 9468-9477.
- [187] A. R. Kennedy, R. E. Mulvey, C. T. O'Hara, G. M. Robertson, S. D. Robertson, *Angew. Chem. Int. Ed.* **2011**, *50*, 8375-8378.
- [188] E. Hevia, R. E. Mulvey, *Angew. Chem. Int. Ed.* **2011**, *50*, 6448-6450.
- [189] P. Garcia-Alvarez, D. V. Graham, E. Hevia, A. R. Kennedy, J. Klett, R. E. Mulvey, C. T. O'Hara, S. Weatherstone, *Angew. Chem. Int. Ed.* **2008**, *47*, 8079-8081.

- [190] D. R. Armstrong, P. Garcia-Alvarez, A. R. Kennedy, R. E. Mulvey, J. A. Parkinson, *Angew. Chem. Int. Ed.* **2010**, *49*, 3185-3188.
- [191] L. Gupta, A. C. Hoepker, K. J. Singh, D. B. Collum, *J. Org. Chem.* **2009**, *74*, 2231-2233.
- [192] P. L. Hall, J. H. Gilchrist, A. T. Harrison, D. J. Fuller, D. B. Collum, *J. Am. Chem. Soc.* **1991**, *113*, 9575-9585.
- [193] P. Garcia-Alvarez, R. E. Mulvey, J. A. Parkinson, *Angew. Chem. Int. Ed.* **2011**, *50*, 9668-9671.
- [194] W.L.F. Armarego, D.D. Perrin, *Purification of Laboratory Chemicals, Vol. 4*, Oxford, **1996**.
- [195] B. E. Love, E. G. Jones, *J. Org. Chem.* **1999**, *64*, 3755.
- [196] C. Schade, W. Bauer, P.v.R. Schleyer, *J. Organomet. Chem.* **1985**, C25.

15 X-ray Crystallographic data

Compound 18 (TMEDA)Li[(*i*Pr)NCH₂CH₂N(H)(*i*Pr)]Zn(*t*Bu)₂

Identification code	pgaross10	
Empirical formula	C ₂₂ H ₅₃ Li N ₄ Zn	
Formula weight	445.99	
Temperature	123(2) K	
Wavelength	1.54180 Å	
Crystal system	TRICLINIC	
Space group	P-1	
Unit cell dimensions	a = 8.8657(5) Å	α = 94.470(5)°.
	b = 10.9105(6) Å	β = 99.423(5)°.
	c = 15.2569(9) Å	γ = 103.390(5)°.
Volume	1405.94(14) Å ³	
Z	2	
Density (calculated)	1.054 Mg/m ³	
Absorption coefficient	1.280 mm ⁻¹	
F(000)	492	
Crystal size	0.1 x 0.08 x 0.04 mm ³	
Theta range for data collection	4.20 to 73.12°.	
Index ranges	-10 ≤ h ≤ 10, -13 ≤ k ≤ 13, -18 ≤ l ≤ 18	
Reflections collected	21097	
Independent reflections	5545 [R(int) = 0.0233]	
Completeness to theta = 73.12°	98.4 %	
Absorption correction	Semi-empirical from equivalents	
Max. and min. transmission	0.27828 and 0.27828	
Refinement method	Full-matrix least-squares on F ²	
Data / restraints / parameters	5545 / 0 / 262	
Goodness-of-fit on F ²	1.061	
Final R indices [I > 2σ(I)]	R1 = 0.0323, wR2 = 0.0888	
R indices (all data)	R1 = 0.0367, wR2 = 0.0905	
Largest diff. peak and hole	0.662 and -0.269 e.Å ⁻³	

Compound 21 (TMEDA)Li[(iPr)NCH₂CH₂CH₂N(iPr)]Zn(tBu)

Identification code	pgaross11	
Empirical formula	C ₁₉ H ₄₅ Li N ₄ Zn	
Formula weight	401.90	
Temperature	123(2) K	
Wavelength	1.54180 Å	
Crystal system	Monoclinic	
Space group	P21/a	
Unit cell dimensions	a = 17.7379(11) Å	α = 90°.
	b = 11.9358(7) Å	β = 90.061(9)°.
	c = 11.4315(10) Å	γ = 90°.
Volume	2420.2(3) Å ³	
Z	4	
Density (calculated)	1.103 Mg/m ³	
Absorption coefficient	1.442 mm ⁻¹	
F(000)	880	
Crystal size	0.12 x 0.08 x 0.08 mm ³	
Theta range for data collection	3.87 to 73.19°.	
Index ranges	-20<=h<=21, -14<=k<=14, -14<=l<=13	
Reflections collected	10300	
Independent reflections	4420 [R(int) = 0.0298]	
Completeness to theta = 65.00°	94.1 %	
Absorption correction	Semi-empirical from equivalents	
Max. and min. transmission	1.00000 and 0.84569	
Refinement method	Full-matrix least-squares on F ²	
Data / restraints / parameters	4420 / 20 / 232	
Goodness-of-fit on F ²	1.061	
Final R indices [I>2sigma(I)]	R1 = 0.0541, wR2 = 0.1206	
R indices (all data)	R1 = 0.0820, wR2 = 0.1289	
Largest diff. peak and hole	0.500 and -0.385 e.Å ⁻³	

Compound 22 $\{(THF)Li[(iPr)NCH_2CH_2N(iPr)]Zn(tBu)\}_2$

Identification code	pgaross19	
Empirical formula	C32 H70 Li2 N4 O2 Zn2	
Formula weight	687.54	
Temperature	123(2) K	
Wavelength	0.71073 Å	
Crystal system	Triclinic	
Space group	P-1	
Unit cell dimensions	a = 8.7028(6) Å	$\alpha = 82.577(5)^\circ$.
	b = 10.0294(7) Å	$\beta = 78.661(6)^\circ$.
	c = 11.2396(7) Å	$\gamma = 81.212(6)^\circ$.
Volume	945.60(11) Å ³	
Z	1	
Density (calculated)	1.207 Mg/m ³	
Absorption coefficient	1.299 mm ⁻¹	
F(000)	372	
Crystal size	0.15 x 0.10 x 0.09 mm ³	
Theta range for data collection	2.63 to 28.99°.	
Index ranges	-11<=h<=11, -13<=k<=13, -15<=l<=15	
Reflections collected	10295	
Independent reflections	4928 [R(int) = 0.0485]	
Completeness to theta = 27.00°	99.6 %	
Absorption correction	Semi-empirical from equivalents	
Max. and min. transmission	multi-scan and 0.94455	
Refinement method	Full-matrix least-squares on F ²	
Data / restraints / parameters	4928 / 13 / 234	
Goodness-of-fit on F ²	0.990	
Final R indices [I>2sigma(I)]	R1 = 0.0448, wR2 = 0.0771	
R indices (all data)	R1 = 0.0754, wR2 = 0.0834	
Largest diff. peak and hole	0.803 and -0.472 e.Å ⁻³	

Compound 25 [(TMEDA)Li(*iPr*)NCH₂CH₂N(*iPr*)Li]₂

Identification code	srcc1001
Empirical formula	C ₂₈ H ₆₈ Li ₄ N ₈
Formula weight	544.66
Temperature	123(2) K
Wavelength	0.71073 Å
Crystal system	Monoclinic
Space group	C 2/c
Unit cell dimensions	a = 19.7144(14) Å α = 90°. b = 9.2884(6) Å β = 94.958(6)°. c = 20.2438(14) Å γ = 90°.
Volume	3693.1(4) Å ³
Z	4
Density (calculated)	0.980 Mg/m ³
Absorption coefficient	0.057 mm ⁻¹
F(000)	1216
Crystal size	0.20 x 0.12 x 0.12 mm ³
Theta range for data collection	3.02 to 28.00°.
Index ranges	-25 ≤ h ≤ 25, -12 ≤ k ≤ 12, -26 ≤ l ≤ 26
Reflections collected	19595
Independent reflections	4435 [R(int) = 0.0544]
Completeness to theta = 26.00°	99.8 %
Absorption correction	Semi-empirical from equivalents
Max. and min. transmission	1.00000 and 0.69706
Refinement method	Full-matrix least-squares on F ²
Data / restraints / parameters	4435 / 3 / 207
Goodness-of-fit on F ²	0.965
Final R indices [I > 2σ(I)]	R1 = 0.0523, wR2 = 0.1418
R indices (all data)	R1 = 0.0907, wR2 = 0.1519
Largest diff. peak and hole	0.300 and -0.333 e.Å ⁻³

Compound 26 [(TMEDA)Li₂[(iPr)NCH₂CH₂N(iPr)]Zn(tBu)H

Identification code	pgaross14	
Empirical formula	C ₂₄ H ₆₀ Li ₂ N ₆ Zn	
Formula weight	512.03	
Temperature	123(2) K	
Wavelength	0.71073 Å	
Crystal system	MONOCLINIC	
Space group	P21/n	
Unit cell dimensions	a = 10.0019(2) Å	α = 90°.
	b = 15.4170(5) Å	β = 96.674(2)°.
	c = 20.5770(6) Å	γ = 90°.
Volume	3151.46(15) Å ³	
Z	4	
Density (calculated)	1.079 Mg/m ³	
Absorption coefficient	0.799 mm ⁻¹	
F(000)	1128	
Crystal size	0.15 x 0.1 x 0.8 mm ³	
Theta range for data collection	2.54 to 27.50°.	
Index ranges	-12<=h<=12, -20<=k<=17, -26<=l<=26	
Reflections collected	22690	
Independent reflections	7213 [R(int) = 0.0485]	
Completeness to theta = 27.50°	99.9 %	
Absorption correction	Semi-empirical from equivalents	
Max. and min. transmission	1.00000 and 0.98604	
Refinement method	Full-matrix least-squares on F ²	
Data / restraints / parameters	7213 / 5 / 328	
Goodness-of-fit on F ²	0.909	
Final R indices [I>2sigma(I)]	R1 = 0.0458, wR2 = 0.0910	
R indices (all data)	R1 = 0.0863, wR2 = 0.0978	
Largest diff. peak and hole	0.466 and -0.354 e.Å ⁻³	

Compound 28 (TMEDA)Li[(iPr)NCH=CHN(iPr)]Zn(Me)

Identification code	pgaross15	
Empirical formula	C15 H35 Li N4 Zn	
Formula weight	343.78	
Temperature	123(2) K	
Wavelength	0.71073 Å	
Crystal system	MONOCLINIC	
Space group	P21/n	
Unit cell dimensions	a = 9.7395(5) Å	$\alpha = 90^\circ$.
	b = 13.6980(7) Å	$\beta = 105.833(5)^\circ$.
	c = 15.4433(7) Å	$\gamma = 90^\circ$.
Volume	1982.15(17) Å ³	
Z	4	
Density (calculated)	1.152 Mg/m ³	
Absorption coefficient	1.238 mm ⁻¹	
F(000)	744	
Crystal size	0.1 x 0.09 x 0.03 mm ³	
Theta range for data collection	2.63 to 26.00°.	
Index ranges	-12<=h<=12, -16<=k<=15, -19<=l<=18	
Reflections collected	12642	
Independent reflections	3872 [R(int) = 0.0657]	
Completeness to theta = 26.00°	99.5 %	
Absorption correction	Semi-empirical from equivalents	
Max. and min. transmission	1.00000 and 0.92523	
Refinement method	Full-matrix least-squares on F ²	
Data / restraints / parameters	3872 / 0 / 199	
Goodness-of-fit on F ²	0.803	
Final R indices [I>2sigma(I)]	R1 = 0.0391, wR2 = 0.0423	
R indices (all data)	R1 = 0.0923, wR2 = 0.0471	
Largest diff. peak and hole	0.917 and -0.354 e.Å ⁻³	

Compound 30 (THF)₃Na[(iPr)NCH=CHN(iPr)]Zn(tBu)

Identification code	pgapga18
Empirical formula	C ₂₄ H ₄₉ N ₂ Na O ₃ Zn
Formula weight	502.01
Temperature	123(2) K
Wavelength	1.54180 Å
Crystal system	TRICLINIC
Space group	P-1
Unit cell dimensions	a = 9.6661(3) Å α = 81.497(4)°. b = 9.8248(5) Å β = 88.765(3)°. c = 15.2836(7) Å γ = 84.978(3)°.
Volume	1429.93(11) Å ³
Z	2
Density (calculated)	1.166 Mg/m ³
Absorption coefficient	1.521 mm ⁻¹
F(000)	544
Crystal size	0.25 x 0.2 x 0.10 mm ³
Theta range for data collection	4.57 to 64.99°.
Index ranges	-11 ≤ h ≤ 10, -11 ≤ k ≤ 11, -17 ≤ l ≤ 14
Reflections collected	15955
Independent reflections	4793 [R(int) = 0.1020]
Completeness to theta = 64.99°	98.5 %
Absorption correction	None
Refinement method	Full-matrix least-squares on F ²
Data / restraints / parameters	4793 / 0 / 356
Goodness-of-fit on F ²	1.061
Final R indices [I > 2σ(I)]	R1 = 0.0582, wR2 = 0.1663
R indices (all data)	R1 = 0.0611, wR2 = 0.1701
Largest diff. peak and hole	1.357 and -0.828 e.Å ⁻³

Compound 31 {(TMEDA)Na[(iPr)NCH₂CH₂N(iPr)]Zn(tBu)}₂

Identification code	pgapga21
Empirical formula	C _{38.25} H _{91.25} N ₈ Na ₂ Zn ₂
Formula weight	840.16
Temperature	123(2) K
Wavelength	1.54180 Å
Crystal system	Monoclinic
Space group	P21/c
Unit cell dimensions	a = 14.0362(12) Å α = 90°. b = 19.0750(14) Å β = 93.665(7)°. c = 18.1701(14) Å γ = 90°.
Volume	4854.9(7) Å ³
Z	4
Density (calculated)	1.149 Mg/m ³
Absorption coefficient	1.627 mm ⁻¹
F(000)	1835
Crystal size	0.20 x 0.15 x 0.12 mm ³
Theta range for data collection	3.92 to 70.00°.
Index ranges	-17<=h<=16, -23<=k<=21, -22<=l<=14
Reflections collected	20032
Independent reflections	9140 [R(int) = 0.0534]
Completeness to theta = 70.00°	99.4 %
Absorption correction	Semi-empirical from equivalents
Max. and min. transmission	1.00000 and 0.95334
Refinement method	Full-matrix least-squares on F ²
Data / restraints / parameters	9140 / 5 / 480
Goodness-of-fit on F ²	0.944
Final R indices [I>2sigma(I)]	R1 = 0.0605, wR2 = 0.1422
R indices (all data)	R1 = 0.1111, wR2 = 0.1515
Largest diff. peak and hole	0.761 and -0.369 e.Å ⁻³

Compound 32 {(TMEDA)Na[(*i*Pr)NCH₂CH₂N(*i*Pr)]Mg(*n*Bu)}₂

Identification code	pgapga24
Empirical formula	C36 H86 Mg2 N8 Na2
Formula weight	725.73
Temperature	123(2) K
Wavelength	1.54180 Å
Crystal system	Triclinic
Space group	P-1
Unit cell dimensions	a = 9.5128(16) Å α = 98.088(15)°. b = 11.395(2) Å β = 94.008(14)°. c = 11.903(2) Å γ = 113.187(16)°.
Volume	1163.1(3) Å ³
Z	1
Density (calculated)	1.036 Mg/m ³
Absorption coefficient	0.875 mm ⁻¹
F(000)	404
Crystal size	0.12 x 0.12 x 0.05 mm ³
Theta range for data collection	3.79 to 59.99°.
Index ranges	-10 ≤ h ≤ 8, -12 ≤ k ≤ 12, -13 ≤ l ≤ 13
Reflections collected	8970
Independent reflections	3431 [R(int) = 0.0472]
Completeness to theta = 59.99°	99.3 %
Absorption correction	Semi-empirical from equivalents
Max. and min. transmission	1.00000 and 0.95608
Refinement method	Full-matrix least-squares on F ²
Data / restraints / parameters	3431 / 30 / 224
Goodness-of-fit on F ²	0.881
Final R indices [I > 2σ(I)]	R1 = 0.0538, wR2 = 0.1283
R indices (all data)	R1 = 0.0889, wR2 = 0.1397
Largest diff. peak and hole	0.304 and -0.315 e.Å ⁻³

Compound 33 (TMEDA)Li[N(*i*Pr)CH₂CH₂N(*i*Pr)]Al(Me)₂

Identification code	pgaross42	
Empirical formula	C ₁₆ H ₄₀ Al Li N ₄	
Formula weight	322.44	
Temperature	123(2) K	
Wavelength	0.71073 Å	
Crystal system	Monoclinic	
Space group	P2 ₁ /n	
Unit cell dimensions	a = 9.5430(7) Å	α = 90°.
	b = 21.8634(18) Å	β = 98.807(7)°.
	c = 10.2111(8) Å	γ = 90°.
Volume	2105.3(3) Å ³	
Z	4	
Density (calculated)	1.017 Mg/m ³	
Absorption coefficient	0.099 mm ⁻¹	
F(000)	720	
Crystal size	0.15 x 0.08 x 0.03 mm ³	
Theta range for data collection	2.72 to 29.00°.	
Index ranges	-13<=h<=11, -29<=k<=29, -13<=l<=13	
Reflections collected	22327	
Independent reflections	5597 [R(int) = 0.0440]	
Completeness to theta = 27.00°	99.9 %	
Absorption correction	Semi-empirical from equivalents	
Max. and min. transmission	1.00000 and 0.90088	
Refinement method	Full-matrix least-squares on F ²	
Data / restraints / parameters	5597 / 0 / 248	
Goodness-of-fit on F ²	0.913	
Final R indices [I>2sigma(I)]	R1 = 0.0394, wR2 = 0.0945	
R indices (all data)	R1 = 0.0672, wR2 = 0.1006	
Largest diff. peak and hole	0.274 and -0.174 e.Å ⁻³	

Compound 34 $\{(\text{THF})_{3\text{Na}}[(\text{Bz})\text{NCH}_2\text{CH}_2\text{N}(\text{Bz})]\text{Zn}(\text{Me})\}_2$

Identification code	rc1009
Empirical formula	C ₅₈ H ₉₀ N ₄ Na ₂ O ₆ Zn ₂
Formula weight	1116.06
Temperature	123(2) K
Wavelength	0.71073 Å
Crystal system	Monoclinic
Space group	P 21/c
Unit cell dimensions	a = 12.5662(5) Å α = 90°. b = 22.9173(6) Å β = 113.429(5)°. c = 11.1736(4) Å γ = 90°.
Volume	2952.5(2) Å ³
Z	2
Density (calculated)	1.255 Mg/m ³
Absorption coefficient	0.877 mm ⁻¹
F(000)	1192
Crystal size	0.20 x 0.12 x 0.12 mm ³
Theta range for data collection	3.26 to 27.00°.
Index ranges	-15 ≤ h ≤ 16, -29 ≤ k ≤ 26, -14 ≤ l ≤ 14
Reflections collected	16516
Independent reflections	6444 [R(int) = 0.0217]
Completeness to theta = 27.00°	99.8 %
Absorption correction	Semi-empirical from equivalents
Max. and min. transmission	1.00000 and 0.89212
Refinement method	Full-matrix least-squares on F ²
Data / restraints / parameters	6444 / 4 / 345
Goodness-of-fit on F ²	0.909
Final R indices [I > 2σ(I)]	R1 = 0.0287, wR2 = 0.0648
R indices (all data)	R1 = 0.0505, wR2 = 0.0679
Largest diff. peak and hole	0.501 and -0.298 e.Å ⁻³

Compound 35 (THF)Li[(Bz)N(H)CH₂CH₂N(Bz)]₂Zn₂[(Bz)NCH₂CH₂N(Bz)](tBu)

Identification code	srrc1003	
Empirical formula	C ₅₆ H ₇₃ Li N ₆ O Zn ₂	
Formula weight	983.88	
Temperature	123(2) K	
Wavelength	0.71073 Å	
Crystal system	Triclinic	
Space group	P -1	
Unit cell dimensions	a = 10.3900(2) Å	α = 105.867(2)°.
	b = 12.7832(2) Å	β = 94.283(2)°.
	c = 22.0921(4) Å	γ = 98.910(2)°.
Volume	2767.14(8) Å ³	
Z	2	
Density (calculated)	1.181 Mg/m ³	
Absorption coefficient	0.908 mm ⁻¹	
F(000)	1044	
Crystal size	0.20 x 0.12 x 0.02 mm ³	
Theta range for data collection	3.50 to 27.00°.	
Index ranges	-13 ≤ h ≤ 13, -16 ≤ k ≤ 16, -28 ≤ l ≤ 28	
Reflections collected	38150	
Independent reflections	12063 [R(int) = 0.0363]	
Completeness to theta = 27.00°	99.8 %	
Absorption correction	Semi-empirical from equivalents	
Max. and min. transmission	1.00000 and 0.79505	
Refinement method	Full-matrix least-squares on F ²	
Data / restraints / parameters	12063 / 6 / 560	
Goodness-of-fit on F ²	1.033	
Final R indices [I > 2σ(I)]	R1 = 0.0489, wR2 = 0.1345	
R indices (all data)	R1 = 0.0765, wR2 = 0.1418	
Largest diff. peak and hole	0.635 and -0.661 e.Å ⁻³	

Compound 36 [(THF)Li(DIBA)]₂

Identification code	rem464
Chemical formula (moiety)	2Li ⁺ ·2NC ₈ H ₁₈ ⁻ ·2C ₄ H ₈ O
Chemical formula (total)	C ₂₄ H ₅₂ Li ₂ N ₂ O ₂
Formula weight	414.56
Temperature	150(2) K
Radiation, wavelength	MoKα, 0.71073 Å
Crystal system, space group	triclinic, P $\bar{1}$
Unit cell parameters	a = 8.9424(4) Å α = 86.254(13)° b = 9.0436(17) Å β = 84.619(14)° c = 17.607(3) Å γ = 81.057(13)°
Cell volume	1398.5(4) Å ³
Z	2
Calculated density	0.984 g/cm ³
Absorption coefficient μ	0.060 mm ⁻¹
F(000)	464
Crystal colour and size	colourless, 0.38 × 0.36 × 0.06 mm ³
Reflections for cell refinement	6302 (θ range 2.5 to 27.5°)
Data collection method	Nonius KappaCCD diffractometer φ and ω scans
θ range for data collection	5.1 to 25.0°
Index ranges	h -10 to 10, k -10 to 10, l -20 to 20
Completeness to θ = 25.0°	98.0 %
Reflections collected	19528
Independent reflections	4835 (R _{int} = 0.0254)
Reflections with F ² >2σ	3781
Absorption correction	semi-empirical from equivalents
Min. and max. transmission	0.9777 and 0.9964
Structure solution	direct methods
Refinement method	Full-matrix least-squares on F ²
Weighting parameters a, b	0.0446, 0.5686
Data / restraints / parameters	4835 / 12 / 298
Final R indices [F ² >2σ]	R1 = 0.0438, wR2 = 0.1024
R indices (all data)	R1 = 0.0615, wR2 = 0.1141
Goodness-of-fit on F ²	1.024
Largest and mean shift/su	0.001 and 0.000
Largest diff. peak and hole	0.21 and -0.18 e Å ⁻³

Compound 37 {(TMEDA)[Li(DIBA)]₂}_∞

Identification code	srrc1001
Empirical formula	C ₂₈ H ₆₈ Li ₄ N ₈
Formula weight	544.66
Temperature	123(2) K
Wavelength	0.71073 Å
Crystal system	Monoclinic
Space group	C 2/c
Unit cell dimensions	a = 19.7144(14) Å α = 90°. b = 9.2884(6) Å β = 94.958(6)°. c = 20.2438(14) Å γ = 90°.
Volume	3693.1(4) Å ³
Z	4
Density (calculated)	0.980 Mg/m ³
Absorption coefficient	0.057 mm ⁻¹
F(000)	1216
Crystal size	0.20 x 0.12 x 0.12 mm ³
Theta range for data collection	3.02 to 28.00°.
Index ranges	-25 ≤ h ≤ 25, -12 ≤ k ≤ 12, -26 ≤ l ≤ 26
Reflections collected	19595
Independent reflections	4435 [R(int) = 0.0544]
Completeness to theta = 26.00°	99.8 %
Absorption correction	Semi-empirical from equivalents
Max. and min. transmission	1.00000 and 0.69706
Refinement method	Full-matrix least-squares on F ²
Data / restraints / parameters	4435 / 3 / 207
Goodness-of-fit on F ²	0.965
Final R indices [I > 2σ(I)]	R1 = 0.0523, wR2 = 0.1418
R indices (all data)	R1 = 0.0907, wR2 = 0.1519
Largest diff. peak and hole	0.300 and -0.333 e.Å ⁻³

Compound 40 (TMEDA)Na(DIBA)₂Zn(*t*Bu)

Identification code	pgaross6	
Empirical formula	C ₂₆ H ₆₁ N ₄ Na Zn	
Formula weight	518.15	
Temperature	123(2) K	
Wavelength	1.54180 Å	
Crystal system	MONOCLINIC	
Space group	P21/n	
Unit cell dimensions	a = 9.79870(10) Å	α = 90°.
	b = 19.5516(2) Å	β = 91.2790(10)°.
	c = 16.5289(2) Å	γ = 90°.
Volume	3165.82(6) Å ³	
Z	4	
Density (calculated)	1.087 Mg/m ³	
Absorption coefficient	1.327 mm ⁻¹	
F(000)	1144	
Crystal size	0.1 x 0.1 x 0.05 mm ³	
Theta range for data collection	3.50 to 69.26°.	
Index ranges	-8<=h<=11, -23<=k<=23, -20<=l<=19	
Reflections collected	19219	
Independent reflections	5797 [R(int) = 0.0187]	
Completeness to theta = 67.50°	99.4 %	
Absorption correction	Semi-empirical from equivalents	
Max. and min. transmission	1.00000 and 0.47280	
Refinement method	Full-matrix least-squares on F ²	
Data / restraints / parameters	5797 / 0 / 304	
Goodness-of-fit on F ²	1.002	
Final R indices [I>2sigma(I)]	R1 = 0.0304, wR2 = 0.0764	
R indices (all data)	R1 = 0.0433, wR2 = 0.0791	
Largest diff. peak and hole	0.497 and -0.216 e.Å ⁻³	

Compound 41 (C₁₀H₇)[N(*t*Bu)₂]C=N[Zn(*t*Bu)₂]Li(TMEDA)

Identification code	pgaross3	
Empirical formula	C ₃₃ H ₅₉ Li N ₄ Zn	
Formula weight	584.15	
Temperature	123(2) K	
Wavelength	0.71073 Å	
Crystal system	MONOCLINIC	
Space group	P21/c	
Unit cell dimensions	a = 14.8452(3) Å	α = 90°.
	b = 10.9327(3) Å	β = 89.893(2)°.
	c = 21.5683(5) Å	γ = 90°.
Volume	3500.49(14) Å ³	
Z	4	
Density (calculated)	1.108 Mg/m ³	
Absorption coefficient	0.726 mm ⁻¹	
F(000)	1272	
Crystal size	0.10 x 0.08 x 0.05 mm ³	
Theta range for data collection	2.50 to 30.86°.	
Index ranges	-21<=h<=20, -12<=k<=15, -30<=l<=29	
Reflections collected	28580	
Independent reflections	10145 [R(int) = 0.0436]	
Completeness to theta = 29.00°	99.4 %	
Absorption correction	Semi-empirical from equivalents	
Max. and min. transmission	1.00000 and 0.93748	
Refinement method	Full-matrix least-squares on F ²	
Data / restraints / parameters	10145 / 0 / 367	
Goodness-of-fit on F ²	0.919	
Final R indices [I>2sigma(I)]	R1 = 0.0471, wR2 = 0.0788	
R indices (all data)	R1 = 0.1038, wR2 = 0.0887	
Largest diff. peak and hole	0.532 and -0.340 e.Å ⁻³	

Compound 43 (TMEDA)Zn(*t*Bu)OC(=CH₂)Mes

Identification code	jkros1
Empirical formula	C ₂₁ H ₃₈ N ₂ O Zn
Formula weight	399.90
Temperature	123(2) K
Wavelength	0.71073 Å
Crystal system	Monoclinic
Space group	P2(1)/c
Unit cell dimensions	a = 12.8329(5) Å α = 90°. b = 12.4467(7) Å β = 101.587(4)°. c = 14.5624(6) Å γ = 90°.
Volume	2278.61(18) Å ³
Z	4
Density (calculated)	1.166 Mg/m ³
Absorption coefficient	1.088 mm ⁻¹
F(000)	864
Crystal size	0.1 x 0.1 x 0.1 mm ³
Theta range for data collection	2.53 to 27.00°.
Index ranges	-14<=h<=16, -12<=k<=15, -18<=l<=15
Reflections collected	10472
Independent reflections	4716 [R(int) = 0.0502]
Completeness to theta = 27.00°	94.5 %
Absorption correction	Semi-empirical from equivalents
Max. and min. transmission	1.00000 and 0.85335
Refinement method	Full-matrix least-squares on F ²
Data / restraints / parameters	4716 / 0 / 236
Goodness-of-fit on F ²	1.019
Final R indices [I>2σ(I)]	R1 = 0.0553, wR2 = 0.0884
R indices (all data)	R1 = 0.0997, wR2 = 0.0983
Largest diff. peak and hole	0.485 and -0.420 e.Å ⁻³

Compound 44 [(Et₂O)₄Na]₄Cr₂Me₈

Identification code	rem515mo
Chemical formula (moiety)	C ₂₄ H ₆₄ Cr ₂ Na ₄ O ₄
Chemical formula (total)	C ₂₄ H ₆₄ Cr ₂ Na ₄ O ₄
Formula weight	612.71
Temperature	123(2) K
Radiation, wavelength	MoK α , 0.71073 Å
Crystal system, space group	tetragonal, I4/m
Unit cell parameters	a = 14.5304(7) Å $\alpha = 90^\circ$ b = 14.5304(7) Å $\beta = 90^\circ$ c = 8.7463(14) Å $\gamma = 90^\circ$
Cell volume	1846.6(3) Å ³
Z	2
Calculated density	1.102 g/cm ³
Absorption coefficient μ	0.657 mm ⁻¹
F(000)	664
Crystal colour and size	yellow, 0.20 × 0.16 × 0.04 mm ³
Reflections for cell refinement	1110 (θ range 3.0 to 29.6°)
Data collection method	Oxford Diffraction Xcalibur diffractometer ω scans
θ range for data collection	3.9 to 25.0°
Index ranges	h -17 to 16, k -15 to 12, l -10 to 7
Completeness to $\theta = 25.0^\circ$	97.7 %
Reflections collected	2343
Independent reflections	859 ($R_{\text{int}} = 0.0279$)
Reflections with $F^2 > 2\sigma$	629
Absorption correction	semi-empirical from equivalents
Min. and max. transmission	0.880 and 0.975
Structure solution	direct methods
Refinement method	Full-matrix least-squares on F^2
Weighting parameters a, b	0.0730, 0.0000
Data / restraints / parameters	859 / 27 / 74
Final R indices [$F^2 > 2\sigma$]	R1 = 0.0394, wR2 = 0.1025
R indices (all data)	R1 = 0.0602, wR2 = 0.1091
Goodness-of-fit on F^2	0.926
Largest and mean shift/su	0.002 and 0.000
Largest diff. peak and hole	0.25 and -0.33 e Å ⁻³

Compound 45 [(TMEDA)Na]₃Cr₂Me₇

Identification code	srrc06	
Empirical formula	C ₂₅ H ₆₉ Cr ₂ N ₆ Na ₃	
Formula weight	626.83	
Temperature	123(2) K	
Wavelength	0.71073 Å	
Crystal system	Orthorhombic	
Space group	P n a 21	
Unit cell dimensions	a = 16.6194(13) Å	α = 90°.
	b = 12.2037(13) Å	β = 90°.
	c = 18.3601(17) Å	γ = 90°.
Volume	3723.8(6) Å ³	
Z	4	
Density (calculated)	1.118 Mg/m ³	
Absorption coefficient	0.640 mm ⁻¹	
F(000)	1368	
Crystal size	0.20 x 0.16 x 0.06 mm ³	
Theta range for data collection	2.97 to 30.33°.	
Index ranges	-21<=h<=22, -17<=k<=15, -25<=l<=25	
Reflections collected	21684	
Independent reflections	9508 [R(int) = 0.0278]	
Completeness to theta = 27.50°	99.9 %	
Absorption correction	Semi-empirical from equivalents	
Max. and min. transmission	1.00000 and 0.77540	
Refinement method	Full-matrix least-squares on F ²	
Data / restraints / parameters	9508 / 1 / 465	
Goodness-of-fit on F ²	0.899	
Final R indices [I>2sigma(I)]	R1 = 0.0287, wR2 = 0.0507	
R indices (all data)	R1 = 0.0419, wR2 = 0.0525	
Absolute structure parameter	-0.024(9)	
Largest diff. peak and hole	0.306 and -0.164 e.Å ⁻³	

Compound 46 [(TMCDANa)₃Cr₂Me₇]

Identification code	srrc1105	
Empirical formula	C ₃₇ H ₈₇ Cr ₂ N ₆ Na ₃	
Formula weight	789.10	
Temperature	123(2) K	
Wavelength	0.71073 Å	
Crystal system	Monoclinic	
Space group	P 21	
Unit cell dimensions	a = 12.0585(3) Å	α = 90°.
	b = 15.7116(5) Å	β = 103.980(3)°.
	c = 12.5776(4) Å	γ = 90°.
Volume	2312.35(12) Å ³	
Z	2	
Density (calculated)	1.133 Mg/m ³	
Absorption coefficient	0.528 mm ⁻¹	
F(000)	864	
Crystal size	0.20 x 0.20 x 0.16 mm ³	
Theta range for data collection	3.12 to 28.67°.	
Index ranges	-15 ≤ h ≤ 15, -21 ≤ k ≤ 19, -16 ≤ l ≤ 12	
Reflections collected	14038	
Independent reflections	8711 [R(int) = 0.0201]	
Completeness to theta = 26.00°	99.8 %	
Absorption correction	Semi-empirical from equivalents	
Max. and min. transmission	1.00000 and 0.96422	
Refinement method	Full-matrix least-squares on F ²	
Data / restraints / parameters	8711 / 1 / 529	
Goodness-of-fit on F ²	1.020	
Final R indices [I > 2σ(I)]	R1 = 0.0282, wR2 = 0.0650	
R indices (all data)	R1 = 0.0308, wR2 = 0.0667	
Absolute structure parameter	-0.013(10)	
Largest diff. peak and hole	0.391 and -0.187 e.Å ⁻³	

Compound 47 [(TMEDA)Na]Mo₂Me₈

Identification code	srrc902
Empirical formula	C ₃₂ H ₈₈ Mo ₂ N ₈ Na ₄
Formula weight	868.94
Temperature	123(2) K
Wavelength	0.71073 Å
Crystal system	Monoclinic
Space group	P 2 ₁ /n
Unit cell dimensions	a = 11.3776(2) Å α = 90°. b = 17.0310(4) Å β = 105.031(2)°. c = 12.7810(3) Å γ = 90°.
Volume	2391.86(9) Å ³
Z	2
Density (calculated)	1.207 Mg/m ³
Absorption coefficient	0.589 mm ⁻¹
F(000)	928
Crystal size	0.26 x 0.20 x 0.16 mm ³
Theta range for data collection	2.78 to 29.16°.
Index ranges	-15 ≤ h ≤ 15, -22 ≤ k ≤ 22, -16 ≤ l ≤ 17
Reflections collected	15939
Independent reflections	5647 [R(int) = 0.0358]
Completeness to theta = 27.50°	97.4 %
Absorption correction	Semi-empirical from equivalents
Max. and min. transmission	1.00000 and 0.99090
Refinement method	Full-matrix least-squares on F ²
Data / restraints / parameters	5647 / 0 / 264
Goodness-of-fit on F ²	0.851
Final R indices [I > 2σ(I)]	R1 = 0.0275, wR2 = 0.0438
R indices (all data)	R1 = 0.0495, wR2 = 0.0461
Largest diff. peak and hole	0.422 and -0.272 e.Å ⁻³

Compound 50 (MDME)Li(TMP)Al(*i*Bu)₃

Identification code	srrc1109	
Empirical formula	C ₂₆ H ₅₈ Al Li N ₂ O	
Formula weight	448.66	
Temperature	123(2) K	
Wavelength	0.71073 Å	
Crystal system	Triclinic	
Space group	P -1	
Unit cell dimensions	a = 10.9347(4) Å	α = 118.627(4)°.
	b = 17.4600(7) Å	β = 90.683(3)°.
	c = 17.8524(8) Å	γ = 97.079(3)°.
Volume	2959.1(2) Å ³	
Z	4	
Density (calculated)	1.007 Mg/m ³	
Absorption coefficient	0.086 mm ⁻¹	
F(000)	1008	
Crystal size	0.20 x 0.14 x 0.10 mm ³	
Theta range for data collection	2.95 to 27.00°.	
Index ranges	-13<=h<=13, -22<=k<=21, -22<=l<=22	
Reflections collected	30177	
Independent reflections	12880 [R(int) = 0.0521]	
Completeness to theta = 27.00°	99.8 %	
Absorption correction	Semi-empirical from equivalents	
Max. and min. transmission	1.00000 and 0.91722	
Refinement method	Full-matrix least-squares on F ²	
Data / restraints / parameters	12880 / 0 / 601	
Goodness-of-fit on F ²	1.026	
Final R indices [I>2sigma(I)]	R1 = 0.0931, wR2 = 0.2278	
R indices (all data)	R1 = 0.1724, wR2 = 0.2907	
Largest diff. peak and hole	1.210 and -0.402 e.Å ⁻³	

Compound 51 (THFFA)Li(TMP)Al(*i*Bu)₃

Identification code	srrc1106
Empirical formula	C ₂₈ H ₆₀ Al Li N ₂ O
Formula weight	474.70
Temperature	123(2) K
Wavelength	0.71073 Å
Crystal system	Monoclinic
Space group	P2(1)/c
Unit cell dimensions	a = 11.0215(4) Å α = 90°. b = 17.0737(4) Å β = 106.110(3)°. c = 17.1412(6) Å γ = 90°.
Volume	3098.93(17) Å ³
Z	4
Density (calculated)	1.017 Mg/m ³
Absorption coefficient	0.086 mm ⁻¹
F(000)	1064
Crystal size	0.20 x 0.16 x 0.08 mm ³
Theta range for data collection	3.07 to 28.00°.
Index ranges	-13<=h<=14, -19<=k<=22, -22<=l<=22
Reflections collected	16787
Independent reflections	7289 [R(int) = 0.0271]
Completeness to theta = 27.00°	99.8 %
Absorption correction	Semi-empirical from equivalents
Max. and min. transmission	1.00000 and 0.82990
Refinement method	Full-matrix least-squares on F ²
Data / restraints / parameters	7289 / 12 / 352
Goodness-of-fit on F ²	1.020
Final R indices [I>2sigma(I)]	R1 = 0.0549, wR2 = 0.1298
R indices (all data)	R1 = 0.0838, wR2 = 0.1441
Largest diff. peak and hole	0.412 and -0.346 e.Å ⁻³

Compound 52 (DME)Li(TMP)Al(*i*Bu)₃

Identification code	srec1201	
Empirical formula	C ₂₅ H ₅₅ Al Li N O ₂	
Formula weight	435.62	
Temperature	123(2) K	
Wavelength	0.71073 Å	
Crystal system	Monoclinic	
Space group	C c	
Unit cell dimensions	a = 9.5982(3) Å	α = 90°.
	b = 18.7837(7) Å	β = 99.987(3)°.
	c = 16.1448(6) Å	γ = 90°.
Volume	2866.64(18) Å ³	
Z	4	
Density (calculated)	1.009 Mg/m ³	
Absorption coefficient	0.089 mm ⁻¹	
F(000)	976	
Crystal size	0.16 x 0.16 x 0.14 mm ³	
Theta range for data collection	3.24 to 29.58°.	
Index ranges	-12 ≤ h ≤ 10, -24 ≤ k ≤ 23, -22 ≤ l ≤ 19	
Reflections collected	6393	
Independent reflections	4179 [R(int) = 0.0229]	
Completeness to theta = 27.50°	97.5 %	
Absorption correction	Semi-empirical from equivalents	
Max. and min. transmission	1.00000 and 0.69133	
Refinement method	Full-matrix least-squares on F ²	
Data / restraints / parameters	4179 / 2 / 307	
Goodness-of-fit on F ²	1.027	
Final R indices [I > 2σ(I)]	R1 = 0.0472, wR2 = 0.1111	
R indices (all data)	R1 = 0.0552, wR2 = 0.1173	
Absolute structure parameter	0.15(18)	
Largest diff. peak and hole	0.684 and -0.277 e.Å ⁻³	

Compound 53 (MDME*)Li(TMP)Al(*i*Bu)₂

Identification code	srrc1114
Empirical formula	C ₂₂ H ₄₈ Al Li N ₂ O
Formula weight	390.54
Temperature	123(2) K
Wavelength	0.71069 Å
Crystal system	Monoclinic
Space group	P 2 ₁ /n
Unit cell dimensions	a = 14.2282(5) Å α = 90°. b = 10.5076(4) Å β = 90.171(5)°. c = 16.7736(7) Å γ = 90°.
Volume	2507.71(17) Å ³
Z	4
Density (calculated)	1.034 Mg/m ³
Absorption coefficient	0.093 mm ⁻¹
F(000)	872
Crystal size	0.24 x 0.20 x 0.20 mm ³
Theta range for data collection	2.70 to 29.65°.
Index ranges	-14 ≤ h ≤ 18, -13 ≤ k ≤ 14, -23 ≤ l ≤ 19
Reflections collected	9718
Independent reflections	5330 [R(int) = 0.0278]
Completeness to theta = 26.00°	86.9 %
Absorption correction	Semi-empirical from equivalents
Max. and min. transmission	1.00000 and 0.97879
Refinement method	Full-matrix least-squares on F ²
Data / restraints / parameters	5330 / 0 / 279
Goodness-of-fit on F ²	1.023
Final R indices [I > 2σ(I)]	R1 = 0.0435, wR2 = 0.0881
R indices (all data)	R1 = 0.0592, wR2 = 0.0961
Largest diff. peak and hole	0.208 and -0.156 e.Å ⁻³

Compound 54 (THFFA*)Li(TMP)Al(*i*Bu)₂

Identification code	srrc1201
Empirical formula	C ₂₄ H ₅₀ Al Li N ₂ O
Formula weight	416.58
Temperature	123(2) K
Wavelength	0.71073 Å
Crystal system	Triclinic
Space group	P-1
Unit cell dimensions	a = 9.4405(8) Å α = 72.873(8)°. b = 10.5033(9) Å β = 87.596(7)°. c = 14.8984(14) Å γ = 69.653(8)°.
Volume	1320.7(2) Å ³
Z	2
Density (calculated)	1.048 Mg/m ³
Absorption coefficient	0.092 mm ⁻¹
F(000)	464
Crystal size	0.12 x 0.12 x 0.02 mm ³
Theta range for data collection	2.93 to 26.00°.
Index ranges	-11 ≤ h ≤ 11, -12 ≤ k ≤ 12, -18 ≤ l ≤ 18
Reflections collected	26903
Independent reflections	5179 [R(int) = 0.0317]
Completeness to theta = 26.00°	99.8 %
Absorption correction	Semi-empirical from equivalents
Max. and min. transmission	1.00000 and 0.95101
Refinement method	Full-matrix least-squares on F ²
Data / restraints / parameters	5179 / 72 / 322
Goodness-of-fit on F ²	1.043
Final R indices [I > 2σ(I)]	R1 = 0.0921, wR2 = 0.2442
R indices (all data)	R1 = 0.1080, wR2 = 0.2583
Largest diff. peak and hole	1.827 and -0.825 e.Å ⁻³

Compound 55 {(THFFA)[Li(TMP)]₂LiCl}₂

Identification code	srrc1107
Empirical formula	C ₅₀ H ₁₀₂ Cl ₁₂ Li ₆ N ₆ O ₂
Formula weight	931.92
Temperature	123(2) K
Wavelength	0.71073 Å
Crystal system	Monoclinic
Space group	P 21
Unit cell dimensions	a = 12.5637(7) Å α = 90°. b = 14.9562(8) Å β = 106.186(4)°. c = 15.9663(6) Å γ = 90°.
Volume	2881.2(2) Å ³
Z	2
Density (calculated)	1.074 Mg/m ³
Absorption coefficient	0.152 mm ⁻¹
F(000)	1024
Crystal size	0.18 x 0.14 x 0.14 mm ³
Theta range for data collection	2.72 to 28.22°.
Index ranges	-16<=h<=16, -19<=k<=12, -20<=l<=20
Reflections collected	12343
Independent reflections	8995 [R(int) = 0.0300]
Completeness to theta = 26.00°	99.8 %
Absorption correction	Semi-empirical from equivalents
Max. and min. transmission	1.00000 and 0.51123
Refinement method	Full-matrix least-squares on F ²
Data / restraints / parameters	8995 / 131 / 637
Goodness-of-fit on F ²	1.046
Final R indices [I>2sigma(I)]	R1 = 0.0704, wR2 = 0.1420
R indices (all data)	R1 = 0.1021, wR2 = 0.1611
Absolute structure parameter	0.03(12)
Largest diff. peak and hole	0.323 and -0.239 e.Å ⁻³

Compound 57 (TMDAE*)Li(TMP)Al(*i*Bu)₂

Identification code	rc1117
Empirical formula	C ₂₅ H ₅₅ Al Li N ₃ O
Formula weight	447.64
Temperature	123(2) K
Wavelength	0.71073 Å
Crystal system	Orthorhombic
Space group	Pmn2(1)
Unit cell dimensions	a = 12.8948(8) Å α = 90°. b = 11.0717(5) Å β = 90°. c = 10.1824(5) Å γ = 90°.
Volume	1453.71(13) Å ³
Z	2
Density (calculated)	1.023 Mg/m ³
Absorption coefficient	0.089 mm ⁻¹
F(000)	500
Crystal size	0.20 x 0.20 x 0.16 mm ³
Theta range for data collection	3.16 to 27.99°.
Index ranges	-16 ≤ h ≤ 17, -14 ≤ k ≤ 14, -8 ≤ l ≤ 13
Reflections collected	5099
Independent reflections	2513 [R(int) = 0.0365]
Completeness to theta = 27.00°	99.7 %
Absorption correction	Semi-empirical from equivalents
Max. and min. transmission	1.00000 and 0.86314
Refinement method	Full-matrix least-squares on F ²
Data / restraints / parameters	2513 / 13 / 224
Goodness-of-fit on F ²	1.041
Final R indices [I > 2σ(I)]	R1 = 0.0472, wR2 = 0.1111
R indices (all data)	R1 = 0.0610, wR2 = 0.1208
Absolute structure parameter	-0.2(2)
Largest diff. peak and hole	0.385 and -0.210 e.Å ⁻³

16 Extended Acknowledgements

First I would like to justify the exceptional length of this acknowledgement. As well as being a reflection of how thankful I am to all who I have worked with during my studies, I have also learned through personal experience that, for most people, this will probably be the only part of this thesis, on which I have slaved for so long, that will actually be read. My hope is that through this heartfelt acknowledgement the reader, whether a past, present or future member of the Mulvey, Hevia and O'Hara conglomerate, can appreciate that, no matter how enjoyable their time has been, my time (for which I take no personal credit) was truly the golden age!

I will start, as is and should be customary, by thanking Prof. Mulvey, the man who gave me the opportunity to experience this golden age and who has played no small part in allowing it to flourish. Rab has helped immeasurably with all things chemistry; conceiving projects and guiding them, the preparation and delivery of oral presentations, and the proof reading of papers and reports, including this thesis for which the reader should also be eternally thankful. More than this though, he has been a regular part of the Friday night drinking party, a key instigator of group traditions such as Friday lunch or the annual Christmas trip to Rothesay, has invited me (along with others) to his flat for dinner (I should at this point thank Barbara for her wonderful cooking and also for doing me the honour of dancing the Gay-Gordens), a purveyor of many humorous stories excellently delivered (even if occasionally embellished...), is a surprising dab hand in the art of drinking Jenga and has always made the well-being of all in the lab his number one concern at all times. For all this and much more I will always be eternally grateful. He even took me to Hawaii!

Next I would like to thank Eva. Firstly, it was she who found my next job, via the Spanish chemical society, and, as well as Rab, wrote me a beautiful reference that I shall now have to work doubly hard to live up to! While she has not been able to attend every social gathering, there has not been an event that was not richer for her presence. And in my time she has been especially busy, not only receiving the first of which I'm

completely certain will be many promotions on her road to world domination, but also the birth of the beautiful baby Lucia. The regularity with which she and Gordon have been on holiday to coincide with the Glasgow half marathon has been highly suspicious however...

To complete this most significant of all chemistry triads, we now come to Charlie. As well as consistently taking the time to thoroughly help with any chemistry problem I may have thrust upon him while he was unwittingly passing by, he may also be almost solely responsible for the smooth running of every computer program in the office. Certainly my many battles with MS word have (in most instances...) ended in victory with him by my side. Charlie and Claire were also significant members of our cohort that travelled to Hawaii, Claire's role as my surfing buddy a particular highlight (though not the blatant assault that followed!).

Next I would like to recognise the members of the "fun gang". Jan, Stuart and Pablo have all ensured that our "gang's" name is not a misnomer! All three have been much more than just the three most dependable people come drink o'clock on a Friday night, though this they have surely been! For example, Jan and I have scaled the mighty cobbler together, have partaken in the odd game of chess and I even convinced him to go to a Killie game! Stuart's stag weekend in Belfast was legendary, and the wedding was also a fantastic night. I'm also sure his many lessons in the ways of North American language and sport shall soon be highly valued. Finally, Pablo had an uncanny knack for being a catalyst for providing many a great night, whether within our own research group, with people from other groups, his hand ball crowd, or with his countless other mates in Glasgow. My social calendar certainly took a hit when he returned to Spain. He was also the founder of our infamously "successful" 5 a side football team. All three also deserve many thanks for their X-ray analysis of most of the compounds found within this thesis. For this special thanks also go to Alan Kennedy (who has also proved a source of limitless wit, particularly on our trips to Rothesay, and is also a true pool shark, or at least one of the few who could give Stuart some competition) and Luca Russo and Bill Clegg at Newcastle. While I'm thanking people from other research groups I should also

mention Tell Tuttle, Jörg Saßmanshausen and Daniel Cannon for their help with DFT calculations, Eva Rentschler and Luca Carrella for performing magnetic susceptibility analysis, and Eric McInnis and Stephen Sproules for their help with EPR spectroscopy, particularly Stephen who looked after me diligently during my trip to Manchester.

Next, I turn to the three who started with me way back in 2008, Matt, Gemma and Liam. “Almost perfect Matt” (so coined by Eva, she wasn’t too far wrong) founded, though refused to join, “the fun gang”. Whenever he could be prised from under Kirsty’s thumb, not always an easy task, you would always be glad of his company. This might also explain why if you could persuade Matt to come out and play the rest would surely follow. He also was a regular taker of my ridiculous bets, and I didn’t always lose... Gemma I’ve known longer than anyone else in the lab. We have borne our thesis writing together for the last six months in R520 (an office she procured for the group herself), and there is probably not a diagram or formatting related issue within this thesis that has not benefited from her, almost obsessive compulsive help. The good times shall live longer in the memory though, such as the LA roller coasters en-route to Hawaii (boy can that girl scream!). Liam provided our football team with an otherwise lacking dose of flair, at least until he got fed up by the long string of heavy defeats. Amongst the many good times, the night of “Tam Crowley” was a particular laugh, though I reckon my Carlsberg would have tasted a whole lot better without the acetone!

The first tranche of students to start after me included Zoe, Ben, Sharon and Elaine. Zoe had a habit for watching the same gritty crime dramas as myself and many an hour in the lab has been whittled away (whilst simultaneously working very hard) trying to guess who did it, much to Matt’s amusement. We were pretty good too! Particular highlights include the times she got us all out to the Stand comedy club, and her Go Ape/house warming combo. Ben manages to love the works of Shakespeare, Sister Act 2, Leona Lewis, Pantera, exquisite French cuisine and McDonalds all in equal measure; the man’s capable of anything! He can also sing like you wouldn’t believe, even when standing seemed beyond him, truly the Van Gough of his time in the art of “gettin mad wae it”! Sharon is simply, and effortlessly, cool. None of her many acts of greatness demonstrate

this more than the time she went home and single-handedly, with a little help from her family, made the first prototype of our game, 3D noughts and crosses. I promise I won't forget you when the money starts rolling in from toys'r'us! Finally, the bis TMP aluminate that provides much of the success in chapter 12 was long ago christened "Elaine's Base" for a reason, her help with this work was needed and appreciated in equal measure. On a more personal note, I'm sure no one involved in our Karaoke rendition of Aqua's only "classic" will ever be able to forget it, however hard we might try!

The next year provided only one new start, which may have been considered slim pickings if it wasn't Jenni; they always say it's quality, not quantity that counts. Jenni not only bore the unfortunate need to share a glovebox with me with infinite grace, but also, facing me in the lab means she also bore the lion's share of my senseless ramblings as well! A glutton for punishment, she also agreed to run the Glasgow half marathon with me and, if it wasn't for my imminent departure, we would have tackled the full Marathon this May (sorry Jenni, but good luck!). And she's not that posh...

And at last we reach our new contingent, they may have arrived as my studies were reaching their conclusions but, nevertheless, they have made their mark over these past few months. Donna has seemingly acquired the "skill" of finding everything and anything genuinely, and I emphasise genuinely, hilarious. You'll never know anyone to laugh so much though, unlike Rab, she "sucks" at drinking Jenga! In keeping with a common theme for our newest members Sarah has the admirable ability to see the beauty in almost anything, though nothing could possibly compete with greyhounds of course! Not only has her company in the office, often long after almost everyone else has sensibly left for home, been thoroughly enjoyed (hopefully mutually...), but Jenni and I had the pleasure of her friendship during a Munro bagging exercise near Killin. Finally, whilst it feels like cheating to class you with the newbies it at least holds with my theme. Emma holds the ability to be cynical about just about anything which, combined with her razor sharp wit, has made for highly amusing lunchtimes. It can also be said with authority that, had she started in earnest in 2008, she would have been an instant member of "the fun gang".

The many final years that have passed through our ranks in my time also deserve a shout out, from Scottish Graham to our very own Spanish angel. Of special note were Paul and Rachael, who were both “lucky” enough to come under my stewardship. I can confidently say that Paul will be the only final year in R526 who, when confronted with a poorly draining sink in the lab, without hesitation proceeded to dismantle the U-bend and fix the problem. Rachael had the misfortune of requiring my help at the same time as I was writing this thesis. Fortunately she is someone that no one could have the heart to refuse, a joy to behold, and she provided many distractions that have doubtless helped me keep my relative sanity these past few months.

There are many others who deserve my gratitude but the acknowledgements should not exceed the length of the final thesis! However, others who have added to my time here include my initial mentor Lorna, “geography teacher” Vicki, Conway, just for being Conway, the immeasurably glamorous (and wonderful) Leslie, Janie Anne, the Colonel, and Chris for sorting all that ever needed sorting, and certainly not forgetting big Tam and his much appreciated positivity! To all, for making our lab an amazing place to work, for our various excursions bowling, go-karting and the likes, and for the countless acts of generosity that have been too quickly forgotten to mention, I am eternally grateful. And while much of what I have written here is of a personal rather than professional nature, there is not a person in the lab who has not been subjected to my infinite supply of chemistry problems, musings, and inspirations and I can’t and don’t want to understand how anyone could complete a PhD, or any research, without this level of support.

Och I slutsats måste jag tacka Sverige, för det är det bästast landet i hela världen!

Ross Campbell

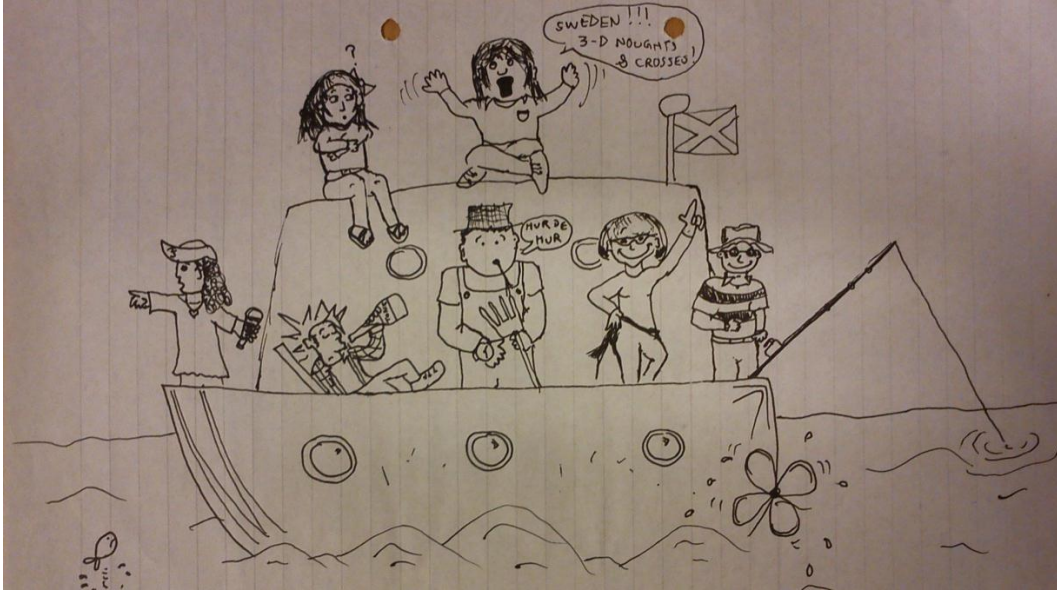


Figure A1: Doodle by Ben which beautifully encapsulates all that has made ours, truly, the golden age! (top left, Elaine; top right, me; bottom left to right: Jenni, Ben, Matt, Gemma, Jan).